

**A MULTICHANNEL SINGLE FIBER  
EMG RECORDING SYSTEM**

**A MULTICHANNEL SINGLE FIBER  
EMG RECORDING SYSTEM**

by

**John C. Smerek, B. Sc. E. E.**

**A thesis**

**Submitted to the Faculty of Graduate Studies**

**in partial fulfillment of the requirements**

**for the degree**

**Master of Engineering**

**McMaster University**

**April 1990**

Masters (1990)  
Electrical Engineering

McMaster University  
Hamilton, Ontario

Title:

A MULTICHANNEL SINGLE FIBER  
EMG RECORDING SYSTEM

Author:

John C. Smerek B.Sc. E.E.  
(GMI Engineering and Management Institute)

Supervisor:

Dr. H. DeBruin

Number of Pages:

xxii, 349

## Abstract

A multichannel single fiber EMG recording system has been developed and tested. This system is based on a multichannel needle electrode which has the ability to record EMG signals from multiple sites within the muscle under study without reinsertion. Therefore, not only is the recording volume of the electrode increased but also enhancement of the single channel electrodes is possible through spatial filtering.

The recording system, currently implemented on a PDP-11/34 computer, amplifies, filters and digitally stores the multichannel EMG signals for further signal processing. Signal processing techniques were developed to detect and extract motor unit action potentials from the EMG signal. Due to the large amount of data recorded by the multichannel electrode, slower sampling rates for digitizing the action potentials were required. High resolution feature extraction using a simple Discrete Fourier Transform interpolation algorithm was then done on the extracted motor unit action potentials. Even with near Nyquist sampled signals the accuracy of this technique was shown to be nearly equivalent to conventional extraction of action potential features samples at four times the Nyquist rate. Finally, the problem of superpositioning of action potentials was addressed. By modifying the interpolation routine an algorithm for resolving superpositions was developed.

## **Acknowledgements**

Special recognition should be given to Dr. H. deBruin for his support and help and suggestions throughout the writing of this thesis. Special mention should also be made to the Biomedical Engineering Staff at Chedoke Hospital for their camaraderie, helpfulness and support shown for the completion of my research. I would also like to thank my fellow students and friends for their assistance and encouragement. Finally, I would like to thank my parents and family, without whose support this thesis would not have been possible.

You should see the pumpkins my brother has grown.

## Table of Contents

List of Illustrations		xiii
List of Photographs		xx
Glossary of Terms		xxi
Chapter One: Introduction		1
Chapter Two:	Generation and Recording of Motor Unit Action Potentials	6
2.0	Introduction	6
2.1	Generation of the Motor Unit Action Potential	7
2.1.1	Motor Unit	7
2.1.2	Muscle Fiber	9
2.1.3	Rest State	11
2.1.4	Active State	13
2.1.5	Volume Conduction	18
2.1.6	Factors Affecting MUAP Characteristics	21
2.2	Recording of Motor Unit Action Potentials	28
2.2.1	Electrodes	29
2.2.2	Electrode Characteristics	30
2.2.3	Electrode Configurations	32
2.2.4	Positioning of the Electrode	34
2.2.5	Multichannel Recording Electrode	35
Chapter Three:	Analysis of Motor Unit Action Potentials	38

3.0	Introduction	38	
3.1	Interference Pattern	38	
3.2	Motor Unit Action Potential Analysis	41	
3.2.1	Motor Unit Action Potential Shape Analysis	41	
3.2.2	Features of Motor Unit Action Potential Shape	43	
3.2.3	Motor Unit Action Potential Train Analysis	54	
3.2.4	Properties of Motor Unit Action Potential Trains	55	
3.2.5	Muscle Control	58	
3.2.6	Separation of MUAPs into MUAPTs	60	
3.2.7	Pattern Recognition Techniques Applied to MUAPT Analysis	60	
Chapter Four:	Collection of Motor Unit Action Potentials		71
4.0	Introduction	71	
4.1	Hardware Implementations	73	
4.1.1	Multichannel Single Fiber Recording Electrode	73	
4.1.2	Arm Jig	76	
4.1.3	Multichannel EMG and Force Preprocessor	78	
4.1.3.1	Multichannel Amplifier and Filter	78	
4.1.3.2	Action Potential Detector/Firing Rate Display	80	
4.1.3.3	Force Signal Amplification/Filtering and Target Generation	82	

4.1.3.4	Muscle Control	82	
4.1.3.5	Data Collection Using the Hardware Preprocessor	83	
4.1.3.6	Safety Considerations	87	
4.2	Software Implementations	88	
4.2.1	Collection Algorithm	89	
4.2.2	Display Algorithms	95	
4.2.3	Preprocessing Algorithms	105	
Chapter Five:	Preliminary MUAP Analysis		123
5.0	Introduction	123	
5.1	Detection and Extraction of a MUAP from the IP	124	
5.1.1	Feature Selection for MUAP Detection	124	
5.1.2	Envelope Detector	126	
5.1.3	Background Noise	132	
5.1.4	Detection Sensitivity	136	
5.1.5	Extraction	136	
5.1.6	Classification of MUAPs Extracted	144	
5.2	Single Motor Unit Action Potential Analysis	151	
5.2.1	Feature Representation	153	
5.2.2	Properties of the Fourier Transform	154	
5.2.3	Extraction of MUAP Features	179	
5.2.3.1	Duration	180	

5.2.3.2	Modified Newton's Method	180
5.2.3.3	Amplitude of Peaks of a MUAP	186
5.2.3.4	Overall Characteristics	194
5.2.4	Comparison Between Straightforward and Interpolation Methods	196
5.3	Preliminary MUAPT Analysis	202
5.3.1	Alignment Algorithm	210
5.3.2	Rough Alignment	216
5.3.3	Fine Resolution Alignment	217
5.3.4	Minimization Method	220
5.3.5	Superpositions	228
5.3.6	Rough Alignment	233
5.3.7	Fine Resolution	234
5.3.8	Multidimensional Minimization Method	236
Chapter Six:	Conclusions and Recommendations	248
Appendix A:	Hardware Preprocessor Design	253
A.0	Introduction	253
A.1	Instrumentation Amplifier	253
A.2	Amplifier	257
A.3	Filtering	258
A.4	Action Potential Detector	265
A.4.1	Amplitude Detection	265
A.4.2	Slope Detection	269
A.4.3	Detection Circuit	277

A.4.4	Aggregate Display Counter	280	
A.5	Force Signal Amplification/Filtering and Target Generation	283	
Appendix B:	Power Spectral Density of Motor Unit Action Potentials		287
B.0	Introduction	287	
B.1	Calculating the Power Spectral Density	287	
B.2	Results	289	
Appendix C:	Hardware Preprocessor Functions		293
C.1	Front Panel	293	
C.1.1	EMG Preprocessor Switch Settings	293	
C.1.2	Force Preprocessor Switch Settings	295	
C.2	Back Panel	296	
C.2.1	EMG Preprocessor Inputs/Outputs	296	
C.2.2	Force Preprocessor Inputs/Outputs	297	
Appendix D:	Reference Electrode Placement		301
D.0	Introduction	301	
D.1	Reference Electrode Placement	303	
D.1.1	Comparison Measures	304	
D.1.2	Results	308	
Appendix E:	Proof of Theorems		313
E.1.1	Continuous Time	313	
E.1.2	Time Shifting	314	

E.1.3	Differentiation	315
E.1.4	Integration	316
E.2	Discrete Time	317
E.2.1	Discrete Time Shifting	318
E.2.2	Discrete Differentiation	320
E.2.3	Discrete Integration	324
E.2.4	Discrete Minimization	325

References:

329

## List of Illustrations

- 2.1 the motor unit 8
- 2.2 the muscle fiber 10
- 2.3 conductivity changes during depolarization 14
- 2.4 model of muscle fiber 16
- 2.5 muscle fiber equivalent circuit 20
- 2.6 the transmembrane action potential and it's first and second derivatives 22
- 2.7 phase distribution of motor unit action potentials 24
- 2.8 equivalent electrode/electrolyte interface circuit 31
- 2.9 multichannel single fiber EMG recording electrode 36
- 3.1 IP pattern – strong contraction 40
- 3.2 analysis of EMG activity 42
- 3.3 IP pattern – low contraction 44
- 3.4 features of the MUAP 47
- 3.5 peak to peak amplitude distribution of MUAPs 49
- 3.6 duration distribution of MUAPs 50
- 3.7 turns distribution of MUAPs 51
- 3.8 variation in MUAP shape 52
- 3.9 skeletal muscle control 59
- 4.1 collection hardware setup 72

4.2	multichannel single fiber recording electrode	74
4.3	preprocessor layout	79
4.4	muscle control with visual feedback	84
4.5	PDP 11/34 data digitization setup	90
4.6	collection algorithm	91
4.7	data buffer storage	93
4.8	multichannel EMG	96
4.9	multichannel EMG – continued	97
4.10a	single channel EMG	99
4.10b	single channel EMG – continued	100
4.11a	moderate isotonic contraction	101
4.11b	high isotonic contraction	102
4.12a	ramp contraction with offset	103
4.12b	ramp to isotonic contraction	104
4.13a	undifferenced EMG	108
4.13b	undifferenced EMG – continued	109
4.14a	differenced EMG	110
4.14b	differenced EMG – continued	111
4.15	frequency effects on differencing EMG signal	113
4.16a	undifferenced MUAP	114
4.16b	MUAP –frequency domain	115
4.16c	differenced MUAP	116
4.16d	MUAP – frequency domain	117

4.17a	undifferenced MUAP	118
4.17b	MUAP – frequency domain	119
4.17c	differenced MUAP	120
4.17d	MUAP – frequency domain	121
5.1	frequency response of smoothing filter	130
5.2	detection envelope output	131
5.3a	background noise	133
5.3b	typical amplitude distribution of the background noise	134
5.4a	envelope of a MUAP	138
5.4b	envelope of a MUAP – continued	139
5.4c	envelope of a MUAP – continued	140
5.5a	extraction of a MUAP	141
5.5b	extraction of a MUAP – continued	142
5.5c	extraction of a MUAP – continued	143
5.6a	extraction of a superposition	146
5.6b	extraction of a superposition – continued	147
5.6c	extraction of a superposition – continued	149
5.6d	extraction of a superposition – continue	150
5.7	classification procedure	152
5.8a	derivatives of a MUAP	164
5.8b	derivatives of a MUAP – continued	165
5.9a	integrals of a MUAP	166

5.9b	integrals of a MUAP – continued	167
5.10a	first nyquist derivative	169
5.10b	second nyquist derivative	170
5.10c	first nyquist derivative	171
5.10d	second nyquist derivative	172
5.11a	first nyquist integral	173
5.11b	second nyquist integral	174
5.11c	first nyquist integral	175
5.11d	second nyquist integral	176
5.12a	zero crossings of a MUAP	187
5.12b	zero crossings of a MUAP – continued	188
5.12c	zero crossings of a MUAP – continued	189
5.13a	peaks of a MUAP	191
5.13b	peaks of a MUAP – continued	192
5.13c	peaks of a MUAP – continued	193
5.14a	zero crossings for area	197
5.14b	MUAP area calculations	198
5.15a	interpolated characteristics	199
5.15b	interpolated characteristics – continued	200
5.15c	interpolated characteristics – continued	201
5.16a	over sampled characteristics	203
5.16b	over sampled characteristics – continued	204

5.16c	over sampled characteristics – continued	205
5.17a	nyquist characteristics	206
5.17b	nyquist characteristics – continued	207
5.17c	nyquist characteristics – continued	208
5.18	comparison of methods	209
5.19a	nyquist sampled MUAP	212
5.19b	nyquist sampled MUAP – continued	213
5.19c	nyquist sampled MUAP – continued	214
5.20	distances between two different unaligned MUAPs	215
5.21	minimization function	223
5.22a	alignment of a MUAP	225
5.22b	alignment of a MUAP – continued	226
5.22c	alignment of a MUAP – continued	227
5.23a	different MUAPs	229
5.23b	alignment of MUAPs	230
5.24	distances between to different aligned MUAPs	231
5.25a	superpositioned MUAPs	241
5.25b	initial alignment	242
5.25c	alignment of MUAPs to MUAP complex	243
5.26a	superpositioned MUAPs	244
5.26b	initial alignment	245
5.26c	alignment of MUAPs to MUAP complex	246

A.1	input amplifier	255
A.2	amplifier	259
A.3	fourth order low pass Butterworth filter	262
A.4	fourth order high pass Butterworth filter	264
A.5	band pass filter response of single fiber channel	266
A.6a	amplitude detection circuit	267
A.6b	amplitude detection circuit – continued	268
A.7a	slope detection circuit	270
A.7b	slope detection circuit – continued	273
A.7c	slope detection circuit – continued	274
A.8	phase response of constant time delay filter	276
A.9a	MUAP detection circuit	278
A.9b	MUAP detection circuit – continued	279
A.10a	display circuit	281
A.10b	display circuit – continued	282
A.11a	force signal amplification and filtering circuit	284
A.11b	force target signal generation circuit	285
B.1a	cannula and single fiber EMG	290
B.1b	cannula PSD	291
B.1c	single fiber PSD	292
C.1	EMG preprocessor – front panel	299

C.2	EMG preprocessor – back panel	300
D.1	reference electrode positions	302
D.2	moderate contraction	305
D.3	high contraction	306
D.4	cross correlations	309
D.5	cross correlations – continued	310
D.6	rms vs cross correlation	311

## **List of Photographs**

Photograph 4.1: arm jig set up 77

Photograph 4.2: data collection set up 85

## Glossary of Terms

- action potential (AP)** — the brief regenerative electrical potential that propagates along a single axon of muscle fiber membrane
- conduction velocity** — the speed of propagation of an action potential along a nerve or muscle fiber
- contraction** — a voluntary or involuntary reversible muscle shortening that is accompanied by action potentials
- electromyography (EMG)** — the study of the recording and analysis of spontaneous and voluntary electrical activity of muscle
- firing pattern** — a qualitative and quantitative description of the sequence of discharges of potential waveforms recorded from muscle or nerve
- firing rate** — a frequency of repetition of an action potential
- interference pattern (IP)** — the electrical activity recorded from a muscle with a needle electrode during voluntary effort
- macro motor unit action potential** — the average electrical activity of that part of an anatomic motor unit that is within the recording range of the macro-EMG electrode
- maximum voluntary contraction** — the largest force of contraction possible by the muscle under study
- motor unit** — the anatomic unit of an anterior horn cell, its axon, the neuromuscular junctions and all the muscle fibers innervated by the axon
- motor unit action potential (MUAP)** — an action potential reflecting the electrical activity of a single anatomic motor unit
- motor unit action potential train (MUAPT)** — the firing history of a single anatomic motor unit as shown by its sequence of recorded MUAPs
- movement artifact** — the change in the recorded activity caused by movement of the recording electrodes
- nerve action potential (NAP)** — an action potential recorded from a single nerve fiber
- recording volume** — the volume of muscle from which electrical activity is recorded by the recording electrode

**recruitment** — the successive activation of the same and additional motor units with increasing strength of voluntary muscle contraction

**volume conduction** — the spread of current from a potential source through a conductive medium such as body tissues

## **Chapter One**

### **Introduction**

The study of electromyography (EMG) involves the detecting and subsequent interpretation of the electrical signals generated by muscle [1]. Of particular importance is the EMG associated with skeletal muscle which is characterized by short duration high amplitude wavelets. These wavelets are known as action potentials (APs) or more formally defined as motor unit action potentials (MUAPs) A typical wavelet is the summation of the action potentials created by all the muscle fibers innervated by one motor neuron, (Chapter Two) hence the formation of the motor unit action potential.

In any system, whether it be linear or nonlinear, the classical way to get a handle on the actual behavior of the system is to observe how the outputs of the system vary with a variety of inputs. This can be done with any system including models for the functional analysis of muscle. Essentially, this is what is required for the analysis of skeletal muscle. There are really only two ways to do a functional analysis on skeletal muscle; either through evoked stimulus of the muscle where the electrical reaction of the muscle is interpreted as a response to the stimulus input or through the non-stimulus recording of muscle activity during normal muscle function. Evoked potential analysis of skeletal muscle has been studied elsewhere [2]. The initial intent of this thesis is to do the latter type of analysis namely to take a look at the functional behavior of skeletal muscle during normal muscle actions. This analysis requires a lot of ground work in order for it to be done properly. It is this ground work on the analysis of MUAPs which is attempted in

this thesis. Ultimately, the preliminary work presented here will lead to the overall analysis of MUAPs.

There are a wide variety of ways in which the MUAP can be detected. Typically, these methods fall into two basic categories an intrusive and a non-intrusive recording systems. Non-intrusive refers to detection methods which do not break the skin barrier and are generally represented by surface recording electrodes. Invasive detection techniques break this skin barrier and are typified by needle recordings. Although a case can be made for non-invasive recording techniques being less stressful to the patient and muscle under study, they fail to give a thorough understanding of what is going on within the muscle since only superficial muscle activity is recorded. The muscle activity within the belly of the muscle itself is not well recorded with these types of electrodes. Thus invasive techniques using needle or wire electrodes are more selective and record from inside the actual muscle under study and thus give a better understanding of muscle function and physiology.

Various studies have been done with needle recorded EMG [3]. However, this in itself is not sufficient to totally determine muscle control parameters. The recording volume or the area from which the electrode records electrical activity is essentially small when compared to the overall volume of the muscle. Thus the results one obtains from a needle recorded EMG signal are biased toward that one particular area of the muscle. This is not what is wanted. What is required is an overall model for the particular muscle under study. A straightforward way to do this is to simply increase the recording volume of the electrode. This can be done by recording from more than one electrode at a time within the same muscle. Multichannel recording has been shown to be feasible and is the method adopted in

this thesis.

Before any actual analysis can be done on MUAPs recorded from skeletal muscle one must back up and determine more fully what we are studying, and determine some of the problems which may be encountered. This is what is attempted in Chapter Two. This chapter describes the fundamental concepts behind the generation and subsequent recording of EMG signal. In particular it stresses the interrelationship between generation and recording of MUAPs and concludes that the EMG signal recorded from the muscle is highly dependent on the method of recording. Indeed the two cannot be separated. This chapter closes with the presentation of the recording method used in this thesis, namely the multichannel recording electrode.

Assuming one is able to collect EMG signals then the next logical step is to analyze them in order to try and come to some sort of an understanding of muscle physiology. Chapter Three attempts to present the analysis of EMG in a logical and progressive way starting with interference pattern (IP) analysis and ending with motor unit action potential train (MUAPT) analysis. Again, as before, a background on the present state of analysis done on EMG is essential in order to both determine what information can be obtained from this activity and to consider other areas of analysis which might be done. Furthermore, it is also shown that the analysis is directly associated with the recording technique used, with some analyses only suitable for certain recording techniques. Finally, the chapter closes with a discussion of some pattern analysis techniques that have been used to classify MUAP's into MUAPT's.

With the aforementioned ground work covered in Chapters Two and Three we are now ready for the first step in the implementation of a multichannel single

fiber recording system. The first step is covered in Chapter Four; collection of EMG signals. This chapter follows a basic fundamental design philosophy; design the best analog recording system possible first before any attempt is made at digitizing the signals. The hardware and software used to record EMG and force signals from the first dorsal interosseus (FDI) muscle is presented in chapter four. The design details of the analog hardware are described in Appendix A to ease the readability of this chapter. The hardware and software used to digitize and display the EMG and force data are also presented here. Finally the chapter concludes with some preliminary preprocessing of the multichannel EMG signals in order to assist in the subsequent MUAP analysis.

Finally an important goal in EMG analysis is to learn something about the actual physiological control mechanism in the muscle. Some of the preliminary methods developed to do this are presented in Chapter Five. The only valid method by which this can be done is to determine the rate coding and recruitment schemes imposed by the muscle control mechanism onto motor units in the muscle. Essentially, the only way this can be done with any exactness involves the separation of the MUAPs in the IP into MUAPT's for each active motor unit or in other words find out the time history of activation of each motor unit. With the time recorded history of the EMG the determination of the firing history of a motor unit involves first identifying when a particular MUAP has occurred and then determining if this MUAP has fired before. This latter fact is essentially a pattern recognition problem based on the assumption (albeit a very good one) that MUAP wavelets have unique shapes or features by which they can be differentiated from each other. Such being the case though does not guarantee separation of MUAPs into MUAPTs especially when the EMG signals are sampled at the Nyquist rate. This

problem is overcome by essentially representing the MUAP by its discrete Fourier coefficients as determined by the discrete Fourier Transform (DFT). Therefore the theorems relating the discrete time to the discrete frequency domain can be brought to bear on this problem, which, as shown, turns out to be essentially a one dimensional minimization problem. Furthermore, this analysis can be extended to the resolution of superimposed MUAPs which play a large role in EMG analysis since they occur frequently.

Finally, Chapter Six presents the conclusions resulting from this work. Recommendations for improvements in the techniques and analyses are also presented here as well as further fields of study.

## Chapter Two

### Generation and Recording of Motor Unit Action Potentials

#### 2.0 Introduction

The generation, recording and analysis of motor unit action potentials (MUAPs) is a complex often misunderstood process. The complexity arises from the inherent unknown characteristics of the recorded action potential (AP). No precise information about the characteristics of a particular MUAP is known a priori; rather only loosely generalized information about MUAPs can be hypothesized. The misunderstanding comes into play with the failure to recognize that the characteristics of the generated action potential are directly dependent on the method used to record the action potential and which subsequently will affect any analysis to be done on the MUAP. Furthermore, the apparent contradictions in reported data on MUAP behavior not only demonstrate that the action of muscle during contraction is poorly understood but also points to the fact that too few studies on a wide variety of differently behaving muscles have been done [4]. Physiologically, the generation of the MUAP is in no way influenced by the recording method. However, what the recording method does affect is the characteristics (size, shape, frequency content, etc.) of the action potential. Therefore, any analysis of the MUAP must take into account the affects of the recording method. Likewise, to understand how the recording of the action potential affects the characteristics of the action potential, an understanding of the generation of the action potential must first be obtained.

The generation, recording and analysis of MUAPs and all other electrical activity associated with muscle is more generally known as the study of electromyography or EMG [1]. EMG signals referred to in this thesis are the electrical signals recorded by an electrode from muscle. Valid EMG signals contain information about the fundamental structure of the muscle from which they were recorded. In order to determine whether or not the signals recorded are valid, an understanding of the basis of EMG signals is required. The purpose of this chapter is to describe the physiological generation of the MUAP and how the recording of the action potential affects its characteristics.

## **2.1 Generation of the Motor Unit Action Potential**

### **2.1.1 Motor Unit**

On the neural level, the fundamental initiation and control of muscle contraction is performed by the motor unit [5]. It is the basic contractile element of force [6]. The motor unit, as shown in Figure 2.1 , consists of the motor neuron, its axon, the neuromuscular junctions and all the muscle fibers innervated by the axon [7][8][9]. The motor neuron consists of a nucleus, cell body, dendrites, axon, synaptic contacts and afferent nerve terminals. The function of the motor neuron is to receive signals via afferent contacts, process these inputs and decide whether or not to form an efferent response to these inputs by the initiation and generation of nerve action potentials (NAP). These NAPs travel down the axon of the motor neuron to the muscle fibers it innervates.

The muscle fibers receive their stimulation via the neuromuscular junction.

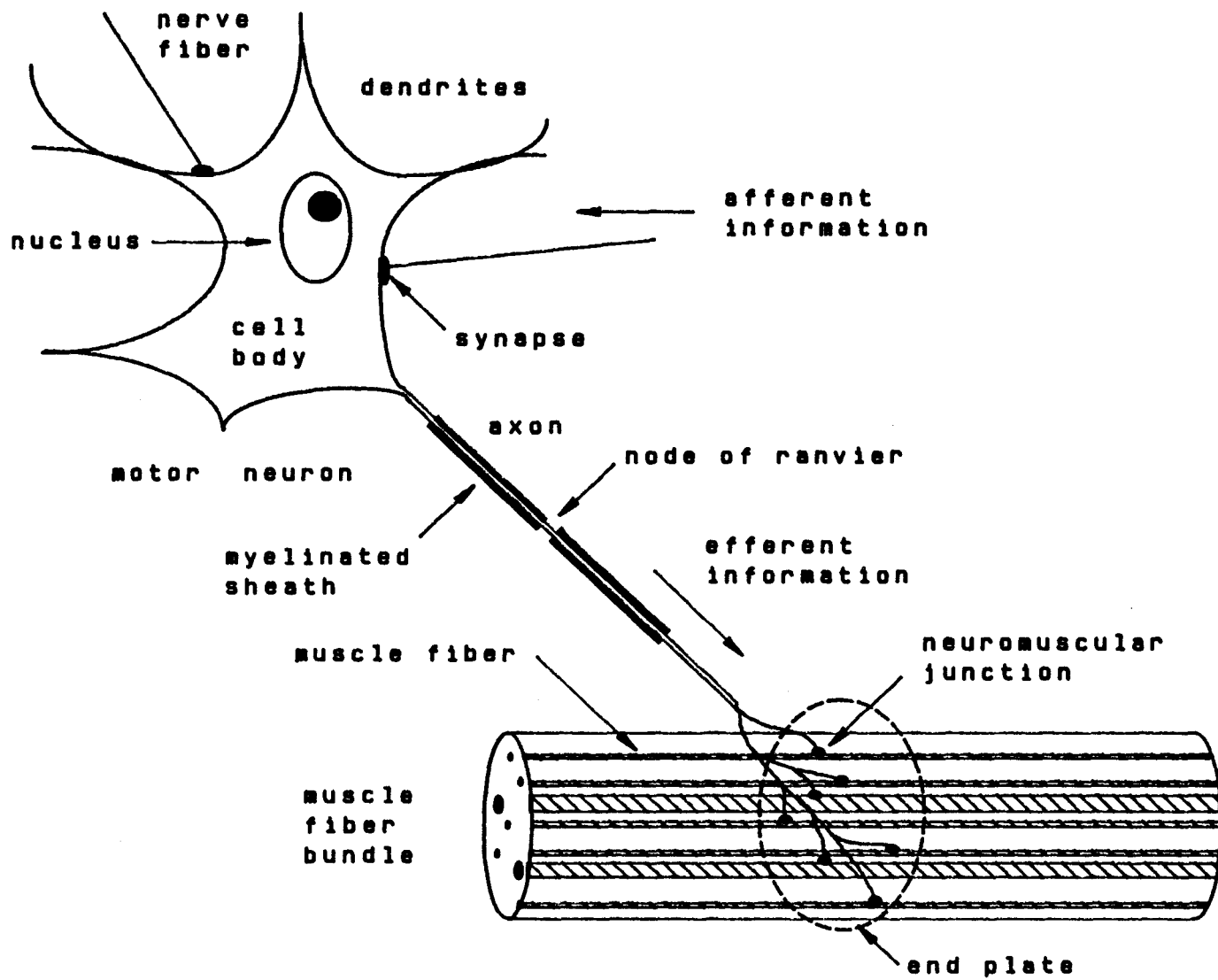


Figure 2.1 The motor unit

In the presence of a NAP the neuromuscular junction releases the neural transmitter acetylcholine (Ach). This neural transmitter crosses the transmembrane gap to chemical receptors located on the muscle fibers. It is the reception of this neural transmitter which initiates the firing of an action potential in the muscle fiber. As shown in Figure 2.2, this muscle fiber action potential (AP) travels bidirectionally along the muscle fiber from the point of innervation. The generation of the action potential is associated with the flow of ions between the muscle fiber and its surrounding medium. It is the electrical field created by this flow of ions that is recorded by an electrode as an action potential. The presence of an action potential along the muscle fiber causes that muscle fiber to contract and produce force. In order to understand how muscles generate this flow of ions to produce action potentials an understanding of the properties of the muscle fiber in its rest and active states is required.

### 2.1.2 Muscle Fiber

The contractile element of skeletal muscle is the muscle fiber. The muscle fiber is a multi-nucleated cylindrical cell with an overall diameter of approximately  $50\mu\text{m}$  and a membrane thickness of 7–15Å. As suggested by Figure 2.1, a whole muscle consists of parallel bundles of muscle fibers called fascicles [6]. Each muscle fiber is in turn composed of parallel bundles of filaments of contractile protein. These contractile proteins are approximately 150nm in diameter and are known as fibrils [6]. The important elements of the muscle fiber in regards to the generation of the action potential are the intercellular fluid, the intracellular fluid and the active muscle fiber membrane. Ultimately, the generation of the action potential

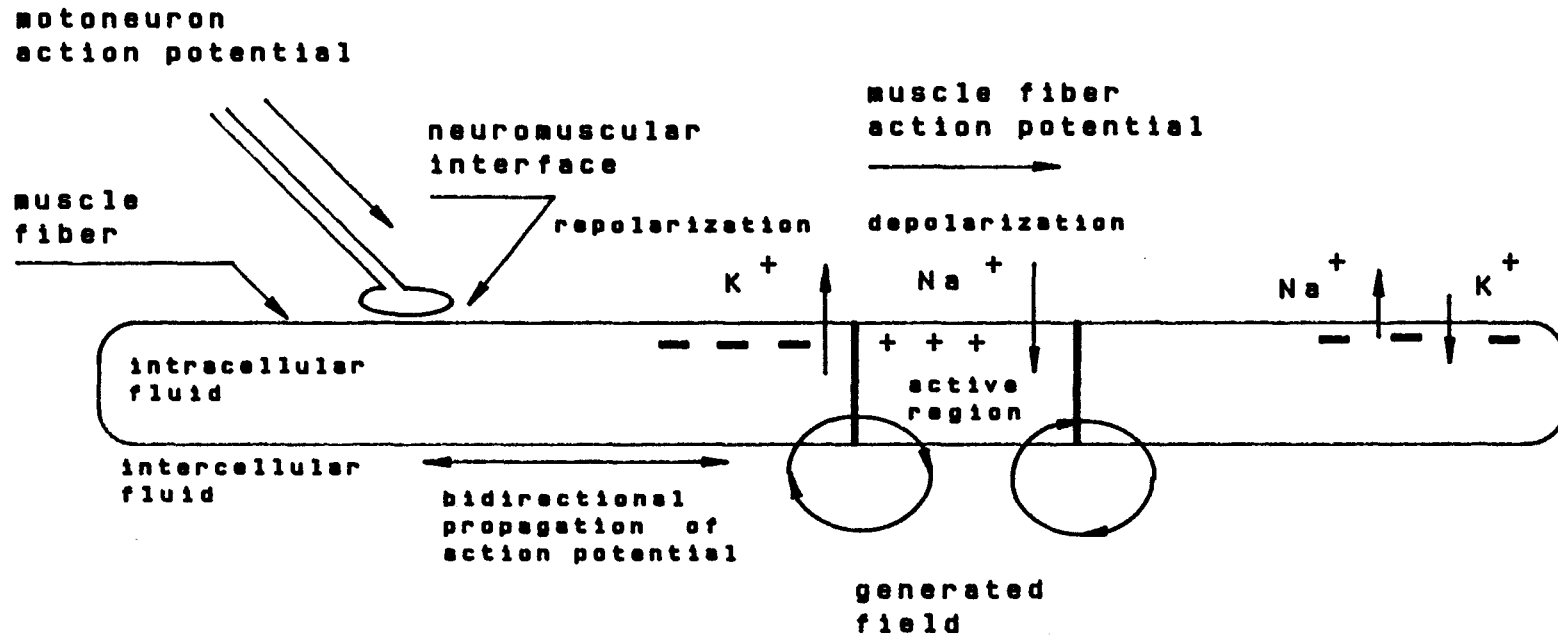


Figure 2.2 The muscle fiber

along a muscle fiber is accomplished by the unique properties exhibited by the cell membrane when it is in either a rest or active state.

### 2.1.3 Rest State

The muscle fiber membrane in a rest state is a semi-permeable active membrane which maintains a potential difference between the intercellular and intracellular fluid. In this state the muscle fiber is generally referred to as a leaky capacitor and there is no generation of APs [10]. The underlying driving force in the generation of this potential difference is the concentration gradients of ions. The important ions regarding the generation of the action potential are potassium ions ( $K^+$ ), sodium ions ( $Na^+$ ) and to a lesser extent chloride ions ( $Cl^-$ ). In steady state, the muscle fiber membrane is semi-permeable in the sense that it is permeable to  $K^+$  ions and  $Cl^-$  ions and only slightly permeable to  $Na^+$  ions. In fact the membrane is 50–100 times more permeable (conductive) to  $K^+$  ions than it is to  $Na^+$  ions in this state. The concentration of  $K^+$  ions inside the muscle fiber ( $[K^+]_i$ ) is also much higher than the concentration of  $K^+$  ions outside the fiber ( $[K^+]_o$ ) (as opposed to  $[Na^+]_i$  being less than  $[Na^+]_o$ ) thereby setting up a diffusion gradient. As  $K^+$  ions move from the inside to the outside of the muscle fiber across the membrane the non-diffusible anions are left inside. Thus, the membrane, acting as a charge separator, produces a net charge across itself with the intercellular medium being more positive relative to the intracellular medium.

Inherent in the structure of the membrane are pores which allow the diffusion of ions across it. Several different diffusible ions would have individual equilibrium transmembrane potentials across the membrane and the total potential difference

across the membrane would be the net effect of these multiple ions. This is not the case due to the presence of a sodium/potassium pump in the membrane which actively moves  $K^+$  ions into the muscle fiber and  $Na^+$  ions out of the muscle fiber thus maintaining the concentration gradients. This is shown in Figure 2.2 in the rest state where  $K^+$  ions are moved into the fiber and  $Na^+$  ions are drawn out of the muscle fiber. The net effect of the passive diffusion and active transportation of these ions across the membrane results in a steady state equilibrium being established. The effect of this equilibrium is to set up a potential difference across the membrane. Since this potential is the result of an actively maintained concentration imbalance it can be described in terms of a Nernst equation. The Nernst equation gives the equilibrium potential,  $V_m$ , across the muscle fiber membrane in rest state as:

$$V_m = \frac{RT}{F} \ln \left[ \frac{P_K[K]_o + P_{Na}[Na]_o + P_{Cl}[Cl]_i}{P_K[K]_i + P_{Na}[Na]_i + P_{Cl}[Cl]_o} \right] \quad 2.1$$

:where  $R$  is the universal gas constant,  $T$  is the absolute temperature,  $F$  is Faradays constant,  $P_x$  is the permeability of the membrane to ion  $X$ ,  $[X]_i$  is the concentration of ion  $X$  inside the muscle fiber, and  $[X]_o$  is the concentration of ion  $X$  outside the muscle fiber [7]. For muscle fiber at rest state, the equilibrium potential  $V_m$  is on the order or 50–100 mV. The process of maintaining a potential difference across the membrane is called polarization (Figure 2.2); hence the muscle fiber is said to be polarized in this state.

#### 2.1.4 Active State

The active state of the muscle fiber refers to its ability to generate and maintain an action potential along its length. It is this action potential which enables a muscle fiber to contract. The generation of an action potential is initiated by the depolarization of the fiber membrane past a threshold level. The depolarization of the membrane takes place when a NAP stimulates the neuromuscular junction. The origin of the action potential and hence the depolarization of the muscle fiber lies in the time dependent changes in the conductivity (permeability) of the muscle fiber membrane to  $Na^+$  ions and  $K^+$  ions. This time dependent quality of the membrane is shown in Figure 2.3, the conductivity changes during depolarization. The response of the membrane to depolarization is loosely based on Le Chateilers principle which states that when a system at equilibrium is disturbed it will respond in such a way as to counteract the change [11].

When the membrane potential exceeds that membrane's, and therefore that muscle fiber's threshold (usually  $-40mV$ ) the membrane's conductivity to  $Na^+$  ions increases dramatically. As shown in Figure 2.3, the steepness of the leading edge of the  $Na^+$  ions conductivity curve exemplifies the fact that once this threshold is exceeded complete depolarization of the membrane is inevitable. In fact, once it starts it is irreversible and the membrane potential approaches the Nernst equilibrium potential for  $Na^+$  ions. Thus the membrane becomes depolarized in a very short time (about one millisecond). Also shown in the graph is the conductivity of the membrane to  $K^+$  ions. The membrane's conductivity to potassium ions increases at a slower rate than for the  $Na^+$  ions. After the

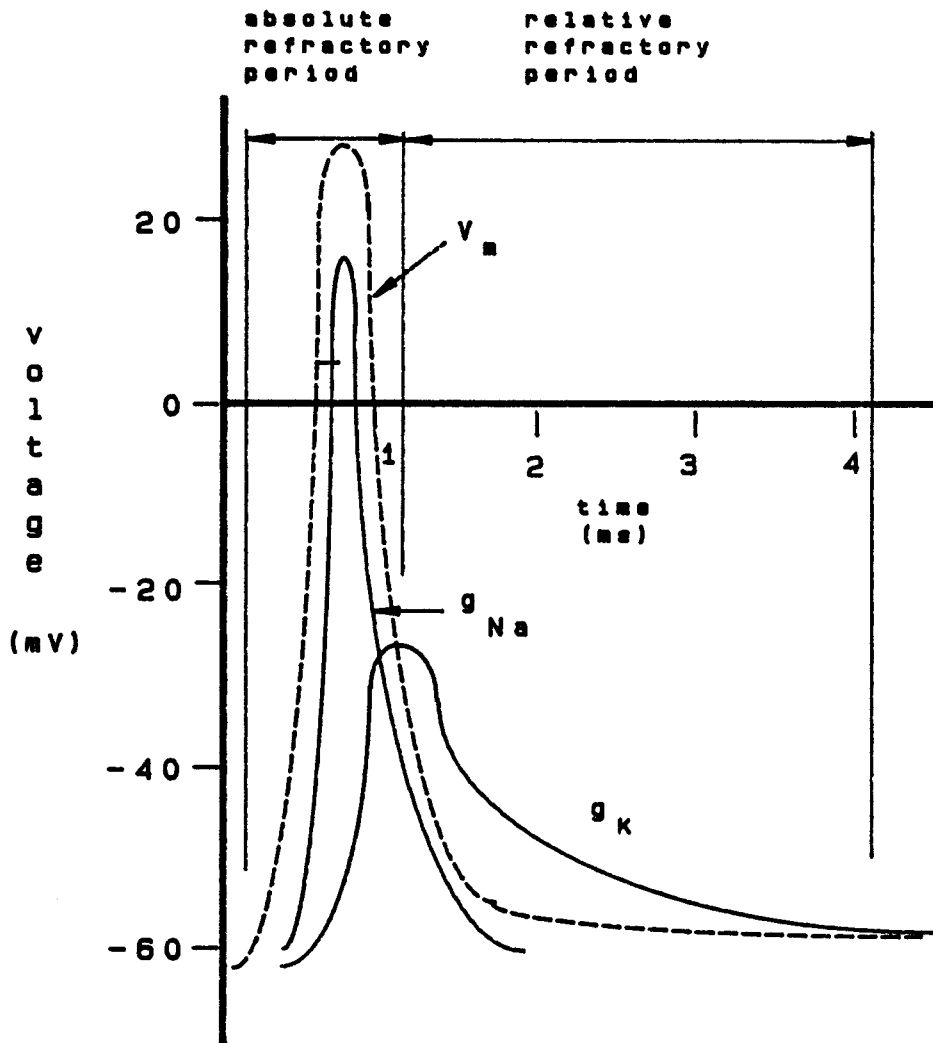


Figure 2.3 Conductivity changes during depolarization

membrane has been depolarized the conductivity of the membrane to sodium ions decreases sharply while at the same time its conductivity to potassium ions increases; thereby repolarizing the membrane to its initial resting state. This lag between the membrane's conductivity to sodium and potassium ions is responsible for creating the action potential. The change in conductances is the driving force behind the change in ionic flow and hence the voltage observed across the membrane. The potential difference,  $V_m$ , is the transmembrane action potential and as shown in Figure 2.3 is essentially monophasic.

Electrically speaking, the muscle fiber membrane can be represented by the equivalent circuit, shown in Figure 2.4 [10]. This is the per unit ( $dz$ ) equivalent circuit of the membrane either in active or rest states. The intercellular and intracellular fluids can be represented as resistive media ( $R_m$  and  $R_i$ , respectively) that are for the most part not dependent on time. The conductances of the membrane to  $K^+$  ions,  $Na^+$  ions and  $Cl^-$  ions along with  $V_m$  and  $C_m$  are time dependent. However, equilibrium potentials,  $E_{Na}^+$ ,  $E_K^+$  and  $E_{Cl}^-$  across the membrane are not time dependent since relatively few ions cross the membrane during an action potential. This circuit can be simplified by making the correct assumption that the sodium and potassium ions are the major ions necessary in creating the action potential. In the rest state then  $g_{Na} \ll g_K$  and therefore the voltage across the membrane  $V_m$ , is essentially the potassium ion's equilibrium potential  $E_K^+$ . At the height of depolarization the converse is true (i.e.  $g_{Na} > g_K$ ) and the potential difference across the membrane is essentially the equilibrium potential of the sodium ion's  $E_{Na}^+$ . This equivalent circuit therefore provides an intuitive grasp of the workings of the dynamic cell membrane.

Once an action potential has been initiated in a muscle fiber membrane it

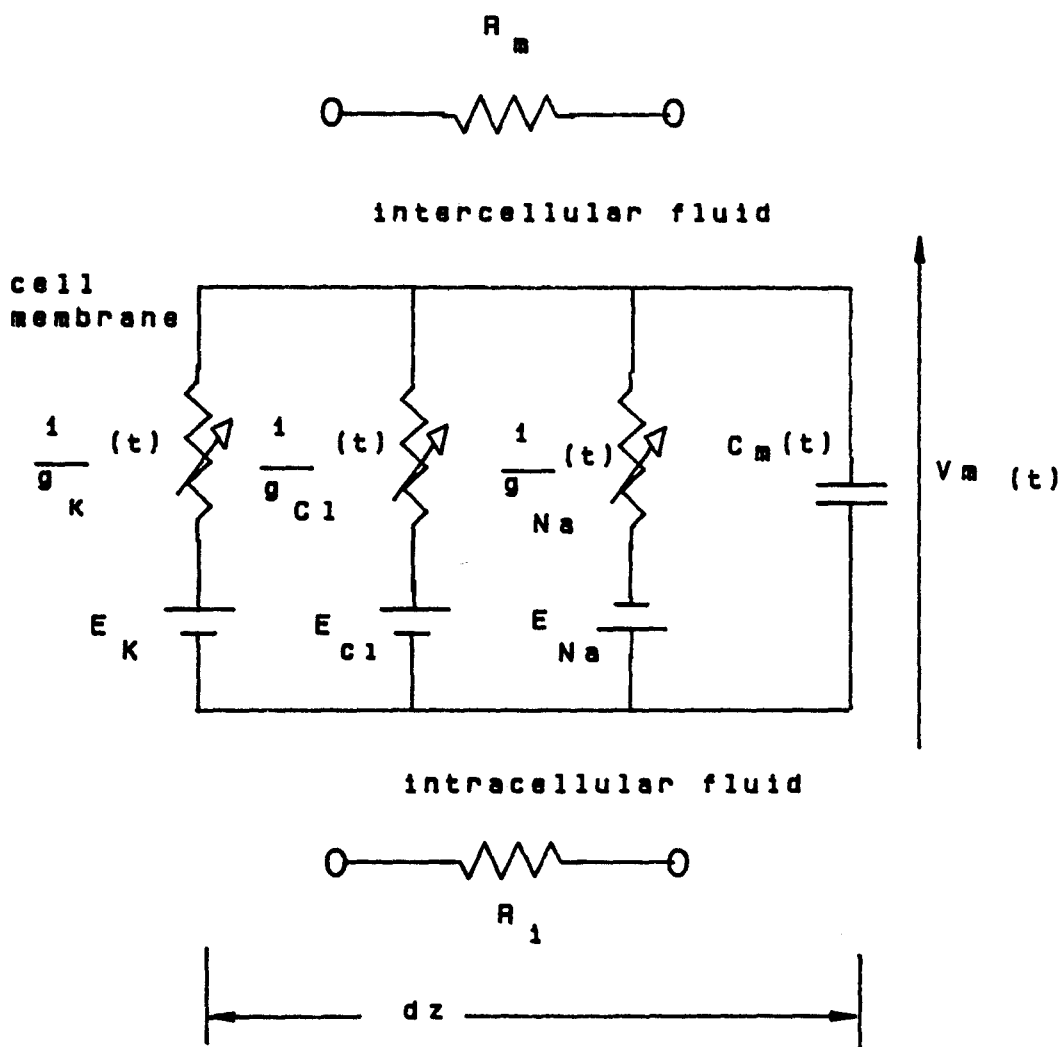


Figure 2.4 Model of muscle fiber

travels bidirectionally from the neuromuscular junction to the fiber ends. Furthermore, the actual active region in the muscle fiber for a single stimulated response is small when compared to the length of the fiber. The bidirectional travel of the action potential in the membrane occurs for the following reason. The muscle fiber is initially polarized throughout; therefore when an action potential is initiated at a point the depolarization travels in both directions away from the junction. The sudden depolarization and subsequent generation of an action potential at any particular position along the muscle fiber creates ionic current flows causing the surrounding polarized membrane to depolarize. The successive depolarization of the membrane is the means whereby the action potential travels down the muscle fiber [7]. Due to the small size of the active region in the membrane it would seem that the presence of an action potential would stimulate a response in not only its forward direction of travel but also in the reverse direction. This is simply not true for a very good reason. The finite rate of change of the membrane's ability to conduct various ions limits the frequency that action potentials can be generated in a muscle fiber. This is represented in Figure 2.3 as the absolute and relative refractory periods. The absolute refractory period is that time following an action potential during which no stimulus, no matter how large can evoke another action potential. The relative refractory period is that time following an action potential during which an abnormally large stimulus is required to evoke another action potential. The membrane in the wake of the travelling action potential is still in a refractory state and therefore cannot respond. By the time the membrane has reached a potentially depolarizable state, the stimulus from the action potential is far below the fiber's threshold level of response [7].

The actual depolarized region travelling down the muscle fiber as depicted in

Figure 2.2, can be considered as a moving dipole. The leading edge is the positive end of the dipole while the following edge is the negative end of the dipole [12]. Due to the refractive state of the trailing edge of the action potential in the muscle fiber this simple dipole model is not quite right. In order to compensate for this a tripole model has generally been used where it is assumed that the charge is concentrated at three points along the center line of the fiber [13][14][15]. The motivation for the modeling of the active region of the muscle fiber as a moving charge is to determine mathematical models for the shape of the extracellular potential recorded at any point outside the fiber. This extracellular potential is recorded as the muscle fiber action potential (MFAP). Various analyses have been done in order to come to a better understanding of the generation of the action potential. The common basis of all these analyses, however, is the modeling of the action potential and its associated biological tissue as a volume conduction phenomenon [15].

### 2.1.5 Volume Conduction

The muscle fiber can be regarded as a cylindrical conductor generating action potentials in a volume conductor [7][16]. As shown in Figure 2.4, the potential difference across the membrane,  $V_m$ , is essentially monophasic. Since most recording electrodes are extracellular they record the potential change caused by ion flow within the extracellular fluid and not the transmembrane potential. It would therefore be beneficial to derive the shape of the single fiber action potential external to the membrane. Considering the medium where the muscle fiber is located as a salt bath (external ions) then the action potential travelling along the muscle fiber generates ion flows which in turn generates moving fields (Figure 2.2).

Assuming that the muscle fiber is a conductor and that the AP is self generating in the direction of propagation (i.e. no losses) then one can consider a small section  $dz$  of the muscle fiber as being represented by Figure 2.5 [7]. Essentially, the muscle fiber can be considered as having a per unit internal impedance  $Z_i$  along it's center line and a per unit impedance  $Z_m$  across the membrane. Although the impedance along the fiber  $Z_i$  is essentially time invariant, the impedance across the membrane  $Z_m$  is only constant when the muscle fiber is in steady state. Nevertheless, the relatively short duration of the action potential over the whole length of the fiber makes the assumption of a constant  $Z_m$  a viable approximation. The voltage across the membrane at time  $t$  and position  $z$  is given by  $V_m(z, t)$ . Similarly the current along the fiber is given by  $I(z, t)$ . Considering a unit length of fiber  $dz$ , then from Figure 2.5 it is clear that:

$$V(z+dz, t) - V(z, t) = -Z_i I(z, t) dz \quad 2.2$$

Dividing through by  $dz$  and taking the limit as  $dz$  approaches zero gives:

$$\frac{dV_m}{dz}(z, t) = -Z_i I_L(z, t) \quad 2.3$$

Similarly:

$$\frac{dI_L}{dz}(z, t) = -\frac{V_m}{Z_m}(z, t) \quad 2.4$$

From Figure 2.5 it can be noted that the current along the fiber, the

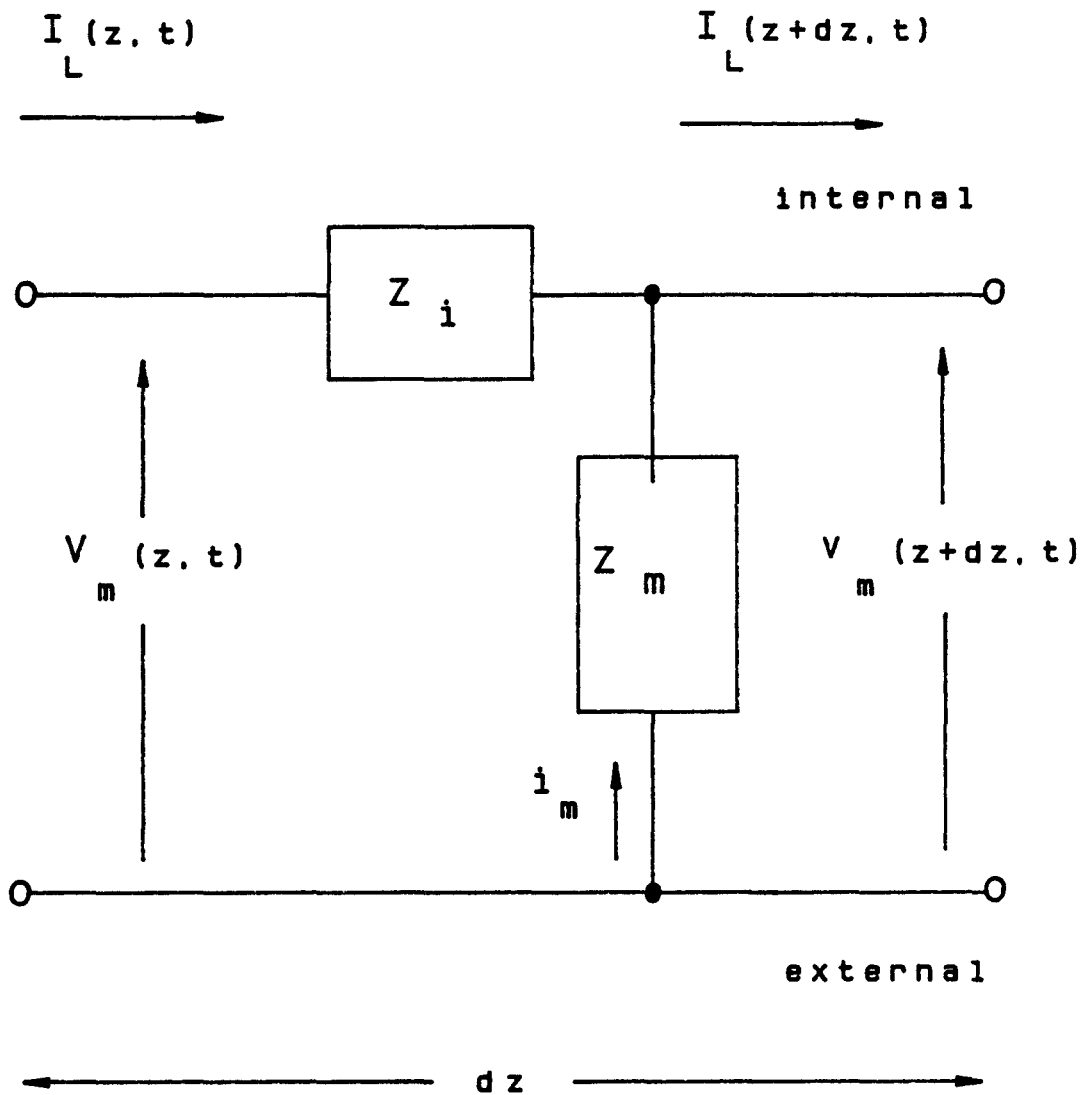


Figure 2.5 Muscle fiber equivalent circuit

longitudinal current  $I_L$  is given by  $I_L(z, t)$ . Likewise, the membrane current  $I_m$ , which is essentially ionic flow is given by:

$$\frac{V_m(z, t)}{Z_m(z)} = -I_m \quad 2.5$$

Taking the second derivative with respect to  $z$  of equation 2.3 and combining it with equations 2.4 and 2.5 gives a new expression for the membrane current:

$$I_m = \frac{d^2}{dz^2} V_m(z, t) \frac{1}{Z_i} \quad 2.6$$

Assuming  $Z_m$  and  $Z_i$  to be constant, then the current across the membrane flowing into the volume conductor is directly related to the second derivative of the voltage across the membrane. Since the monophasic shape of the voltage across the membrane  $V_m$  is known from Figure 2.3, and knowing that the membrane current  $I_m$  is directly related to the voltage in the volume conductor  $V_m(z, t)$  then equation 2.6 tells us that the second derivative of this voltage is the waveform that is seen at the surface of the membrane. As shown in Figure 2.6 this waveform recorded from the volume conductor is ideally triphasic. Furthermore Figure 2.6 also indicates that the action potentials created by muscle fibers in a volume conductor are ac signals.

### 2.1.6 Factors Affecting MUAP Characteristics

One of the main determinants of the characteristics of the action potential is the structure of the muscle. From the previous section it would seem that the

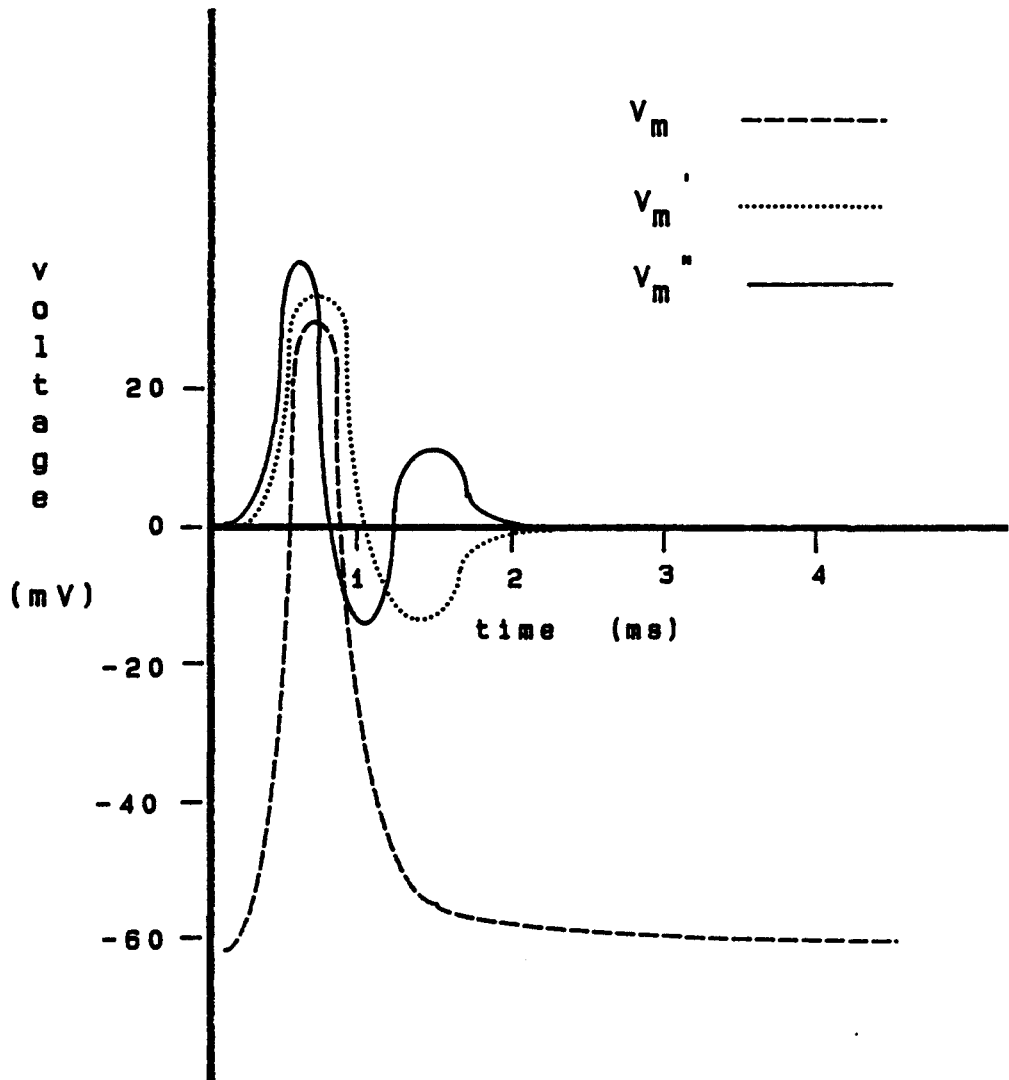
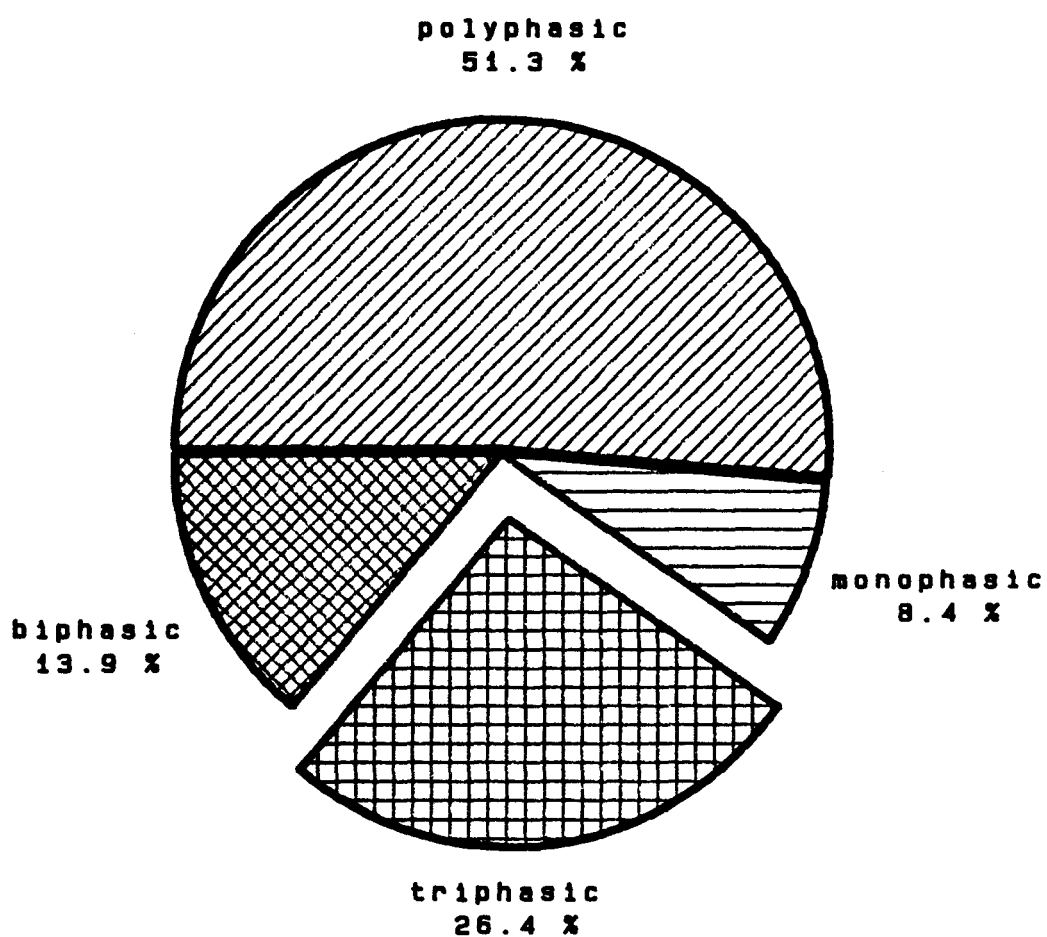


Figure 2.6 The transmembrane action potential and its first and second derivatives

majority of the action potentials recorded externally from a muscle fiber by an electrode referenced remotely would be triphasic. A typical recording of action potentials was done with a needle electrode and the results are shown in Figure 2.7. As shown only a small percentage of the whole group of muscle fiber action potentials are triphasic. There are a variety of reasons for this. Most have to do with the structure of the muscle itself. First and foremost the action potential recorded is not typically an action potential generated by a single muscle fiber; rather, as suggested by Figure 2.1, it is the summation of the activity of the individual muscle fibers innervated by a single motor neuron. Depending on functionality a single motor neuron may innervate as few as 10 muscle fibers or as many as 1000 muscle fibers [4][17]. The nearly synchronous generation of action potentials in all the muscle fibers innervated by a single motor neuron results in the superpositioning of these action potentials in the volume conductor. This summation of the muscle fiber action potentials from a motor neuron,  $S(t)$ , can be expressed as:

$$S(t) = \sum_{i=1}^N s_i(t) \quad 2.7$$

where  $s_i(t)$  is the  $i$ 'th individual muscle fiber action potential. It is this superpositioned signal that is recorded by the electrode and is known as the motor unit action potential (MUAP) [18][19]. Typically, the MUAP is the summation of 2 to 12 muscle fibers for highly selective needle electrodes. If these individual action potentials are exactly superimposed, then the summation of any or all would still be triphasic in shape, however, this is not the case. Muscle fibers are innervated at



**Figure 2.7 Phase distribution of Motor Unit Action Potentials**

approximately the middle of the muscle fiber at what is known as the end plate region. This is not always exact as shown in Figure 2.1. The slight misalignment of the individual innervation regions of the fibers will cause action potentials of individual fibers to be misaligned with respect to one another resulting in a variety of multiphasic waveforms  $S(t)$ . Furthermore, the size of the individual muscle fibers associated with a particular motor unit varies by approximately 10%. From field theory a travelling wave can be expressed as:

$$\frac{d^2}{dz^2} V(z, t) = \frac{1}{c^2} \frac{d^2}{dt^2} V(z, t) \quad 2.8$$

:where  $c$  is the velocity of the wave [20]. Furthermore, since the per unit impedance of the muscle fiber can be expressed as:

$$Z_i = \frac{z\rho l}{\pi r_f^2} \quad 2.9$$

:where  $r_f$  is the radius of the muscle fiber and  $l$  is it's length. Combining the above two equations with equation 2.6 we find that:

$$c \propto \frac{1}{\sqrt{r_f}} \quad 2.10$$

The velocity of the action potential is inversely related to the square root of the diameter of the muscle fiber [7]. The larger the diameter of the muscle fiber the slower the action potential and the more misaligned it becomes with the faster action potentials. Thus the synchronous alignment of the action potential fibers

changes with distance from the point of innervation. Additionally, the diameter of any particular muscle fiber tends to decrease with distance from the point of innervation leading to a further dispersion of the fiber action potentials [7]. The overall misalignment of MFAPs is known as spatial dispersion.

Not only does the size of the muscle fiber affect the conduction velocity of the action potentials but it also affects the size of the action potentials created. The amplitude is found to increase with increasing fiber diameter according to the equation:

$$V = ka^{1.7} \quad 2.11$$

:where  $V$  is the amplitude of the action potential,  $k$  is a constant and  $a$  is the radius of the muscle fiber [4]. Thus larger muscle fibers produce larger MFAPs. This is reasonable since the surface area of the muscle fiber membrane increases with muscle fiber size and therefore a larger flow of ions should produce a stronger electrical field. In developing equation 2.6 it was assumed that the impedance  $Z_m$  was not only the transmembrane impedance but also the impedance of the surrounding muscle tissue. If it is assumed that the transmembrane impedance is  $Z_m$  and  $Z_o$  is the impedance of the tissue then equation 2.6 becomes:

$$I_m(z, t) = \frac{1}{(Z_o + Z_i)} \frac{d^2}{dz^2} V(z, t) \quad 2.12$$

Again the external potential is a function of  $z$  only and if the above equation is combined with equation 2.9 it can be seen that the amplitude of the MUAP varies inversely with the distance from the needle electrode to the muscle fiber. If  $R_o$  is

distance of the recording electrode to the surface of the muscle fiber then the potential at the electrode is given by the expression:

$$V_r = \frac{kV_m}{R_0} \quad 2.13$$

:where  $k$  is some constant and  $V_r$  is the recorded potential and  $V_m$  is the potential at the muscle fiber surface. Further studies have suggested that the muscle tissue displays filtering characteristics which are better described by taking the impedance of the tissue into account for a particular distance  $R_0$  as measured from the recording electrode to the muscle fiber. This is given as:

$$|T(j, \omega)_R| = \frac{k}{\sqrt{(1 + \omega^2)}} \quad 2.14$$

:where  $k$  is a constant,  $\omega$  is the frequency and  $|T(j, \omega)_R|$  is the attenuation at distance  $R$  [21]. This is basically a low pass filter and can be characterized by a simple  $RC$  lumped circuit. The low pass filtering characteristics are shown to vary with different distances and positions of the electrode from the muscle fiber. This would account for reports that the size of the potential diminishes exponentially with radial distance from the active muscle fiber and that the recorded MFAPs have a lower frequency content as this distance increases [22][23][24][25]. Therefore the distance to the electrode is of great importance in determining the size and frequency content of the action potential.

Muscle fibers innervated by any particular motor neuron are randomly distributed over a considerable portion of the muscle. Depending on the type and

functionality of the muscle, the muscle fibers from a particular motor neuron can be distributed anywhere within  $1/3$  to  $1/2$  or more of the entire volume of the muscle [7]. This implies that any particular region can contain muscle fibers from 20–50% of all the motor units located in that muscle [26][27][4]. This means that for any particular location in the muscle volume the electrode will record MUAPs from more than one motor unit depending on the level of muscle contraction. It should be noted that the firing of a motor unit may not be entirely independent of the firing of any other motor neuron. Motor unit action potentials may discharge at the same or nearly the same times with respect to one another during high level fatigue inducing contractions [28][29]. Under normal contractions however, MUAPs are generated asynchronously and can add, subtract or superimpose in any imaginable fashion. This can result in a complex waveform being generated.

Further complexity of MUAP shapes is due to the fact that skeletal muscle actually consists of two different types of muscle fibers; slow twitch and fast twitch fibers. The percentage and type of fibers not only depends on the functionality of the muscle but also the location of the fibers in the muscle. Although, regeneration is not an issue in normal cases, muscle fibers reinnervated by a motor neuron tend to be grouped together in a bundle and not dispersed throughout the muscle. This can change the shape of the MUAPs recorded. All in all, the generation of MUAPs is a complex process influenced by many physiological factors which must be considered when trying to record and analyze them.

## **2.2 Recording of Motor Unit Action Potentials**

Up until now only the generation and physiological influences of the motor

unit have been discussed. Of equal and related importance is the method used to record the MUAP. As stated earlier, the method of recording plays a large role in determining the characteristics of the action potentials recorded.

### 2.2.1 Electrodes

There are many types of electrodes used to collect MUAPs. They fall into two basic groups; surface (noninvasive) and needle (invasive) electrodes. They have fundamentally different characteristics and hence the signals recorded are quite different. An action potential recorded by the electrode is the average of all the potentials existing at the electrode's surface [4] and therefore is a function of the electrode's recording area. Furthermore, an increase in the recording area of the electrode implies that the electrode will record from a larger number of muscle fibers and hence more spatial averaging is present [30]. This results in a decrease in both the frequency content and the amplitude of the signals recorded. Additionally, the filtering effects of muscle tissue are more pronounced for surface electrodes since they are by design further away from the muscle fibers recorded from [31] and their action potentials will also have lower frequency content.

The recording of EMG signals is accomplished through the use of three electrodes: the recording electrode, the reference electrode and the ground electrode. The recording electrode and the reference electrode are always required since differential amplification is necessary to remove large common mode signals. The ground electrode is used as a common return for the recording circuitry and is usually a surface electrode. The recording or active electrode is the electrode which is close to the source of activity (MUAPs) to be recorded. The reference electrode is

generally the electrode located further away from the source.

### 2.2.2 Electrode Characteristics

There are several important properties of the electrodes and their configuration. These include the electrode's filtering properties, the separation distance between the reference and recording electrode's and the electrode/tissue impedance [4][6]. These properties can best be described with the aid of an equivalent circuit as shown in Figure 2.8. As shown, the recording configuration consists of three main facets: the recording electrode, the reference electrode and the instrumentation amplifier. The recording and reference electrodes may be of the same type and material or different. For the equivalent circuit,  $Z_i$  is the input impedance to the amplifier and is significant only when the impedance of the recording or reference electrodes are a sufficient fraction of this impedance. The shunt capacitance,  $C_s$  is the capacitance to ground from the electrodes to the amplifier. This shunt capacitance includes the capacitance from the cables and wires used to connect the amplifier to the electrodes. The resistive part of the electrodes are represented by  $R_1$  and  $R_2$ . The capacitance of the electrode/electrolyte interfaces are shown as  $C_1$  and  $C_2$ . The leakage resistance of the electrodes is represented by  $R_{f1}$  and  $R_{f2}$  and is defined as the flow of ions travelling across the electrode/electrolyte barrier. The half cell potential created by the electrode/electrolyte interface are represented by  $E_1$  and  $E_2$ . If the half cell potentials are not the same, the difference may appear as a dc offset to the instrumentation amplifier. Finally, the impedance of the muscle tissue is represented by  $Z_m$  while the action potentials generated by the muscle fibers is

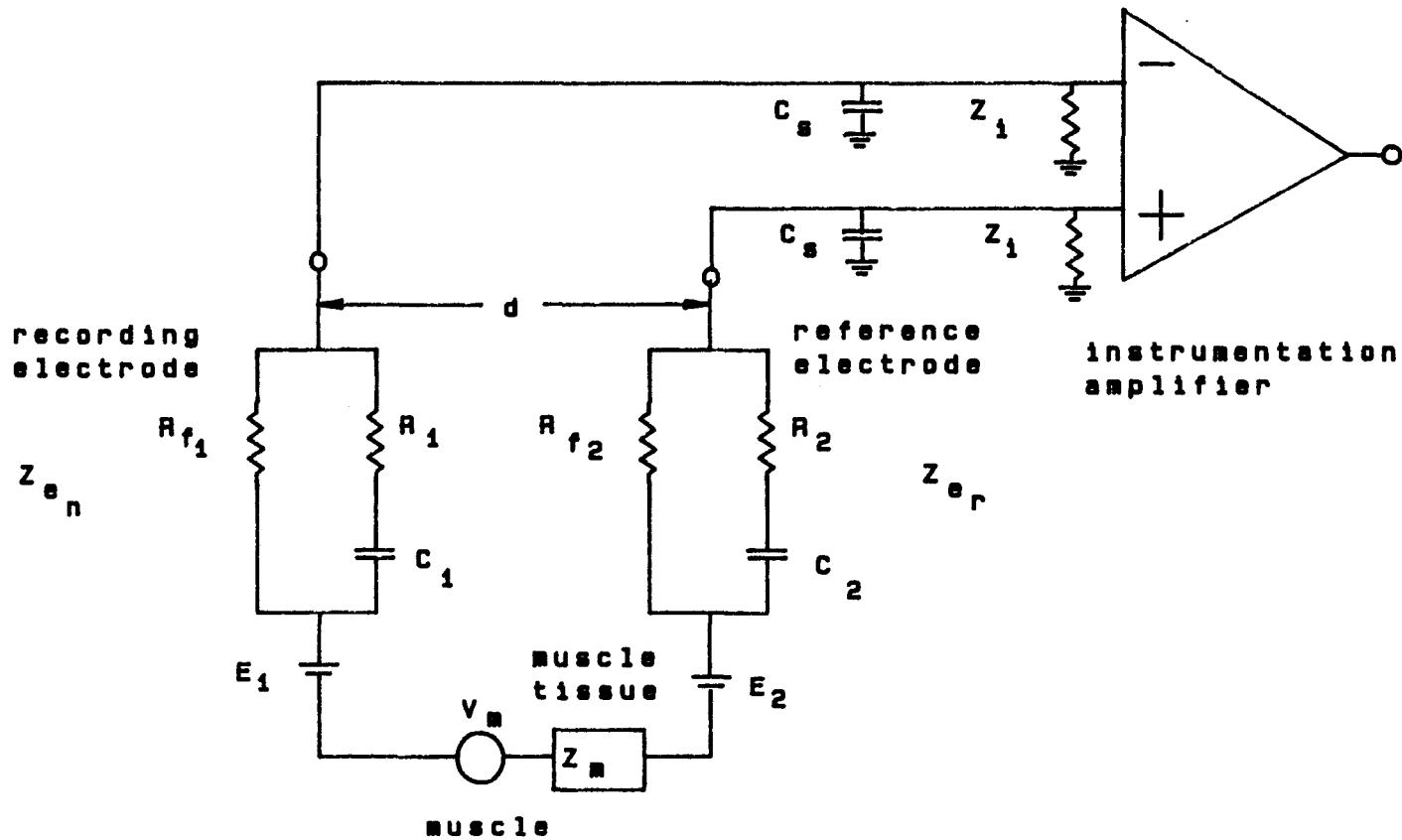


Figure 2.8 Equivalent electrode/electrolyte interface circuit

represented as  $V_m$ . All of these parameters are frequency dependent, thus the electrodes act as filtering devices. The filtering properties of an electrode are a function of their size, the distance between the recording and reference electrodes and the chemical properties of the electrode/electrolyte interface [6][32]. The electrode impedance,  $Z_e$  is inversely proportional to both the recording area of the electrode and the frequency of the action potential and directly proportional to the current density (in terms of ion flow) of the measured potential. Since the impedance of an electrode interface decreases with either an increase in the frequency of the action potential measured or a decrease in electrode area, then the greatest electrode impedance will occur at lower frequencies in small area recording electrodes.

### 2.2.3 Electrode Configurations

There are a variety of different recording configurations. Depending on the relative size and location of the electrode surfaces they may be referred to as monopolar, concentric, bifilar (bipolar), single fiber, and macro EMG needle electrodes. Monopolar recording is accomplished with the recording electrode being positioned in muscle and either a surface electrode or another needle electrode located over inactive tissue at quite a distance apart (larger than the duration of the action potential). This is a remote referenced signal. Monopolar electrodes have been used by a variety of researchers [33][34][35][36] with various parameters recorded for action potentials. Due to their size and configuration these electrodes can be used to obtain information about individual motor units in the muscle [37][38]. Bipolar or bifilar needle recording electrodes have the recording and

reference electrodes located relatively close together [39]. The spacing of the electrodes determines to a great extent the shape of the signals recorded since the recording is basically a differencing of the potential at two points. Many investigations have shown that a variety of action potential shapes can be recorded due to the spacing and orientation of the recording surfaces to the muscle fibers generating the action potentials. Very selective recordings of action potentials can be obtained using this method [32][40][41] and the action potentials tend to be of smaller amplitude and shorter duration than those recorded monopolarly [42][43][44][45]. Concentric needle electrode configurations measure the potential difference between the end of an insulated wire and the bare shaft of a steel needle or cannula through which it is inserted. Concentric needle electrodes are also known as coaxial electrodes. The outer cannula acts as the reference and the central fine wire as the recording electrode. The purpose of the cannula is to act as a shield, effectively blocking out any low frequency activity from distant fibers [5][34][46][47][48]. Due to this filtering effect the durations of the action potentials recorded by this configuration are shorter than those recorded monopolarly [49]. Single fiber recording is done with the same configuration as the concentric needle only the wire electrode is much smaller (usually  $25\mu\text{m}$  diameter) and ideally records a single muscle fiber action potential. In reality they measure one to two MFAP [50][51][52][53] whose durations are very short. Macro EMG is recorded with a modified single fiber electrode. The Macro EMG is the synchronous average of cannula responses using a single fiber electrode as a trigger channel [54][55][56][57][58][59][60]. The response from the cannula is used in conjunction with the single fiber to find the response of the entire motor unit within the recording region of the cannula.

### 2.2.4 Positioning of the Electrode

As previously mentioned, not only is the distance from the muscle fiber to the electrode important but also the positioning of the needle electrode relative to the central innervation zone is important in order to eliminate spatial dispersion of the generated MUAP.

Uptake volume of the recording electrode is also an important parameter to consider when recording MUAPs. The uptake volume of the needle electrode is defined as that volume of tissue around an electrode from which practical MFAPs can be recorded [1]. This practical limit on the recording distance is due both to the attenuation of action potentials with distance as previously stated and the area of the recording electrode. Therefore there is only a limited number of muscle fibers that can be recorded from by a needle electrode at any particular position. This limits the number of MFAPs that will summate to form the recorded MUAP, thus greatly affecting its shape.

Motion artifact in the collection of MUAPs can come about in a variety of ways. The first and foremost cause of motion artifact is the changing of the electrode position. This movement may cause low frequency noise resulting from electrode/electrolyte interface changes and even connecting cable motion to corrupt the recorded signal especially if the electrode has high impedance to begin with.

Changing electrode position also has another affect. The occurrence of an action potential causes the muscle fiber to contract. This contraction is associated with force and movement of the muscle. This movement, however slight, will cause a change in the position of the electrode to the recording volume (uptake area) and

thus as previously discussed affect the resulting action potential recorded. Thus we can and will expect a change in the shape of the action potential produced by the same muscle fiber with different levels of force and with successive recordings due to the changing geometric arrangement of electrode and fiber. Secondly, small movements may in fact place the recording needle in a different muscle area and hence a different motor unit population, creating discontinuities in the recorded action potentials. This can be especially annoying when trying to follow the successive firing of a motor unit. This is a major problem when using highly selective needles [61].

### 2.2.5 Multichannel Recording Electrode

The configuration of the electrodes used in this thesis is shown in Figure 2.9. As shown, the ground and reference electrodes are surface electrodes. These electrodes are disc shaped silver chloride electrodes. The recording electrode is a multichannel fine wire electrode. There are three fine wires (50.0  $\mu\text{m}$  dia.) placed in a steel needle shaft (0.5mm dia.) called, as stated previously, the cannula by epoxy. The fine wires are only exposed at their ends and are isolated from each other as well as from the cannula. It should be noted that the cannula in this configuration provides shielding for the fine wires from distant EMG activity. The recording configuration, as shown, is monopolar. This does not mean that the EMG activity to be analyzed has to be a monopolar recording. The beauty of a multichannel recording lies in its ability to be configured in a variety of different ways. For example, after data has been collected by computer, the EMG activity of one fine wire channel can be subtracted from the EMG activity of any of the

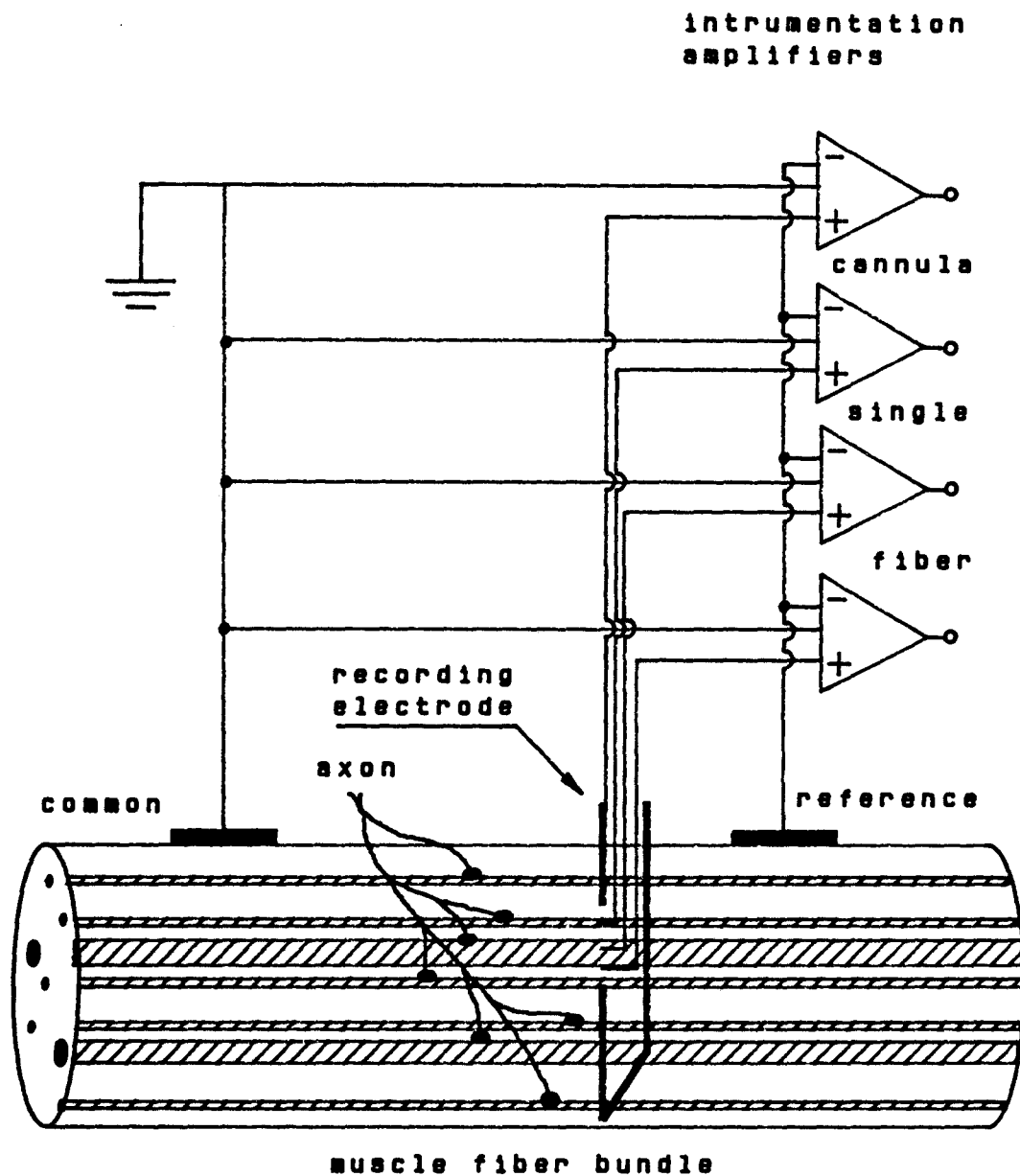


Figure 2.9 Multichannel single fiber EMG recording electrode

other two fine wire channels to form essentially a bipolar recording of the action potentials. If the EMG activity of the cannula is subtracted instead the resulting activity would be very similar to that recorded with a concentric needle electrode.

## **Chapter Three**

### **Analysis of Motor Unit Action Potentials**

#### **3.0 Introduction**

The next logical step after considering the generation and recording of MUAPs is to consider how they are analyzed. The analysis of MUAPs can be separated into two main categories:

- (1) interference pattern analysis and
- (2) motor unit action potential analysis which includes:
  - (a) motor unit action potential shape analysis and
  - (b) motor unit action potential train (MUAPT) analysis.

The motivation for each analysis is an attempt to come to a better understanding of the subtle intricacies of muscle behavior and structure. When used for medical diagnostic purposes inherent is the basic belief that the measured parameters of the EMG activity will be different between neuromuscular pathology and normal structure and function. The purpose of this chapter is to present the various forms of analysis that have been done on the EMG.

#### **3.1 Interference Pattern**

During strong muscle contractions the signal recorded from muscle tends to

form an interference pattern (IP) [1]. The IP is a function of the recording electrode and the strength of the contraction. It is a function of the electrode, specifically the electrode's size, since the larger the recording area the larger the number of motor units it can record from simultaneously and the more random the signal will look especially at higher contraction levels when more motor units are activated. A needle recorded IP is shown in Figure 3.1. As shown, individual MUAPs cannot be readily discerned in many segments of the recording. Nevertheless these patterns can still be analyzed. Individual MUAPs overlap in time and space depending on the number of active motor units, their size and spatial distribution, and firing times [4]. Essentially this is a stochastic process. The IP reflects the relative number, size and firing rates of the active motor units in the muscle. Increasing the amount of force or contraction of the muscle increases the complexity of the IP [62][63][64][65][66]. While early attempts at IP analysis used photographic plates more modern approaches have studied various parameters or features.

Analyses have shown that the IP can yield useful clinical data about the muscle [4][67][68][69][70]. A few of the parameters considered are turns per second, mean amplitude of turns [71][72], amplitude rise per second [73], mean phases [74], positive phase durations and negative phase durations [75][76]. In an effort to reduce the dependence of the measured features of the IP on the level of contraction the ratio of the log of the number of turns to the log of the the mean amplitude has been proposed as a parameter [77][78][79]. Frequency analysis of the IP has also been done [80][81][82][83].

The interference pattern can also be used in a variety of other analyses from the simple determination of whether or not a particular muscle is active to determining whether or not there is crosstalk between muscles. In short any

**SINGLE FIBER EMG**

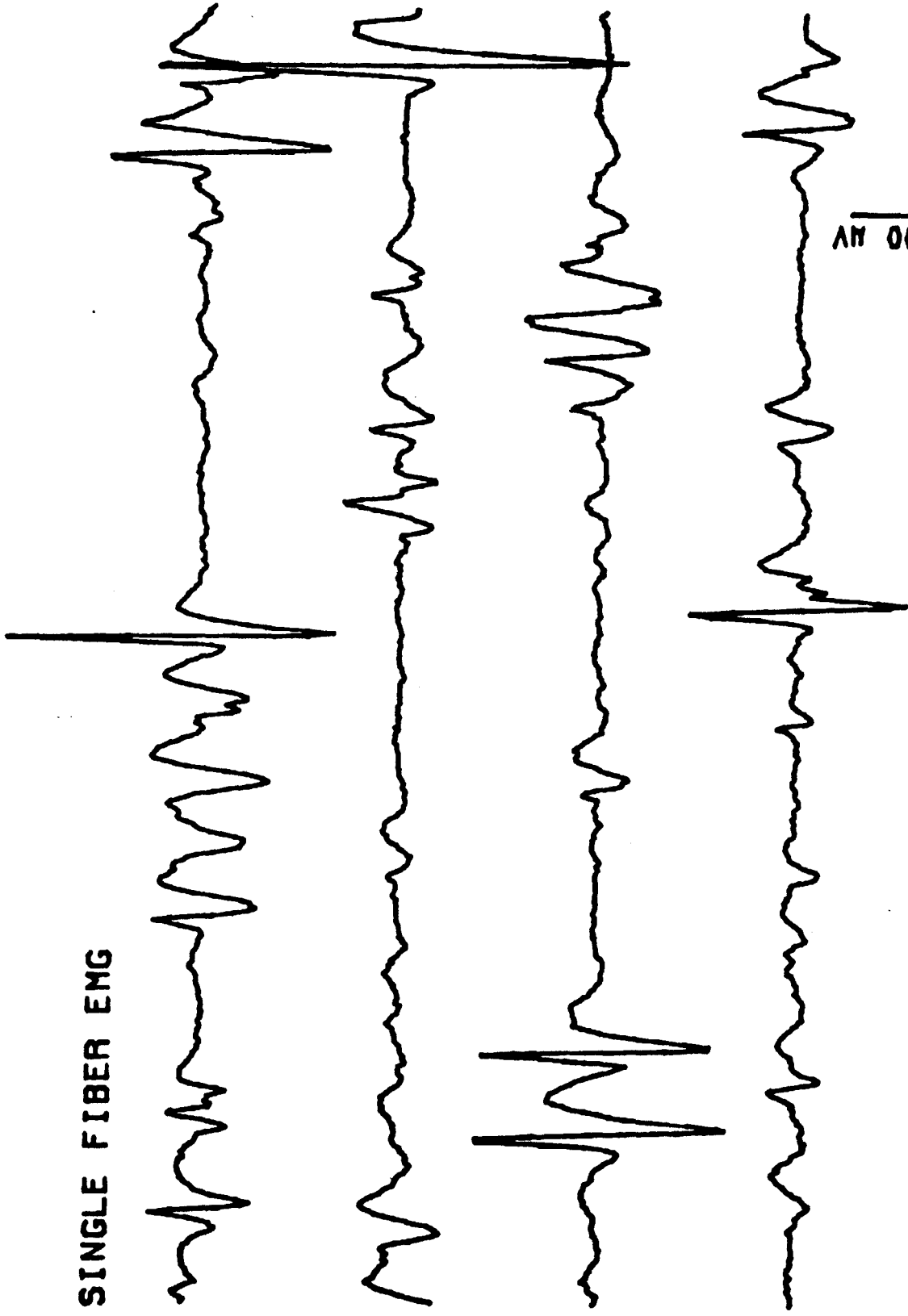


**FIGURE 3.1 IP PATTERN - STRONG CONTRACTION**

analysis applicable to stochastic processes may be applied to the analysis of the interference pattern[84][85][86][87][88].

### **3.2 Motor Unit Action Potential Analysis**

As previously pointed out, individual MUAPs can only be analyzed when the MUAPs do not superimpose or do so rarely. At high levels of contraction superposition is dominant. Therefore this type of analysis breaks down due to the inability to separate individual MUAPs from the recorded EMG activity.

The field of individual MUAP analysis attempts to look at the individual MUAPs located in the recorded EMG and consists of both MUAP shape analysis and MUAP train analysis. There is a logical progression in the analyses going from single MUAP analysis to MUAP train analysis. This is shown in Figure 3.2. In this figure the first step after recording the EMG signal is to extract the MUAP from the EMG record. This is a very important step in MUAP analysis since the method of extraction determines which MUAPs are recognized and used in the further analyses.

Once the MUAP has been extracted from the EMG activity either MUAP shape analysis or MUAP train analysis can be done. These are now described in turn.

#### **3.2.1 Motor Unit Action Potential Shape Analysis**

The analysis of MUAP shape involves the determination of selected features of individual MUAPs. Low levels of muscle contraction are necessary so that

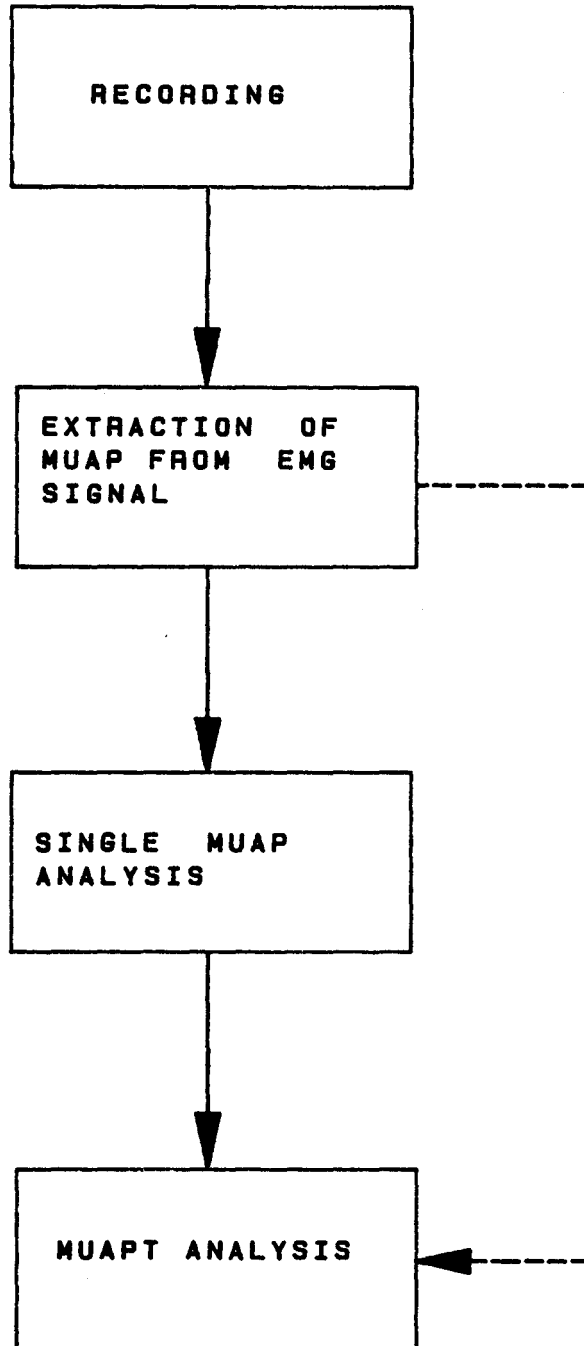


Figure 3.2 Analysis of EMG activity

relatively few, if any, overlappings of the MUAPs occur. A typical needle recording is shown in Figure 3.3. From this figure it can be seen that the MUAPs are relatively far apart and there is virtually no background noise. The remaining basal noise is not important to this analysis and may be discarded. Furthermore, the times which these action potentials occur with respect to each other is also not important for this type of analysis. Only the actual action potential is important. In MUAP shape analysis the MUAPs are analyzed collectively to determine a normal statistical range for each feature measured. This is due to the wide variety of factors previously discussed which affect the shape of the action potentials measured. Furthermore, recording from a needle electrode limits the volume of muscle which can be analyzed with one recording. Therefore, a series of recordings over the whole muscle volume should be obtained in order to more completely characterize the muscle under study. The resulting features will then provide electrical morphological information about the muscle's structure.

### 3.2.2 Features of Motor Unit Action Potential Shape

From a physiological point of view the following features are considered standard for the description of MUAPs. After the electrode is placed to minimize the rise time (which by convention should be less than 0.5ms) then the following features are measured [1]:

- (1) amplitude (peak to peak (uV)),
- (2) duration (mS),
- (3) number of phases (mono, bi, tri, polyphasic),

SINGLE FIBER EMG

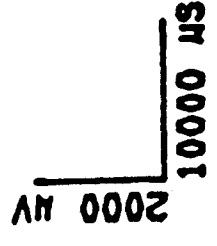
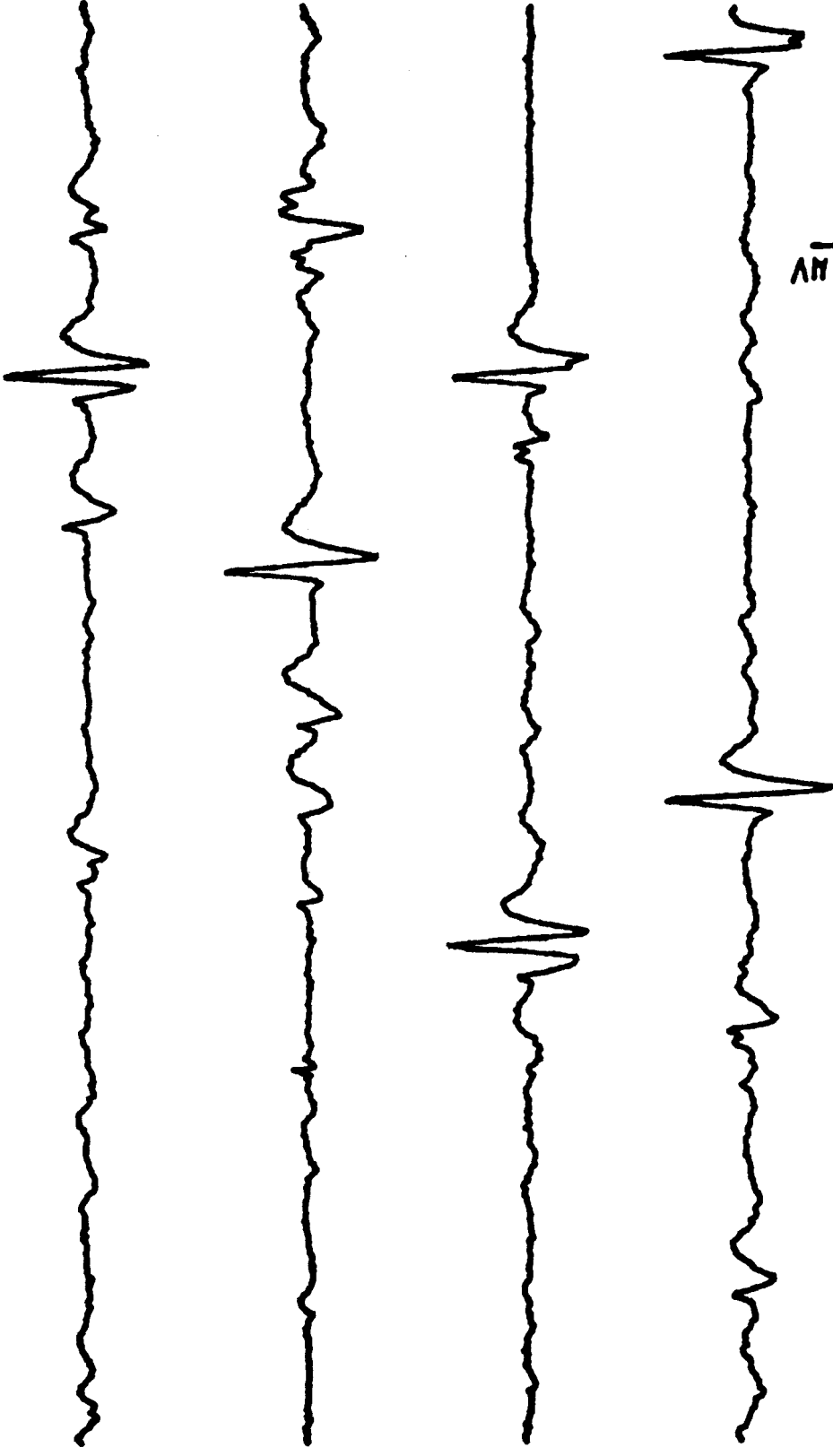


FIGURE 3.3 IP PATTERN - LOW CONTRACTION

- (4) sign of each phase (+,-),
- (5) number of turns,
- (6) variation in shape and
- (7) presence of satellite potentials if any.

The rise time is defined as the time an action potential wave takes to go from baseline to the first peak. The above rise time convention is a compromise so that the MUAPs recorded are not too distant from the recording electrode and therefore are significant action potentials. As one can see all the properties of the action potentials are defined in terms of time domain characteristics. This is directly attributable to the physiologists preference for the time domain. As listed the amplitude of the action potential is defined as the voltage difference between the most positive and the most negative peak of the potential recorded [1]. This to some degree represents the relative size of the MUAP and is an indication of the number of muscle fibers from a particular motor neuron that are located in the recording area of the electrode. In fact, peak to peak amplitudes depend on the number of contributing fibers (number of fibers innervated [4]), size of the fibers, spatial dispersion of the innervation zone, distance from the electrode and the electrode impedance and configuration [4]. Typical amplitudes from needle electrodes are from a few microvolts to millivolts.

The duration of the action potential refers to the total time (mS) between the action potential first deflecting from the baseline and its final return to the baseline [1]. The duration reflects the spatial dispersion of the end plate region, variance of muscle fiber conduction velocities and the number of fibers within the recording volume. An increase in electrode size will cause more spatial averaging

and hence longer duration times. Generally, with monopolar needle recorded action potentials, longer duration times mean larger motor units. It should be pointed out that the duration of MUAPs is inversely proportional to the conduction velocity of the MUAP along the muscle fibers. A general range for conduction velocities is 2–6 m/s [4] with typical durations ranging from 1ms to 13 ms [33][89][90].

The number of phases of an action potential is the number of times the action potential departs from and returns to the baseline [1]. This is an indication of the homogeneity of the action potential when recorded with a monopolar electrode. The greater the number of phases the more fractionization of the motor unit [91]. Of course the sign of the phase depends on whether the action potential deflects to the positive or negative side of the baseline. The signs of the phases are dependent on the relative direction of travel of the depolarization wave along the muscle fibers, hence what side of the innervation zone the recording electrode is on.

A turn in the action potential is defined as the point of change in direction of the waveform and is associated with the potential magnitude between each change [1]. Essentially this is just another way of saying a change in the sign of the slope of the action potential recorded. These last two features are intimately related to the number of phases in the MUAP. Variation in shape attempts to take into consideration motion artifact, the change in the spatial relation between the needle and the muscle fibers recorded from and the change in number of contributing fibers. Satellite potentials are waveforms which are separated from the main action potential waveform by a relatively constant time shift either before or after the main waveform.

These features are illustrated in Figure 3.4. The purpose of these features is an attempt to describe the individual motor unit characteristics that might best

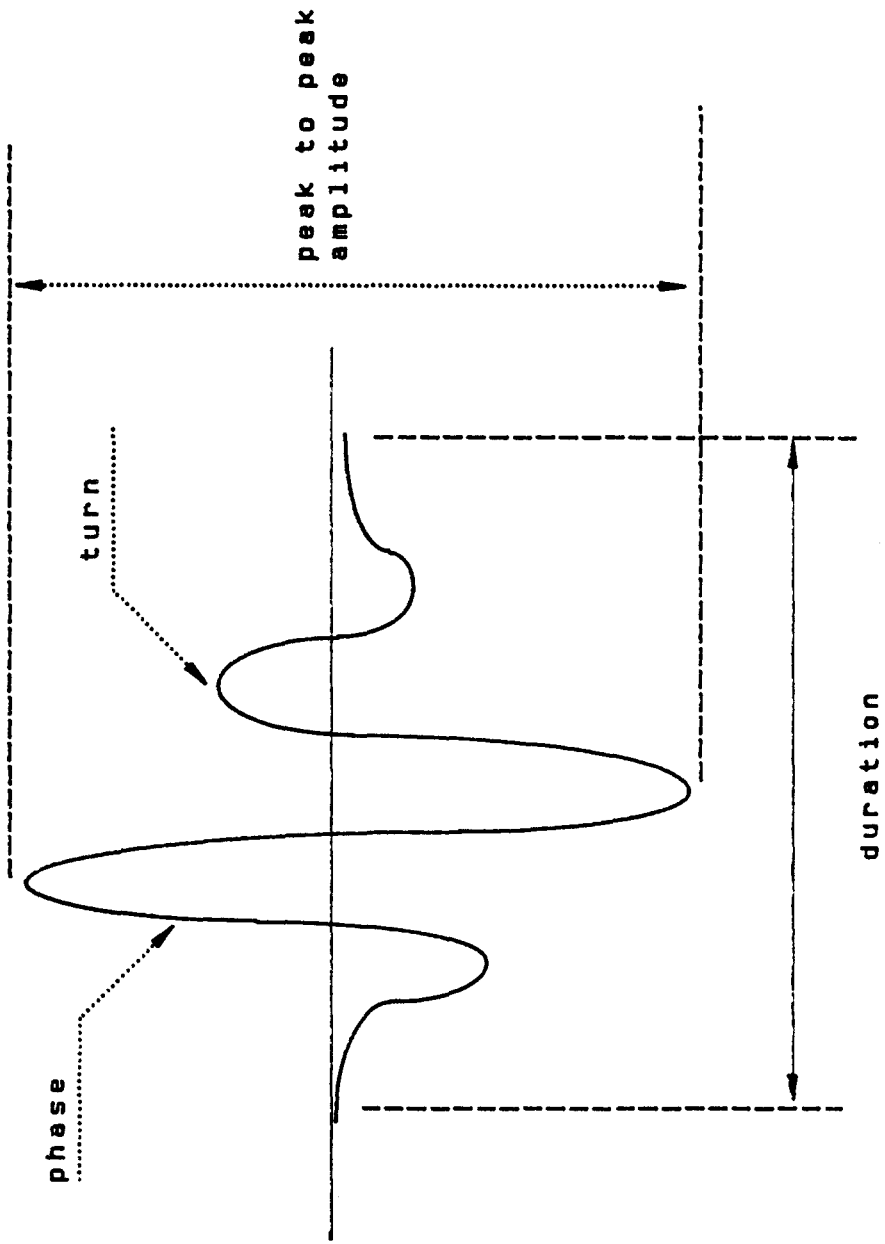


Figure 3.4 Features of the MUAP

differentiate between normal and abnormal muscle. It is generally known that myopathies, i.e. diseases relating to the muscle, tend to produce shortened polyphasic action potentials with smaller amplitudes, while neuropathies, i.e. diseases relating to the motor neuron, tend to produce longer less polyphasic action potentials of higher amplitude[24].

With the aforementioned electrode configuration used in this thesis, monopolar recordings from a single fine wire channel were recorded from muscle under moderate contraction. The MUAP features previously listed were then measured for each individual MUAP and binned according to range. The results are shown in Figures 3.5 through 3.8. Various other researchers have defined ranges for these characteristics typical of normal and abnormal muscle. However, since these features are highly dependent on both the uniqueness of the electrode configuration and the placement of the electrode the variance in the features tends to be large.

Many other time characteristics of the MUAP have been measured and analyzed. Absolute area, rms values, interpeak intervals are all such parameters. In brief, the idea of using the area under the curve of the action potential is based on the notion that no part of the signal should be disregarded and that the total amount of energy in the envelope is the best indicator of the motor unit characteristics. Frequency characteristics of the action potential have also been recorded and used in MUAP shape analysis. In fact the frequency spectrum of needle recorded action potentials has been found to have a range of 5 – 5000 Hz [5]. Which parameters of the frequency spectrum are the most important depends not only on the recording and filtering effects of the electrode used, but also on the type of fibers present in the recording area. The frequency content of MUAPs is an important piece of information that must be considered when designing the

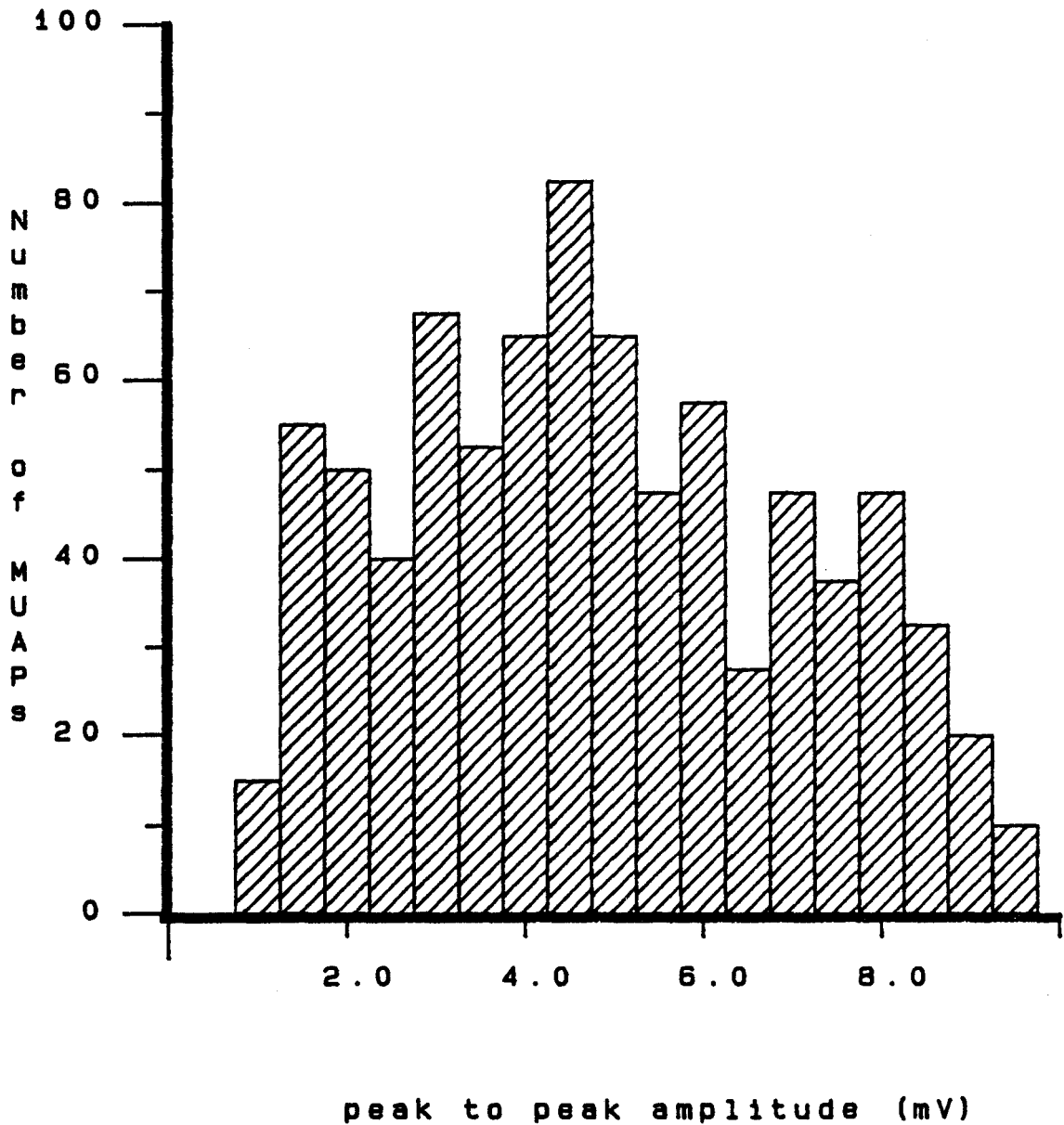


Figure 3.5 Peak to peak amplitude distribution of MUAPs

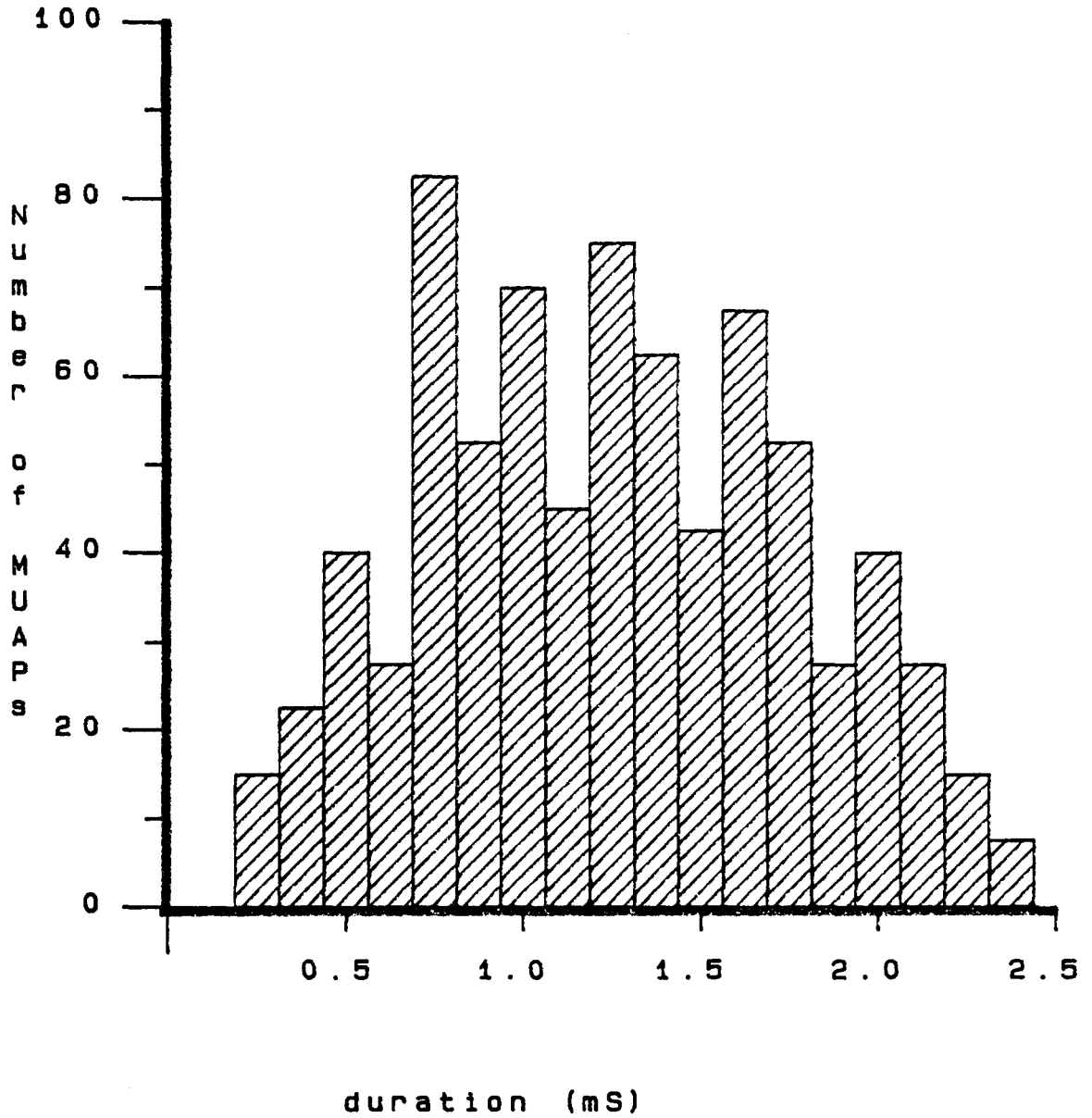
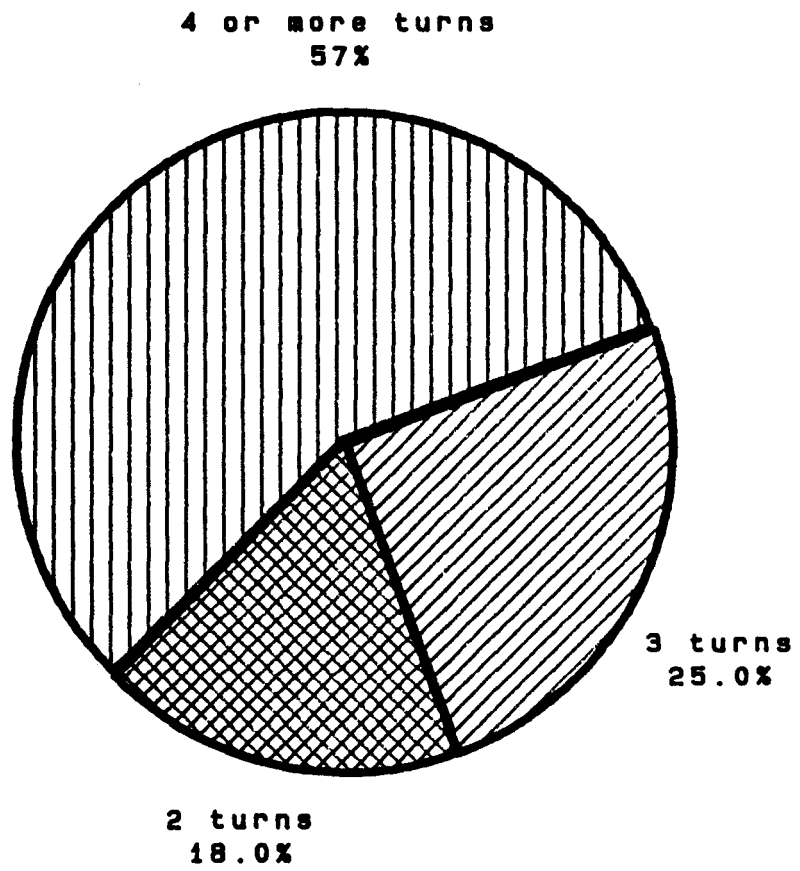


Figure 3.6 Duration distribution of MUAPs



**Figure 3.7** Turns distribution of MUAPs

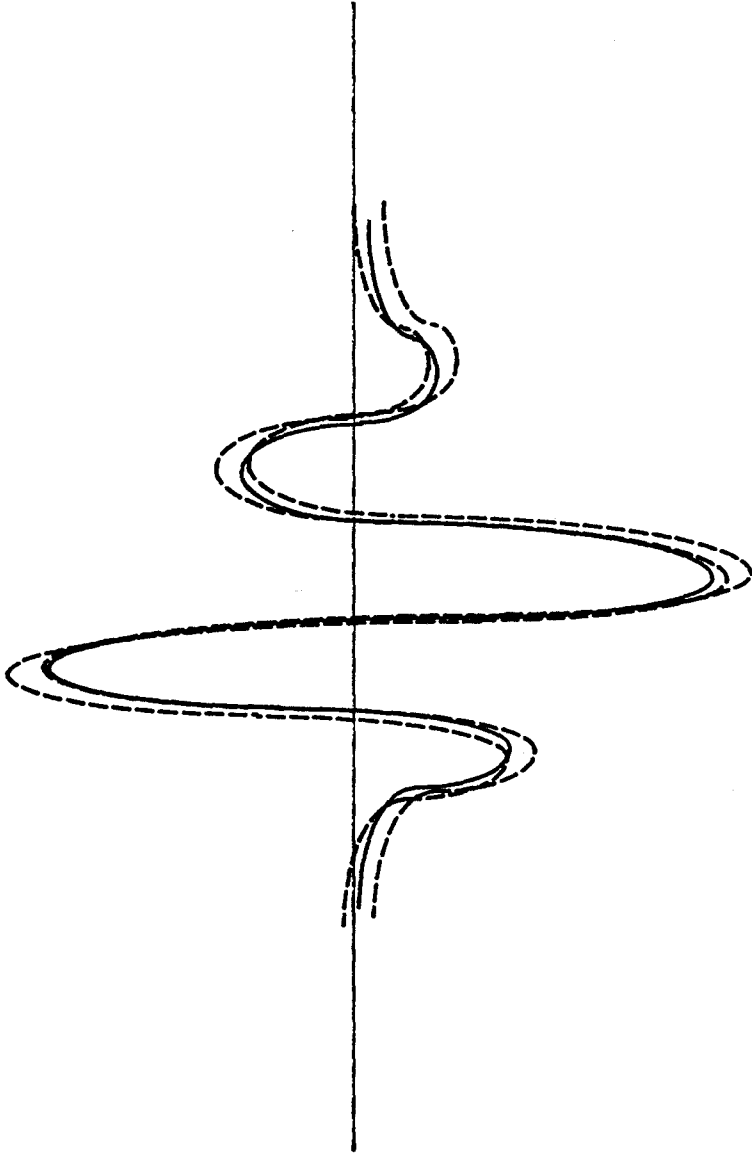


Figure 3.8 Variation in MUAP shape

recording hardware.

Further analyses using individual MUAPs have been done. Single fiber EMG analysis may also be used to find out information about single motor units and motor unit fiber densities. With this recording technique it is possible to measure jitter. Jitter is defined as the variability with consecutive discharges of the time interval between two muscle fiber action potentials belonging to the same motor unit [1]. This is an indicator of the variability of neuromuscular transmissions. If one muscle fiber of a motor neuron fires and the other does not then there is a neuromuscular transmission failure in that muscle fiber. Jitter has been found to have a gaussian bimodal distribution [92]. This type of recording can also be used to study firing patterns of motor units [5][93].

Macro EMG is used to extract the average electrical activity of a motor unit within the recording volume of the electrode. The features most used to describe this signal are:

- (1) peak amplitude of the waveform,
- (2) area contained by the waveform and
- (3) number of phases in the waveform.

It is important to note that the area is more of an indicator of the size of the motor unit than the peak to peak amplitude [4]. Various analyses have been done to separate abnormal from normal macro EMGs [94][95][96][97][98][99][100][101][102][103].

Finally, scanning EMG analysis though not mentioned yet, attempts to investigate the organization of the motor unit within the muscle. Two electrodes

are used in close conjunction. The EMG electrode is moved along the muscle in discrete steps while the second needle electrode is used as a trigger to synchronously average the responses recorded by the first needle. In this way both temporal and spatial information about the motor unit over the whole muscle can be found. This gives an idea of the territory and grouping (fractionization) of the motor unit's muscle fibers within the muscle.

In an attempt to better determine the relationship between the firing history of MUAPs and associated muscle contractions it is necessary to obtain the dynamic behavior between MUAPs and the force level of contraction. This is accomplished by extracting the motor unit action potential train (MUAPT) for each active motor unit from the EMG activity. The analysis of MUAPTs is an attempt to better understand this control mechanism in muscle.

### **3.2.3 Motor Unit Action Potential Train Analysis**

As stated previously, when an action potential is propagated over the entire muscle fiber a single contraction twitch follows within about one millisecond. The fiber recovers electrically before the full force of the contraction is reached. The twitch is present in all of the muscle fibers innervated by a motor neuron. The larger the number of muscle fibers and the larger their diameter in a motor unit the greater the force of the twitch. There is a linear relationship between the twitch tension and recruitment force [104][105][106][107][108][109][110][111]. At the same time when a motor unit is stimulated more frequently the twitches in each motor unit fuse until a tetonic contraction is reached which develops a force several times

stronger than the twitch itself. Therefore, the force of the muscle is controlled by both the frequency of the firing and the number of the motor units active at any particular moment in time.

In single fiber monopolar recordings using a  $50\mu\text{m}$  needle the volume uptake of the needle is such that there will be several different (up to 12) MUAPs recorded from the first dorsal interosseus muscle. For most contractions the different motor unit's will fire asynchronously. The successive firing of a particular MUAP over time is called the motor unit action potential train (MUAPT). The MUAPT reflects that motor units contribution to a muscle contraction. As the level of contraction increases, the electrical activity recorded by the electrode becomes more complex. If the individual MUAPs can be separated from the EMG record then information about motor unit activity can still be obtained even for higher level contractions.

### 3.2.4 Properties of Motor Unit Action Potential Trains

The presence of a MUAP and subsequently the MUAPT is a function of the force that must be generated by the muscle. The larger the force the more active the motor unit. With an increase in force, new motor units are recruited. Recruitment is the successive activation of the same or additional motor units with increasing strength of voluntary muscle contraction [1]. There are two basic principles of recruitment. These are:

- (1) size order of recruitment and
- (2) threshold level of recruitment.

The first principle simply states that larger motor units are recruited when large forces of contraction are required [112][113][114]. Similarly for smaller forces, smaller motor units are recruited. To clarify, in this discussion the size of the motor units refers to the number of muscle fibers innervated by the motor neuron. The larger the number of muscle fibers innervated, the larger the motor unit.

The threshold level of recruitment is less understood. It states that a motor unit will be recruited at a particular force threshold [115][116][117][118]. Different motor units have different force thresholds. A motor unit recruited at a particular force threshold will remain active until the level of force goes below a derecruitment threshold [4][5]. The concept of a force threshold is an important one. It also requires that the forces produced by the muscle be recorded along with the EMG activity. The force may not be precisely quantified due to the difficulty of the measurement process. Also the wide disparity between forces of contraction for the same muscle for the same joint position amongst different individuals requires that the measurement values be normalized. That is, instead of measuring the force in terms of absolute values it can be measured in relative terms where the force exerted by the muscle is measured relative to the maximum voluntary contraction (MVC) that an individual can exert with that particular muscle and joint position. Various levels of contraction can then be referred to as a percentage of the MVC for that individual.

An increase in the force is accompanied by an increase in the firing rate (discharge rate) of the action potential. Larger motor units tend to have lower firing rates than smaller motor units [119][120]. The way in which the firing rate of the motor unit varies with contraction levels is termed rate coding. The rate coding depends not only on the force level of contraction but also the rate of change of the

force [5]; hence, in normal muscle this firing rate is not constant. Another way of expressing the firing rate of a MUAP is by its reciprocal which is known as the interpulse interval (IPI). The IPI has generally been described as a nonstationary independent gaussian renewal process [4][5]. Furthermore there is an interplay between rate coding and recruitment depending on the muscle. In the first dorsal interosseus it is found that under low contraction levels (less than 50% MVC) the major increased production of force is by recruitment. Above these contraction levels the major increased production of force is by an increase in the firing rate [4][5]. From the above discussion, there are several important properties of the MUAPT that are of physiological importance. These are:

- (1) threshold of activation (first recruitment, low, high threshold),
- (2) onset frequency,
- (3) recruitment frequency or IPI and
- (4) firing rate history.

The threshold of activation refers to the force levels that a particular motor unit is recruited and derecruited at. The onset frequency refers to the lowest stable firing frequency of a particular motor unit. Recruitment frequency is the firing rate of the motor unit at recruitment. Finally, the firing rate history is the record of how the firing rate of a motor unit changes with varying or constant levels of contraction.

The relevant information to be extracted from this interference pattern then is not only to determine the number of motor units active at any one time (recruitment) along with their firing rates but to also determine how they are

influenced by both changing and static muscle forces (rate coding). To determine the recruitment and rate coding of a particular EMG recording each individual MUAP must be sorted or separated into its respective MUAPT. In short its firing time history must be known. Fundamentally, since the characteristics of the action potential are so dependent on the spatial orientation of the electrode with respect to the muscle fibers, the innervation separation of the fibers and the number of muscle fibers of a motor unit in the recording volume the individual action potentials will appear to have different shapes. It is this fact alone which enables the separation of MUAPs into their respective MUAPTs. Since MUAPs are essentially one dimensional patterns the methods and algorithms developed for pattern recognition are generally applicable to the separation of MUAPs into MUAPTs [121][122].

### 3.2.5 Muscle Control

Muscle control is a complex process. It can either be predominantly a closed loop system or an open loop system depending not only on the dynamic behavior of the muscle but also the sensory inputs used [123]. Figure 3.9 shows the model of skeletal muscle control. In brief then, the response of a muscle (motor units) is determined by information from sensors for position, velocity and force (Golgi tendon organs) coupled with information exchanged between interconnections of other motor neurons and the upper motor neurons of the central nervous system (CNS). The resulting output of the system is a force produced by the muscle in response to all these inputs. It is assumed (albeit a very good assumption) that the rate coding and recruitment of a motor unit are directly related to force. It should be pointed out here that this relationship need not be a linear one; rather like many

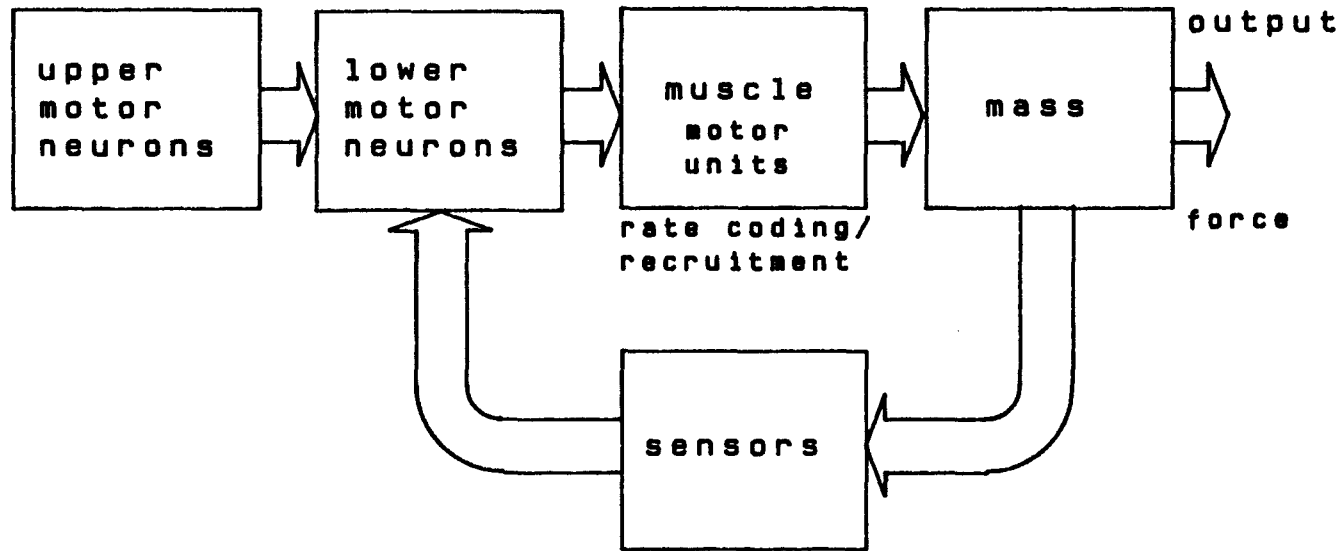


Figure 3.9 Skeletal Muscle control

biological systems this relationship is most likely nonlinear.

### 3.2.6 Separation of MUAPS into MUAPTs

At this point it is assumed that the MUAPs have been extracted from the EMG record. Historically, classification of MUAPs into MUAPTs has gone from visual inspection [3][24][124] to automatic classification done by computer [125][126][127][128][129][130][131][132][133][134][135][136][137][138][139][140][141]. Not only is the human mind quite adept at discriminating action potentials into their respective trains but it is also capable of accurate and repeatable analyses of action potentials. The problem with employing a human visual system is that it is not very efficient. A tremendous amount of time is required in order to make the MUAP identifications and precise firing time measurements. Automatic systems have recently been developed which use high speed computers. These systems are faster and more efficient than visual systems. Lack of accuracy in sorting action potentials is the primary downfall of automatic systems. As a result many hybrid systems such as the method used by LeFever and DeLuca [142][143][144], have been developed that employ automatic systems with visual intervention in order to maintain MUAP sorting accuracy.

### 3.2.7 Pattern Recognition Techniques Applied to MUAPT Analysis

Pattern classification techniques work on the basic assumption that different signals have different shapes and statistical properties. As previously mentioned, this is true for MUAPs. Mathematically speaking, there are two basic pattern

recognition techniques that can be applied to EMG analysis: statistical (decision theoretic) and syntactic. Syntactic pattern recognition relies on the fact that the signal to be classified has a highly structured form such as the electrocardiogram (ECG). The EMG does not have a highly structured form suitable for syntactic pattern recognition techniques. The other area of promise, the statistical approach, can be further divided into either supervised or unsupervised classification. On the one hand, supervised classification techniques assume that all the training samples used to define a classifier belong to one of a set of  $N$  classifications and various techniques are used to label samples as to whether they belong to one group or another. An unsupervised classification scheme, on the other hand, does not assume that a sample belongs to one of a particular set of  $N$  classifications but classifies samples on the fly according to some separation criteria (nearest neighbor, maximum likelihood, Bayes criteria etc.). It should be noted however, that many separation techniques used by supervised classification systems for separating classes can be used in one form or another in unsupervised classification systems.

As seen from the previous chapter, the number of motor units active at any particular time for any given contraction is unknown. Furthermore, the actual shapes of the MUAPs are varied and to a large degree the mathematical relationships governing them are crude estimates. In short, no class prototypes are known a priori. Logically, the automatic classification of MUAPs into MUAPTs should be done using unsupervised or clustering techniques.

Whether the classification is done visually or automatically it follows the same general pattern recognition scheme:

- (1) Extraction of features of the signal that the observer knows from previous experience to be significant in separating one group of signals from another.
- (2) Assembly of the numeric values of the selected features in a multi-dimensional space into regions occupied by the different groups based on measurements made on known samples from each group.
- (3) Classification of a new signal based on the region in multi-dimensional space in which it's vector is located [145][146][147].

In terms of EMG data then the purpose of pattern recognition is to determine for a particular MUAP whether it is a member of a certain class or not. The evaluation of whether or not a MUAP belongs to a particular class is based on the features used for classification.

Undoubtedly, in the classification of MUAPs into MUAPTs the process of feature selection is the single most important step since it determines both the speed at which the classification can be accomplished and the accuracy and repeatability of the classification procedure. In many cases, the features extracted from the MUAP signal are statistically dependent. There are several methods which can be used to provide independent features as described by Duda and Hart [146]. The computational cost and time required for the feature extraction process usually dictates the need to reduce the number of features as much as possible. A compromise may have to be made between the demand for accuracy in classification and the speed at which the classifier works. Optimally, the ideal set of features describing the MUAP would be statistically independent and the minimum number

required to successfully differentiate between all MUAPs that could be encountered in any particular study.

The majority of MUAP classification systems devised are based on the traditionally recorded time features of the MUAP (see section 3.2.2). Using these features has the added advantage that the results of the classification can be easily verified using an existing normative data base. However, it is still desirable to determine which choice of features of the MUAP best distinguish it from other MUAPs. Simply stated, the problem in MUAP analysis is to determine which features are most important. Several methods have been proposed. Optimal features can be selected by either divergence or class separability measures as shown by Duda and Hart [146], or by dynamic programming methods.

The MUAP time features most frequently used for identification and classification are amplitude [79][149][150][151][152], number of phases [74][152] [153] and number of peaks [71][72]. Typical applications where amplitude and time features have been used to discriminate between different action potentials were presented by Mischelivich [151], Zalud et al [152] and Cossi and Mazella [79]. For example, the method used by Mischelivich used four amplitude and time discrimination features: maximum amplitude above base line, maximum amplitude below base line, time from maximum amplitude to subsequent base line crossing and time from maximum to minimum amplitudes. This type of classification is very dependent on how the features are defined. Classification is performed by creating scatter diagrams using pairs of variables where for each pair a single data point is plotted corresponding to each MUAP exceeding an amplitude criterion threshold. Ideally then, MUAP features from the same motor unit tend to cluster. MUAPs are separated by boundaries set around the clusters by the operator. These features

were found to be adequate for low contraction levels where little superposition of action potentials occurs.

Other features of the MUAP that have been used to differentiate them into their respective trains are integration [154], turns counting [78][79] and frequency analysis [5][81][83]. In integration it is the area of the rectified action potential that is used as a feature. Turns counting can be defined as the number of reversals in the slope of the MUAP. Like many of the earlier techniques, turns counting was first done using photographic film or storage scopes. In general, the signals to be analyzed were recorded on an oscilloscope and photographs taken which were later analyzed. Needless to say, this method is very time consuming.

Many recent classification techniques make use of frequency analysis in order to differentiate between MUAPs. Frequency characteristics are used rather than time characteristics because they are less prone to noise and can describe a signal in fewer parameters or coefficients than can be done in the time domain [5]. This is because the Fourier representation of the MUAP is one of many representations that used orthonormal basis functions that are optimum in the mean square sense. The use of Fourier coefficients to represent MUAPs also means that the sampling rate can be the minimum Nyquist rate [155][156].

In some cases such as the method used by Kent [48] the Fourier coefficients are used directly in order to separate MUAPs. This method used the first eight Fourier coefficients as the features, and a contour fitted amplitude coefficient window within which action potentials must fit in order to be considered identical. At first, the upper and lower boundaries of the window are user defined and thereafter are continuously updated using the 50 previously accepted action potentials. Thus slow changes in the action potential are accounted for if the needle

orientation to the muscle fibers should happen to change. This method can only sort one action potential at a time.

An offshoot of using the Fourier coefficients is to calculate the power spectrum of the action potentials and use the power spectrum as a template in classifying the action potentials ( e.g. the method employed by Stashuk [5]). The motivation for using the power spectral coefficients is that there is a further reduction in the dimensionality of the feature space. A further reduction of dimensionality is accomplished by removing the mean, thus making the dc coefficient zero. This is justified since the MUAP is an ac signal as shown in the previous section. It must be noted here that using the power spectrum in template matching may lead to some inconclusive results since phase information is eliminated and there is the possibility of different MUAPs having similar power spectra. As an aid in the classification, the time of occurrence of a MUAP can be used as a classification feature. Knowing the previous firing statistics of an active motor unit, a time window was computed which estimated the probable times that the MUAP would occur again.

Once the features have been selected, they are assembled into a multidimensional vector. This amounts to a projection of the action potential feature vector onto the optimized space where the action potentials can then be separated.

Signal representation has been used to reduce the dimensionality of the vector describing the action potential [157][158][159]. Signal representation involves determining a basis which can be used to describe the action potential using the smallest number of components. Intuitively, the basis chosen should be composed of vectors most closely resembling the action potential to minimize the number of

vectors required. Several methods have been proposed and developed for generating orthogonal vectors [157][158]. Sander and Nandedkar [160] use a learning set for the development of a set of basis functions which are based on the MUAPs themselves. These are later used to classify MUAPs in terms of normal or abnormal. Nunez [158] has proposed the use of Fourier–Bessel polynomial representation for dimensionality reduction of signals. In order to utilize these aforementioned basis vectors, they must first be optimized (i.e their dimensionality reduced). A variety of techniques can be employed, with two of the most common used methods being the Karhunen–Loeve expansion (principal component analysis) and Factor Analysis.

A further decrease in the dimensionality can be accomplished by transformations which reduce the dimensionality of the feature vector or space one chooses. One such transformation is Fisher's linear discriminant which reduces the dimensionality of the features by one.

Essentially classification of MUAPs depends on some dissimilarity measure. There are a wide variety of methods used to divide the multidimensional space into subspaces [135][161]. The most generally used method in MUAP analysis is the mean square distance [5][162][163][164]. The mean square distance is one of many distance classifiers that can be used. All work in the same general way. A signal is assigned to the class or division whose template (vector representation of a particular subspace) results in the smallest distance measure when compared to the signal in question. Thus, MUAPs are classified to the division of the multi–dimensional space with the most similar shape.

In the method employed by Stashuk [5], which uses the power spectral coefficients as features, the measure is defined as the sum of the absolute differences of corresponding elements of the feature vectors. Bayes Decision criteria may also

be used if statistics of the MUAPs are known but this is generally not the case. Another method, used by Guber et al [45], uses a nearest neighbor approach to classifying MUAPs.

Usually, templates are updated as new action potentials are classified, as done by Prochazka [165][166][167]. Updating of the templates is necessary to take into account electrode movement effects as previously described. In order to take into account the changing MUAP shapes and to differentiate between MUAPs Studer et al [168] used matched filters. The matched filters are adapted to follow changes in the measurement conditions. In this way MUAPs can be tracked through the interference pattern. One method uses a template in a different way. The method devised by Cossi and Mazella [79] compares two action potentials point by point and if no more than five differences fall outside the threshold levels preset from experience then those two action potentials are considered to be equal. This is essentially a variance measurement and requires a relatively high sampling rate in order to have uniformity in data comparison.

One problem often associated with template matching in the time domain is alignment. One cannot assume that the MUAP and the template to be matched share the same time base even though they are sampled at the same rate. This problem is intensified if the MUAP is sampled at the Nyquist rate. In order to get acceptable matching of even relatively well-aligned similar action potentials without the added time cost of interpolation, the signal must be sampled up to seven times the Nyquist rate. Time warping algorithms may be applied to MUAPs if the warping function is linear and starts at one end but generally should not be used because duration and overall shape of the signal is an important feature for classification.

Another method proposed by McGill and Dorfman [137][138] attempts to perform high resolution alignment on differentiated MUAP spikes which are sampled at the Nyquist rate. A canonically registered discrete Fourier transform is performed on the differentiated action potential which basically interpolates the signal so that the highest peak occurs at some predetermined time in a predetermined window. In this manner all potentials may be compared with the same time base. This sorting technique is composed of four steps: a fast preprocessing filter that suppresses the background noise; aligning of the waveforms; verifying of identified spike trains based on their relative regularity; and back averaging of the signal to eliminate interference caused by other MUAPs. Although the selectivity of the EMG recordings is enhanced by differentiation [169], care must be taken so that important features of the action potential are not distorted which could lead to poor accuracy in recognition. Results using this system indicate that it is able to resolve 30–70 % of individual MUAP occurrences for 20% MVC. To process 10 seconds of EMG data it takes 90 seconds of computer time. This system does not try to deal with the problem of superpositions and has a 30 – 40 % error rate.

There are several limiting factors to successful decomposition of the interference pattern. This is largely due to the characteristics of the MUAP itself. The action potentials have different finite durations, their number and shape are not known in advance, they overlap in time and frequency, they occur at relatively unknown times and at high voluntary contraction they are rarely isolated [4][5]. One major difficulty in decomposing MUAPs into MUAPTs is the resolution of superpositions of two or more action potentials.

Both manual and automatic superposition decomposition techniques have

been proposed [165][170]. Typically, for superimposed signals the method of Prochazka [165] et al is used. Superpositions of MUAPs are separated by subtraction of a known MUAP template from the superimposed signal. The remainders are then compared to see if any fit any of the templates already identified. If no match is found then the next known template is subtracted from the original superimposed signal and the whole procedure is repeated until a match is found or a new template is created. The difficulty with this method is that it is a long exhaustive procedure and is really only able to separate two templates that have been superimposed [165]. It also assumes that the superposition is algebraic which for all intents and purposes is correct since the motor units are sufficiently independent in firing rates and recruitment.

From the above discussion it can be seen that there have been a wide variety of pattern recognition techniques used to separate the MUAPs in EMG activity into MUAPTs. It is by far the most active and mathematically intense area of study in needle recorded EMG analysis. There are a variety of analyses done to EMG signals. By far the most useful analysis for an understanding of muscle control is the analysis of MUAPTs. This turns out to be the most complicated and difficult analysis that can be done since little if any knowledge of a motor unit's behavior or its action potential is known a priori. Various methods and features have been used to classify MUAPs into their respective trains. Of particular interest is the recognition and separation of MUAPs from the interference pattern. Although this step of the identification process has not been concentrated on as much as the classification of MUAPs it is an important part of the overall process.

One of the areas of electromyography that has not been covered yet is the hardware used to collect the actual signals. This is covered in the next chapter.

## Chapter Four

### Collection of Motor Unit Action Potentials

#### 4.0 Introduction

As seen in the previous chapter the recording and analysis of MUAPs are intimately related due to the fact that the recording protocol and instrumentation affects the shape and subsequent analysis of the action potential.

In order to record EMG activity certain essential hardware is required. The collection hardware used in this thesis is shown in Figure 4.1. The equipment used to collect both force and EMG activity included:

- (1) a DEC PDP 11/34 computer,
- (2) a Hewlett Packard 3964A multichannel FM tape recorder,
- (3) a multichannel single fiber recording electrode,
- (4) a jig to present the muscle under study and
- (5) a multichannel EMG and force preprocessor.

The computer used to collect the EMG activity and force signals was a PDP 11/34 with cache memory, floating point processor and a LPS 11 12-bit A/D converter. Due to the speed and storage limitations of this computer, data could not be digitized directly; rather the data was first recorded on a multichannel FM tape recorder at 15 inches per second and then played back through the A/D converter at  $1 \frac{7}{8}$  inches per second. A multichannel EMG and force signal

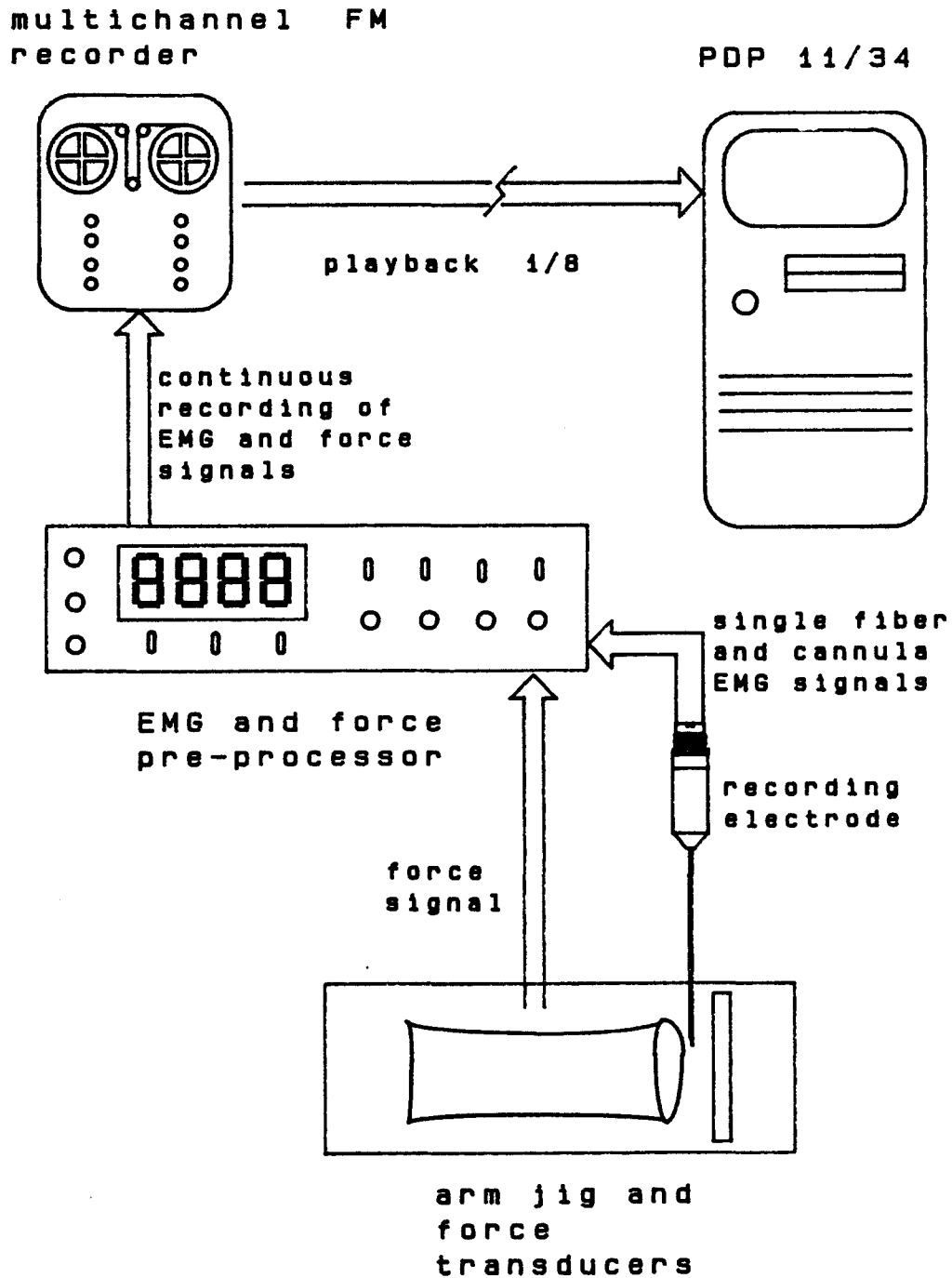


Figure 4.1 Collection hardware setup

preprocessor with supporting hardware were designed and built. This allowed the recording of low noise high quality EMG and force signals. Software was written enabling the computer to continuously sample EMG and force data from the tape recorder and record it to hard disk. The purpose of this chapter is to describe both the hardware and software implementations used to collect both EMG and force signals.

## **4.1 Hardware Implementations**

### **4.1.1 Multichannel Single Fiber Recording Electrode**

The recording configuration for the acquisition of EMG activity has been previously described in chapter two (Figure 2.9). The novelty of this configuration is the multichannel electrode. Figure 4.2 shows how this electrode is constructed. This multichannel electrode consists of three stainless steel fine wires of 0.05 mm diameter drawn through a hypodermic needle of 0.5 mm diameter. A rectangular hole is cut in the side of the needle where the fine wires are threaded through at spacings of 0.5 and 0.7 mm as shown. The needle is then filled with epoxy to lock the wires into place. The wires are then cut flush with the epoxy and the surface of the needle so that only their cross sectional areas are exposed. In this way the needle and the fine wire electrodes are all insulated from each other. The other ends of the fine wires are drawn up through a plastic and brass connector that interfaces this electrode with the rest of the collection hardware. The three fine wires are the single fiber EMG recording electrodes. The cannula of the needle itself is also a recording surface. It should be noted here that the cannula is connected to the

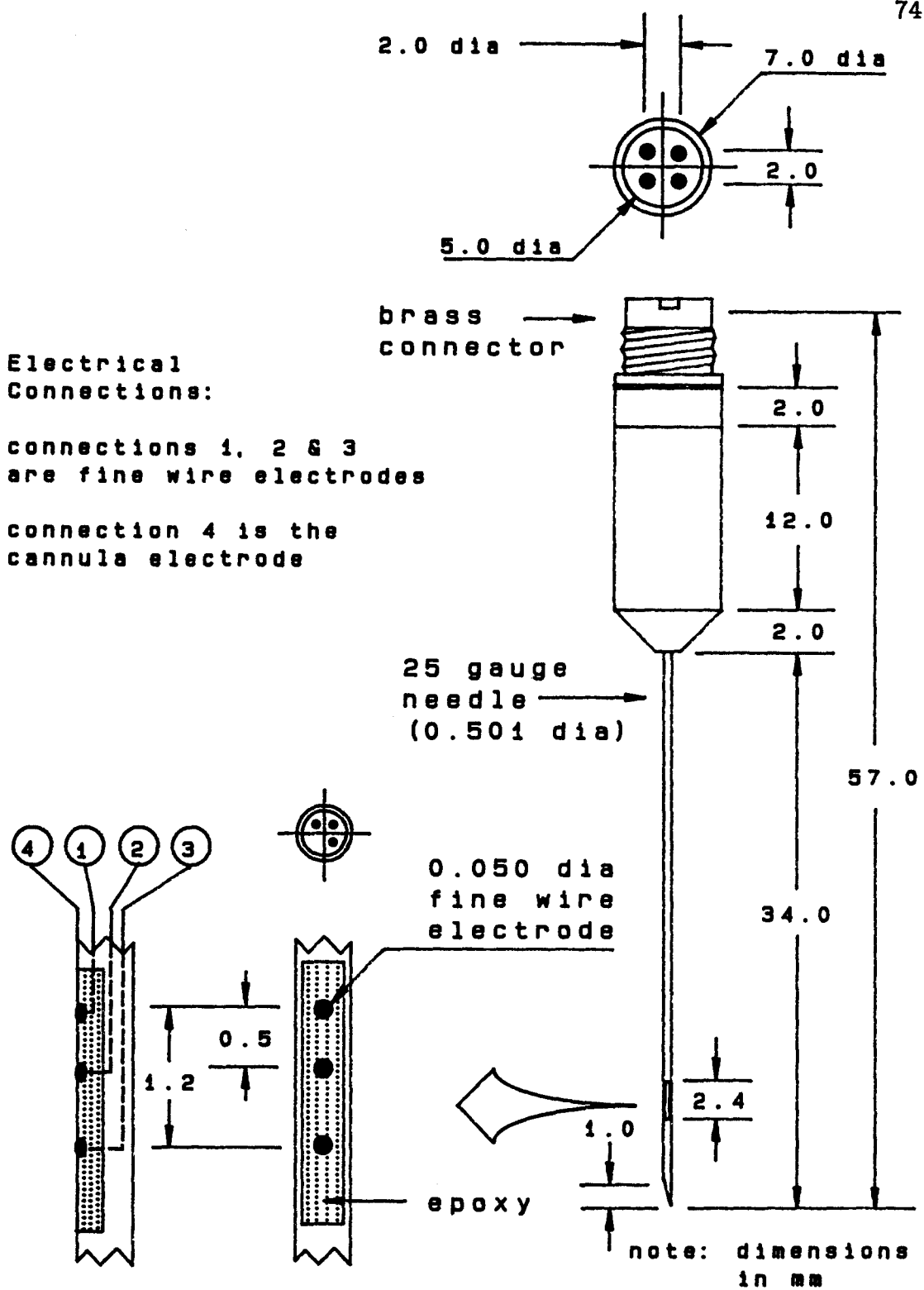


Figure 4.2 Multichannel single fiber recording electrode

outside of the brass connector. The brass connector as shown in the electrical connections of Figure 4.2 has four electrical contacts, three of which are connected to the fine wires and the fourth which is left unconnected. The nominal dimensions of the recording electrode are also shown in the figure.

The supporting apparatus for recording EMG activity was also shown in Figure 2.9. The two surface electrodes used for ground and reference were Beckman 3 mm silver chloride disc electrodes. These electrodes have the property of being stable and largely nonpolarizable and will therefore not cause a dc shift in the recorded ac EMG signal.

There are many characteristics of the electrode which affect the recording of MUAPs as mentioned in the previous chapter. The two most important are electrode size and impedance of the electrode/electrolyte interface. These are inherently related and are of primary concern to the hardware implementation required. The fine wires and cannula are composed of a stainless steel alloy. It has been found that the impedance of fine wire stainless steel electrodes  $Z_e$  is given by:

$$Z_e = \frac{10^{14}}{\left[ \sqrt{2\pi K A f} \right]^{1-\alpha}} \quad 4.1$$

:where  $K$  is a constant,  $A$  is the area in square micrometers,  $f$  is the frequency in Hz and  $\alpha$  is a constant less than one. Thus the impedance is greatest for dc signals and decreases with increasing frequency and surface area of the exposed electrode. The impedance of the single fiber electrodes used in the multichannel recording electrode is calculated to be approximately 10 k $\Omega$  at dc. The impedance of the cannula is not as easily calculated due to its large surface area which is also

dependent on the depth of the needle insertion. However, it is safe to assume that it is much lower than the impedance calculated for the single fiber electrode due to its larger surface area.

This multichannel recording electrode is then interfaced to a signal preprocessor described in this chapter.

#### 4.1.2 Arm Jig

Along with the recording of EMG data is the collection of the force signal produced by the muscle under study. As previously stated, the muscle under study is the first dorsal interosseus (FDI). This muscle is located on the dorsum of the hand, between the thumb and forefinger. As show in Photograph 4.1, the multichannel needle is positioned in the middle of the muscle. The arm is placed in a jig to hold the hand down and prevent it from moving. The arm jig consists of a weighted arm rest and an arm restraining cuff which holds the right forearm in place while EMG activity is being recorded from the FDI muscle. The forefinger is free to move against a tension bar while the thumb and other fingers are prevented from movement by restraining blocks. A lateral force towards the thumb by the forefinger is the motion required to contract the FDI. On this tension bar are attached force transducers arranged in the form of a Wheatstone bridge. The application of force to the tension bar produces a difference in the resistance of the force transducers resulting in a change in the bridge voltage and this change can be amplified and filtered by an electronic circuit.

Photograph 4.1 Arm jig set up

### 4.1.3 Multichannel EMG and Force Preprocessor

In order to collect multichannel EMG activity along with the relative force of the muscle under contraction the preprocessor hardware was developed which includes:

- (1) a multichannel amplifier and filter,
- (2) an action potential detector with aggregate firing rate display and,
- (3) a force signal amplifier/filter and a force target generator.

The general layout of the EMG and force signal preprocessor is shown in Figure 4.3. This preprocessor amplifies, filters and presents both EMG and force activity to be recorded on FM tape. The MUAP aggregate count presented by the hardware is based on the filtered amplified EMG signal. Furthermore, there is a force target generator circuit which generates either a time varying or isotonic (constant) force level target that can be displayed on an oscilloscope. The force produced by the muscle under study is converted via strain gauges in a wheatstone bridge into a voltage signal which is displayed on an oscilloscope at the same time as the generated target signal.

Each part of the hardware is discussed below.

#### 4.1.3.1 Multichannel Amplifier and Filter

The multichannel amplifier and filter consists of four channels of instrumentation preamplifiers, input amplifiers and band pass filters. The overall

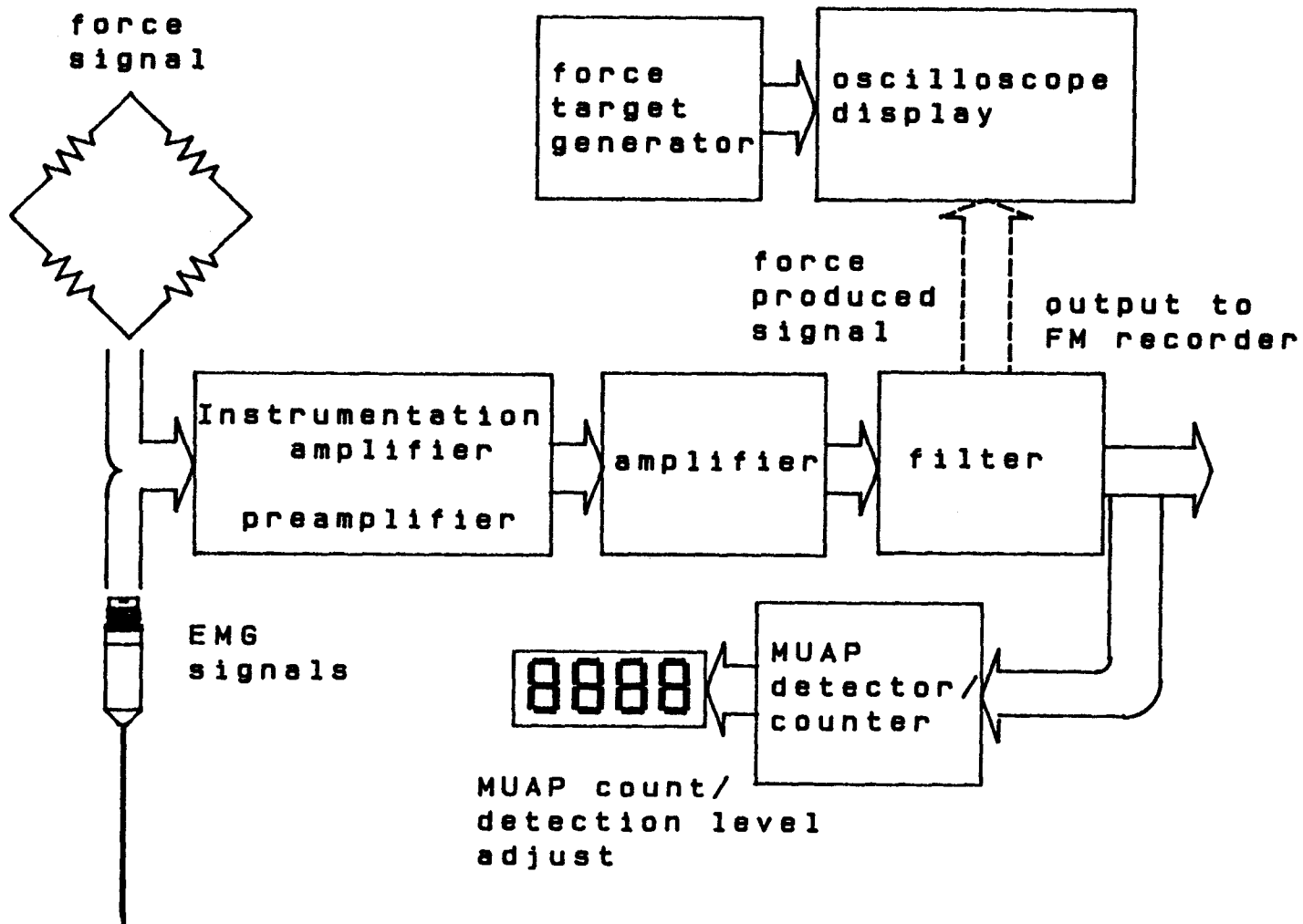


Figure 4.3 Preprocessor layout

gain for the single fiber EMG signal can be varied from 100 to 1000 while the cannula EMG signal can be varied from 50 to 500 times the input [171].

The significant frequencies of the fine wire recorded EMG are between 250 Hz and 4,000 Hz while the significant frequencies of the cannula recorded EMG are between 10 Hz and 3,000 Hz. A detailed discussion of how these frequencies were arrived at is given in Appendix B. In order to collect only these significant frequencies of the EMG signals, they were band pass filtered. Band pass filtering was accomplished by using fourth order Butterworth filters. The pass band frequency for the fine wire EMG is 250 Hz to 5000Hz and for cannula EMG 0.5 Hz to 5000 Hz. Design and circuit details are presented in Appendix A.

#### **4.1.3.2 Action Potential Detector/Firing Rate Display**

A unique feature of the hardware preprocessor is its ability to detect the aggregate firing rate of MUAPs in any one of the three single fiber channels. This is useful for several reasons. First, it gives the electromyographer feedback while locating the multichannel recording electrode in an active part of the muscle during a contraction. Secondly, and just as important, it provides a continuous display during the entire muscle contraction of the aggregate count for the action potentials produced by the muscle. Any change in the geometry as a result of needle or muscle movement between the recording electrode and the muscle fibers recorded from, will be reflected in the aggregate number of action potentials counted. This will then allow the experimentalist to determine whether collection should be continued or terminated.

There are specific reasons for using amplitude and slope or both as detection

criteria. The first reason is historical. Historically, A/D converters on many real time computers use both amplitude and slope criteria for detecting when an event has occurred. They have been shown to be valid criteria for MUAP detection as demonstrated by Stashuk [5]. The use of amplitude and slope together arise from the need to only detect action potentials from fibers near the electrode and having both significant amplitude and fast enough rise time. Slower rise time action potentials tend to be from muscle fibers located at farther distances from the recording electrode while an amplitude threshold is necessary to avoid low amplitude high frequency noise spikes. Thus the selectivity of the needle is greatly increased with the use of these criteria. It should be pointed out here that this process, if used to detect action potentials for later analysis, produces an inherent bias in the type of action potentials detected and in fact is a rudimentary pattern recognition technique with the parameter determined being action potential detection or not.

A special circuit shown in Appendix A was designed to detect action potentials in a data channel. As discussed, both slope and amplitude are used as the discriminant for determining whether or not an action potential has occurred. This is similar to the method used by Stashuk [5]. In this method both amplitude and slope criteria must be satisfied within a certain time window in order for a valid MUAP pulse to be generated, as pointed out in Appendix A.

The choice of which single fiber EMG channel should be used is usually dependent on the amplitude of the action potentials observed in that EMG channel. The larger the action potentials, the closer that particular single fiber electrode is to an active motor unit. In the analysis this channel is usually used as the trigger channel (as marked on the hardware preprocessor). The aggregate number of action

potentials occurring in a selected channel is displayed to the electromyographer using the circuit described in Appendix A.

#### **4.1.3.3 Force Signal Amplification/Filtering and Target Generation**

The circuit that amplifies and conditions the force signal recorded is shown in Appendix A. This involves the use of a dc differential amplifier followed by a low pass filter of 10 Hz cutoff.

Along with the processing of the force signal, a force target signal is created and displayed on an oscilloscope. The force generated by the muscle can then be made to follow the target signal on the oscilloscope. In order to present high and low limits on the signal generated, that the force generated by the muscle must fall between during a collection of data, an error signal was added to the generated waveform. These signals are added together to form the output to one oscilloscope channel. The actual force signal is put into the other channel. With the oscilloscope on alternate display then both signals may be seen on the display at the same time and thus the generated signal can be used as a target to be followed by the muscle under contraction. As stated previously the force may then be represented as a percentage of the maximum voluntary contraction.

#### **4.1.3.4 Muscle Control**

A note must be made on the aspects of the control of the muscle. The normal control of the muscle as described in chapter three (Figure 3.9) is not quite right for the force generated by the muscle (FDI) by the above method. This is due

to the largely visual input used to follow the generated ramp (or isotonic) voltage waveforms.

With the visual input required to follow the force signal on the oscilloscope screen, the experimental control loop as shown in Figure 4.4 is more correct. As shown in this figure the main feedback controller is the visual input rather than the muscle sensors as described in Figure 3.4. Thus the force level of contraction may no longer be uniquely tied to the muscle sensors any more. Nevertheless the same assumptions made in the previous chapter still hold; namely, the fact that rate coding and recruitment are directly related to the force output.

#### 4.1.3.5 Data Collection Using the Hardware Preprocessor

A data collection to multichannel FM tape is shown in Photograph 4.2. All electrical connections are first made between the hardware preprocessor, FM tape recorder and dual channel oscilloscope. The three fine wire recording electrode outputs are recorded as channels one through three on the FM tape while the cannula EMG and force signals are recorded as channels four and five respectively on the FM tape. The strain gauge is adjusted using the BALANCE control (Figure C.2, Appendix C) for zero output from the force produced channel for zero input. The right forearm is then placed in the arm cuff and strapped down in the jig as shown in Photograph 4.1.

Before any actual recording of EMG and force activity is done, the maximum voluntary contraction (MVC) of the FDI muscle under question must be found in order to have a measure of the relative forces produced during a data collection. This can be done using the hardware preprocessor by setting the SET (Figure C.1,

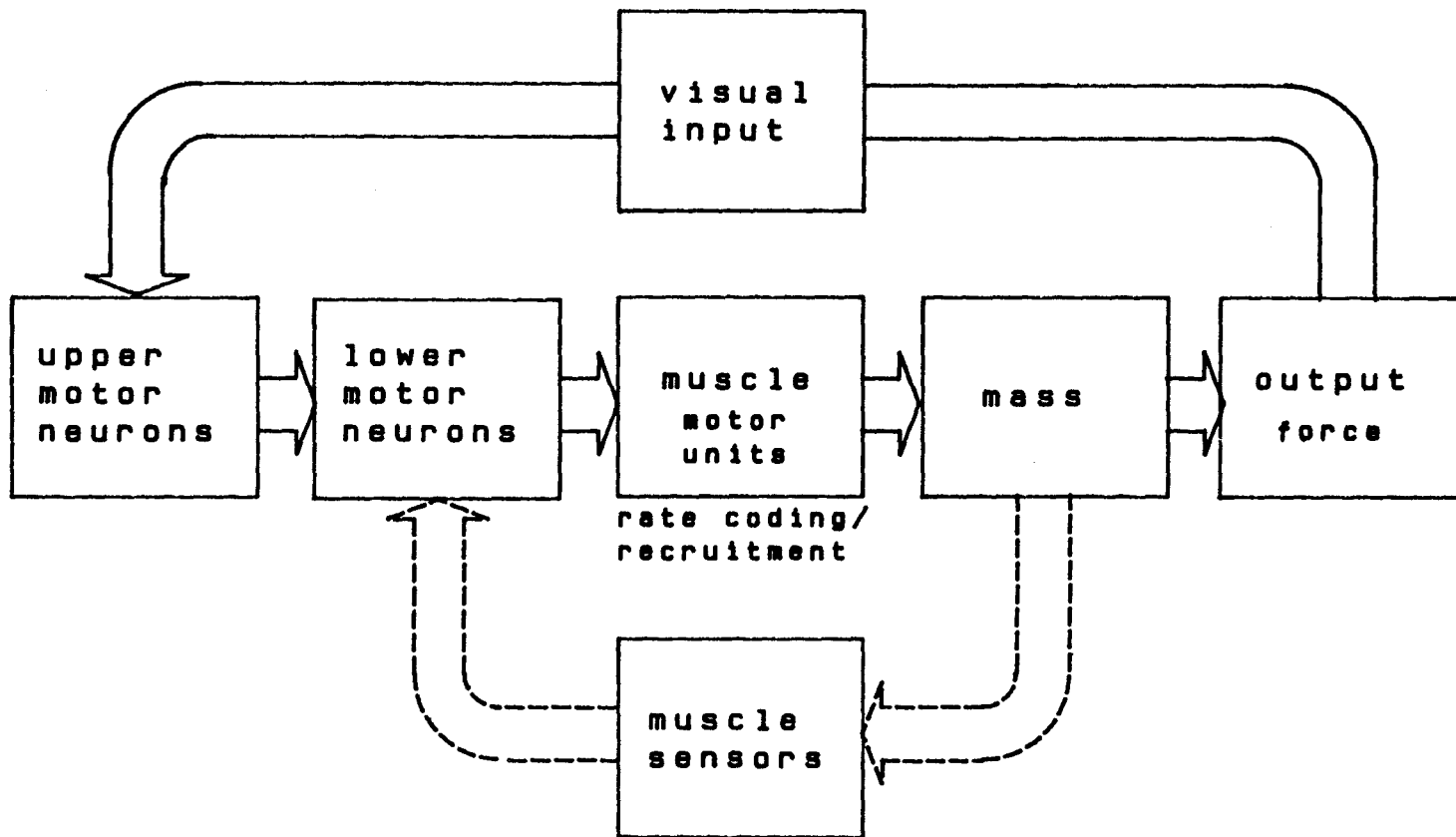


Figure 4.4 Muscle control with visual feedback



Appendix C) switch and selecting the LCD display to show the FORCE as a voltage. A percentage of this maximum voltage then is a percentage of the MVC of that particular FDI muscle. This percentage of the MVC produced by the FDI can be reflected by the amplitude of the generated force target signal (either isotonic or ramp) by the level (F. LEVEL) potentiometer on the hardware preprocessor. Various percentages of the maximum voluntary contraction can therefore be elicited and controlled using this hardware.

The ground electrode is placed on or near the elbow, the common electrode is placed on the triceps (see Appendix D on common electrode placement) and of course the multichannel recording electrode is inserted into the belly of the FDI muscle. As mentioned previously, one of the purposes of the aggregate MUAP count is to find a region of muscle that is active for a particular contraction level. Thus when the multichannel recording needle is inserted the relative level of muscle activity can be seen by simply exercising the FDI muscle. Whether or not a particular region of muscle is active enough for a recording is decided by the electromyographer.

A data collection is started with the resetting (RESET) of the target and actual force signal outputs to the oscilloscope. A real time collection of roughly 30 seconds is done for a particular target force setting. Several recordings are done for each electrode insertion in order to limit the number of times the needle electrode must be inserted. Once recorded to FM tape, the EMG and force records can be analyzed at a later date.

#### 4.1.3.6 Safety Considerations

There are safety precautions which must be considered when collecting multichannel EMG signals using this hardware preprocessor. As with any electrical hardware that comes into contact with the human body, the avoidance of shock hazard must be eliminated. The typical shock hazard that can occur is a ground conductor with the hot shorting to the chassis or ground. When this occurs potentially fatal flows of current through the body via ground can result. This is prevented in the case of the hardware preprocessor above by the use of an isolation transformer which isolates the hot from the ground so that very little if any current can flow through the ground.

Usually, for medical quality equipment, the instrumentation amplifier is isolated from the rest of the circuit. This is done through the use of an isolation amplifier. The isolation amplifier breaks any ground loops in the recording circuit and provides an interface between the rest of the hardware circuitry and the transducer (electrode) which comes in physical contact with the human body. Thus the isolation amplifier ensures high isolation voltages and very low leakage currents. An isolation amplifier was not designed into the circuits described in this chapter (and diagrammed in Appendix A) due to the limited use of the hardware (the hardware preprocessor was not and will not be used in a clinical sense) and the limited amount of time available to design and build the hardware preprocessor. When and if a clinical device is designed in the future, safety precautions such as the isolated amplifier will be designed into the hardware.

As presented, this is the hardware used to collect the EMG and force signals. Again, the circuit details are included in Appendix A. Along with the

hardware used to collect EMG and force signals, an analog signal acquisition system must also be provided. This requires interfacing an A/D converter to FM tape for continuous collection of data.

## 4.2 Software Implementations

As previously mentioned, a PDP 11/34 with cache memory, floating point processor and LPS-11 12 bit A/D was used to collect and analyze EMG data. The method used to collect EMG and force signals by the computer was essentially that presented by Stashuk [5] but with key differences. The first key difference was, as previously stated, the use of a multichannel single fiber electrode. The other difference is in the software acquisition program. Whereas they employed a time discontinuous collection method the method used in this thesis is a continuous time collection. This was required due to the speed of the computer and the amount of data required to be collected from the multichannel single fiber electrode. The software implementation for data collection and subsequent analysis included algorithms to:

- 1) continuously collect EMG and force data,
- 2) display this data to the electromyographer and
- 3) preprocess the data collected.

Each of these algorithms is described below.

#### 4.2.1 Collection Algorithm

A continuous time recording of the EMG and force activity produced by the FDI was collected via the interrupt routine capabilities of the PDP 11/34 [172]. With this method it was possible to collect up to 30 seconds of four channel EMG signals and one channel of force signal at a sampling rate of 10,000 Hz.

The set up for the continuous collection of EMG and force data is shown in Figure 4.5. As shown, EMG and force signals are sampled via a 12 bit A/D converter where the sampling times are controlled by a real time clock. The data collected from the EMG signals are saved via the PDP 11/34 bus to a core memory buffer of 12288 words in length. The software used to continuously collect these data is based on a dual buffering collection system [173][174]. Each buffer of memory is 6144 words in length. As one buffer of memory is being collected a second buffer of memory is being written to hard disk via the interrupt routine capabilities of the PDP 11/34. The recording of the force signal produced by the muscle is stored to a separate core memory buffer and is only written to disk at the end of a data collection. This is possible due to the slower sampling rate used to record the force signal.

The algorithm for accomplishing the collection of EMG and force data is shown in Figure 4.6. The first part of the algorithm initializes the memory buffers, the A/D converter interrupt level and the real time clock used in setting the sampling rate in the collection process. Since the EMG activity is low pass filtered at 5000 Hz (approximately the Nyquist frequency) the sampling rate was set at 10,000 Hz. Of course the EMG could be collected at a faster rate than this but due to the speed and memory limitations of the computer this was not feasible. The FM

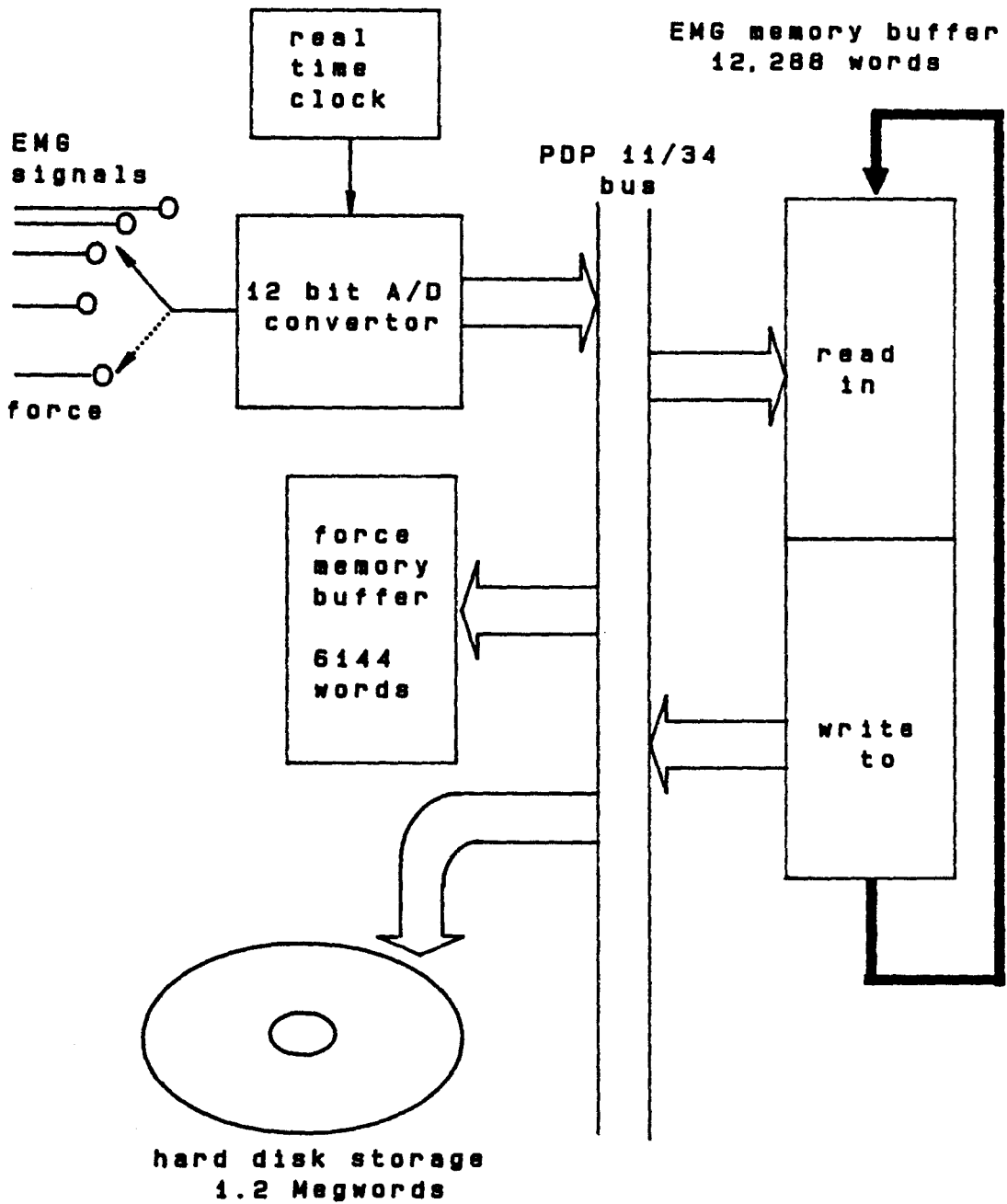


Figure 4.5 PDP 11/34 data digitization setup

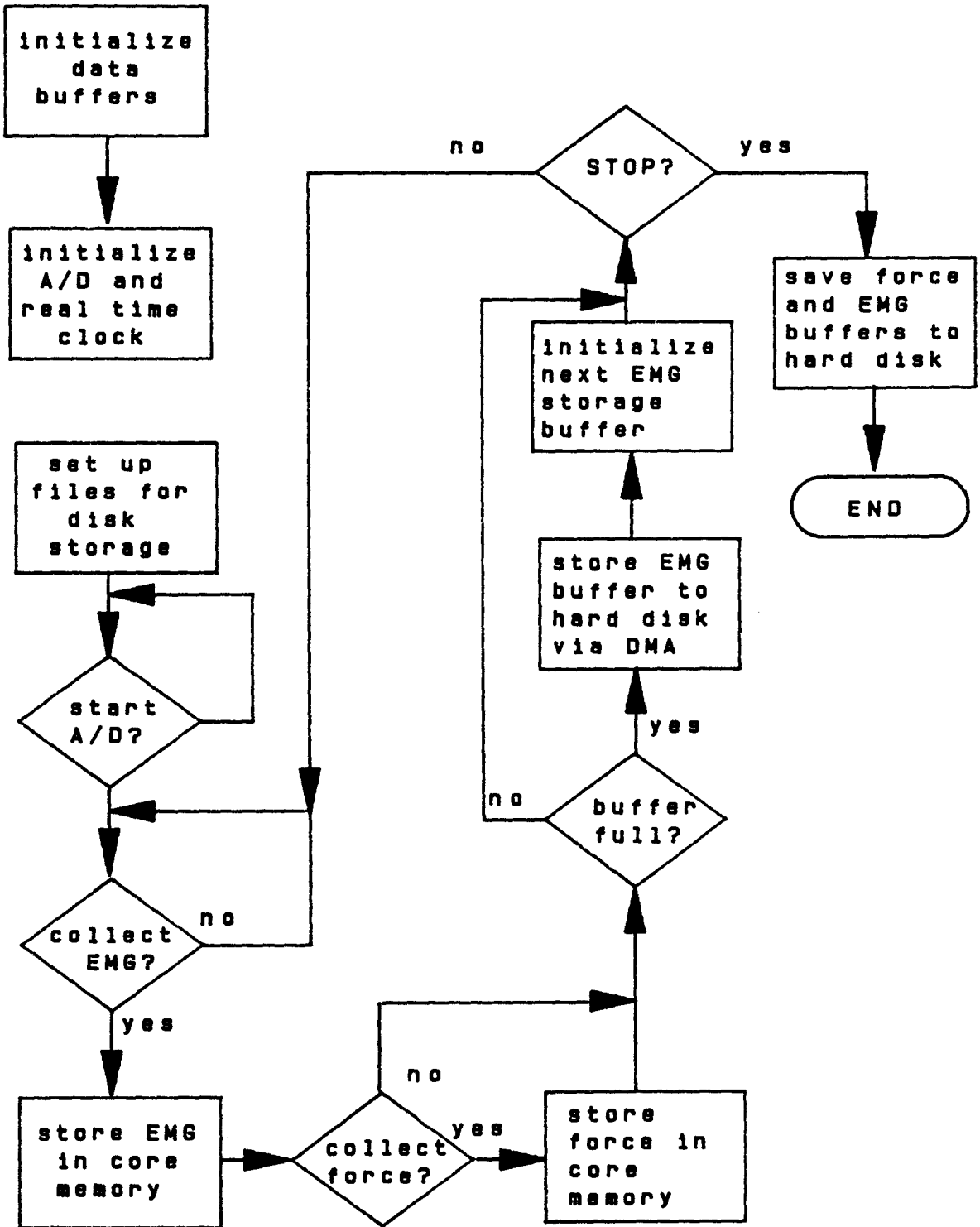


Figure 4.6 Collection algorithm

tape as stated previously was played back to the computer at 1/8 the recording speed therefore the effective sampling rate required per channel of EMG signals was 1250 Hz.

The collection of data occurs when a real time clock set to the frequency above signals the A/D converter to collect data. At this point the A/D converter converts the EMG signal starting at channel one and incrementing up to channel four by means of an on board multiplexer. Thus the three single fiber EMG signals (channels one through three) and the cannula signal (channel four) are sampled and stored to their core memory buffer. The EMG data are stored in a serial manner as shown in Figure 4.7, with every fourth word of data stored being from the same EMG channel. The A/D converter then waits for the next signal from the real time clock. The collection program continuously checks to see if the core memory buffer of EMG data is full. If the memory buffer is full (6,144 words) then that memory buffer is written to disk via the interrupt routine capabilities of the PDP 11/34 and the next memory buffer is used as a temporary storage for the EMG data. In this way then a continuous collection is possible as long as the sampling rates are low enough so that the data written to disk via the PDP 11/34 bus does not conflict with the data being written to memory. This situation is particularly acute in the case of the PDP 11/34 computer due to its inherent hardware architecture [172][175]. This computer does not have a DMA controller in the sense of modern technology where there is a dedicated microprocessor which controls the DMA, rather this is done with the main processor of the PDP 11/34 itself. Therefore, the timing considerations of the dual buffering system are critical for correct operation so that data from the A/D converter being written via the PDP 11/34 bus do not run into the data written from the core memory to the hard disk.

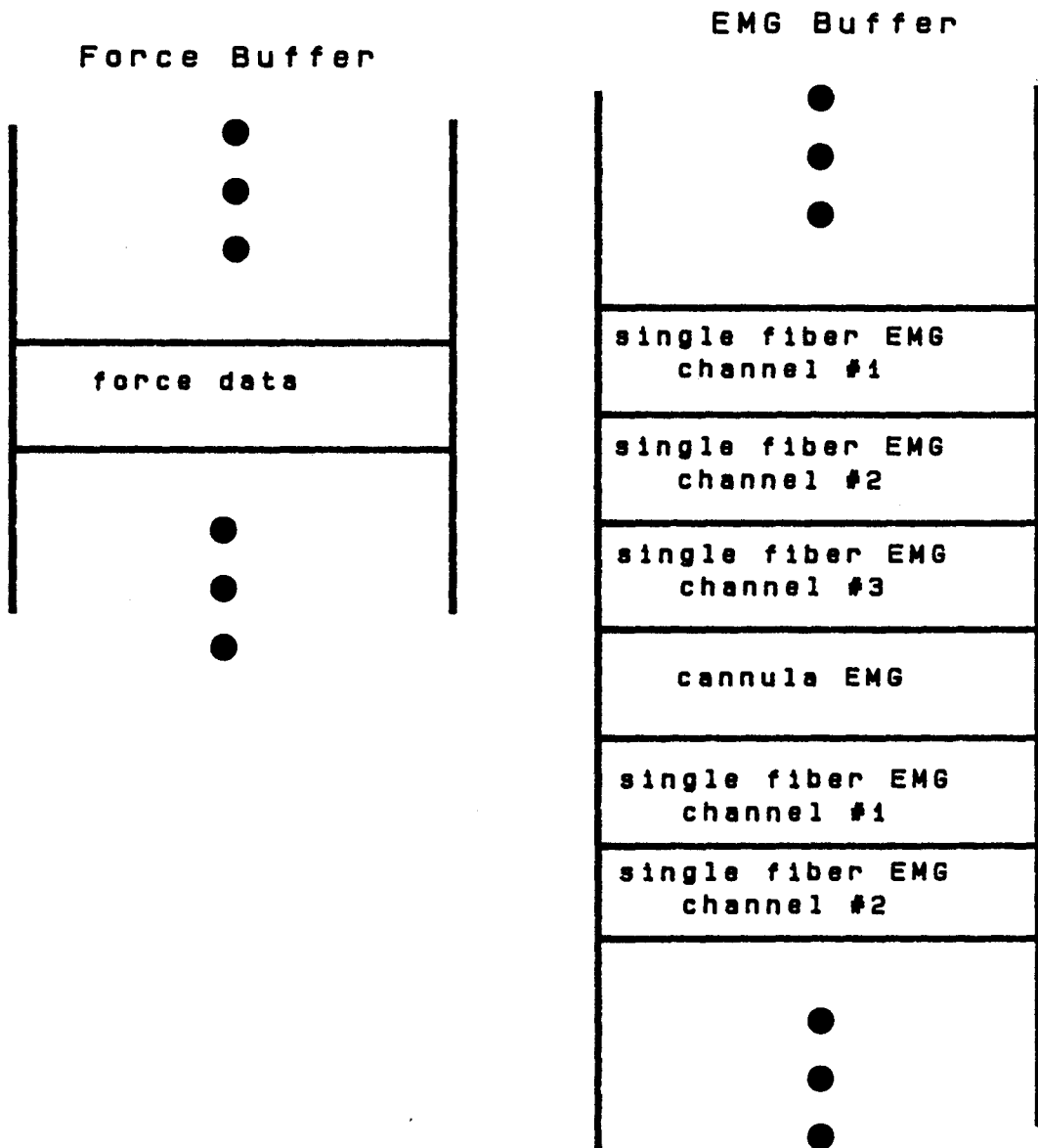


Figure 4.7 Data buffer storage

As stated previously, the size of the memory buffers used in this collection routine are 6,144 words long. There is a specific reason for this. The storage capacity of one track on a RK11 hard disk used by the PDP 11/34 computer as mass storage is only 12,288 words. On one side of one track then, only 6,144 words can be stored. Since one word corresponds to one A/D converted sample, then by choosing this size of buffer to be written to the hard disk, minimizes the the time required to align the disk head to the next track (head seek time) to be written to. The way this works is that after a particular track on the disk is filled, then the disk head position automatically increments to the next track on the disk as the other core memory buffer is being filled with EMG data. The next data buffer is written to the next track on the hard disk since the file containing the sampled EMG signals is stored contiguously. In this way then the DMA speed is optimized since the head seek (on the order of 75 milliseconds) is done while the core memory buffer is being filled. The time taken to fill this memory buffer is dependent on the sampling rate chosen and the number of EMG channels to be sampled. The time taken to write one side of one track of the hard disk is on the order of 69 milliseconds. The maximum sampling rate is therefore dependent on all these times [176]. The theoretical maximum sampling rate can be calculated from these times, however, it is more practical to actually try a variety of sampling rates to determine the maximum rate possible before any errors occur. This was done. It was found that the maximum error free sampling rate that was obtainable with the above algorithm when collecting four channels of EMG signals (and force to memory) was 4,000 Hz per channel. Therefore, the FM tape could have been played back to the A/D computer at 2/5 recording speed. However, the sampling rate was slowed down to 1,250 Hz in order to lessen the phase shift associated with multiplexing.

The limit on the amount of data which can be collected is entirely dependent on the maximum storage capacity of the RK11 hard disk. This storage capacity is approximately 1.2 Megawords. Therefore, the collection of four channels of EMG signals at the true sampling rate of 10,000 Hz per channel results in approximately 30 seconds of real time continuous data for each recording. (This is the reason for recording approximately only 30 seconds of EMG and force activity for a particular contraction level.) At 1/8 the sampling rate (1,250 Hz) the actual time of collection is four minutes.

The collection algorithm collects the force signal as a fifth channel of data. The force is sampled at 1/67 the sampling rate of the EMG activity. Thus the effective sampling rate is 20 Hz. Unlike the EMG activity, the force signal is not saved to disk continuously as it is collected. Due to the slower sampling rate and hence the smaller amount of data, the force activity is saved to a core memory buffer (Figure 4.5) and is only saved to disk at the end of collection. In this manner then a continuous record of the force signal is recorded along with the EMG activity and can then be later used to assess muscle behavior.

#### 4.2.2 Display Algorithms

Display algorithms were written in order to present the multichannel EMG and force signals on a Tektronix 4006-1 vector graphics terminal. A typical multichannel EMG recording is shown in Figures 4.8 and 4.9 for two different levels of contraction. The uppermost signal on both figures is the activity recorded from the cannula. The bottom three signals are the fine wire recorded EMG signals. It should be pointed out the EMG data displayed are the Nyquist sampled EMG data.

CANNULA



SFEMG #1



SFEMG #2



SFEMG #3

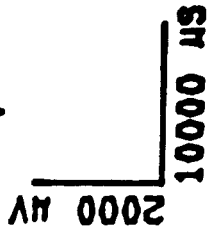


FIGURE 4.8 MULTICHANNEL EMG

CANNULA



SFEMG #1



SFEMG #2



SFEMG #3



FIGURE 4.9 MULTICHANNEL EMG - CONT'D

2000  $\mu$ V  
10000  $\mu$ S

The vertical and horizontal scales of the data are shown in the right hand corner of the figures for reference.

As can be seen from the figures the motor unit action potentials seen in one single fiber channel occur in other channels with some differences. These differences are amplitude, shape and phase shift. Amplitude and shape differences are easily explained by the varying positions of the single fiber electrodes from each other and hence from the motor unit activity recorded. Furthermore, there are inherent differences in identical motor unit action potentials recorded from different positions in the muscle tissue due to the filtering characteristics of the muscle. The phase shift may be due to the fact that the electrodes are not aligned perpendicular to the fiber direction and hence recordings are affected by conduction delays. Furthermore, as shown in the figure, the EMG activity between action potentials is relatively low, therefore little noise is present in the recorded data.

The display of a single channel of fine wire recorded EMG signal is shown in Figures 4.10a and 4.10b. These displays shows a single channel of fine wire activity which is displayed left to right such that the left most part of the signal displayed is continued from the right most part of the signal above. This same signal is then continued from Figure 4.10a to Figure 4.10b. This display is necessary when further analysis and extraction of MUAPs is done. Various force contractions are shown in Figures 4.11a through 4.12b. Figures 4.11a and 4.11b show moderate and high isotonic muscle contractions while Figures 4.12a and 4.12b show typical ramp (triangle) type muscle contractions. The force target bars generated by the hardware preprocessor are also displayed in these figures for comparison. It should be noted that the apparent noise in this force signal is largely due to the small tremors in the muscle that arise when various motor units are firing asynchronously

SINGLE FIBER EMG

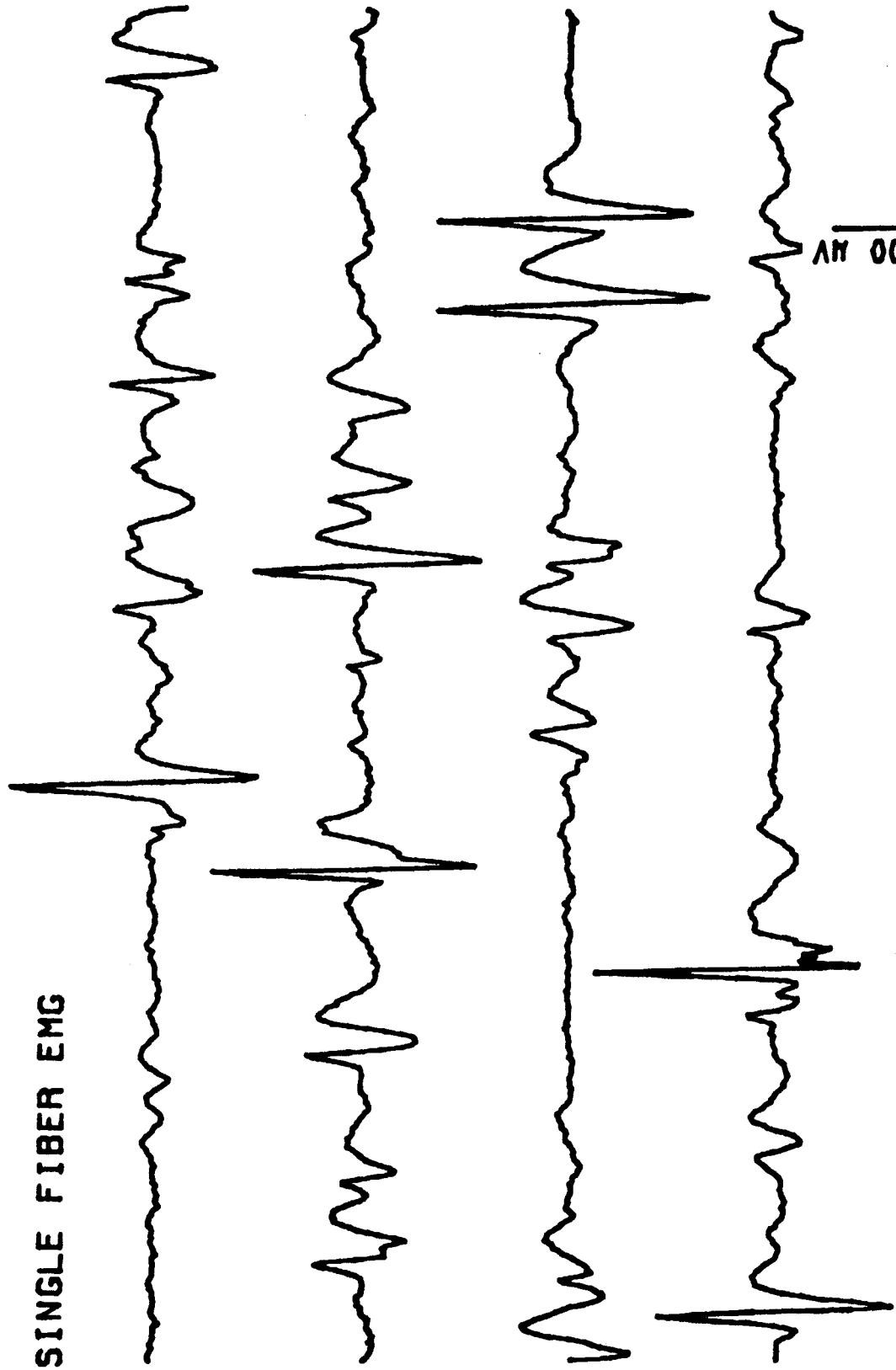


FIGURE 4.10A SINGLE CHANNEL EMG

SINGLE FIBER EMG

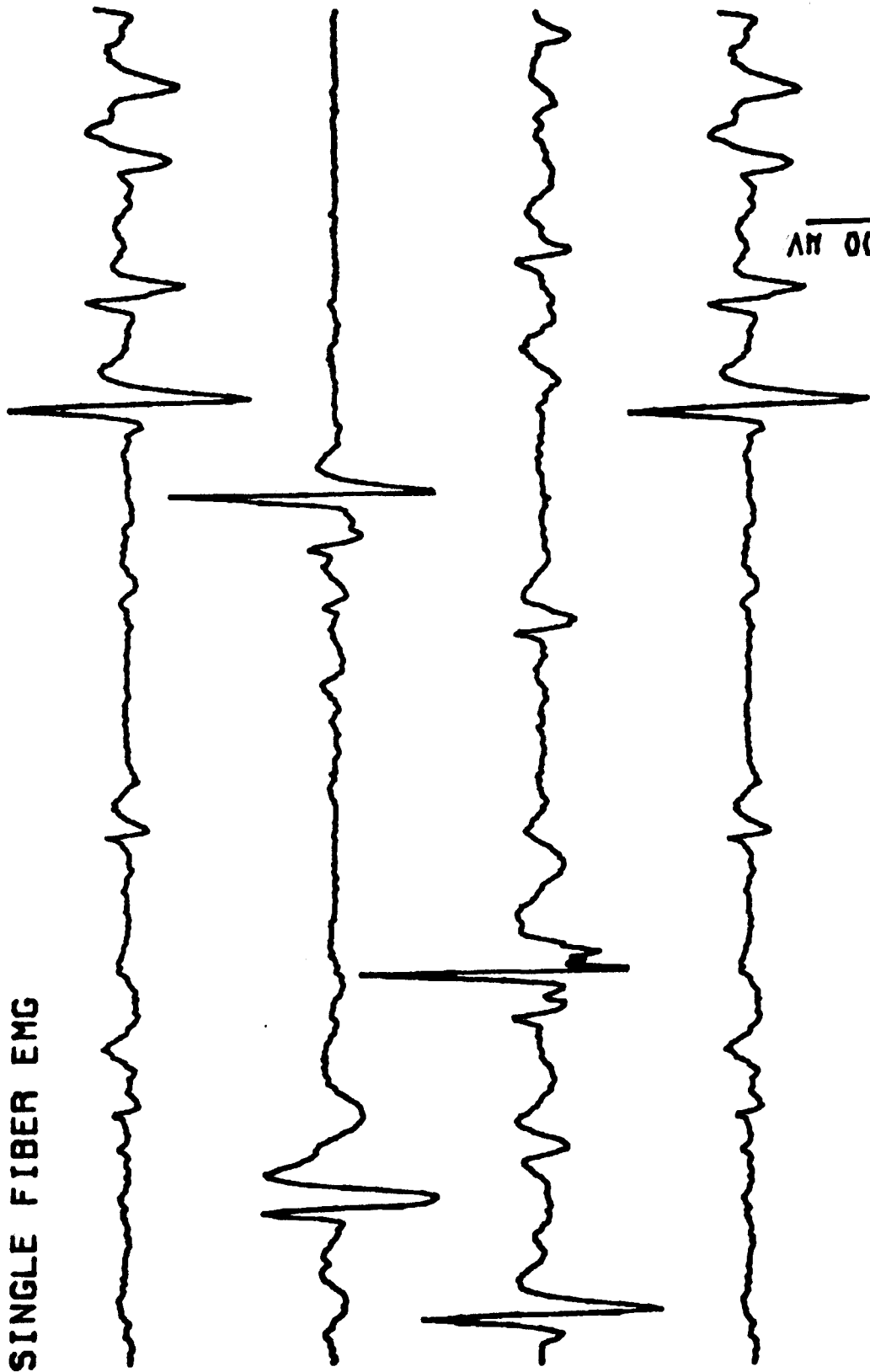


FIGURE 4.10B SINGLE CHANNEL EMG - CONT, 100

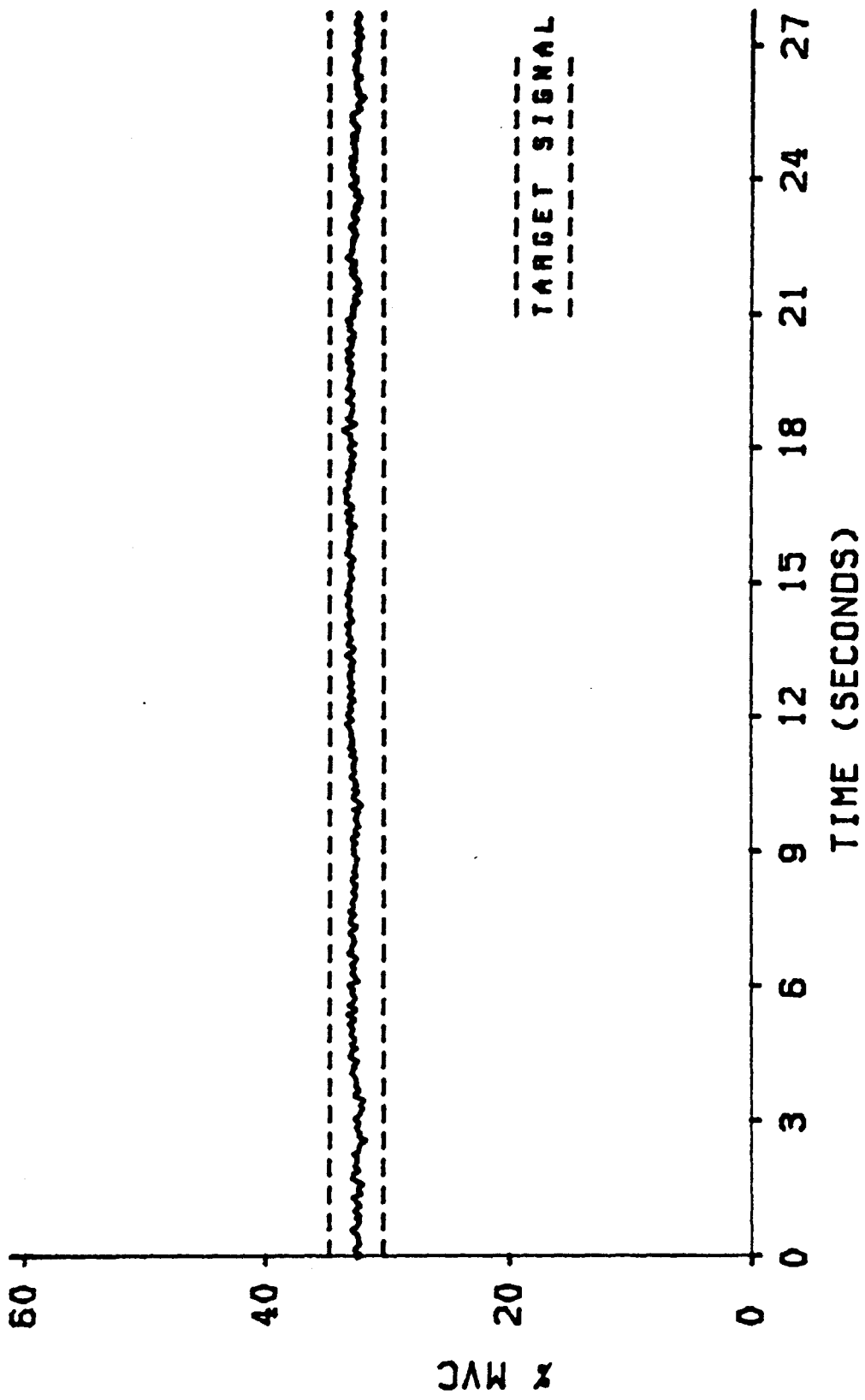


FIGURE 4.11A MODERATE ISOTONIC CONTRACTION

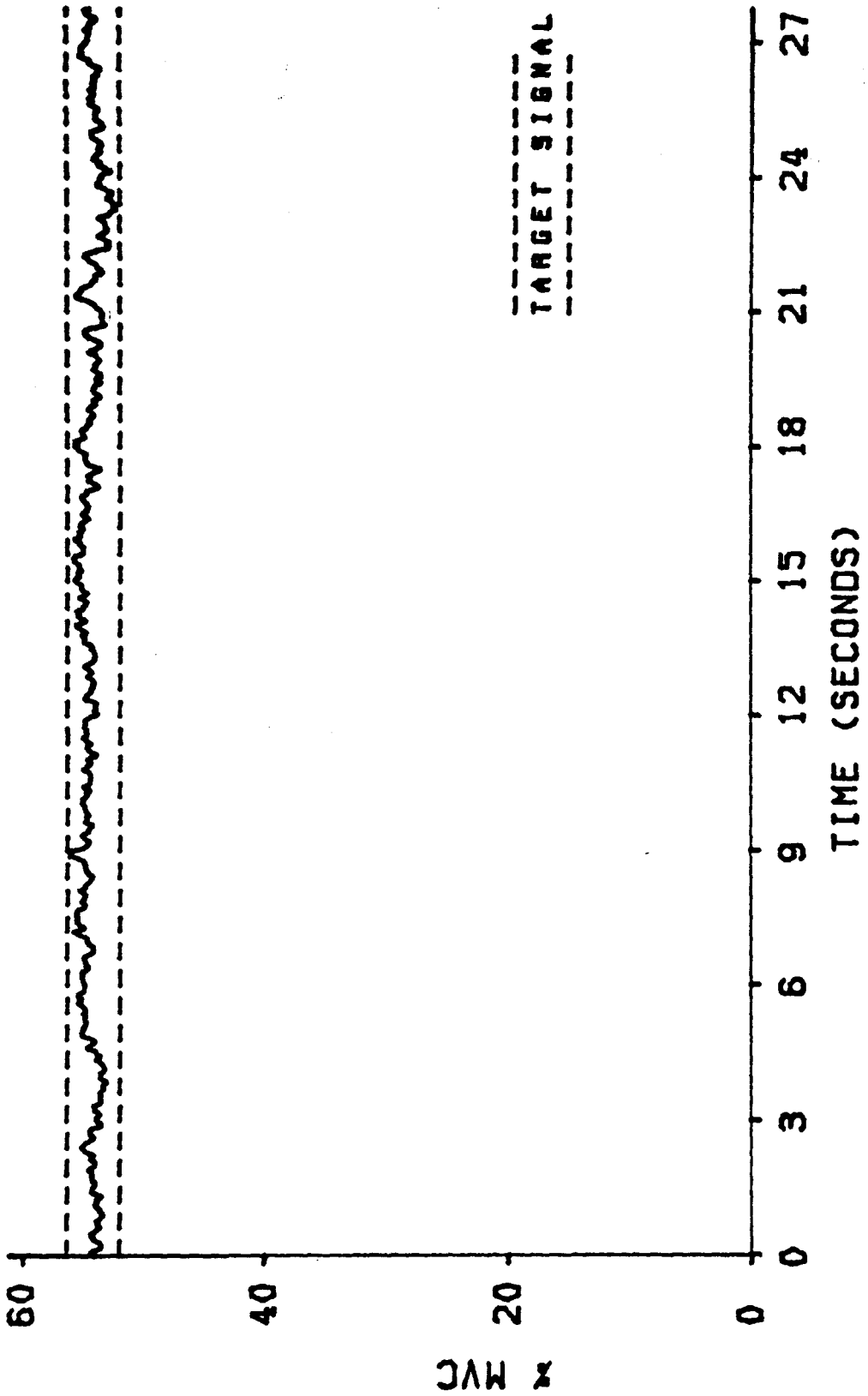


FIGURE 4.11B HIGH ISOTONIC CONTRACTION

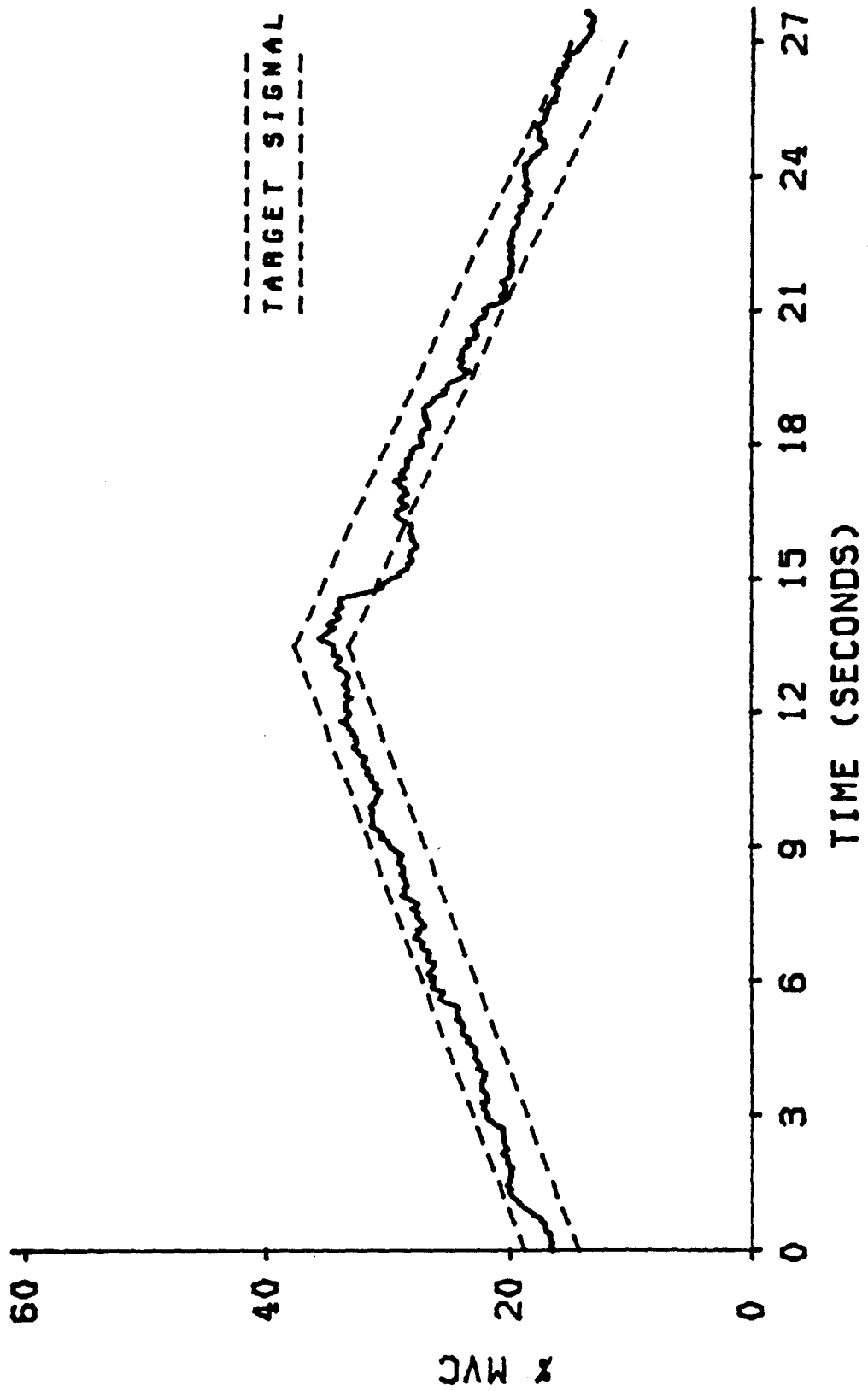


FIGURE 4.12A RAMP CONTRACTION WITH OFFSET

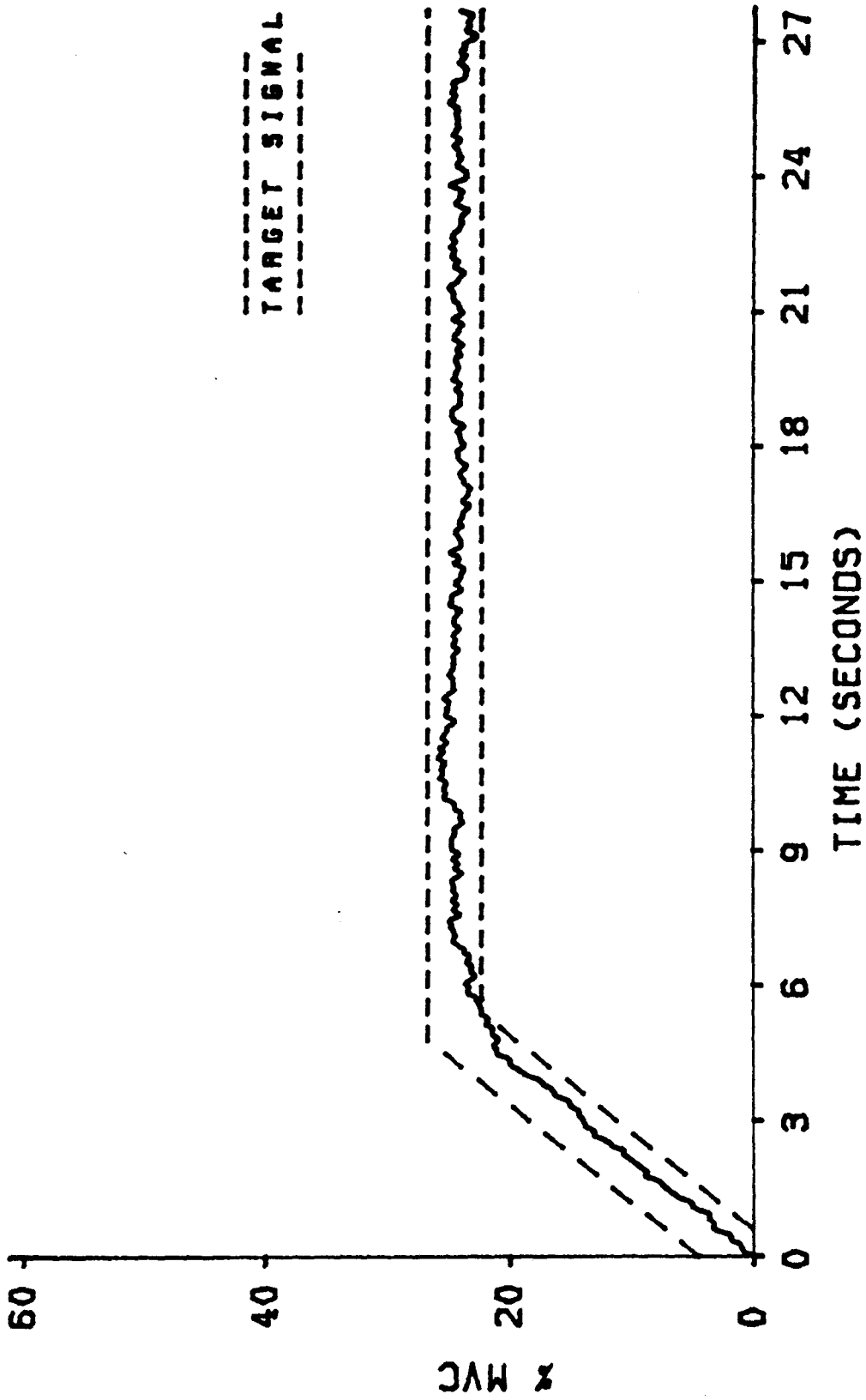


FIGURE 4.12B RAMP TO ISOTONIC CONTRACTION

in order to maintain the contraction level. Due to the large difference in frequency content of the force signal and the EMG signals it is meaningless to plot the EMG signal recorded along with the force signal on the same time scale. However, one can plot the force signal over the time of the collection of the EMG signals as a percentage of MVC.

#### 4.2.3 Preprocessing Algorithms

One of the first steps required in the analysis of EMG activity is preprocessing. Preprocessing of the EMG activity can take on a variety of forms. The preprocessing of the EMG record in this thesis involved:

- 1) removal of the mean from EMG signals and
- 2) differencing of adjacent needle recorded EMG signals.

The removal of the mean is required for later extraction and processing of the EMG signal. It is justifiable to do this since the EMG signals are ideally ac to begin with. The MUAPs generated are ideally ac (zero mean) signals. A dc offset may come about for several reasons. The first and foremost is the dc offset caused by the polarization of the electrodes. This is minimal as pointed out previously for the type of electrodes used in this thesis. However, the dc offset caused by the instrumentation may be significant. This dc offset caused by the instrumentation should be removed since it is not part of the activity recorded. The usual method employed to do this is the continual averaging of EMG activity over a long enough period of time such that a truer average of the time recorded EMG signal can be

obtained. This method is fine if the average is over a long enough period of time. However, what can and will happen when the recorded activity is of short duration when compared to the overall duration of an action potential, is that the average will be biased by motor unit action potentials at the ends of the recorded EMG activity. Since an average over a long period is not possible due to limited computer facilities a calculation of the average which does not include action potentials must be done for the removal of the dc offset. This running average is then subtracted from the EMG

The algorithm for generating a continuous average is given by the equation:

$$A_n = \begin{cases} \frac{s_n - A_{n-1}}{n} + A_{n-1} & \delta \leq \text{threshold} \\ A_{n-1} & \delta > \text{threshold} \end{cases} \quad 4.2$$

where  $A_n$  is the  $n$ 'th average,  $s_n$  is the  $n$ 'th sample,  $A_{n-1}$  is the last average,  $n$  is the  $n$ th points used to calculate the average and  $\delta$  is the threshold value used [177]. The purpose of the threshold value is to average only the background EMG data where no MUAPs are present. The actual value of this threshold is discussed in the next chapter but suffice to say, it should be at least  $3\sigma$  of the background noise level. The average calculated by the above formula is then subtracted from each individual EMG sample in that record. In order to take into account a varying level of dc offset which may occur the maximum value of  $n$  is 64. Thus a moving window average is calculated for each successive point in the record.

The motivation for differencing two fine wire electrode EMG signals is to localize action potentials close to the recording surfaces by eliminating as many low frequency MUAPs and low frequency components of MUAPs as possible. Therefore,

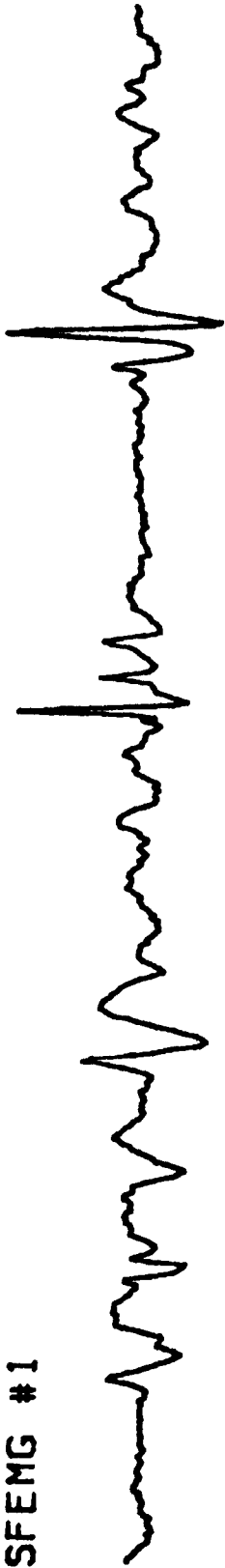
this limits not only the number of MUAPs to those of higher frequency content but it also restricts the lower frequency components of the MUAPs to a minor role in later analysis when MUAPs are to be separated. This last point essentially means that the higher frequency components in the MUAP are much more important in differentiating the shapes of the recorded MUAPs.

There are a variety of single channel differencing techniques which can be done. Essentially, they all follow the same basic equation:

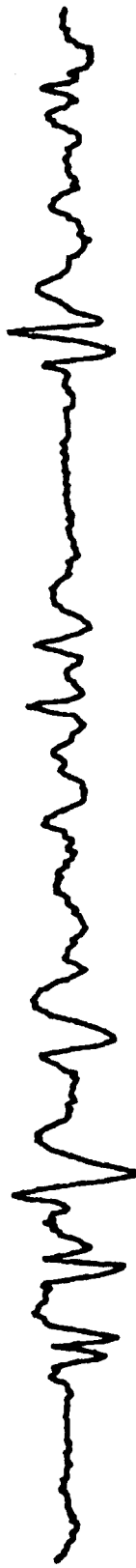
$$\nabla u_n = u_{n+1} - u_n \quad 4.3$$

where the discrete variable  $\nabla u_n$  is replaced by the difference in the successive data points of that variable. This type of differencing can be done for fine wire EMG, however, since there is more than one recorded signal from the same general volume of muscle (due to the small distance of separation of the single fiber electrodes) then the differencing can be done between any of these three fine wire electrode channels. Three different differences could be done. The three undifferenced fine wire EMG recordings are shown in Figures 4.13a and 4.13b. The differenced EMG recording is shown in Figures 4.14a and 4.14b. In comparing the former figures to the latter it can be seen that the motor unit action potentials are more peaked in nature and much of the low frequency components are no longer present. This result has several different explanations. Intuitively, differencing of any two single fiber channels within a similar recording volume results in a bipolar recording configuration with the distance between the single fiber electrodes being the bipolar recording distance. Thus the common EMG activity will be rejected to some degree since this would appear on both fine wire electrodes. Furthermore, due

SFEMG #1



SFEMG #2



SFEMG #3

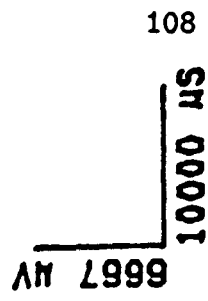
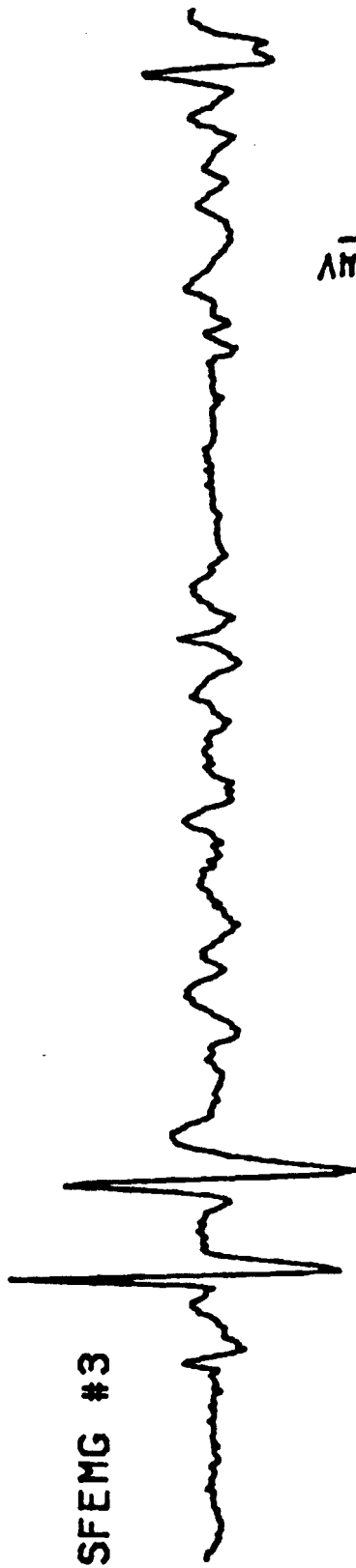


FIGURE 4.13A UNDIFFERENCED EMG

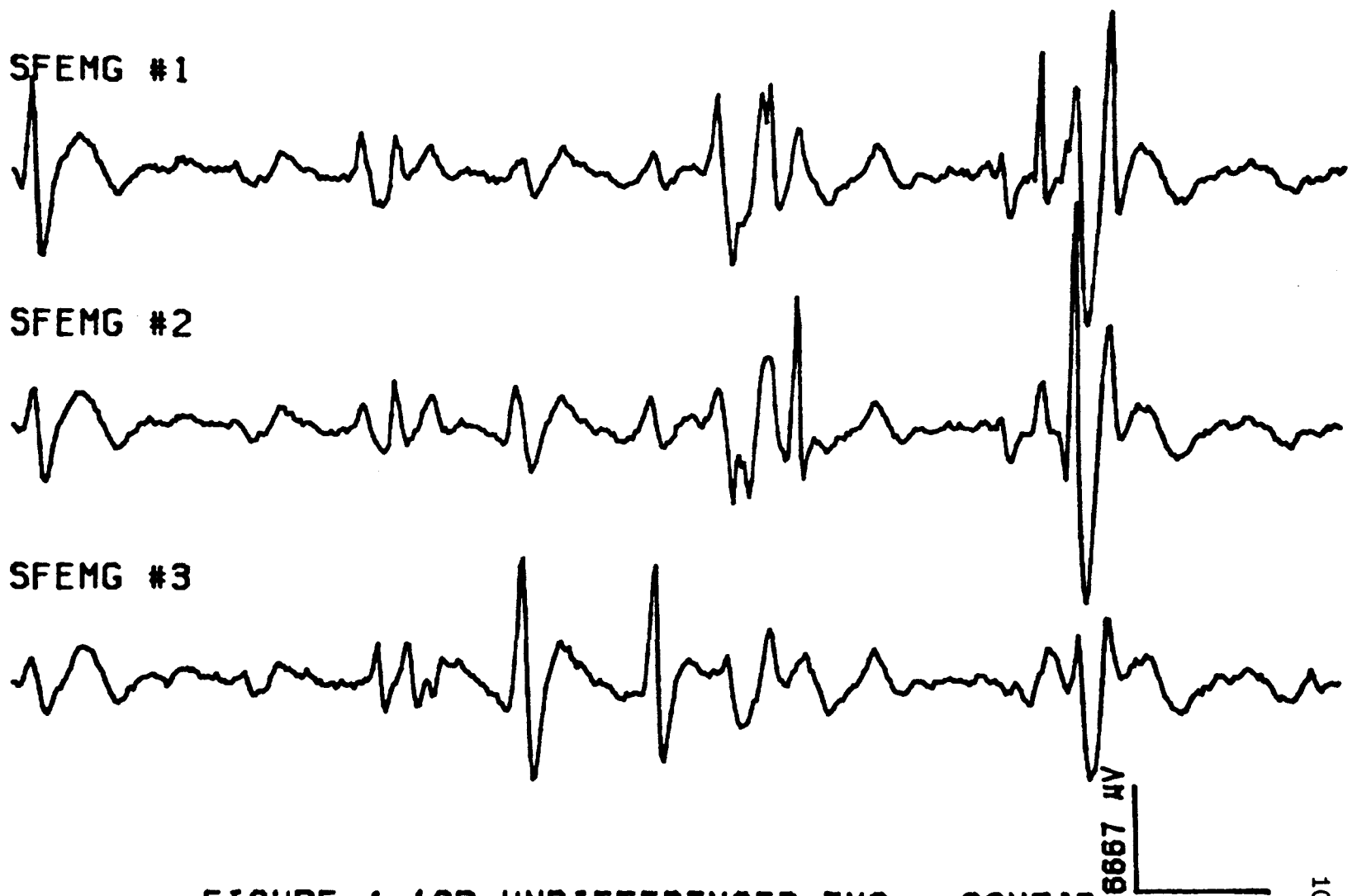
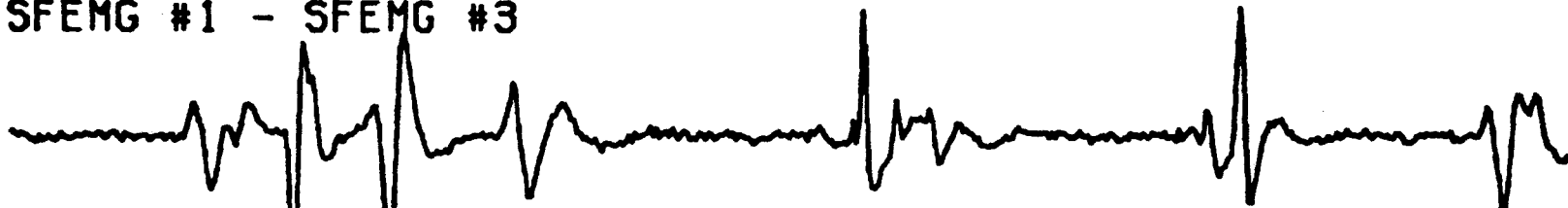


FIGURE 4.13B UNDIFFERENCED EMG - CONT'D

SFEMG #1 - SFEMG #2



SFEMG #1 - SFEMG #3



SFEMG #2 - SFEMG #3

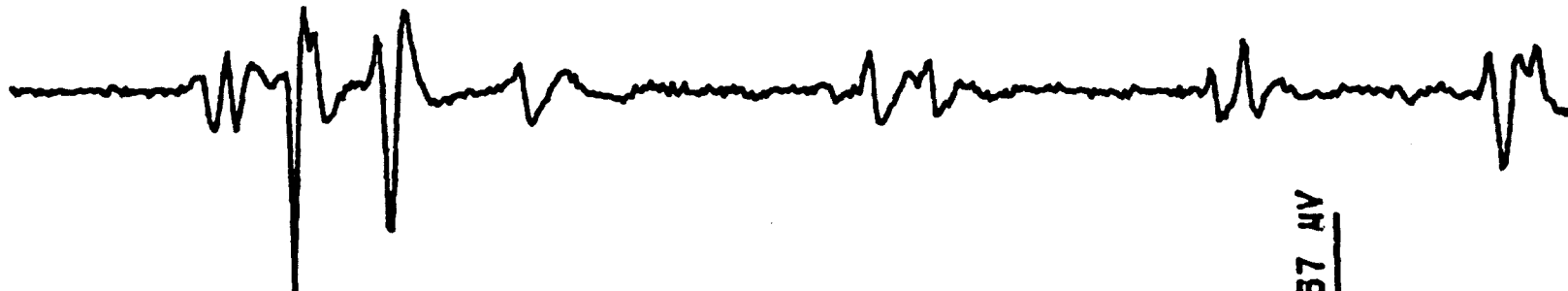
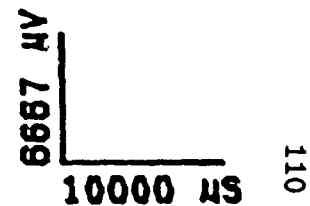


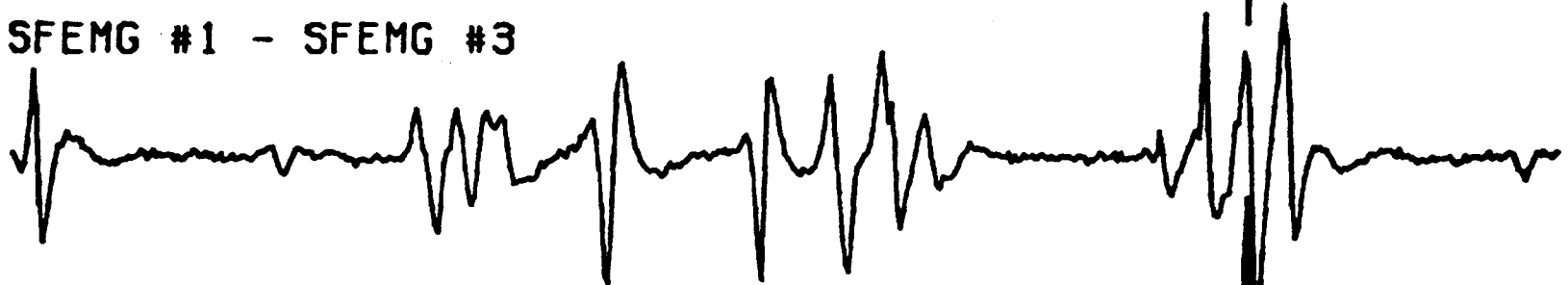
FIGURE 4.14A DIFFERENCED EMG



SFEMG #1 - SFEMG #2



SFEMG #1 - SFEMG #3



SFEMG #2 - SFEMG #3



6667  $\mu$ V  
10000  $\mu$ S

FIGURE 4.14B DIFFERENCED EMG - CONT'D

to both the generation of MUAPs and the filtering properties of the tissue, low frequency MUAPs will appear at both electrodes. Differencing should remove the commonality between these signals. To see the effect of the difference operator on a signal,  $e^{j\omega t}$ , in the volume conductor, the difference between this signal as recorded by two separate fine wire electrodes must be looked at. Assuming no filtering of the signal takes place then the difference between the signal  $e^{j\omega t}$  and the same signal phase shifted by the amount  $\epsilon$  given by  $e^{j\omega(t+\epsilon)}$  is given by the equation:

$$\nabla e^{j\omega\epsilon} = e^{j\omega(t+\epsilon)} - e^{j\omega t} \quad 4.4$$

which can be rewritten by the use of Euler's equation to give:

$$\nabla e^{j\omega\epsilon} = e^{j\omega\epsilon/2} \left[ \frac{2 \sin(\omega\epsilon)}{2} \right]^k e^{j\omega t} \quad 4.5$$

where  $-\pi \leq \omega \leq \pi$  and  $k$  is the number of differences taken (usually one) [178][179]. From the plot of this function in Figure 4.15 it can be seen that the difference operator attenuates the lower one third of the frequencies present in a particular signal and accentuates or increases the upper two thirds of the frequencies present in the signal.

The result of this differencing on an individual motor unit action potential is demonstrated in Figures 4.16a through 4.17b. The time undifferenced and differenced signals are shown in Figures 4.16a and 4.17a respectively. Their respective PSDs (mean square amplitude) are shown in Figures 4.16b and 4.17b. Clearly the frequency bandwidth of the individual signals is decreased in such a way

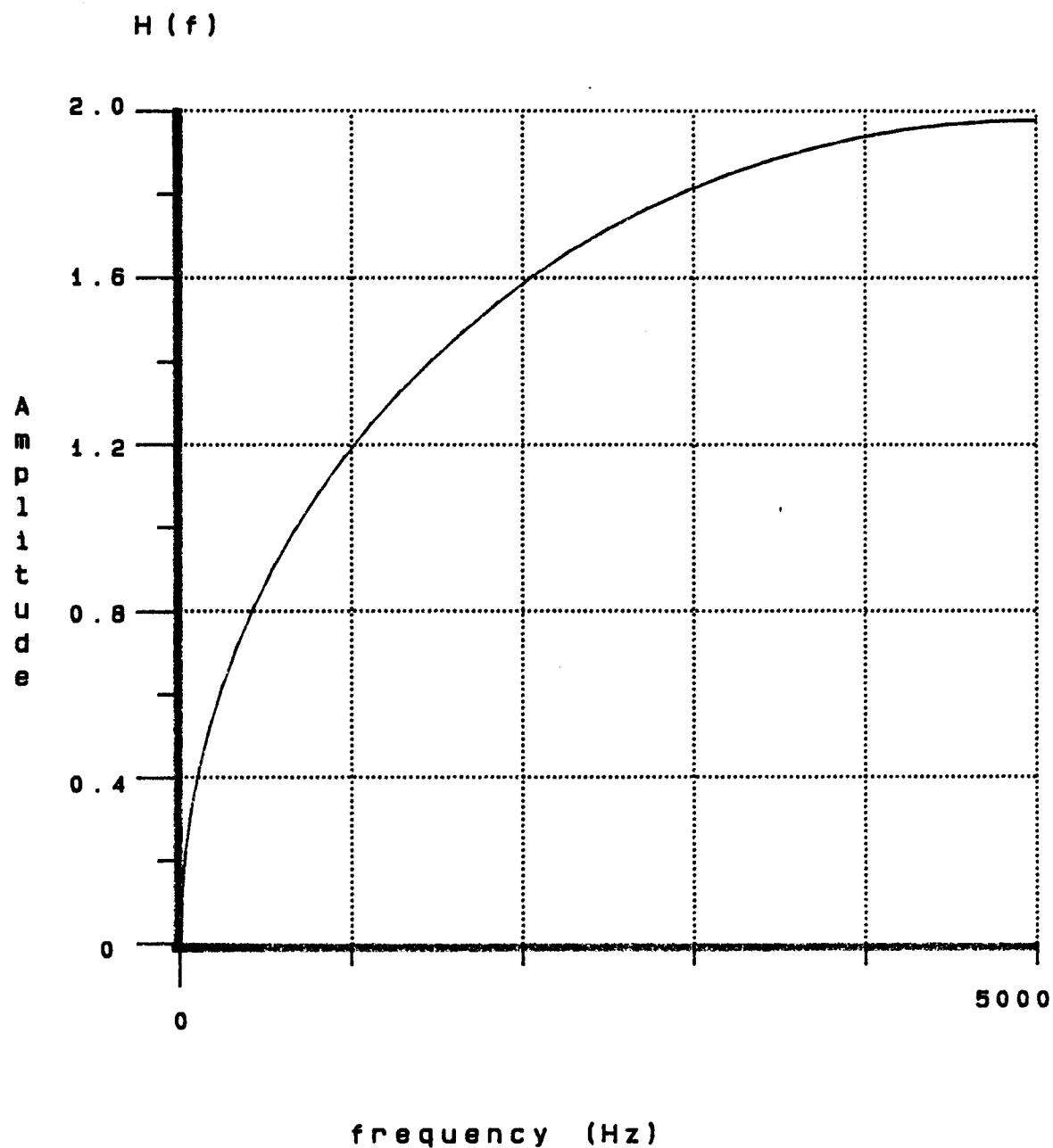


Figure 4.15 Frequency effects on differencing EMG signal

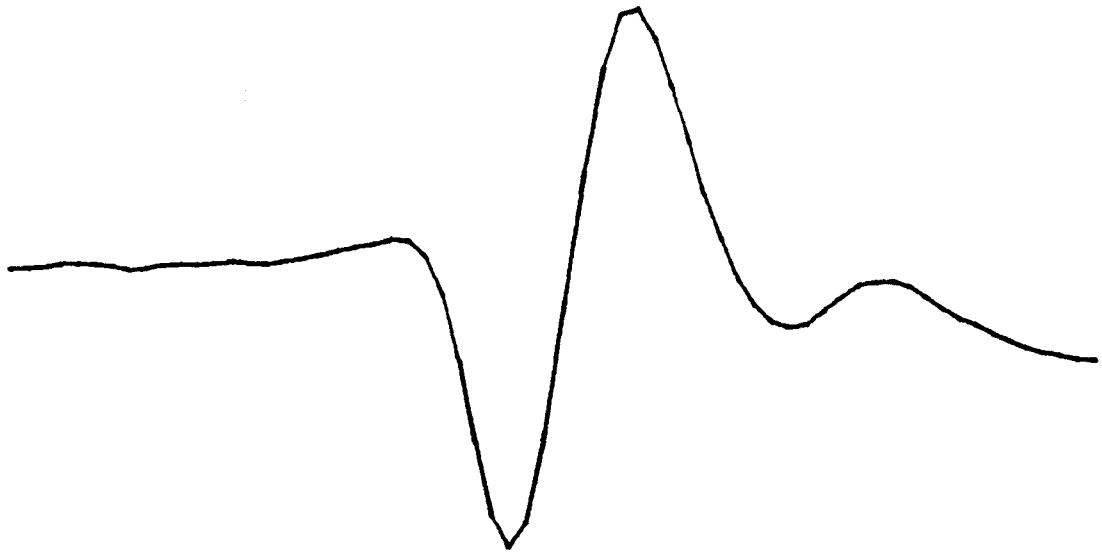
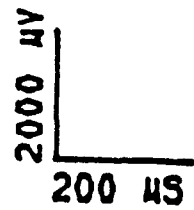


FIGURE 4.16A UNDIFFERENCED MUAP



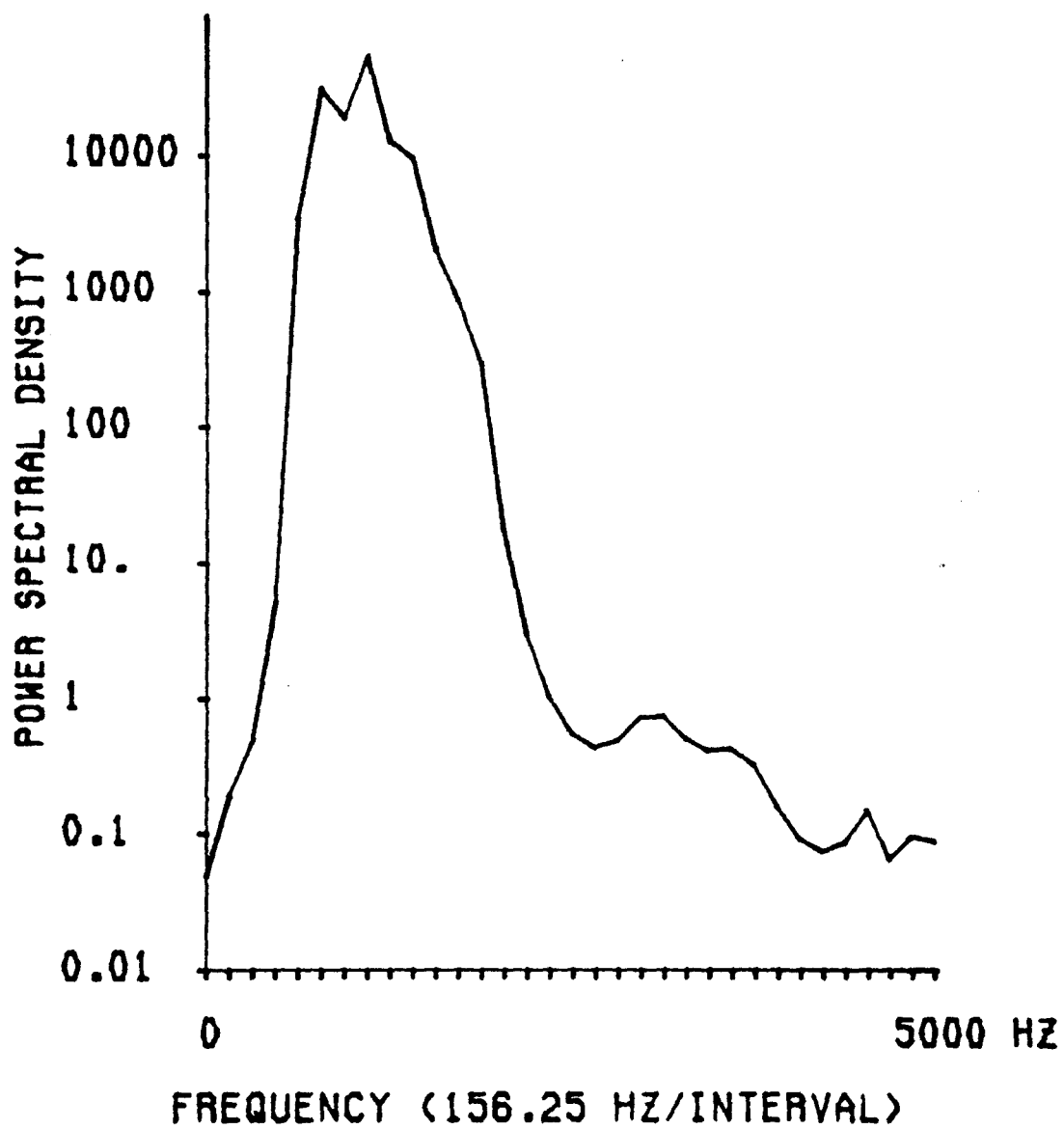


FIGURE 4.16B MUAP - FREQUENCY DOMAIN

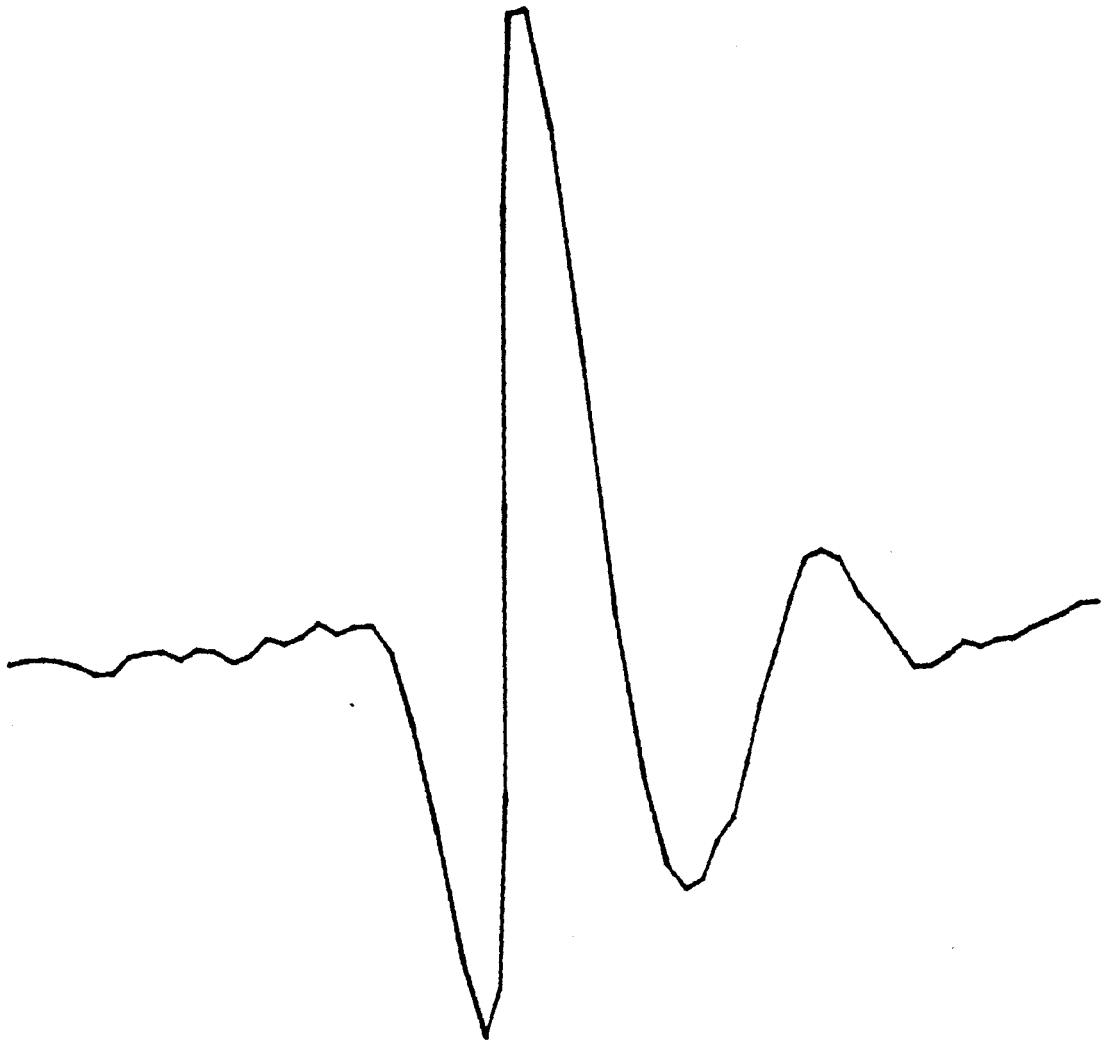


FIGURE 4.18C DIFFERENCED MUAP

2000  $\mu$ V  
200  $\mu$ S

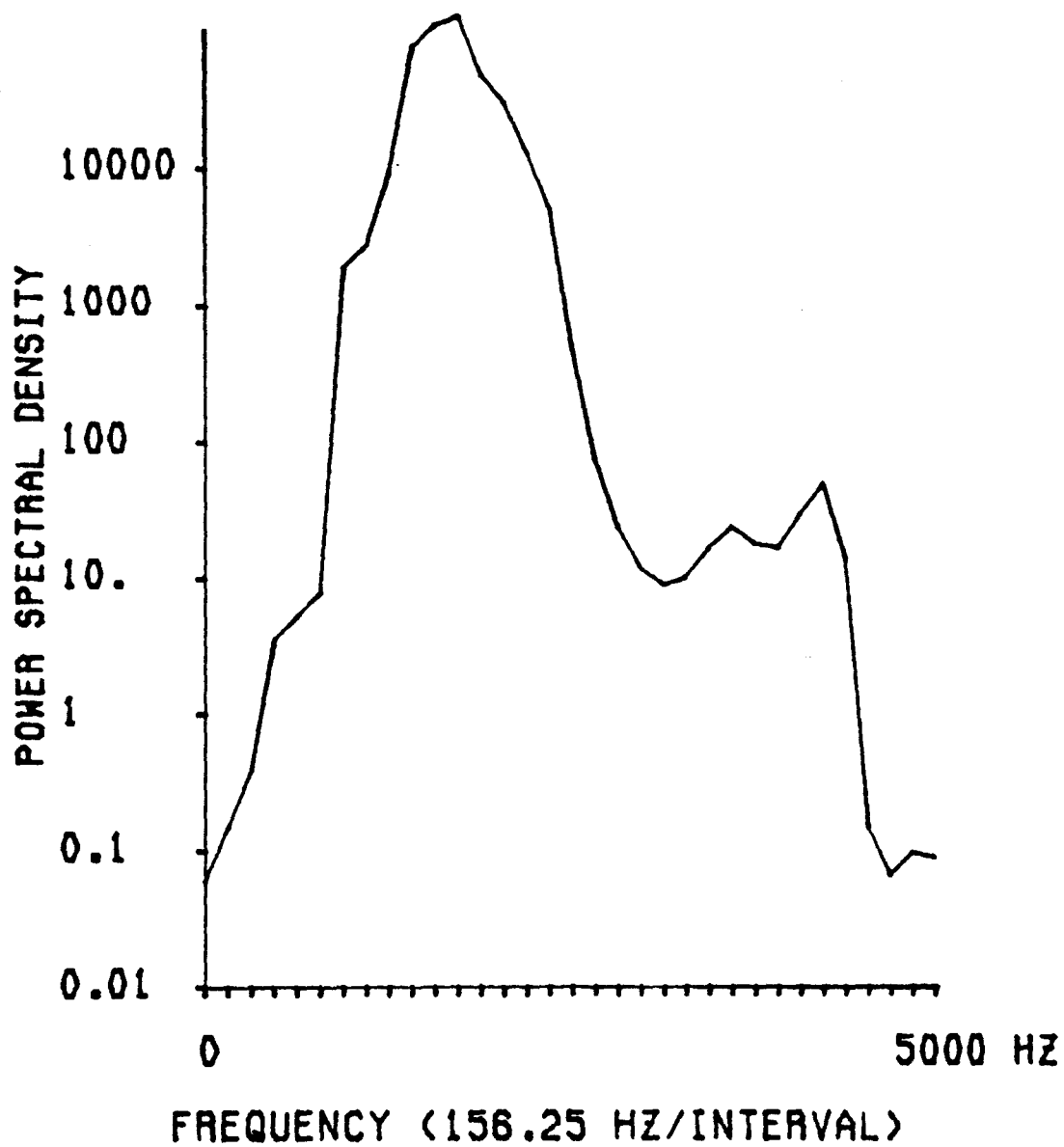


FIGURE 4.18D MUAP - FREQUENCY DOMAIN



FIGURE 4.17A UNDIFFERENCED MUAP

2000  $\mu$ V  
200  $\mu$ S

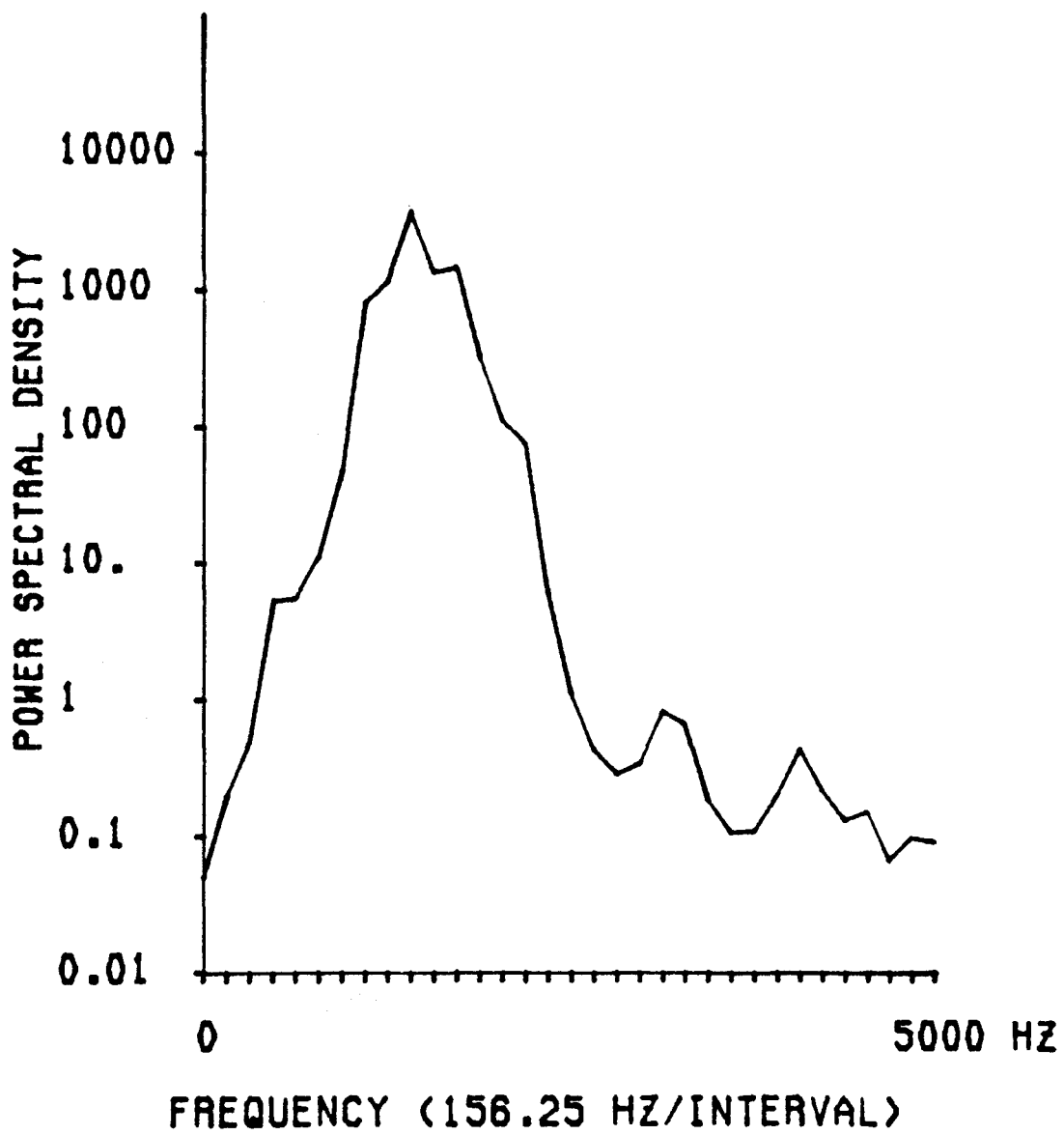


FIGURE 4.17B MUAP - FREQUENCY DOMAIN

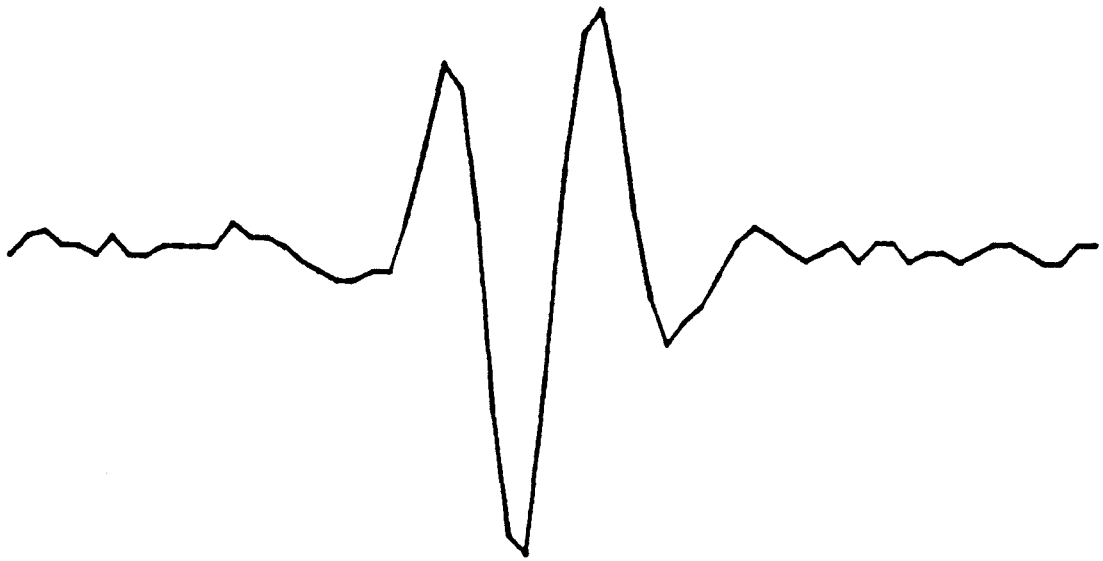
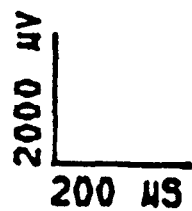


FIGURE 4.17C DIFFERENCED MUAP



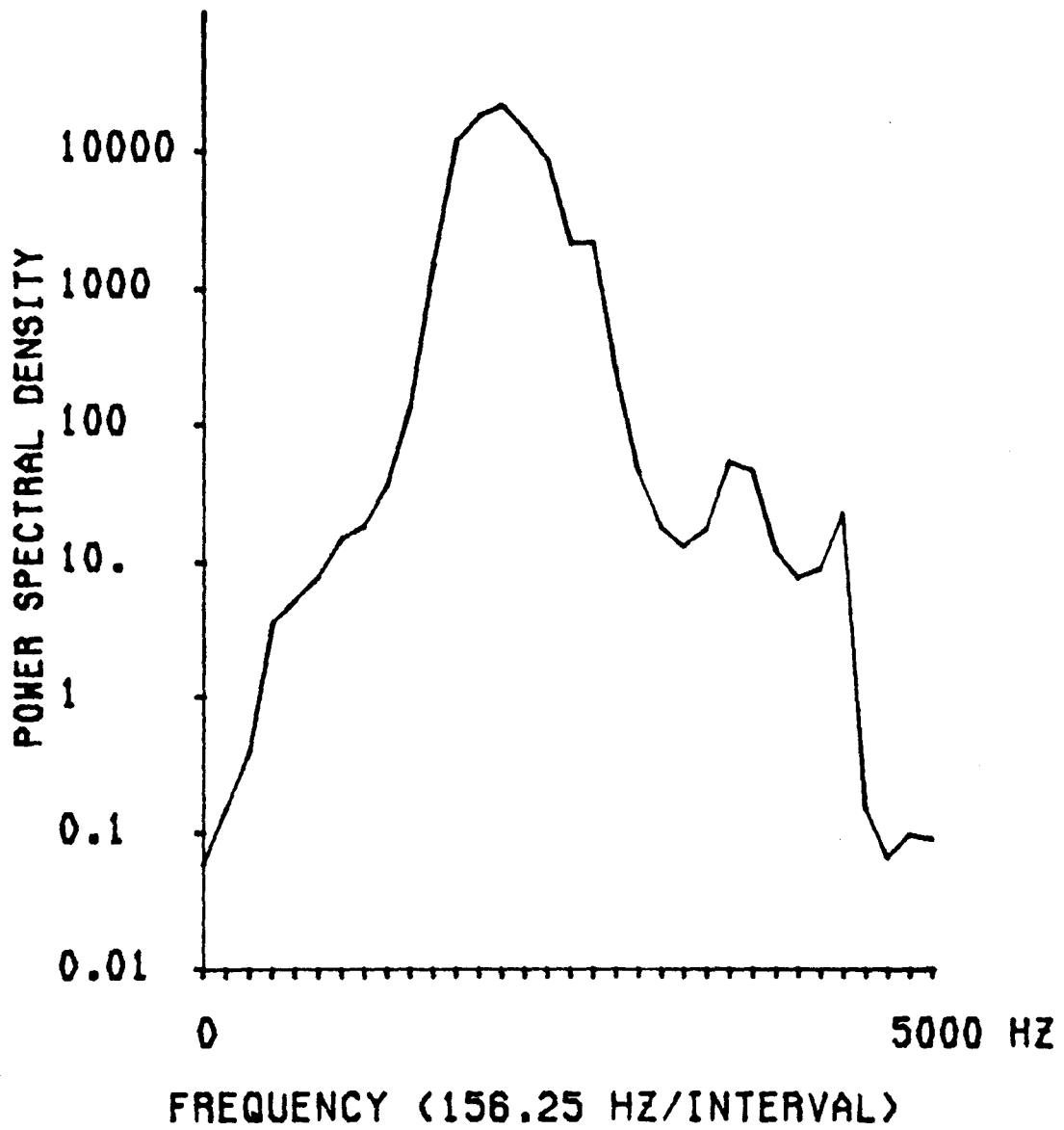


FIGURE 4.17D MUAP - FREQUENCY DOMAIN

as to eliminate the common low frequency components of the signal.

The next step in the analysis of data is to look at data compression of data for which requires the detection of MUAPs in the IP. This is presented in the next chapter.

## Chapter Five

### Preliminary MUAP Analysis

#### 5.0 Introduction

With both hardware and software systems described in the previous chapter continuous recording of EMG signals can be accomplished and therefore further analysis can be done. In chapter three it was pointed out that there are three main areas of EMG analysis; interference pattern (IP), single motor unit action potential (MUAP) and motor unit action potential train (MUAPT). IP analysis looks at the continuous EMG record whereas the other two analyses look at only the action potentials present in the EMG record. IP analysis can be accomplished in a straight forward manner and will not be discussed here. In order to look only at the action potentials present in the interference pattern the action potential must first be detected. As pointed out in chapter three, before any analysis can be done on a signal, the signal must be represented by some sort of feature vector. Ideally, this feature vector representation of the MUAP will sufficiently describe that particular MUAP as a unique signal in that feature space. Furthermore, extraction of MUAP characteristics should be readily and easily discernible from this feature vector in order that MUAP and MUAPT analysis may be done.

The purpose of this chapter is to describe the analysis done on the MUAP. This analysis includes:

- 1) detection and extraction of MUAP from the IP,
- 2) single MUAP analysis including:
  - i) feature representation of the MUAP and
  - ii) extraction of time feature characteristics of the MUAP,
- 3) preliminary MUAPT analysis including:
  - i) alignment of MUAP signal to a class vector and
  - ii) resolving of superimposed MUAPs.

Each analysis is described below.

## 5.1 Detection and Extraction of a MUAP from the IP

Although the hardware and software system described in the previous chapter is capable of collecting up to three fine wire and one cannula EMG signals the subsequent analysis only deals with one channel of single fiber EMG signal. This analysis can be extended to include the other fine wire EMG and cannula signals at a later time when hardware capabilities permit.

### 5.1.1 Feature Selection for MUAP Detection

The question that logically arises in detecting MUAPs is what feature of the MUAP best describes the presence of an action potential in the interference pattern. Intuitively, there are many features which can be

extracted from the IP which can be used to detect APs. Some of the methods used previously for the detection and subsequent extraction of a MUAP from the IP were auto regressive time series models and recursive horizon filters [134][180][181]. In the first detection scheme auto regressive models of MUAP activity and non activity were developed and hence a MUAP is detected when significant changes between the models become evident. In the recursive horizon filters the method used was to constantly measure the variance in the signal to noise ratio. When this SNR becomes greater than a threshold then a MUAP is said to have occurred. Both of these typical methods, although very powerful, have the disadvantage of being very computationally intensive.

Although these methods described above use viable features for the detection of MUAPs, the detection of MUAPs in the IP can be done in a much simpler way. The simplicity and hence computational ease of detecting MUAPs in the IP all depends on the features selected. Logically if one looks at any EMG signal recorded from skeletal muscle, whether it be recorded by surface electrodes or by needle electrodes the single most distinctive feature of these action potentials is their peak. This is a direct consequence of how an action potential is generated and therefore is an inherent feature of any AP located within the recording volume of the electrode. Although MUAPs may vary significantly in the number of phases they have (as shown in chapter three) they tend to have only one significant positive and one significant negative peak if there is no superpositioning of MUAPs. The occurrence of a peak, positive or negative, can then be associated with the occurrence of a MUAP. Thus this common

feature can be used to separate action potentials from the interference pattern. Notice that this feature (like the more complex ones attempted above) does not attempt to differentiate between MUAPs or determine whether or not superpositioning (algebraic summation) of MUAPs is occurring; rather, it only attempts to separate an MUAP from the IP. With a few subtle modifications however the resolving of superpositioned MUAPs can be done to some degree as will be shown later in the chapter.

In order to achieve the detection of a MUAP in the IP by the use of its peak an envelope detector to detect these peaks was used. This is described below.

### 5.1.2 Envelope Detector

After the EMG signal is preprocessed as described in the previous chapter an envelope of the IP is created. This is done in the following way. The first step in creating the envelope is to take the absolute value of the EMG signal in order to eliminate the need to search for both positive and negative peaks present in a single MUAP. The next step is to smooth out this signal to prevent multiple detections of MUAPs when using a threshold detector. This is accomplished by a simple linear equation of the form

$$E = S_p \left( 1 - \frac{n}{\tau} \right) \quad 5.1$$

where  $E$  is the output of the envelope detector,  $S_p$  is the peak of the

signal in the EMG activity,  $n$  is the number of data points away from that peak and  $\tau$  is the time constant which adjusts the decay rate (i.e. slope). Therefore, the slope,  $m$  of this linear equation is given by:

$$m = - \frac{S_p}{\tau} \quad 5.2$$

With this type of envelope detection there is a ripple frequency  $f_r$  that occurs as the non signal area between the peaks is traversed by the envelope generator. The trick is to pick a time constant  $\tau$  such that relatively little decay occurs in the output of the envelope between peaks occurs. In other words  $\tau$  must be much greater than the period of the ripple signal given by  $\frac{1}{f_r}$ . Also the value of  $\frac{1}{\tau}$  must be less than the highest frequency  $f_h$  present in the EMG signal. This highest frequency in the EMG signal was shown to be in the neighborhood of 4kHz. The value of  $\tau$  may then be expressed as satisfying the following equation:

$$\frac{1}{f_r} \ll \tau < \frac{1}{f_h} \quad 5.3$$

Furthermore, the absolute value of the slope of the decay of this detector must be greater than the slope of the signal of the MUAP under study in order to ensure proper detection. In short this can be represented by differences. Thus:

$$|m| = \frac{S_p}{\tau} \geq \frac{s_n - s_{n+1}}{T} \quad 5.4$$

where  $s_n$  and  $s_{n+1}$  are successive sample points of the EMG signal and  $T$  is the sampling interval. It should be noted here that the slopes of the MUAP vary around the peak and that the difference used to calculate this slope is only an approximation of the decay. Nevertheless, the above equation can be rearranged to give a value for  $\tau$  as:

$$\tau \leq \frac{S_p T}{s_n - s_{n+1}} \quad 5.5$$

Thus  $\tau$  must satisfy the two conditions imposed by equations 5.3 and 5.4. A good value for  $\tau$  consistent with these restrictions was found to be approximately  $\frac{1}{4000}$ . The ripple still produced by this detection method is further reduced by smoothing the output of this envelope detector. This smoothing filter has the property that the interpolated value of the detection envelope must be such that it does not lessen the maxima or heighten the minima with respect to the EMG signal recorded; rather it smooths out the higher frequency of the envelope output. These peaks and valleys of the original signal can only be accurately represented by the smoothing filter if higher frequencies ( $f_n$ ) are allowed to pass. The smoothing function used is a simple FIR filter of form:

$$y_n = \sum_{k=-n}^n c_k u_{n-k} \quad 5.6$$

where  $u_{n-k}$  is the unit step function and the values of  $c_k$  are given

by the matrix:

$$\left[ \frac{1}{320} \right] (-3, -66, -5, , 3, 21, 46, 67, 74, 67, 46, 21, 3, -5, -6, --3)$$

The frequency response of this FIR smoothing filter is shown in Figure 5.1 [128][178][182].

Notice that equation 5.6 does not essentially effect the magnitude of the IP signal since the envelope detector and smoothing function are normalized and the dominant frequencies present in the EMG signal are allowed to pass while the ripple frequency is attenuated. Thus the amplitude of the signal output from the envelope detector is more or less the same level as the absolute value of the EMG signal. In this way any detection criteria applied to this signal can be directly related to the actual level of the amplified signal.

The critical aspect of this detection window as pointed out previously is the value of  $\tau$ . This type of envelope detection is equivalent to the demodulation of an AM signal where instead of the entire envelope being used as information, a detection level threshold can be set to determine the presence or absence of a MUAP.

A continuous recording of single fiber EMG is shown in Figure 5.2 along with the output of the MUAP detector. From the diagram it is clearly seen that the peaks in the detection output correspond to MUAPs in the IP. A threshold level can then be set to detect when the envelope goes above a certain level and thus a MUAP is deemed to have occurred. There are several considerations used for the setting of this threshold level.

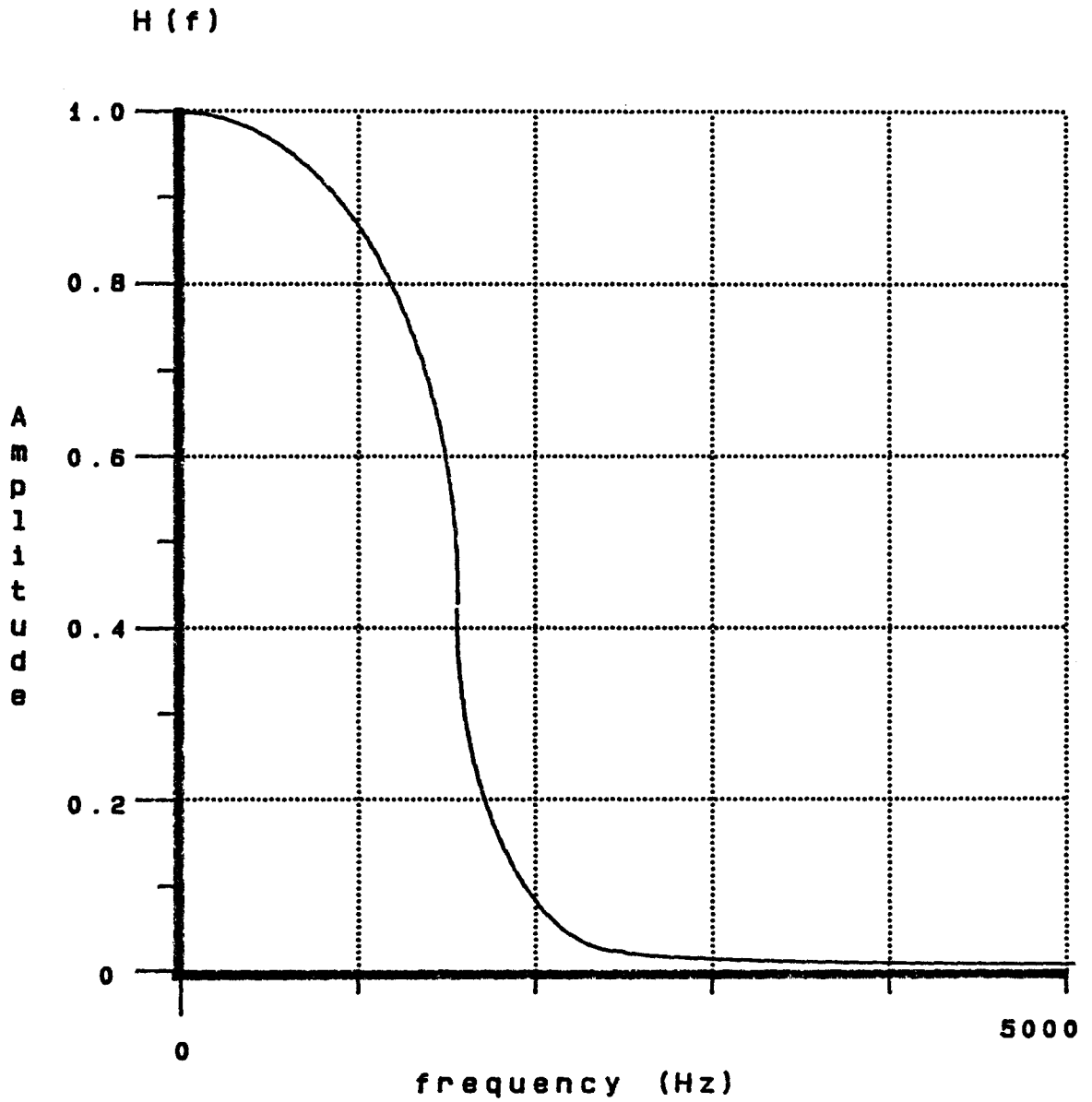
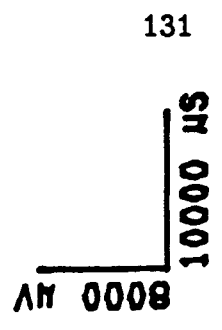
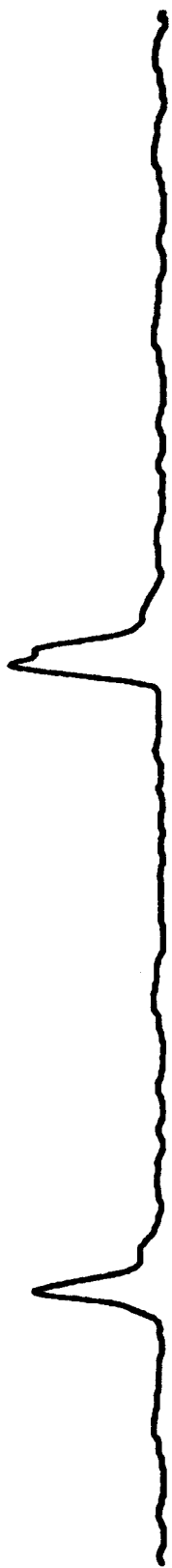
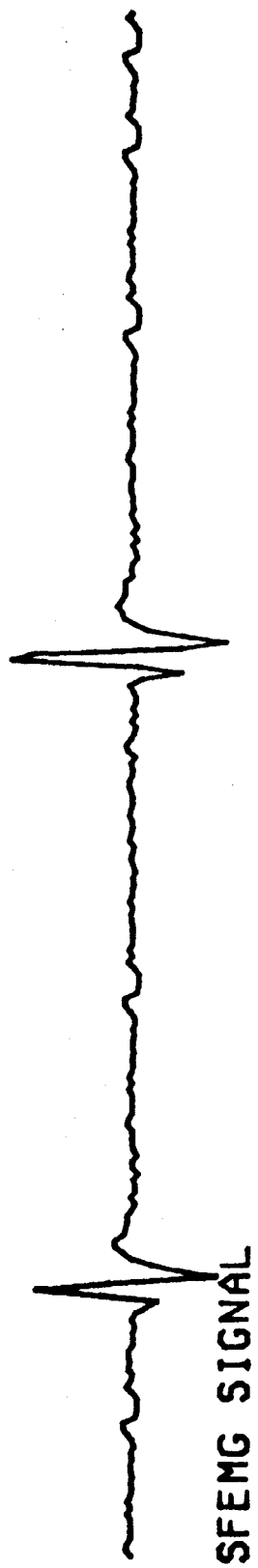


Figure 5.1 Frequency response of smoothing filter



DETECTION ENVELOPE

FIGURE 5.2 DETECTION ENVELOPE OUTPUT

These consideration are:

- 1) background noise and
- 2) detection sensitivity.

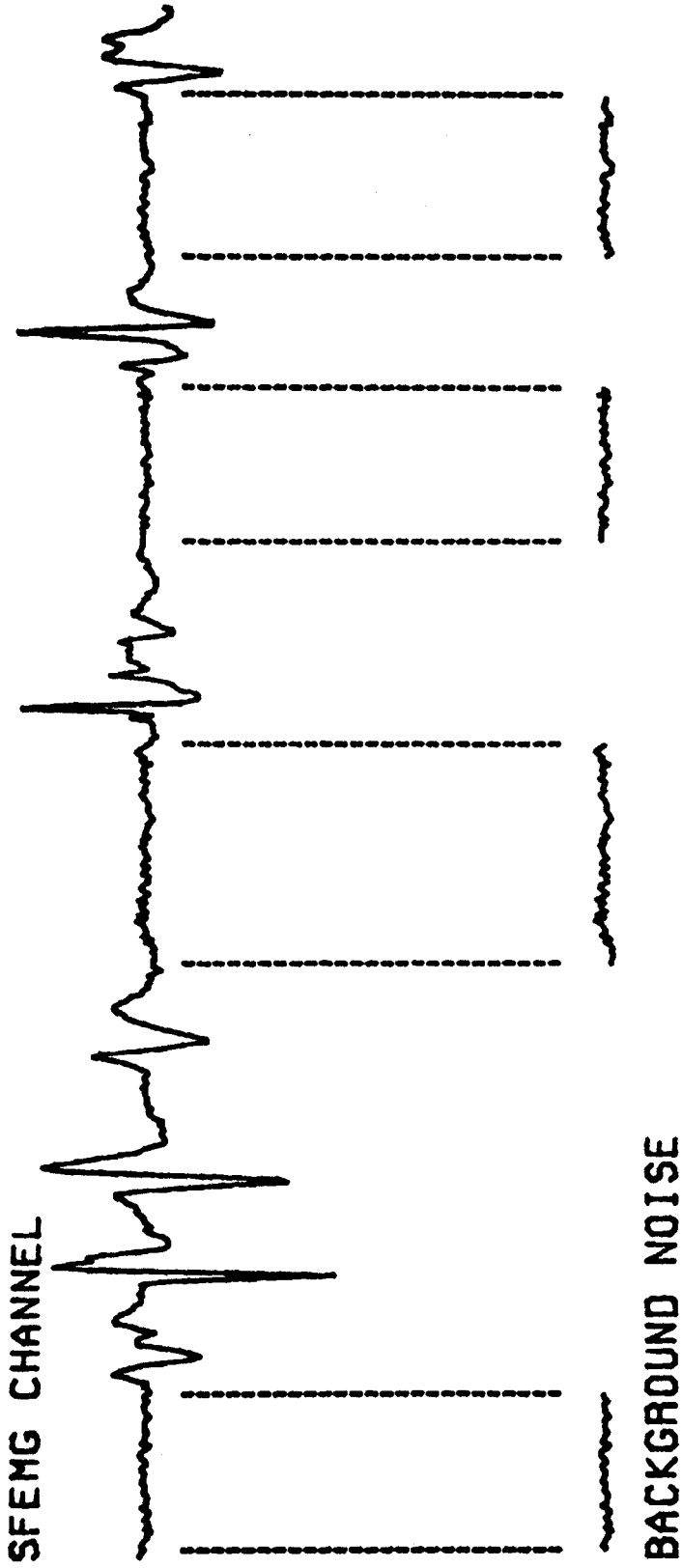
These are discussed below

### 5.1.3 Background Noise:

Due to the inherent design of the hardware the instrumentation noise of the EMG signal is virtually nil. The majority of the background noise consists of background EMG activity. That is, the signals produced by motor units which are located at a distance from the recording surface of the electrode. Typical background noise in the EMG recording is shown in Figures 5.3a and 5.3b.

The detection threshold must be greater than this background level. This background EMG activity is calculated on a continuous basis from the original EMG record if and only if no MUAP is detected. As shown in the figure, this level is found by calculating the standard deviation  $\sigma$  of the EMG signal for the interval of length  $N$  where no MUAP is detected by the following equation:

$$\sigma = \sqrt{\text{var}(s_1 \dots s_N)} = \sqrt{\frac{1}{N} \sum_{i=1}^N (s_i - \bar{s})^2} \quad 5.7$$



8667 MV  
10000 μS

FIGURE 5.3A BACKGROUND NOISE

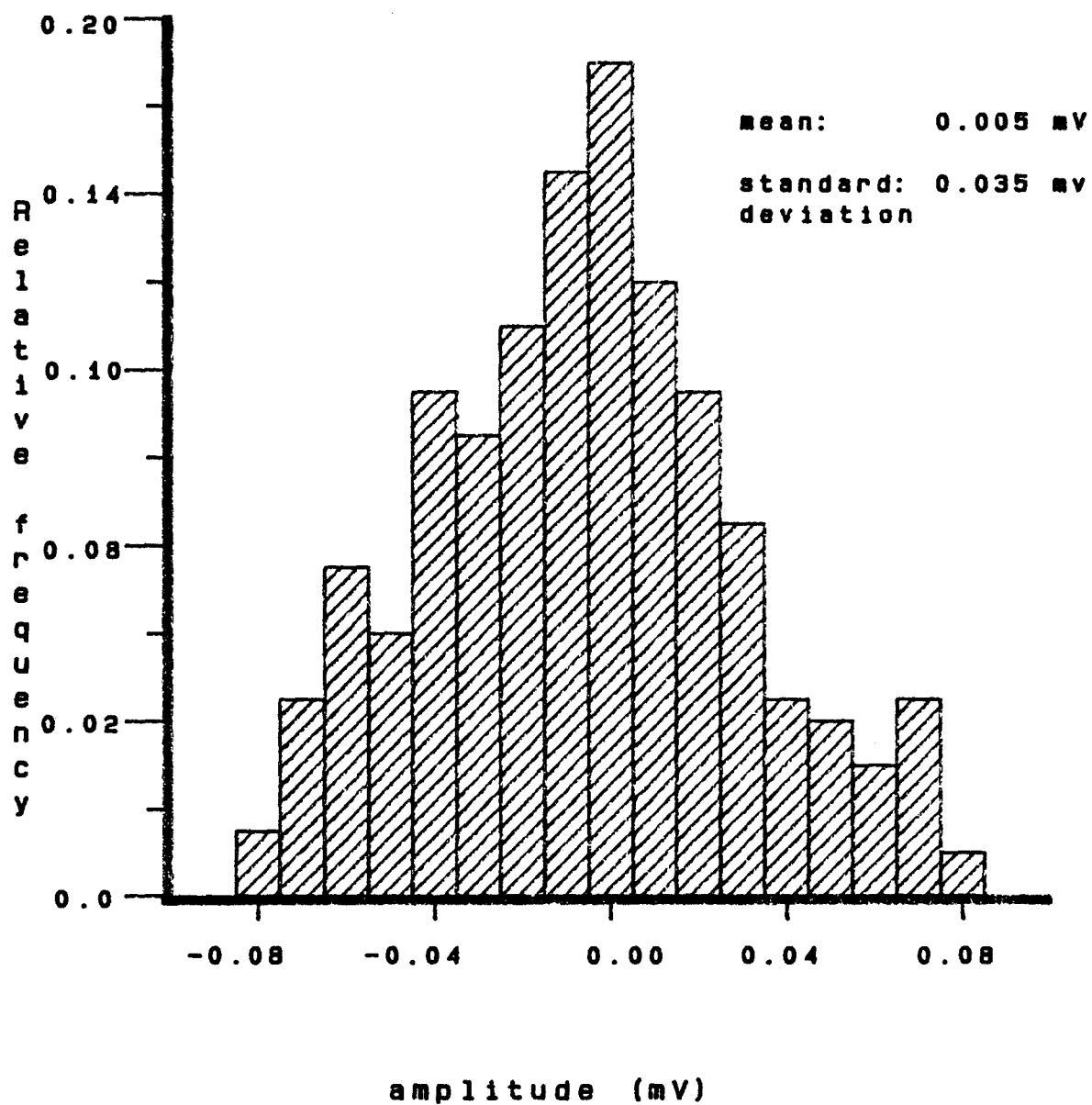


Figure 5.3b Typical amplitude distribution of the background noise

where  $\bar{s}$  is the mean of the signal (the mean may or may not be zero due to MUAPs at the end of the interval) in that particular interval [183][184]. The absolute lowest level of the action potential detection threshold is then stipulated to be  $3\sigma + \bar{s}$ . For Figure 5.3b this is seen to be approximately  $120\mu\text{V}$ . Of course this threshold level will change if the background noise changes. Slow changes in the background noise are accommodated for in the following way. When the standard deviation of a particular interval is calculated it is stored as  $\sigma_I$ . This is similarly done for the next background noise interval. The standard deviation of the background noise is then calculated as a running average of these standard deviations according to the equation:

$$\sigma_A = \frac{\sigma_p - \sigma_{A-1}}{n} + \sigma_{A-1} \quad 5.8$$

where  $\sigma_A$  is the present average standard deviation,  $\sigma_p$  is the latest standard deviation calculated by equation 5.7,  $\sigma_{A-1}$  is the last average standard deviation and  $n$  is the number of standard deviations used in the calculation. A value of five for  $n$  was found to be adequate for following slowly changing SFEMG signals.

It should be noted that the background EMG activity changes relatively little either during isotonic or varying force produced by the muscle undergoing contraction. In this manner then once the detection level is set above the ambient noise present in the EMG signal it remains so for the rest of the activity.

#### 5.1.4 Detection Sensitivity

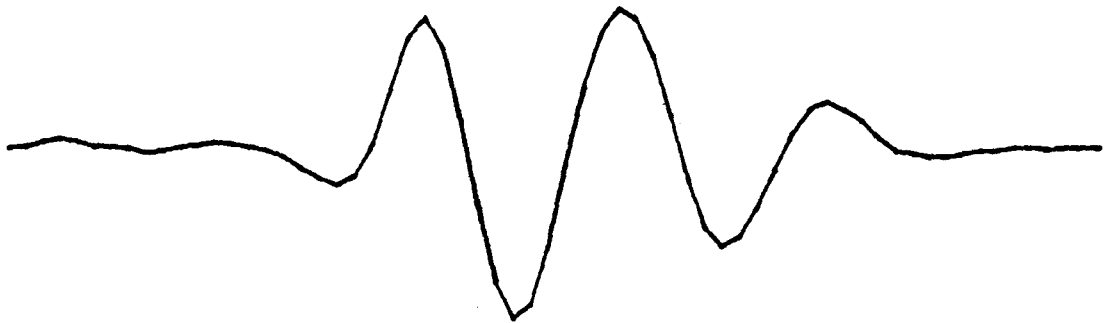
In most cases the detection threshold stipulated in the preceding section is impractical since it includes the detection of many small MUAPs along with large MUAPs. In order to limit the number of MUAPs detected to a reasonable amount and to MUAPs which are more easily distinguished (i.e. larger MUAPs indicate closeness to the needle electrode and thus higher frequency characteristics important to separation are attenuated less) a higher detection level must be set. The choice of this detection level is arbitrary with a reasonable one being able to detect an aggregate count of between 10–30 MUAPs per second when the muscle is undergoing light contraction. The detection level therefore may change with changing contraction force of the muscle but is set to a particular value for a selected contraction level and is not changed during the rest of the muscle contraction unless the standard deviation of the background noise exceeds this level. If this is the case then the detection level is reset to be twice as great as it was previously. Now that the threshold has been set the extraction of MUAPs can be done.

#### 5.1.5 Extraction

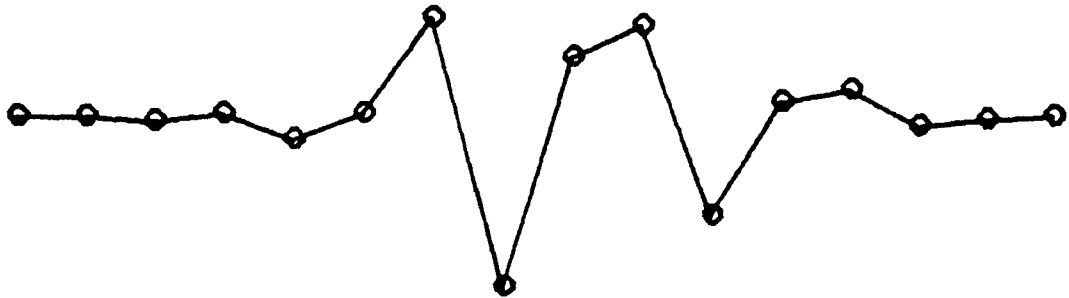
Once the level of the threshold has been set, detection and subsequent extraction of a MUAP from the IP is possible. In order to eliminate multiple detections of the same MUAP the criteria used to detect an action potential is as follows. When the detection threshold  $\delta$  is

exceeded by the output of the envelope detector then this is determined as one of the points (*a*) bracketing the peak of an action potential. When the output of the envelope detector goes below this same detection threshold then this is determined to be the other point (*b*) bracketing the peak of the envelope detector output. The peak of the envelope detection output corresponds to the maximum peak (positive or negative) of the action potential. This is shown in Figures 5.4A, 5.4B and 5.4C. Thus the peak of the MUAP can easily be found by searching for the maximum between points *a* and *b*. Once the peak is determined then extraction of the MUAP can be done.

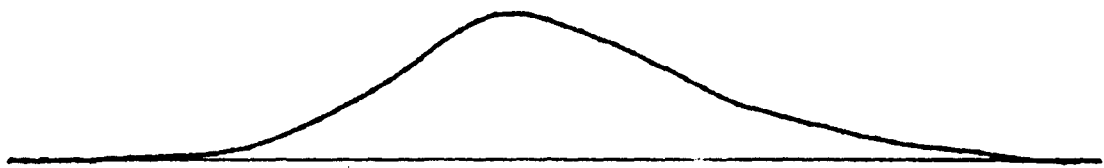
Figures 5.5A, 5.5B and 5.5C show this process for the signals of 5.4A, 5.4B and 5.4C respectively. Originally the MUAP was detected by first finding the peak of the detection envelope and then looking for the points of inflection ( $x_1$ ,  $x_2$ ) that occur on either side of this peak below the detection level and to either side of *a* or *b* as shown in these figures. The points of inflection of the envelope wave were calculated directly from the definition of an inflection point. Namely, a change in the sign of the second derivative of the envelope function denotes the point of inflection. This of course assumes the second derivative of the discrete points denoting an envelope can be calculated accurately. This can be done and will be shown later in the chapter under MUAP analysis. Thus the MUAP detected is determined to be between the points  $x_1$  and  $x_2$ . The width, *N* of the MUAP detected is then given by the integer  $x_2 - x_1$  number of points. This width of the MUAP is then extended out to the nearest power of two length (i.e. 8, 16, 32, 64) in order to ease the computation



(A)

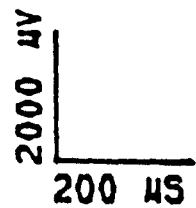


(B)



(C)

FIGURE 5.4A ENVELOPE OF A MUAP



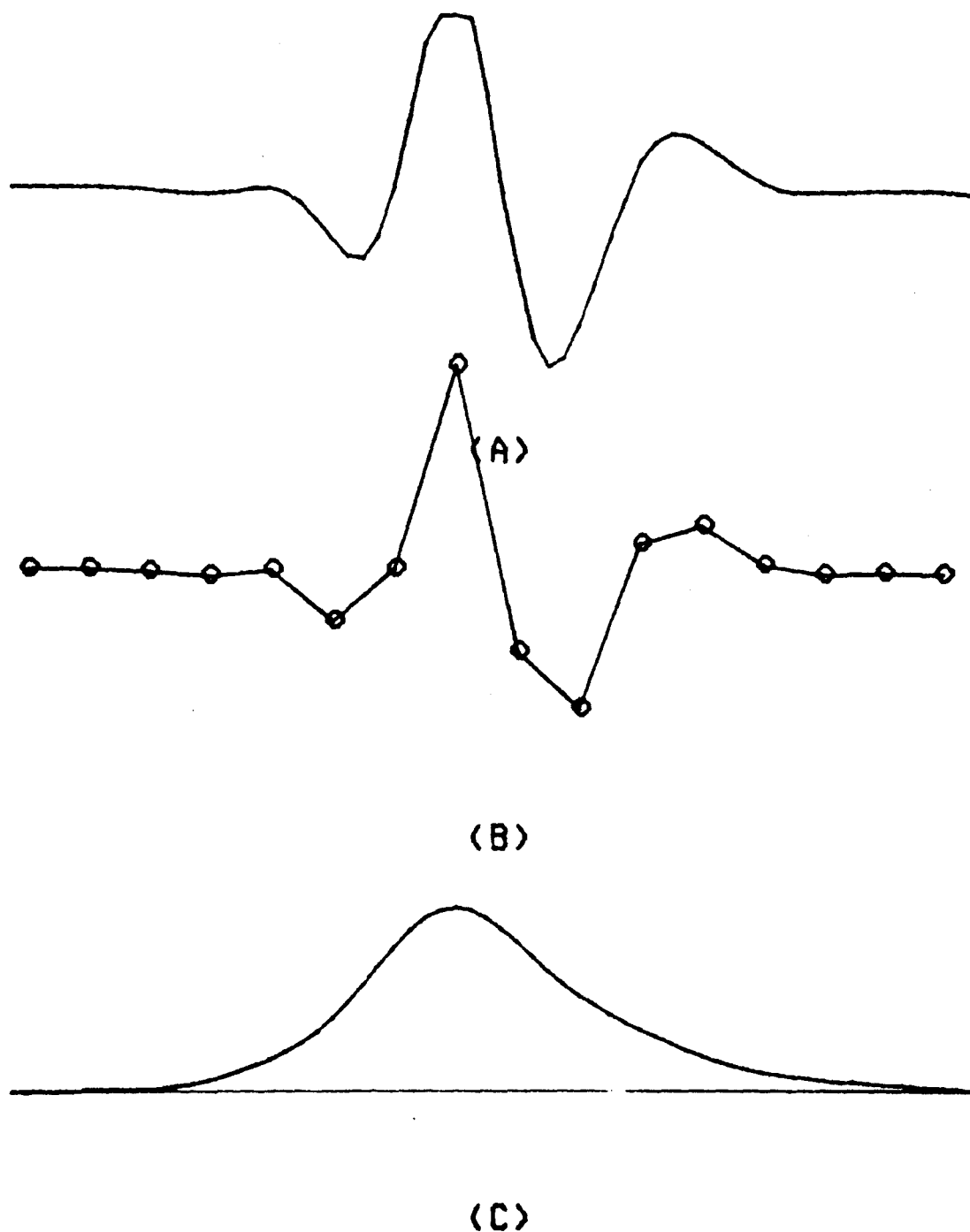
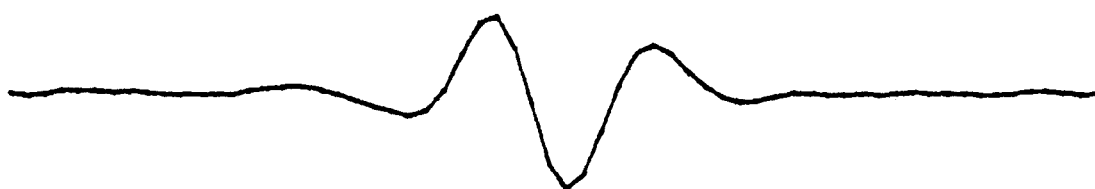
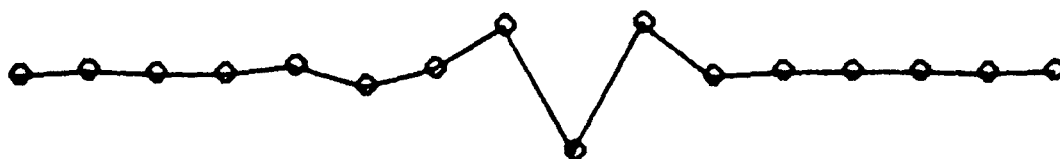


FIGURE 5.4B ENVELOPE OF A MUAP

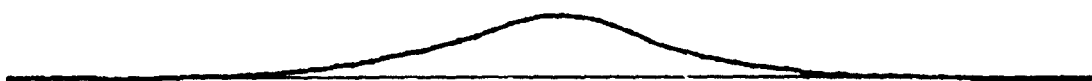
4000  $\mu$ V  
200  $\mu$ S



(A)

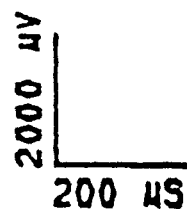


(B)



(C)

FIGURE 5.4C ENVELOPE OF A MUAP



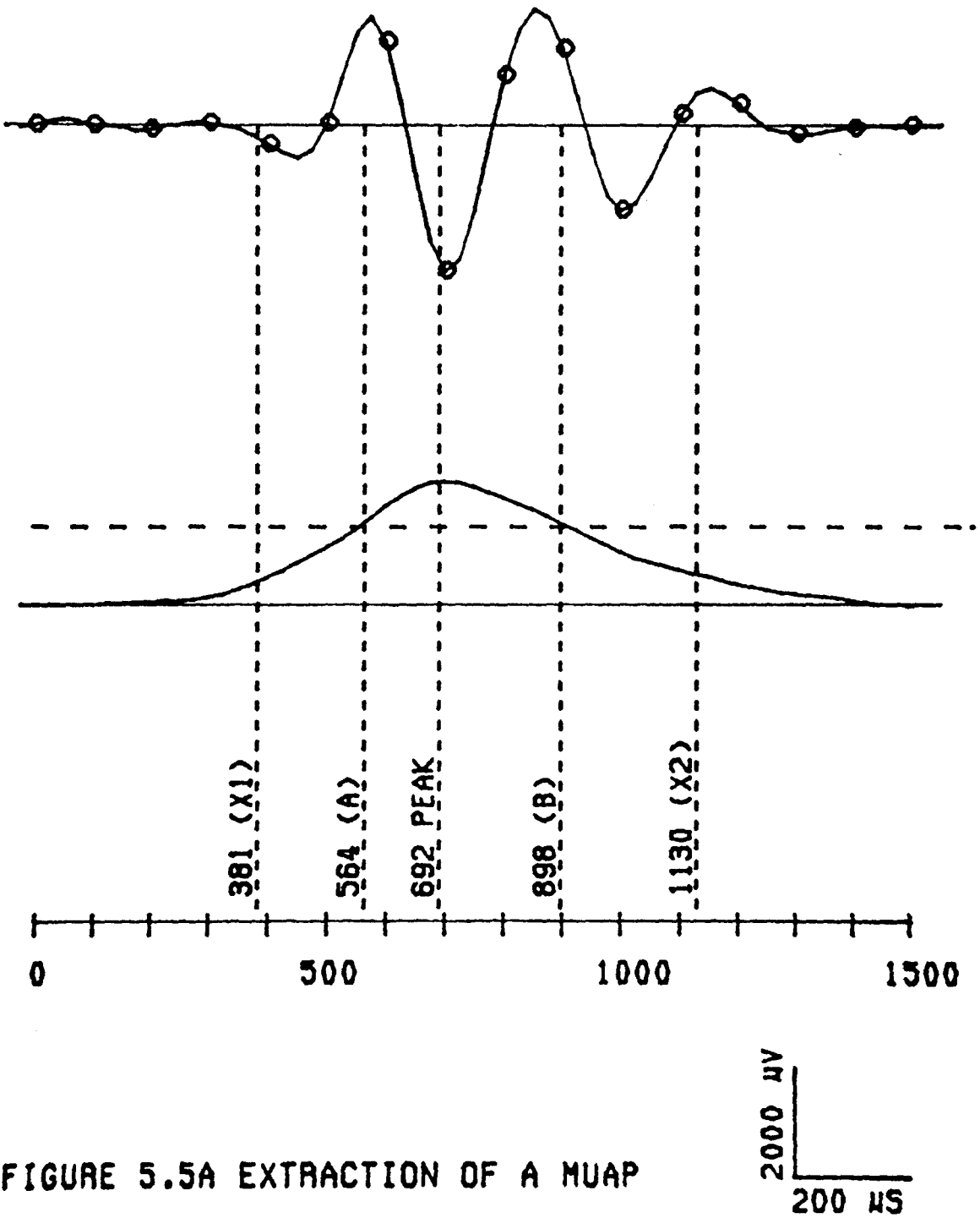


FIGURE 5.5A EXTRACTION OF A MUAP

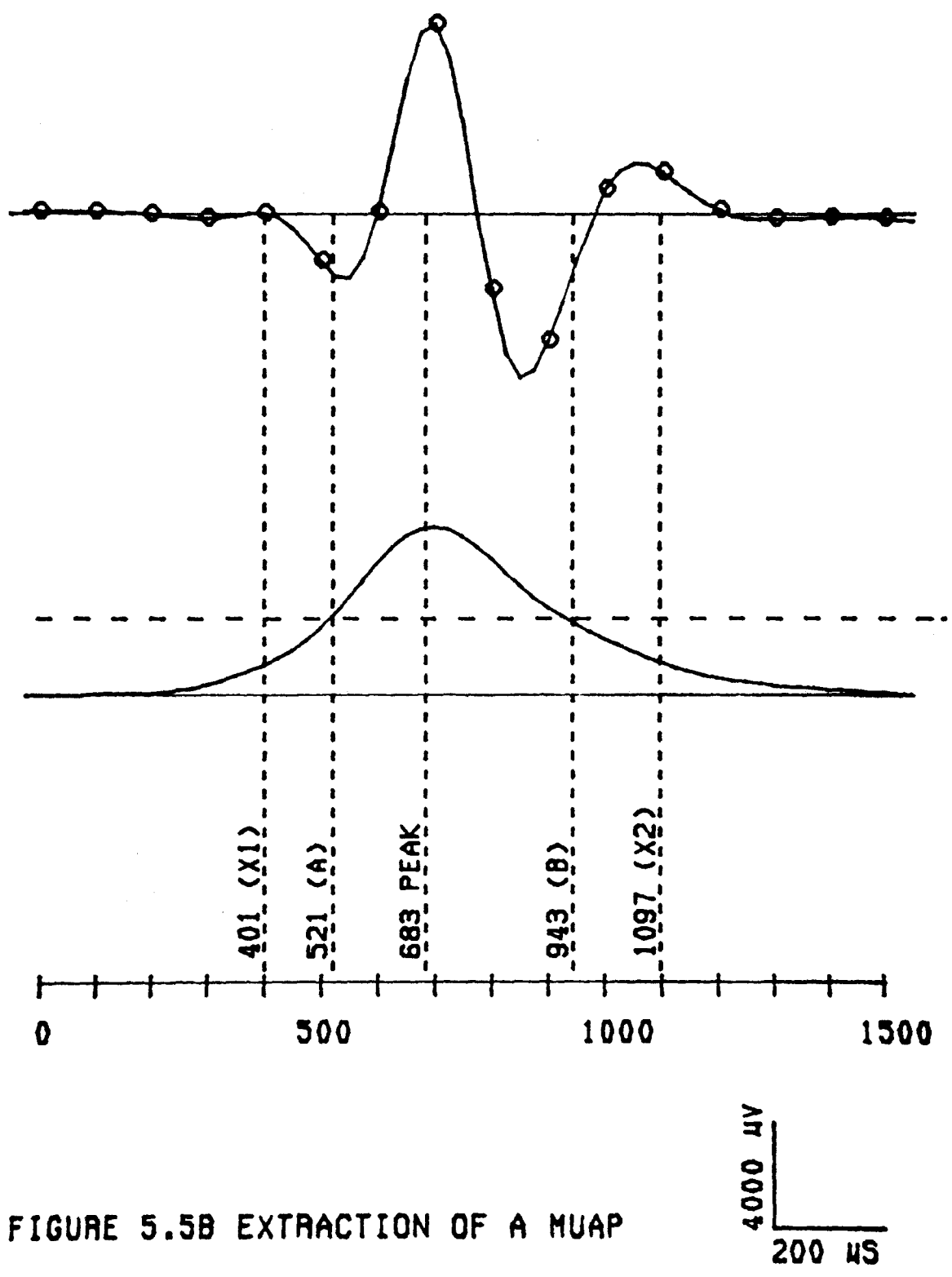


FIGURE 5.5B EXTRACTION OF A MUAP

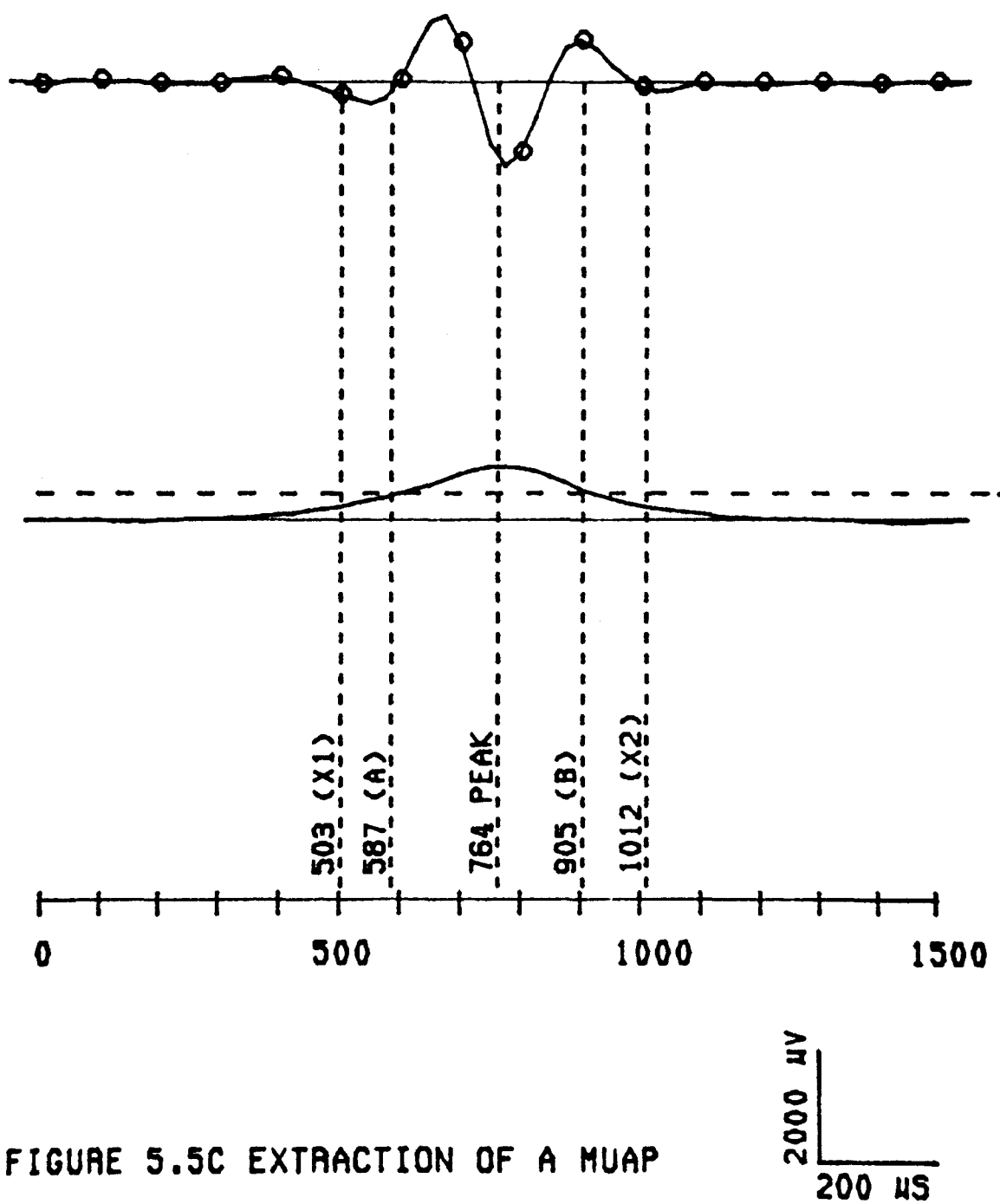


FIGURE 5.5C EXTRACTION OF A MUAP

burden required for later processing. It should be pointed out that this extending out to a power of two of the length of the MUAP is done symmetrically around the peak in an attempt to make the peak of the MUAP occur at roughly the center of the stored signal vector. Furthermore, in order to insure no discontinuities the overall MUAP stored is windowed by a Hamming window of coefficients  $W(n)$  as given by the equation:

$$W(n) = 0.54 + 0.46 \cos \left[ \frac{2\pi n}{W} \right] \quad 5.9$$

where  $W$  is the MUAP length [185]. This method used for the extraction of MUAPs from the IP makes one major assumption. That is it assumes MUAPs are relatively far apart and occur individually with no superpositioning occurring. The probability of superpositioning occurring increases with an increase in the force level of contraction. Under light to moderate contraction, superposition does occur but not to as great an extent as under strong contraction. Nevertheless, when superposition does occur the detection and extraction algorithm can be designed to accommodate this.

#### 5.1.6 Classification of MUAPs Extracted

To accommodate this problem of superpositioning, what is required is a preliminary classification of the MUAPs extracted from the EMG signal into two classes. These classes are:

- 1) single MUAPs and
- 2) superimposed MUAPs.

Furthermore, it would be beneficial if possible to know how many MUAPs are superimposed when superpositioning does occur.

There are several different types of superpositioning of MUAPs which may be detected. The first step is to determine if superposition does occur. Essentially this is reduced by the envelope detection algorithm to determining the number of peaks in the envelope above the detection threshold. The first situation in superposition occurs when an action potential has several peaks of different or the same height between the points *a* and *b* where the detection level threshold is exceeded. This is shown in Figures 5.6A and 5.6B. As can be seen, the two peaks correspond to two MUAPs in the IP. The peaks of the individual superpositioned MUAPs correspond to the peaks of the envelope detection output. It should be pointed out here that a single individual MUAP is assumed to correspond to one and only one peak (of any significant value) produced by the envelope detection method as described above. Therefore, if more than one peak in the detection envelope occurs between the points *a* and *b* then it is highly probable a superposition has occurred. As before, the inflection points are found on either side of the threshold points *a* and *b* and the superimposed MUAP complex is tagged as a superpositioning of two or more MUAPs. If the two MUAPs are superimposing closely in time then the resolution of this algorithm is diminished. As the two peaks of the MUAPs coincide this complex may then be wrongly tagged as a single

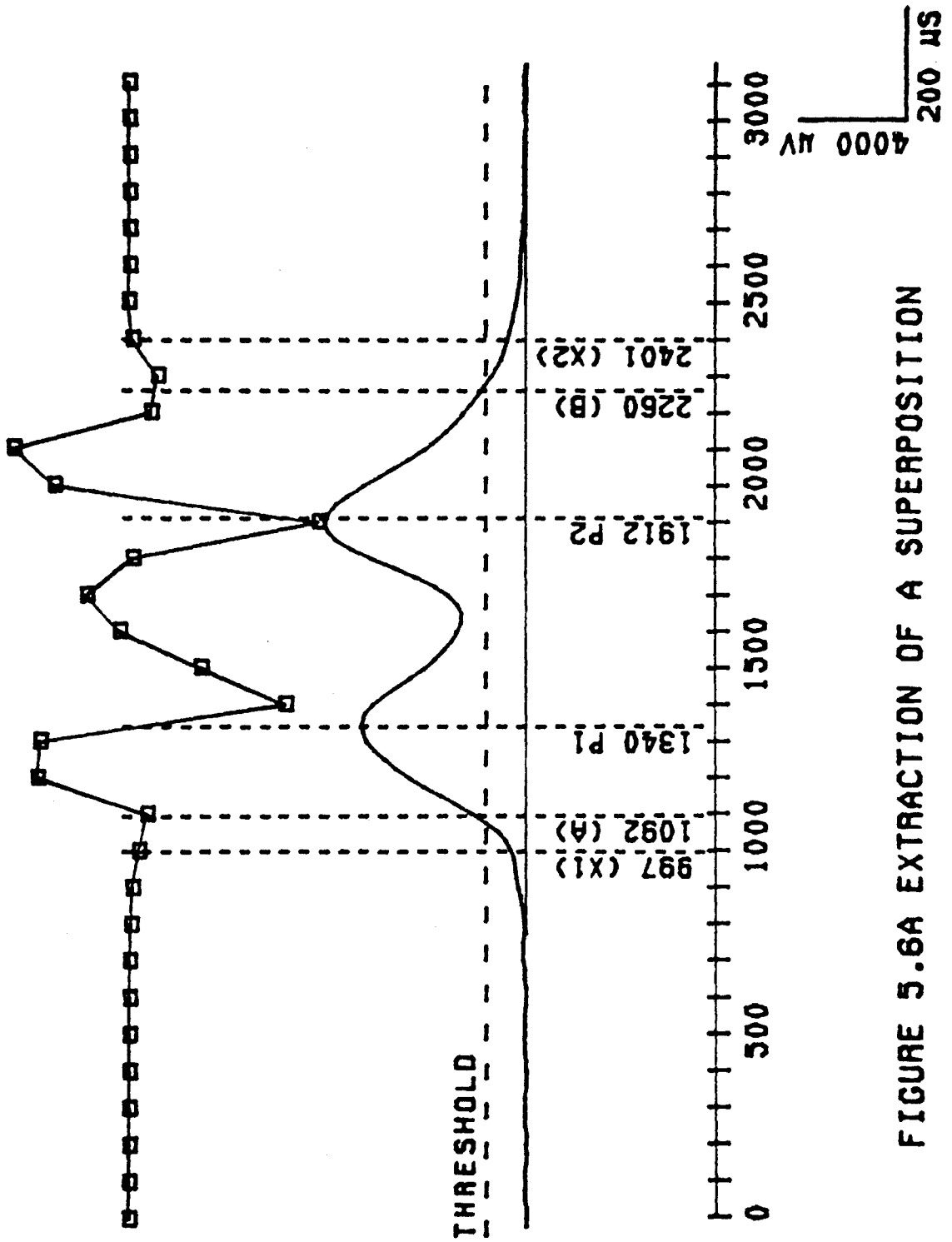


FIGURE 5.6A EXTRACTION OF A SUPERPOSITION

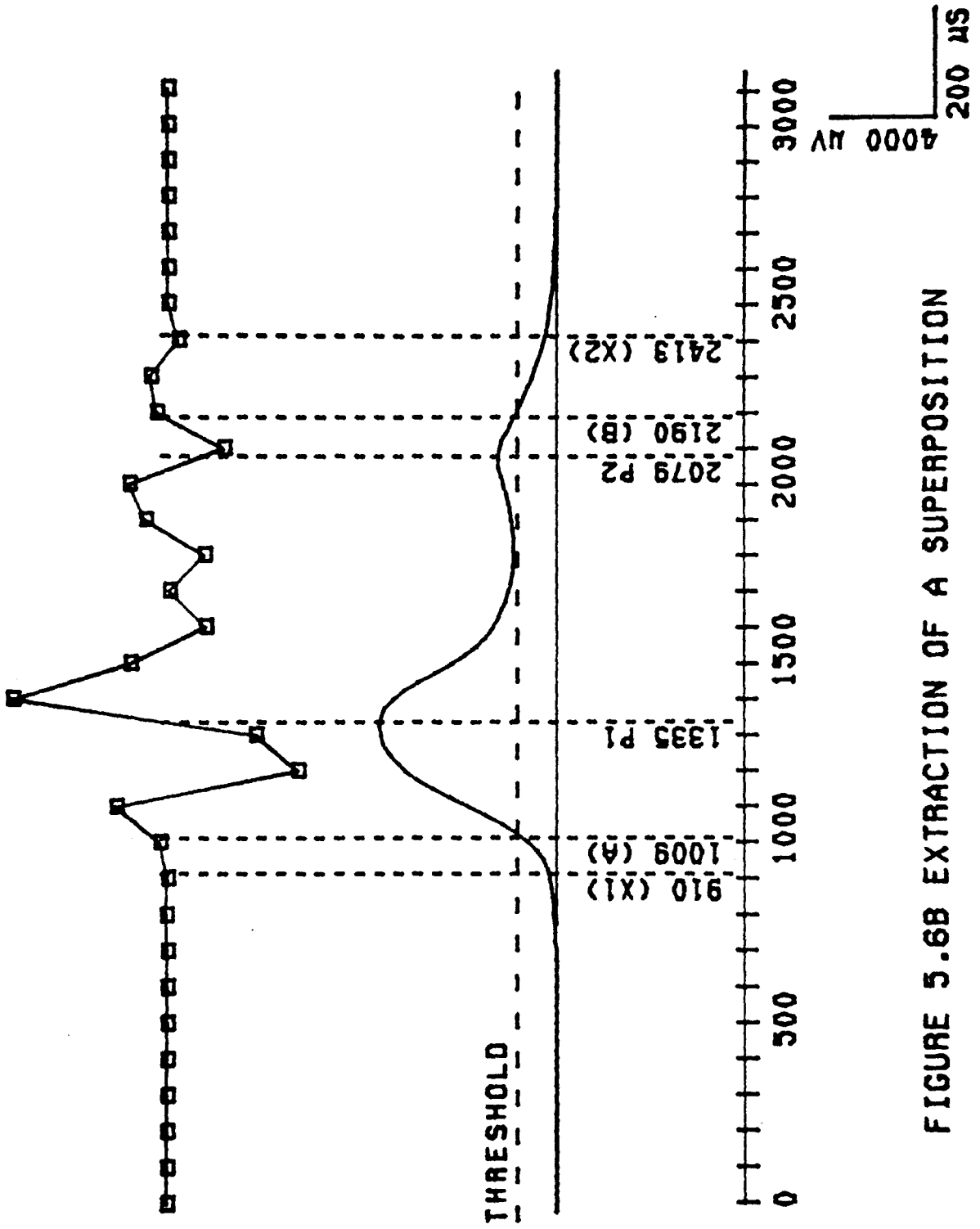


FIGURE 5.6B EXTRACTION OF A SUPERPOSITION

MUAP. The problem of correctly resolving superpositions of this nature is discussed later.

The second situation occurs when MUAPs superimpose at some distance in time. This is shown in Figures 5.6C and 5.6D. As shown in the example there is more than one interval where a peak has occurred. Thus one peak is determined to be between a and b and the other peak between c and d. The closeness of the peaks can be represented as the value of the minimum between b and c. If it does not go below  $3\sigma$  of the ambient noise level then the MUAP complex is said to be composed of two or more individual MUAPs and the entire interval between  $x_1$  and  $x_2$  is stored and later resolved into its constituent MUAPs. In addition since the high pass filter setting is 250 Hz for single fiber EMG activity recorded by the aforementioned hardware then the largest time duration of the action potential is approximately  $1/250$  of a second long. Therefore, when sampling at 10 kHz the maximum approximate duration is 40 samples. Any MUAP over 64 points long can therefore be hypothesized to be formed by the superpositioning of two or more MUAPs. Again as before, the length of this MUAP complex stored is a power of two to ease computational burden later.

So far only the separation of single MUAPs from superimposed MUAPs has been discussed. Further differentiation between single MUAPs can be done by using the envelope detection output and subsequent determination of the inflection points. The approximate duration of the MUAP is given by the length of the MUAP detected and stored. That is to say the lengths of 8, 16, 32, etc. can be used as a crude estimation of

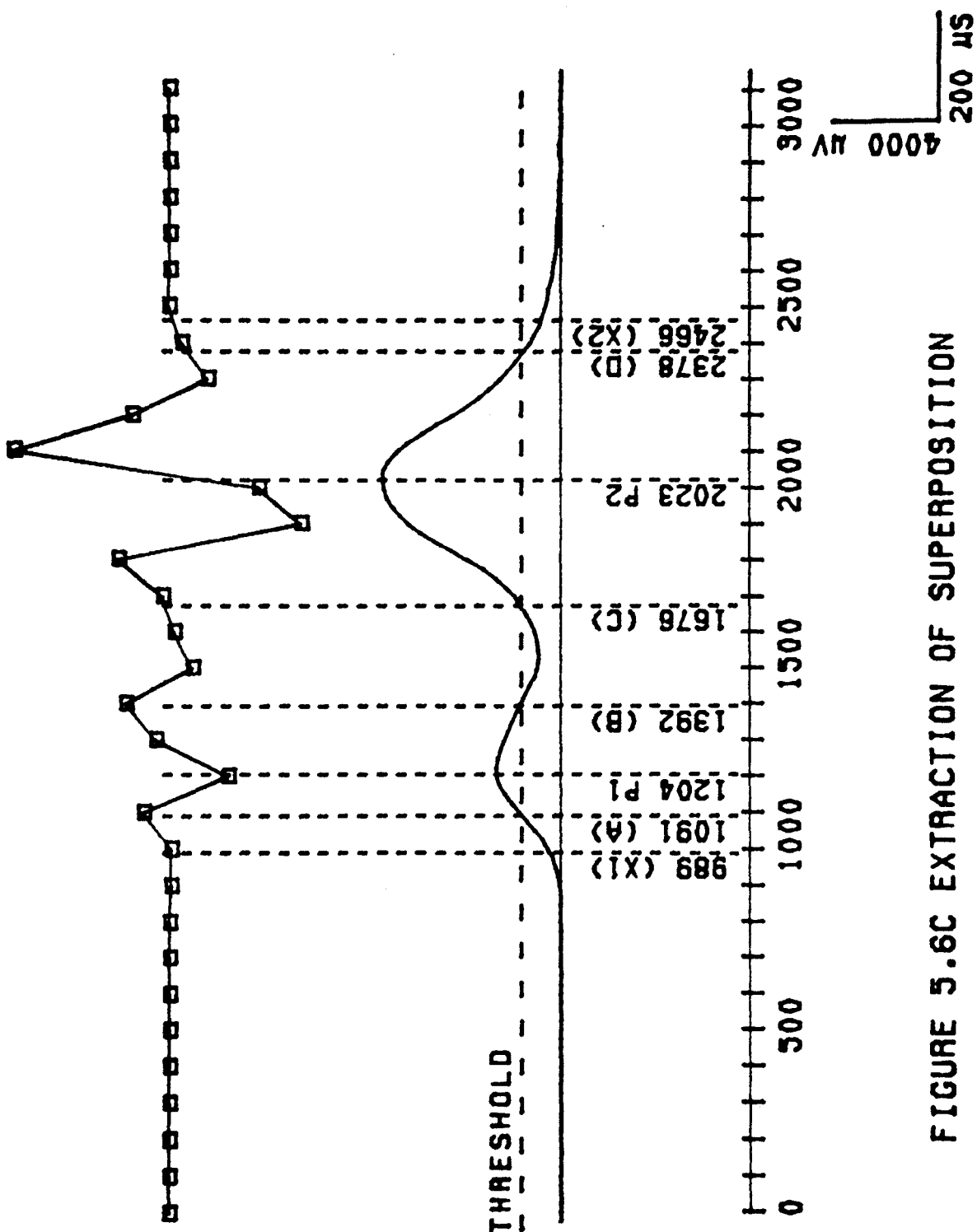


FIGURE 5.6C EXTRACTION OF SUPERPOSITION

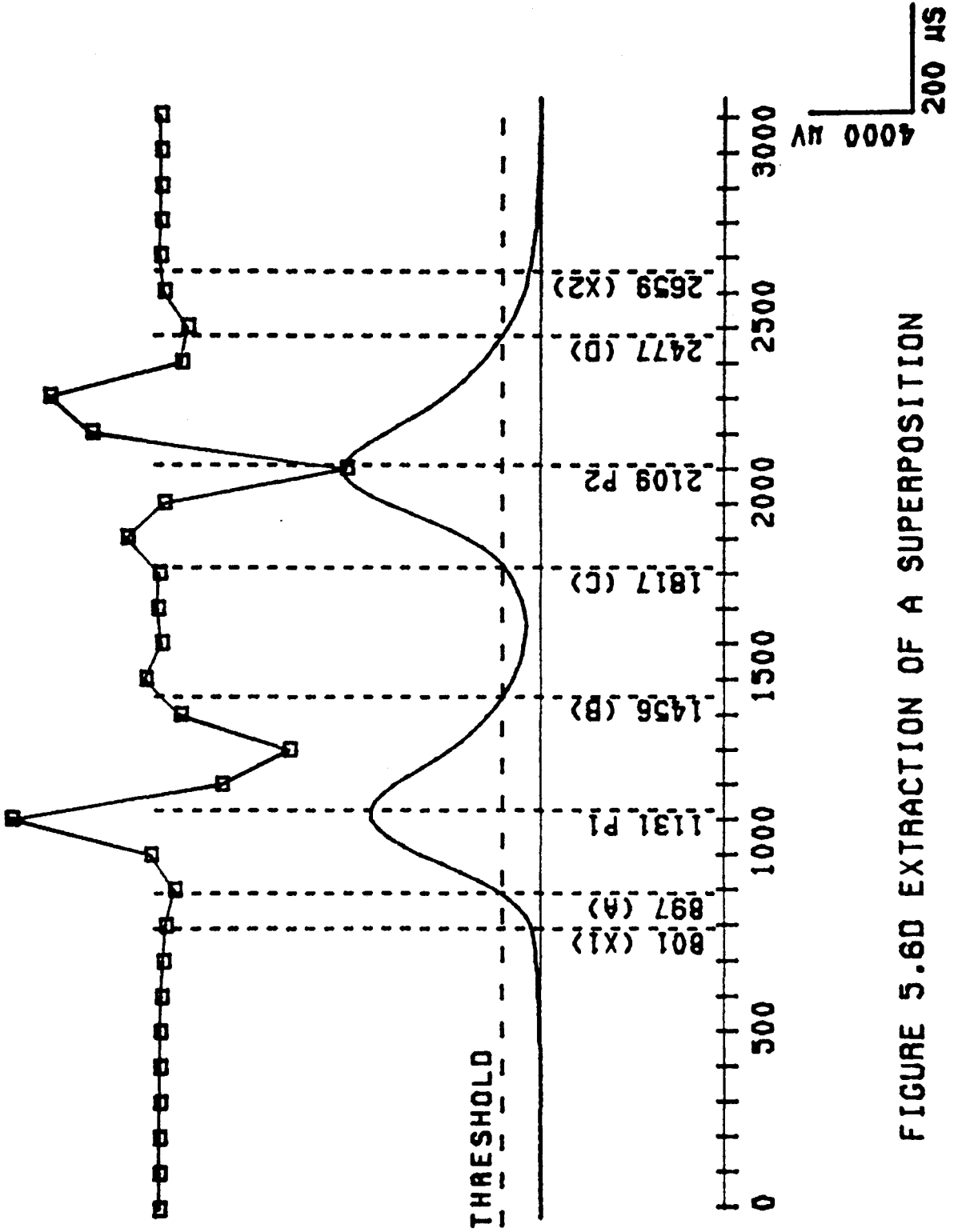


FIGURE 5.6D EXTRACTION OF A SUPERPOSITION

the duration of a particular MUAP. Thus MUAPs of similar durations can be classed together for further analysis later on.

Finally, the MUAPs separated by duration can further be separated using the peak amplitude of the envelope detector output. This is a less reliable parameter than the duration mentioned above. This is inherently due to the large variability in the amplitude of identical MUAPs resulting from Nyquist sampling of the EMG signals and the lack of any a priori knowledge of what the amplitudes of the MUAPs are for a particular contraction level.

Using this information gained from the detection envelope aids in the overall classification procedure of the MUAP. How it helps out can be seen from Figure 5.7. The crucial step in MUAP/MUAPT classification procedure is to first determine whether or not superpositioning has occurred. Furthermore the number of MUAPs superpositioned would also be beneficial. This can be done to some degree with the envelope detector as previously discussed.

## 5.2 Single Motor Unit Action Potential Analysis

Once the single MUAPs have been detected and extracted from the EMG signal further analysis can be done. Ideally for action potentials the time characteristics should be known (chapter 3). In the case of over sampled signals (i.e. significantly greater than the Nyquist rate) this is usually a straight forward procedure since no interpolations between sample points is required for accuracy in determining the characteristics of the

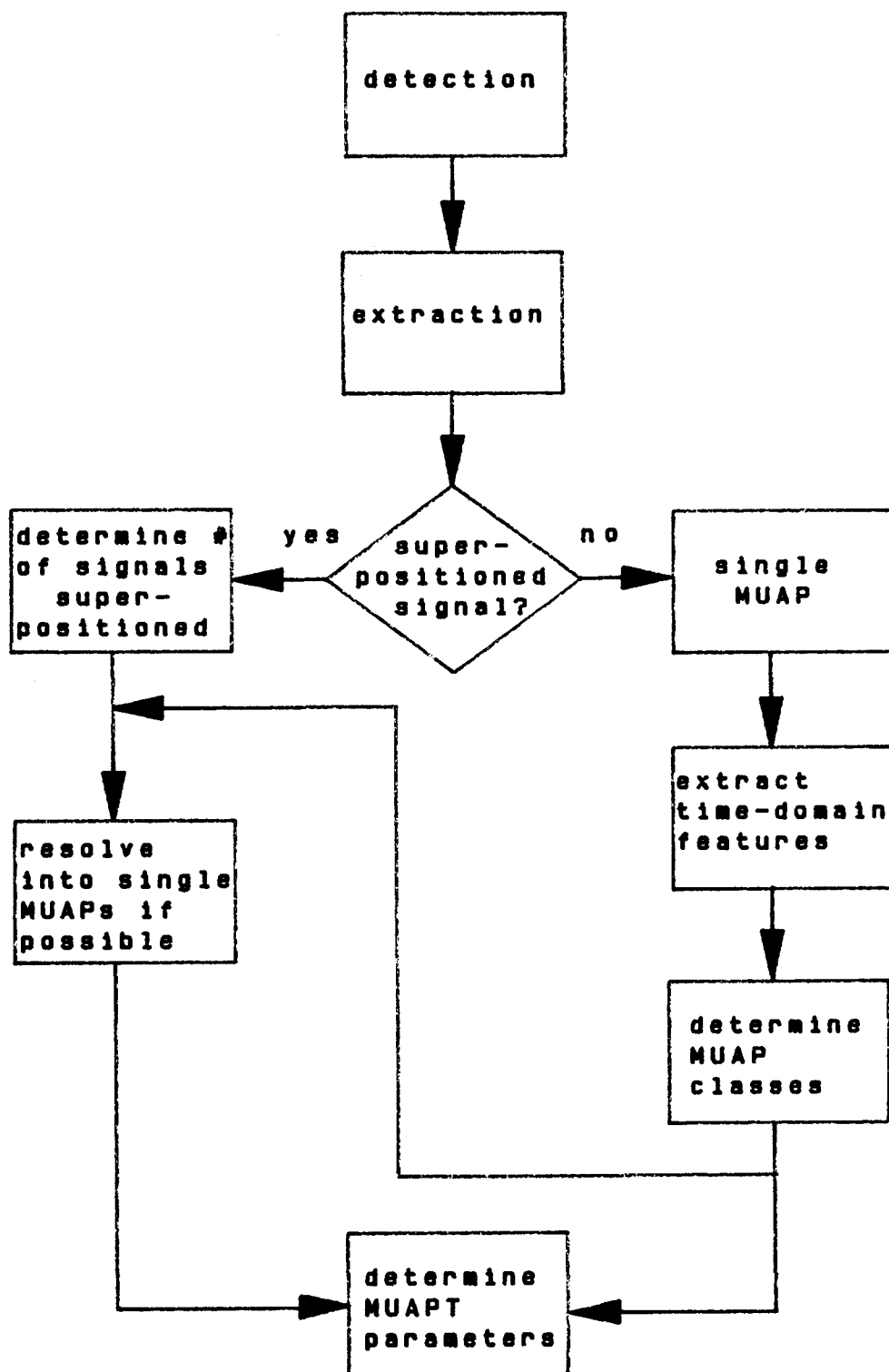


Figure 5.7 Classification procedure

MUAP. In the case of Nyquist sampled signals this straightforward method cannot be used accurately. In order to extract MUAP parameters in this latter case some sort of interpolation must be done on the time sampled action potentials. Several methods have been proposed which interpolate the MUAP by conventional means such as cubic splines. Of particular interest is the method employed by McGill and Dorfman [186] where interpolation amounts to the rotation of a signal vector in the frequency domain. This is the method employed in this thesis and is described below.

### 5.2.1 Feature Representation

One particularly convenient way to represent a vector in the time domain is to convert that vector to the frequency domain by means of the Fourier Transform (FT) [187][188]. In the frequency domain then the full brunt of the theorems and properties of the Fourier Transform may be brought to bear on the signal under question. The Fourier Transform is given by:

$$G(\omega) = \int_{-\infty}^{+\infty} g(t)e^{j\omega t} dt \quad 5.10$$

and it's inverse as:

$$g(t) = \frac{1}{2\pi} \int_{-\infty}^{+\infty} G(\omega)e^{-j\omega t} d\omega \quad 5.11$$

where  $g(t)$  is the time domain representation of a signal and  $G(w)$  is the frequency representation of the signal. The importance of the Fourier Transform lies in both the many properties it exhibits and the efficiency with which it may be computed through the use of the Fast Fourier Transform (FFT) [189].

### 5.2.2 Properties of the Fourier Transform

Of particular importance to the subsequent discussion are the following properties of the Fourier Transform:

- 1) time shifting,
- 2) differentiation,
- 3) integration and
- 3) Parseval's equation.

Adopting the following convention:

$$g(t) \Leftrightarrow G(w) \qquad 5.12$$

where  $g(t)$  is the time domain function which is transformed by the Fourier Transform operator  $\Leftrightarrow$  to the frequency domain function  $G(w)$  provides a convenient way of representing the above mentioned properties.

The time shifting property of the Fourier Transform may be expressed

as

$$g(t-t_0) \Leftrightarrow G(w)e^{j\omega t_0} \quad 5.13$$

where  $t_0$  is the value the function is shifted by in the time domain. As shown the time shifted signal  $g(t-t_0)$  is represented by the Fourier Transform of the original function  $G(w)$  multiplied by a complex exponential.

The time differentiation property of the Fourier Transform may be expressed as:

$$\frac{dg}{dt} \Leftrightarrow j\omega G(w) \quad 5.14$$

where the derivative of a function in the time domain  $g(t)$  is represented by the Fourier Transform of the original function  $G(w)$  multiplied by  $j\omega$ . Equation 5.14 can be generalized for the  $m$ 'th derivative. This is expressed by the equation:

$$\frac{d^m g}{dt^m} \Leftrightarrow (j\omega)^m G(w) \quad 5.15$$

where  $m$  is the order of the derivative.

The integration property of the Fourier Transform may be expressed as:

$$\int_{-\infty}^t g(x) dx \Leftrightarrow \frac{G(w)}{jw} + \pi G(0) \delta(w) \quad 5.16$$

where the integral of the time domain function  $g(t)$  between the time interval  $(-\infty, t)$  is represented by the Fourier Transform of the original function  $G(w)$  divided by  $jw$  and the addition of a constant. The constant  $G(0)$  is simply the area under the function  $g(t)$ . Since for all MUAP's the area under the signal is zero (ac signals ac coupled) equation 5.16 may be expressed as:

$$\int_{-\infty}^t g(x) dx \Leftrightarrow \frac{G(w)}{jw} \quad 5.17$$

Parseval's equation may be expressed as:

$$\int_{-\infty}^{+\infty} g^2(t) dt = \frac{1}{2\pi} \int_{-\infty}^{+\infty} |G(w)|^2 dw \quad 5.18$$

Essentially this states that the integral on the left hand side of equation 5.18 is the energy of the signal  $g(t)$  in the time domain. The right hand side of the equation is the expression of the signal energy in the frequency domain. Of course these must be equal.

A proof of these properties for time shifting, differentiation, and integration is given in Appendix E.

So far the properties described above were presented only in the

continuous time domain. The extension to the discrete time domain comes about from the fact that in the discrete time domain,  $N$  consecutive samples are defined as:

$$g_k = g(t_k) \quad 5.19$$

where  $k=0,1,2, \dots, N-1$  and  $t_k$  is given by:

$$t_k = k\tau \quad 5.20$$

where  $\tau$  is the sampling interval used to sample the continuous time signal. In the case of this thesis this was 1/10000 second.

According to the sampling theorem a band limited signal having its highest frequency content equal to  $f_h$  can be completely specified by its sampled sequence provided that the sampling frequency  $f_s$  is greater than twice the highest frequency of the signal being sampled. Each point of the interpolation is determined by every other sample value according to:

$$g(t) = \sum_{k=-\infty}^{+\infty} g_n \left[ \frac{\sin(\pi(t-k\tau)/\tau)}{\pi(t-k\tau)/\tau} \right] \quad 5.21$$

where  $g(t)$  is the continuous time representation of the signal,  $g_n$  is the discrete time sample of the signal and the value of the bracketed term is usually referred to as the sinc function [190]. The contribution of a sample value roughly decreases monotonically as the interval to the point

increases. The fact that the underlying continuous waveform  $g(t)$  is completely determined by its samples is used extensively in determining the characteristics of the MUAP. In order to use this property in the frequency domain the Discrete Fourier Transform (DFT) must be used.

The discrete version of the Fourier Transform for  $N$  points is given by the equation:

$$G_n = \sum_{k=0}^{N-1} g_k e^{j2\pi kn/N} \quad 5.22$$

and similarly its inverse is given by:

$$g_k = \frac{1}{N} \sum_{n=0}^{N-1} G_n e^{-j2\pi kn/N} \quad 5.23$$

where the DFT of the discrete function  $g_k$  is given by  $G_n$ . In actuality it is important to remember that where any DFT relations are concerned a finite length sequence implies one period of a periodic sequence  $g(n)$ . This is usually represented by the following equation:

$$g(n) = \sum_{r=-\infty}^{+\infty} g(n + rN) \quad 5.24$$

where  $N$  is the length of the sequence and:

$$g(n) = g(n \bmod N) \quad 5.25$$

In short then, as a sample is shifted out of the interval  $(0, N-1)$  where it is defined an identical sample enters the interval at the other end due to the periodic nature of  $g(n)$ . Thus shifting of a discrete time function is equivalent to a cylindrical shift. When using the above time shifting algorithm on MUAPs the amount of shifting required for interpolation (and later on alignment) is small when compared to the interval the discrete MUAP is defined on such that the wrap around that does occur is only at the tail ends of the MUAP which are of relatively low frequency and amplitude (and are reduced by windowing).

Thus the DFT attempts to estimate the Fourier Transform at the discrete frequency points  $f_n$  described by:

$$f_n = \frac{n}{N\tau} \quad n = 0, 1, \dots, N - 1 \quad 5.26$$

Furthermore, it can be seen that the relationship between the DFT and the FT is given by:

$$G(f_n) \cong \tau G_n \quad 5.27$$

where  $G(f_n)$  is the FT of a function  $g(t)$  at frequency  $f_n$  and  $G_n$  is the  $n$ 'th coefficient of the of the DFT of the discrete function  $g_k$ .

Following the convention adopted for the FT, the DFT can be

expressed as

$$g_k \Leftrightarrow G_n \quad 5.28$$

where  $g_k$  is the discrete time domain function which is transformed by the DFT operator to the discrete frequency domain function  $G(w)$ . The above mentioned properties can now be expressed in the discrete domain.

The time shifting property of the DFT can be easily expressed if the following convention  $g(t_k - t_\phi) = g_{k-\phi}$  is adopted then

$$g_{k-\phi} \Leftrightarrow G_n e^{j2\pi\phi n/N} \quad 5.29$$

which follows from equation 5.13. Here the discrete time shift is given by  $t_\phi$  and the discrete shifted function by  $g_{k,\phi}$  where  $\phi$  represents the amount the function is shifted. It should be pointed out here that the shift is a function of the sampling interval  $\tau$  according to the relation  $t_\phi = \phi\tau$ . Thus the rotation (shift) can theoretically be any fraction or multiple of the sampling interval though it only guarantees exactness of the discrete time domain signal vector for shifts that are integer multiples of the sampling interval.

A further simplification of the time shifting property of the DFT can be made by adopting the convention:

$$G_{n,\phi} = G_n e^{j2\pi\phi n/N} \quad 5.30$$

where the DFT of a discrete time domain function rotated (shifted) by  $\phi$  is represented by  $G_{n,\phi}$ .

Applying the above relation to equation 5.23 gives an expression for the discrete time signal of phase shift  $\phi$  as:

$$g_{k-\phi} = \frac{1}{N} \sum_{n=0}^{N-1} G_{n,\phi} e^{-j2\pi kn/N} \quad 5.31$$

This is an important result. What this equation states is that the value of discrete signal  $g_k$  at a particular phase shift  $\phi$  from  $k$  can be found by the normalized summation of the DFT coefficients multiplied by the complex exponential associated with the phase shift  $\phi$ . This complex exponential has a magnitude of one and a phase of  $k\phi$  as expressed by equation 5.30.

The discrete time differentiation property of the DFT may be expressed in a likewise manner. Since  $w = 2\pi f_n$  then from equation 5.26 the discrete radial frequency  $w_k$  can be represented by:

$$w_k = \frac{k2\pi}{N\tau} \quad 5.32$$

If the derivative of a discrete time function is represented by  $\frac{dg(t_k)}{dt_k}$  then the differentiation of a DFT may be expressed as:

$$\frac{dg(t_k)}{dt_k} = \frac{dg_k}{dk} \Leftrightarrow G_n(j\frac{2\pi k}{N}) \quad 5.33$$

where the derivative of the discrete time function  $g_k$  is represented by the DFT of the function  $G_n$  multiplied by  $\frac{j2\pi k}{N}$ . As with the analog case the  $m$ 'th derivative of the discrete time sample is given by:

$$\frac{d^m g_k}{dk^m} \Leftrightarrow G_n \left[ \frac{j2\pi n}{N} \right]^m \quad 5.34$$

where  $m$  is the order of the derivative.

Substituting relation 5.34 into equation 5.23 gives the equation:

$$\frac{d^m g_k}{dk^m} = \frac{1}{N} \sum_{n=0}^{N-1} G_n \left[ \frac{j2\pi n}{N} \right]^m e^{-j2\pi kn/N} \quad 5.35$$

Hence the  $m$ 'th derivative of the discrete time function  $g_k$  is given by the normalized summation of the DFT coefficient  $G_n$  multiplied by the value  $\left[ \frac{j2\pi n}{N} \right]^m$  [133]. Therefore, the derivative of a discrete time function can easily be found from the DFT coefficients.

The discrete time integration property may be expressed as an approximation to the integration of the function  $g(x)$  over the interval  $(a, b)$  given in the continuous time case as:

$$g_I(x) = \int_a^b g(t)dt = \int_{a_k}^{b_k} g(t_k)d(t_k) = \int_{a_k}^{b_k} g_k d_k \quad 5.36$$

where the continuous interval  $(a, b)$  becomes the discrete interval  $(a_k, b_k)$ . This interval can be approximated in discrete time by:

$$\int_{a_k}^{b_k} g_k d_k \Leftrightarrow \frac{G_{b_k}}{\left(\frac{j2\pi n}{N}\right)} - \frac{G_{a_k}}{\left(\frac{j2\pi n}{N}\right)} + G_0(b_k - a_k) \quad 5.37$$

where the discrete integral on the interval  $(a_k, b_k)$  is given by the DFT coefficient  $G_{b_k}$  associated with the discrete frequency  $\frac{b_k}{N}$  divided by the quantity  $\left(\frac{j2\pi n}{N}\right)$  which is added to the negative quantity of the DFT coefficient  $G_{a_k}$  associated with the frequency  $\frac{a_k}{N}$  divided by the quantity  $\left(\frac{j2\pi n}{N}\right)$ . It is important to note that the above relation is not defined at zero frequency (dc values). A dc value  $G_0$  is only present if the signal under scrutiny has a non-zero mean. Thus  $G_0$  is zero for MUAPs. Substituting relation 5.37 into relation 5.23 gives the equation for the integral of a discrete function in terms of the DFT as:

$$\int_{a_k}^{b_k} g_k d_k = \frac{1}{N} \sum_{n=1}^{N-1} \left[ \frac{G_{b_k}}{\left(\frac{j2\pi n}{N}\right)} - \frac{G_{a_k}}{\left(\frac{j2\pi n}{N}\right)} \right] + G_0(b_k - a_k) \quad 5.38$$

Equations 5.38 and 5.35 can be used directly for calculating the integrals and derivatives of a discretely sampled MUAP. Figures 5.8A (5.8B) and 5.9A (5.9B) show the first and second derivatives and integrals of an over sampled (four times the Nyquist rate) MUAP. Clearly the derivatives and integrals plotted in these figures look right. However, over

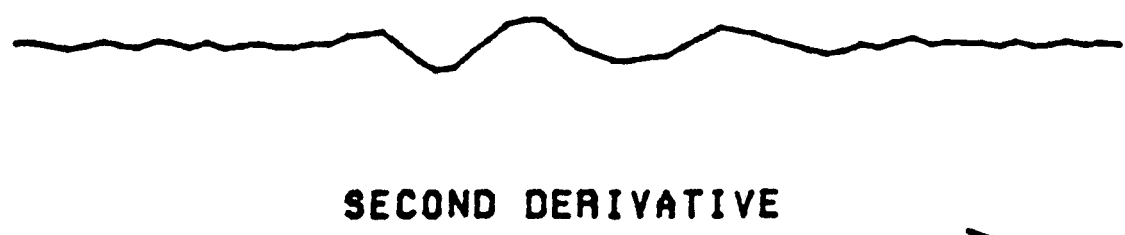
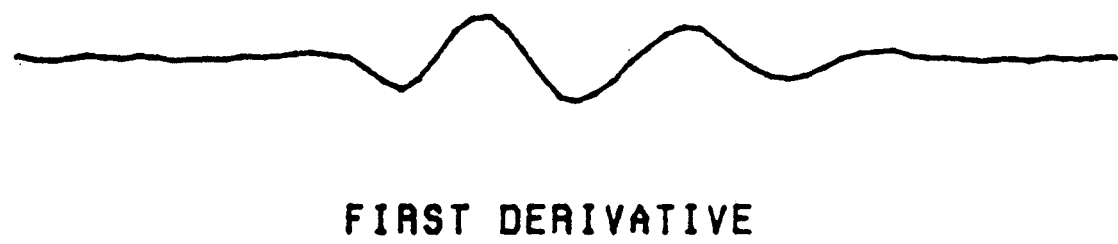
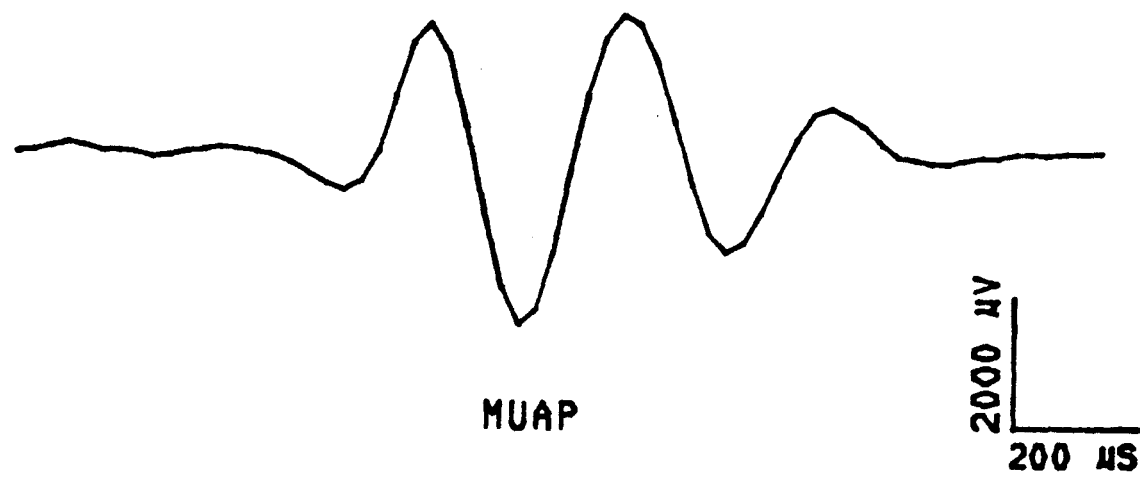
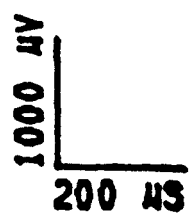


FIGURE 5.8A DERIVATIVES OF A MUAP



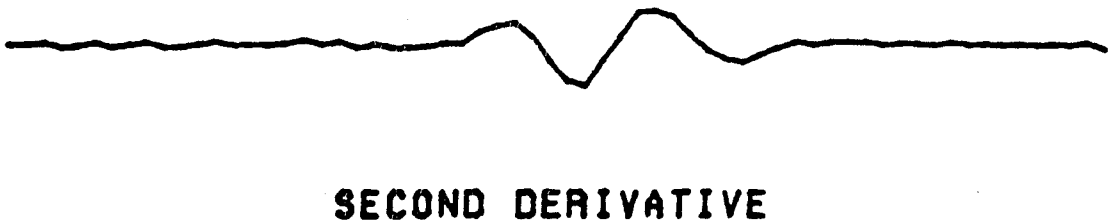
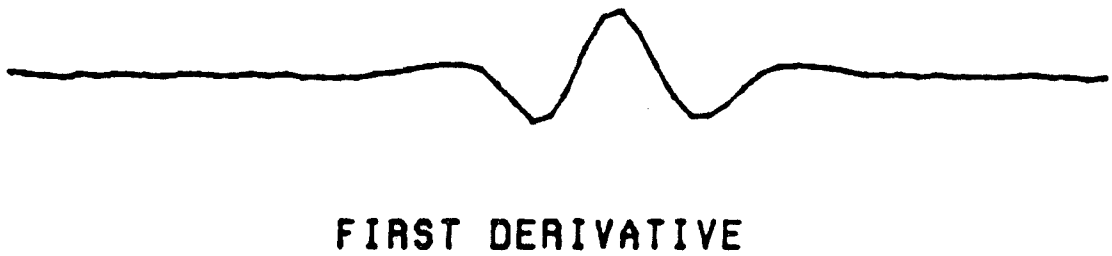
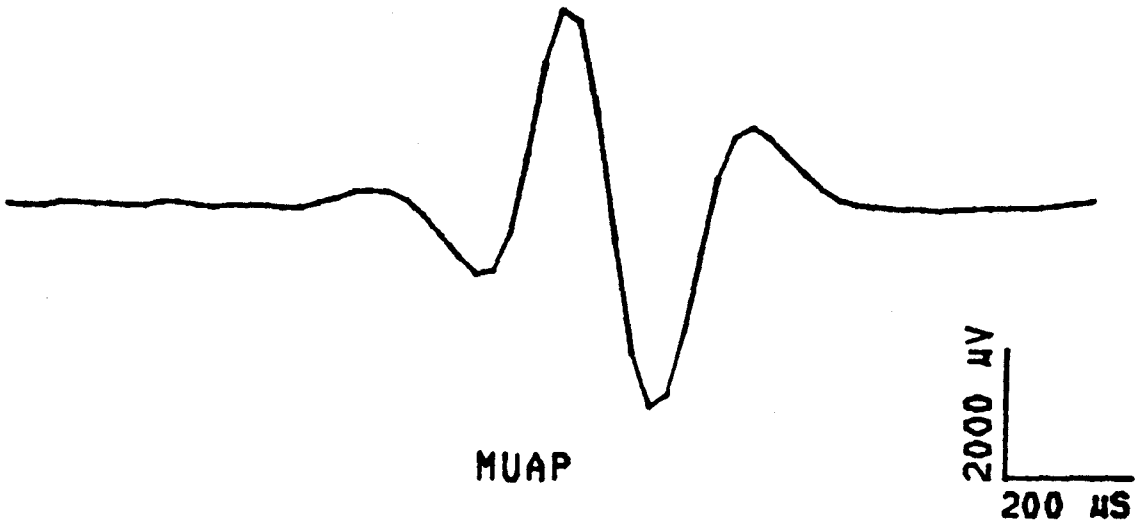
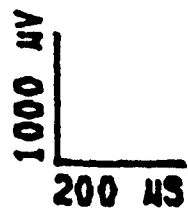


FIGURE 5.8B DERIVATIVES OF A MUAP



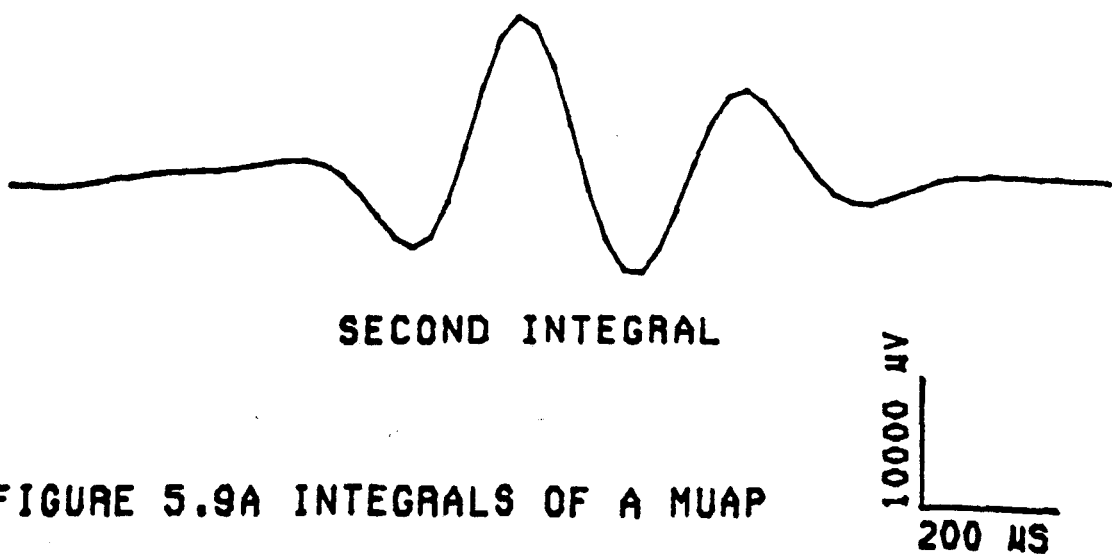
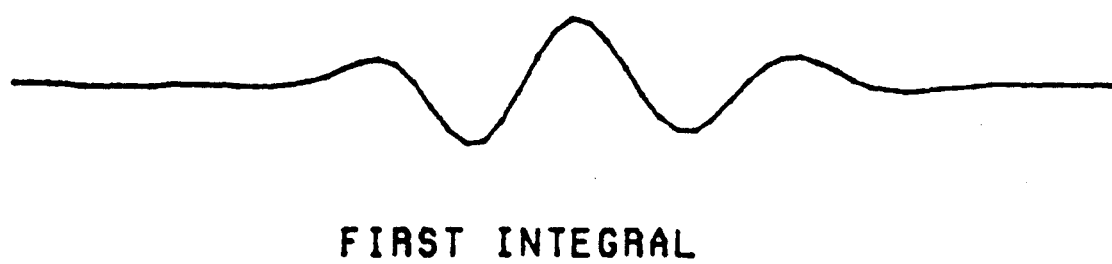
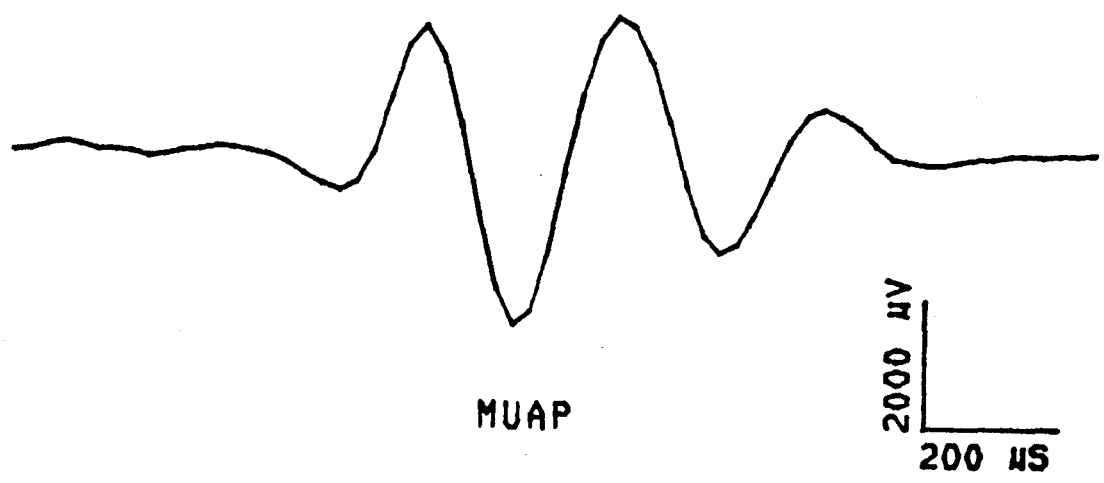


FIGURE 5.9A INTEGRALS OF A MUAP

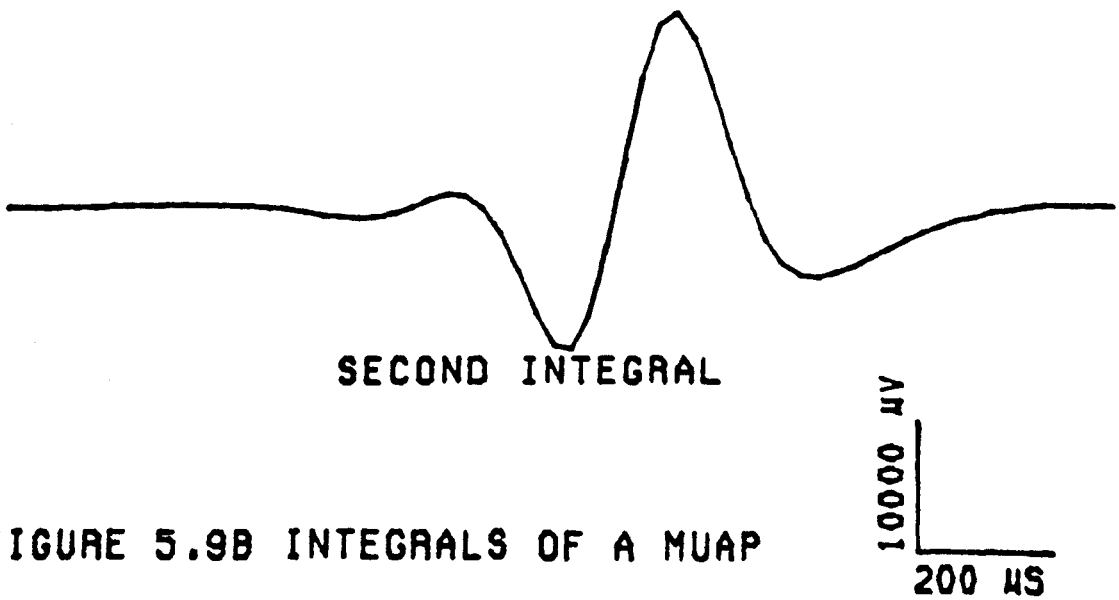
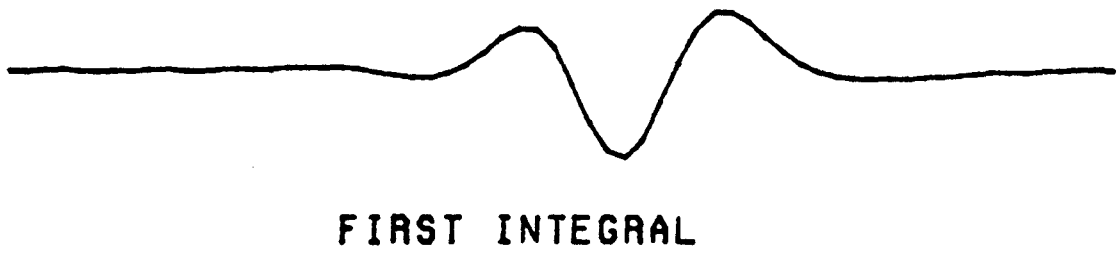
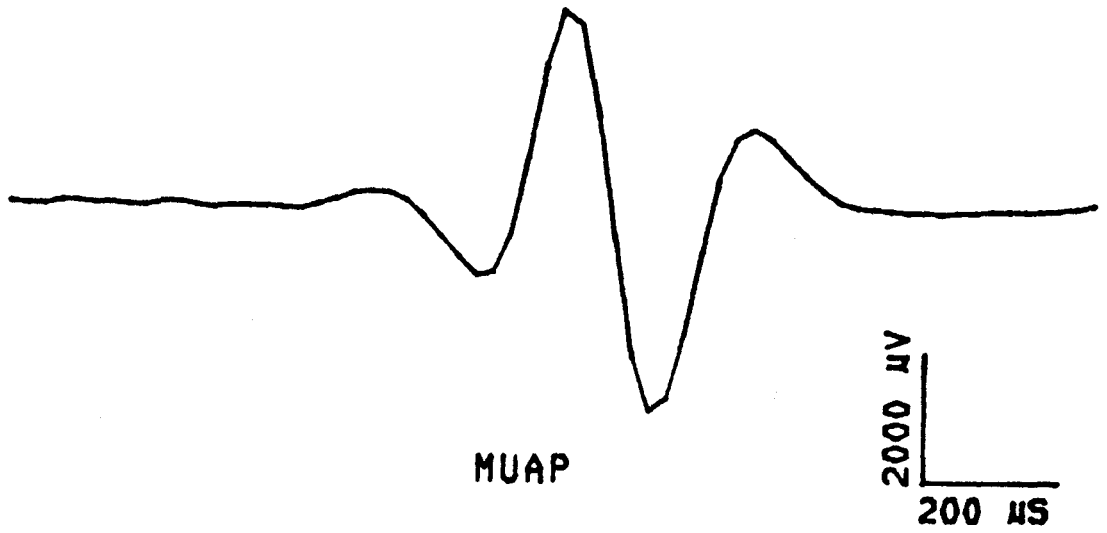


FIGURE 5.9B INTEGRALS OF A MUAP

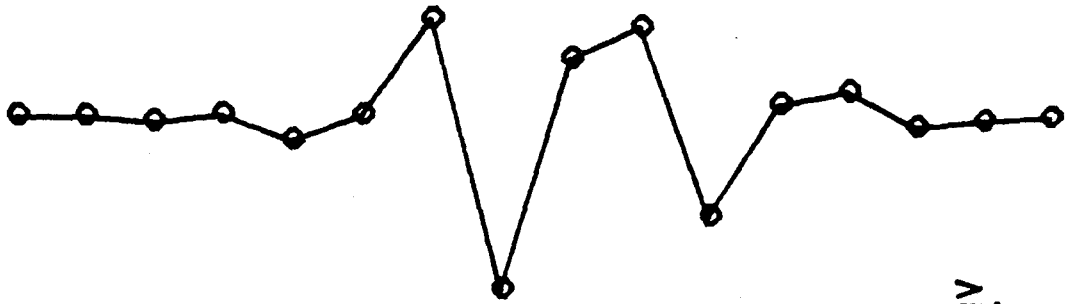
sampled signals are not required. The above derived equations are valid for any sampled signal as long as it meets the Nyquist sampling criterion. Figures 5.10a (5.10c) and 5.10b (5.10d) and Figures 5.11a (5.11c) and 5.11b (5.11d) show the first and second derivatives and integrals respectively of the same Nyquist sampled MUAP. Clearly from Figures 5.10a through 5.10d the effect of differentiation on the MUAP signal is to enhance the higher frequency content of the signal (notice the change in the vertical scales). From Figures 5.11a through 5.11d it can be seen that the effect of integration is to suppress the higher frequency content of the signal. The correctness of these waveforms and hence the equations is demonstrated in the next section when determining MUAP characteristics.

It should be noted that the above equations for the derivative and the integral of the discrete function  $g_k$  can be combined with the time shift property to yield a more powerful equation. For the derivative of a discrete function phase shifted by  $\phi$   $g_{k,\phi}$  the following equation can be derived (Appendix E):

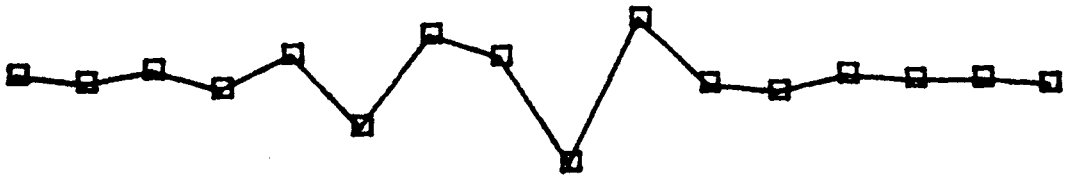
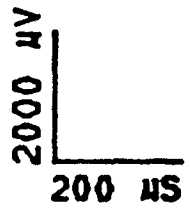
$$\frac{d^m g_{k-\phi}}{d\phi^m} = \frac{1}{N} \sum_{n=0}^{N-1} \left[ \frac{j2\pi n}{N} \right]^m G_{n,\phi} e^{-j2\pi kn/N} \quad 5.39$$

This above equation can be simplified as shown in appendix E to the form:

$$\frac{d^m g_{\theta}}{d\theta^m} = -\frac{2}{N} \sum_{n=1}^{N/2-1} \text{Im} \left\{ G_{n,\theta} \left[ \frac{j2\pi n}{N} \right]^{m-1} \right\} \quad 5.40$$

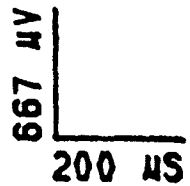


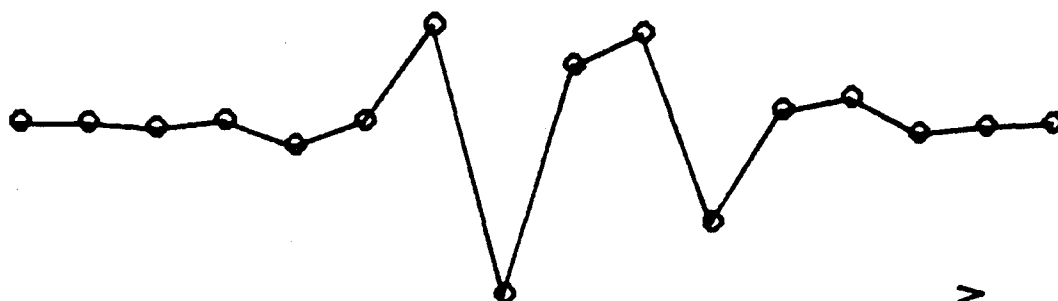
NYQUIST WAVEFORM



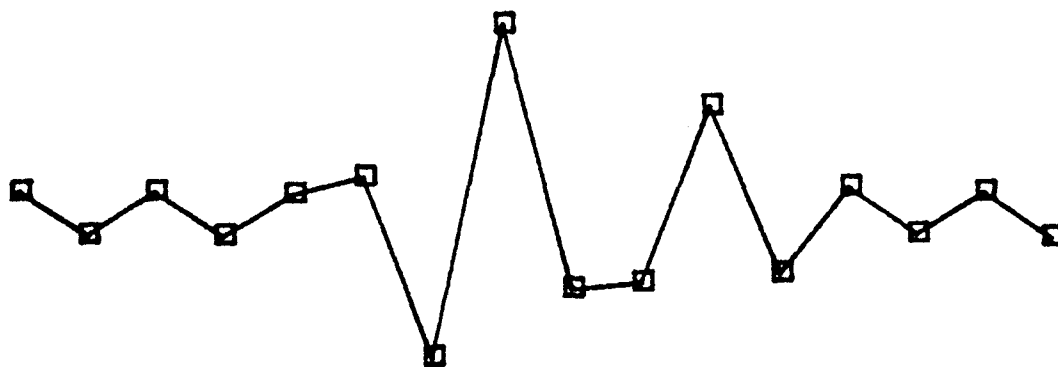
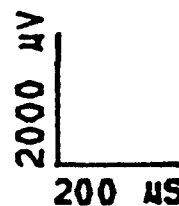
FIRST DERIVATIVE

FIGURE 5.10A FIRST NYQUIST DERIVATIVE





NYQUIST WAVEFORM



SECOND DERIVATIVE

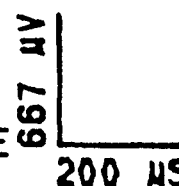
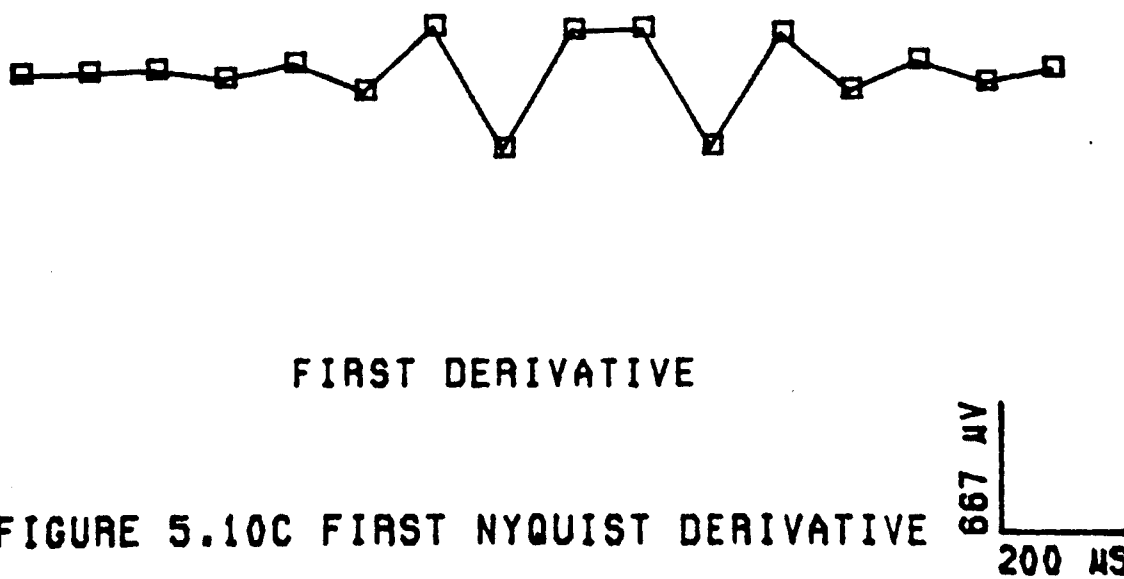
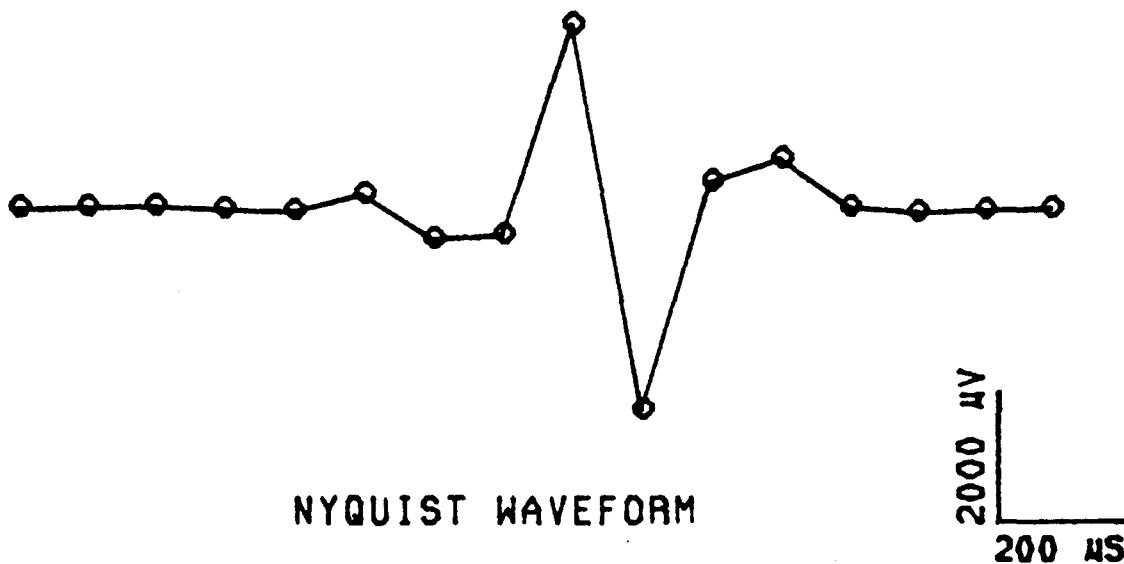
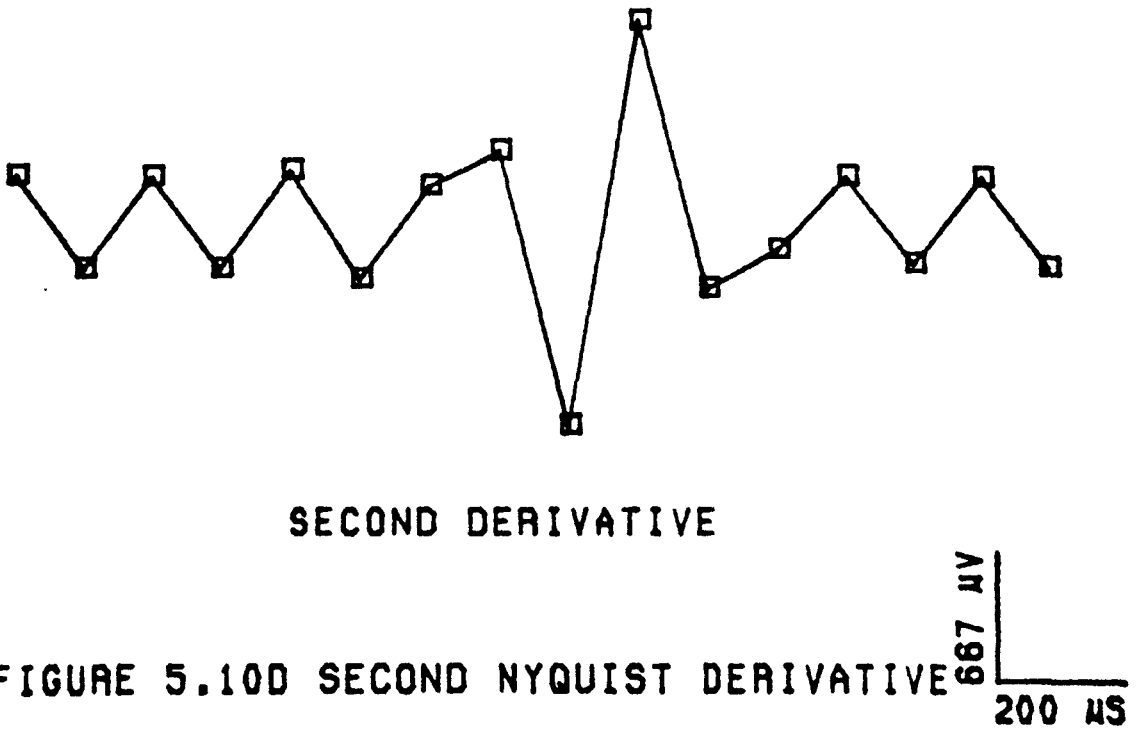
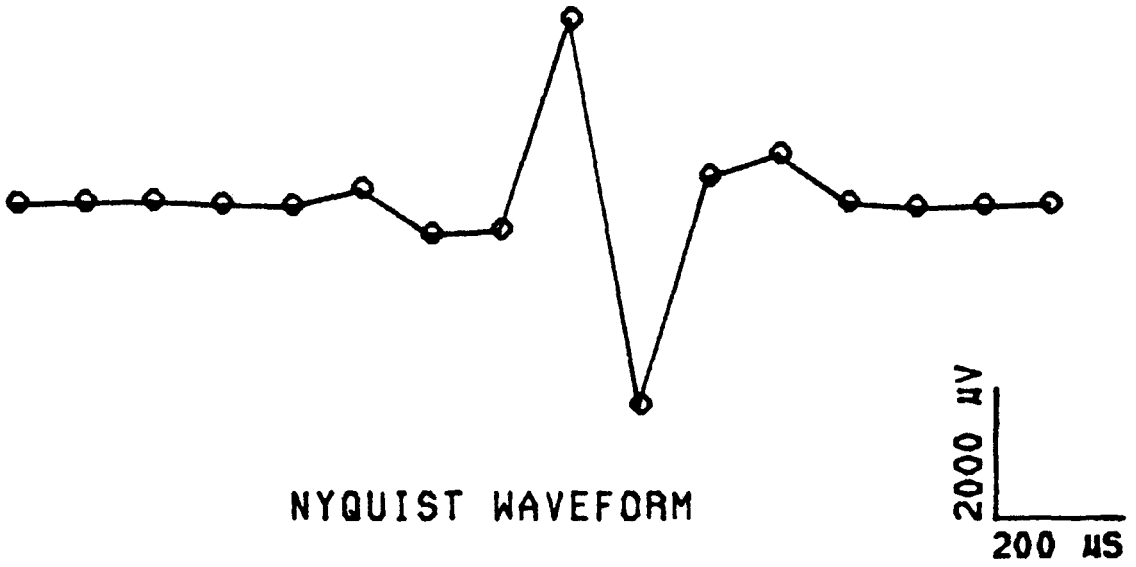
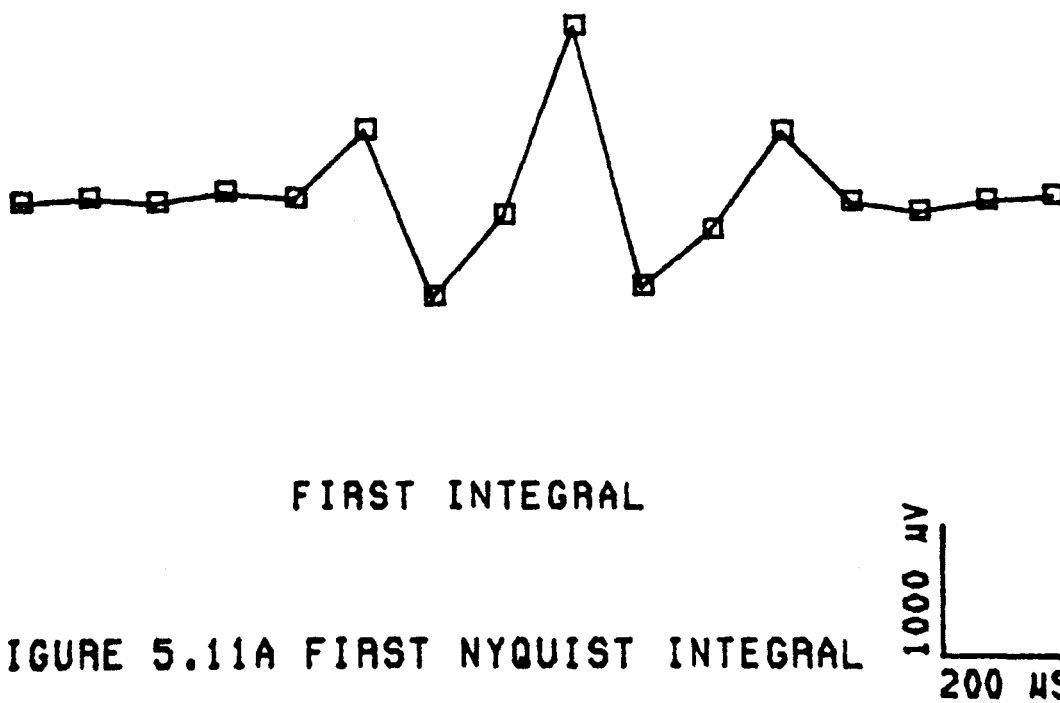
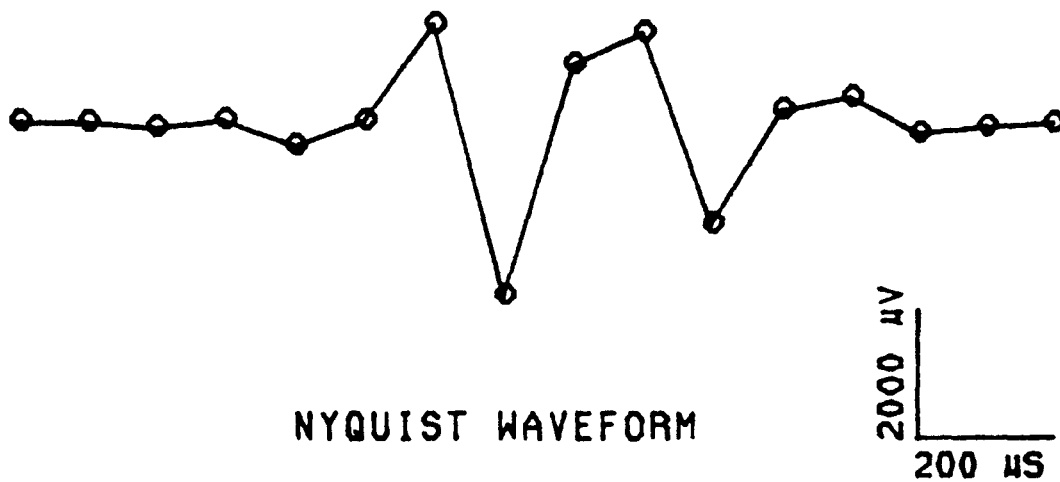
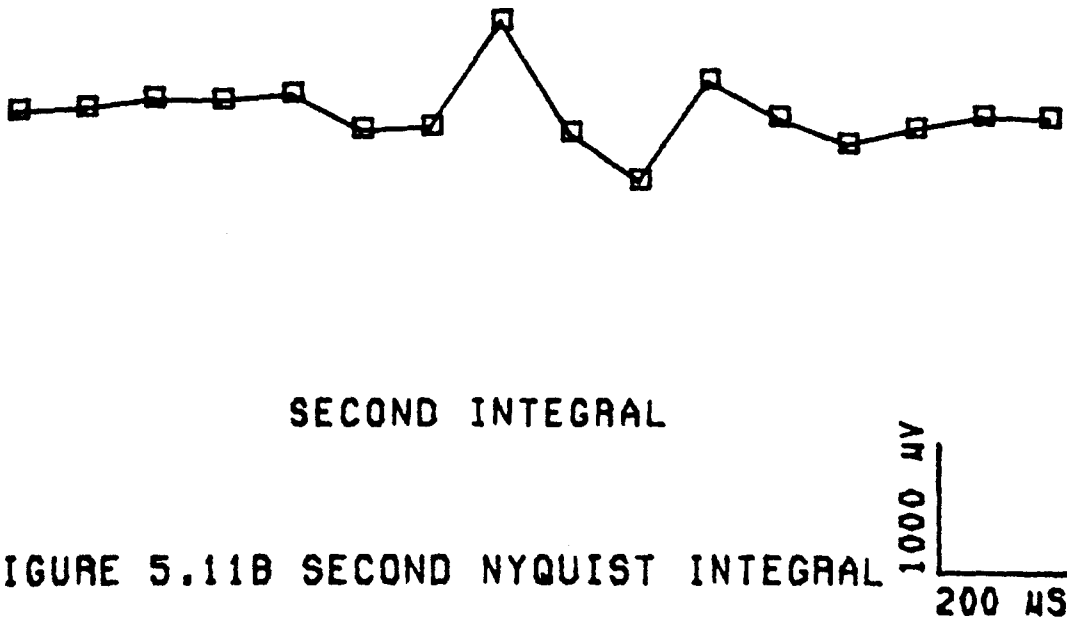
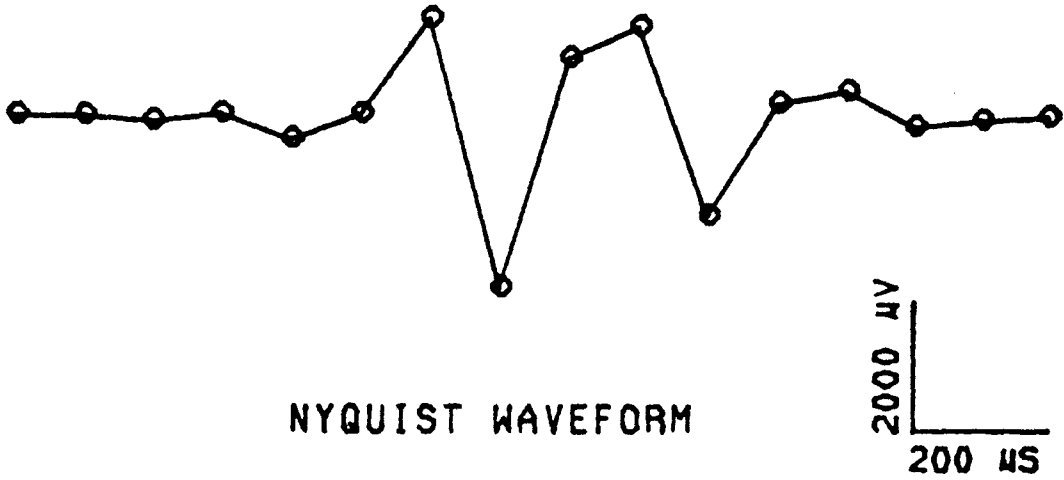


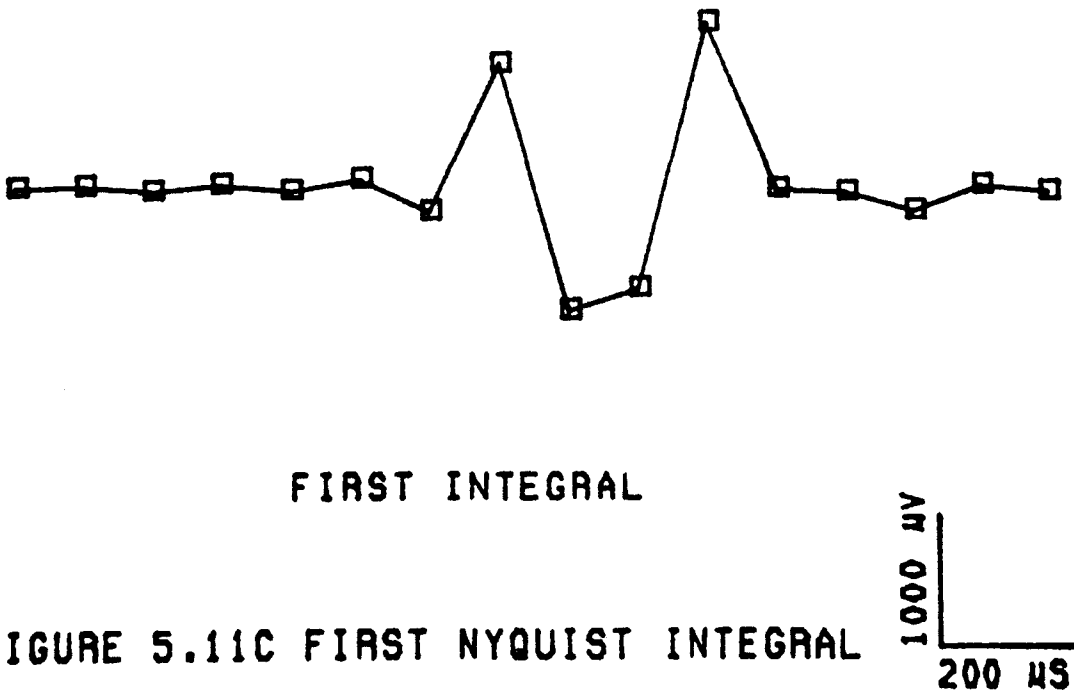
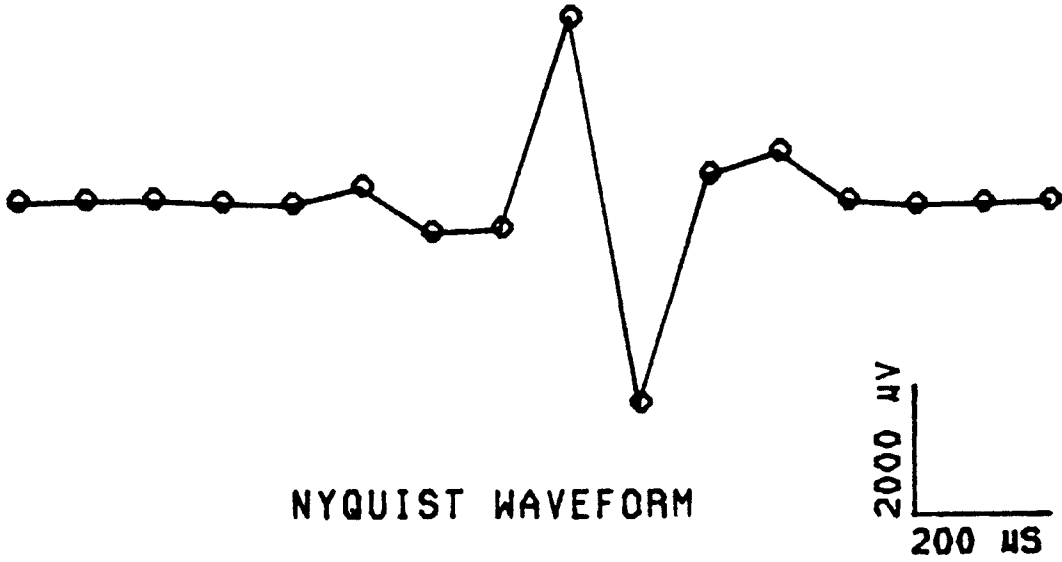
FIGURE 5.10B SECOND NYQUIST DERIVATIVE

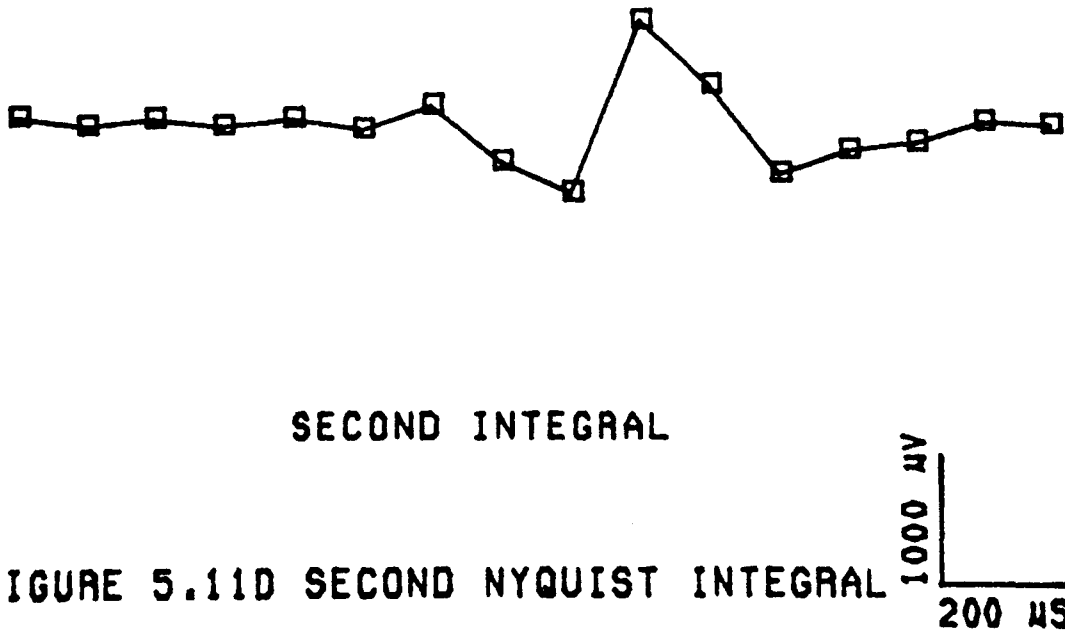
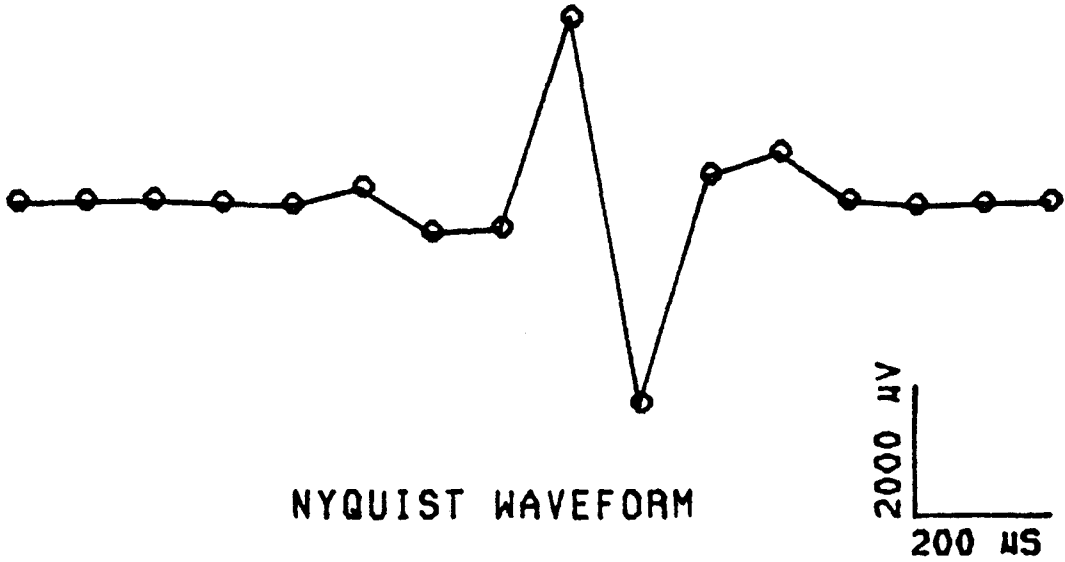












where  $\theta = k - \phi$ .

Similarly the discrete integration formula may be written as:

$$\int_{a_k}^{b_k} g_{k-\phi} = \frac{G}{N} (b-a) + \frac{1}{N} \sum_{n=1}^{N-1} \left[ \frac{G_{n,b}}{(j\frac{2\pi n}{N})} - \frac{G_{n,a}}{(j\frac{2\pi n}{N})} \right] e^{-j2\pi kn/N} \quad 5.41$$

$$\int_{a_k}^{b_k} g_{k-\phi} = \frac{1}{N} \sum_{n=1}^{N-1} \left[ \frac{G_{n,b}}{(j\frac{2\pi n}{N})} - \frac{G_{n,a}}{(j\frac{2\pi n}{N})} \right] e^{-j2\pi kn/N} \quad 5.42$$

These equations can then be used to calculate the integral or derivative of the MUAP at points other than the discretely sampled ones.

In the discrete time domain the representation of Parseval's equation is given by the expression:

$$\sum_{k=0}^{N-1} |g_k|^2 = \frac{1}{N} \sum_{n=0}^{N-1} |G_n|^2 \quad 5.43$$

where  $|G_n|^2$  and  $|g_k|^2$  are the magnitude squared of  $G_n$  and  $g_k$  respectively. This theorem is a direct consequence of the correlation property and in fact is a measure of autocorrelation, hence:

$$\sum_{k=0}^{N-1} x_k^2 = \sum_{k=0}^{N-1} x_k x_k = \frac{1}{N} \sum_{k=0}^{N-1} |X_k|^2 \quad 5.44$$

where the term  $\sum_{k=0}^{N-1} x_k^2$  is the first term of the autocorrelation of  $x_k$ .

The importance of Parseval's equation to MUAP analysis becomes apparent when comparing MUAP classes to individual MUAPs.

At this point it should be noted that the coefficients of a DFT is defined only for the discrete time sampled intervals, i.e.  $k\tau$ . Thus the shifting of a discrete time function is exact only for an integer shift of the sampling intervals. However, time shifts which are a fraction of the sampling interval can be computed by simple rotations (eq. 5.30) to a high degree of accuracy. Furthermore since the discrete values of the function  $g_k$  are by definition periodic in  $N$  there is a wrap around error resulting from the discontinuity between  $x_{N-1}$  and  $x_0$  giving rise to Gibb's phenomenon. This is limited by the filtering of the SFEMG signal and windowing of the MUAP done at extraction time.

Essentially the interpolation is done via the exponential function. For a better approximation, the sinc function could be used but due to its more complex calculation its use is not warranted. Other interpolation formulas have been presented in the past such as cubic splines [191]. Of course the interpolation makes the assumption that the underlying continuous signal from which the sampled signal is taken is continuous in the mathematical sense and also well behaved. This is required for the interpolation to be

accurate. Fortunately the MUAP is a continuous well behaved function. Furthermore the phase shift can be a fractional amount of the sampling interval as long as the noise introduced by the interpolation is less than the ambient noise of the signal.

Finally, and central to the reason for using the DFT equations to represent the MUAP is that they can be computed efficiently using the Fast Fourier Transform (FFT). Thus the interpolation formulas are not only highly accurate but can be computed in a relatively fast time. Conventional interpolation techniques only utilize a few adjacent points to interpolate at a particular point. The power of using these DFT interpolation equations is that they use all of the sample points (essentially a trigonometric interpolation). It should be noted here that because of the monotonically decreasing influence of the adjacent samples on any particular point all the values of the DFT do not have to be used for determining the value of point  $p$ . A similar technique can be performed as is done for determining of the power spectra of a long sequence of data. Data windows can be used (appropriately windowed to reduce end effects) for the interpolation of the function value at a particular point.

With these tools the extraction of features as presented in Chapter Three is possible.

### **5.2.3. Extraction of MUAP Features**

From the Nyquist sampled waveform and the equations presented above, the time features as presented in Chapter Three can now be found

to a high degree of accuracy. In the following discussion the function  $f(x)$  refers to the discrete equation  $g(k, \phi)$  and represents the MUAP by its DFT coefficients. The following characteristics of the MUAP were extracted using the above techniques:

- 1) duration,
- 2) amplitude and time occurrence of the peaks and
- 3) overall characteristics.

Each is explained below.

#### 5.2.3.1 Duration

In order to simplify the problem of finding the duration of a MUAP the overall duration of the MUAP is further broken down into the duration of the individual phases present in the MUAP. The duration of the individual phases of the MUAP can be found by simply finding the zero crossings (ie where the MUAP crosses the baseline). This is done by using a modified Newton's method for determining zero crossings and hence finding the roots of the function  $f(x)$  given by equation 5.31.

#### 5.2.3.2 Modified Newton's Method

Newton's Method for finding zeros of a function is well known. In order to make the method more robust it is modified in order to ensure a

convergence to a zero [192][193].

Essentially, Newton's Method is a one dimensional root finding routine. It requires the use of the function  $g(k, \phi)$  (equation 5.31) and its derivative  $\frac{dg(k, \phi)}{dk, \phi}$  (equation 5.33) over the interval where the zero(s) is located. These functions are easily obtainable for a sample MUAP and for that matter any digitally sampled data as long as they satisfy the Nyquist sampling theorem as presented in the above sections. Once the DFT coefficients of the MUAP are determined then the MUAP can be determined at any point  $\phi$  resolvable to within:

$$\frac{\sigma}{\beta \sqrt{E}}$$

5.45

where  $\sigma$  is the root mean square of the background noise,  $E$  is the energy in the MUAP and  $\beta$  is the normalized root mean square bandwidth of the MUAP signal [186]. Empirically, the achievable resolution is approximately 0.05 of a sampling interval for moderate sized MUAPs. This achievable resolution is also true more or less for the derivative of the MUAP; however the resolution tends to be less due to the enhancement of higher frequencies by the derivative, thus increasing the amplitude of the background noise. Typical achievable resolution was on the order of 0.08 of a sampling interval for the derivative of the MUAP.

The Modified Newton Method is essentially the same as the Newton Method and varies only in modifying the search algorithm for the zero when deemed necessary. In order for the method to work the zero to be found

must first be bracketed in an interval  $(a, b)$ . Then the method involves extending the tangent line at a point  $x_i$  until it crosses zero. The next point  $x_{i+1}$  used is the abscissa of that zero crossing. This method is continued until  $x_i$  and  $x_{i+1}$  differ by only a small amount  $\delta$  and hence the zero resolved.

Mathematically this method derives from the Taylor Series expansion:

$$f(x + \delta) \approx f(x) + f'(x)\delta + \frac{f''(x)}{2\delta^2} + \dots \quad 5.46$$

where for small values of  $\delta$  then:

$$f(\delta + x) = 0 \quad 5.47$$

and for well behaved functions (like the MUAP) the terms beyond the linear are unimportant since the zero or root is bracketed in the interval and is relatively close in a linear sense to the end points. Hence the above equation can be rewritten as:

$$\delta = - \frac{f(x_i)}{f'(x_i)} \quad 5.48$$

where again the step size is  $\delta$ . Of course this can be rewritten by substituting  $x_{i+1} - x_i$  for  $\delta$  to get:

$$x_{i+1} = x_i - \frac{f(x_i)}{f'(x_i)} \quad 5.49$$

which gives the approximation for the next point.

The powerful feature of the Newton Method is its rate of convergence. If  $x_r$  represents the true root of the function  $f(x)$  then:

$$\epsilon_{i+1} = x_r - x_{i+1} \quad 5.50$$

and similarly:

$$\epsilon_i = x_r - x_i \quad 5.51$$

where  $\epsilon_{i+1}$  and  $\epsilon_i$  are the next and current errors respectively. It can be shown then that the rate of convergence of the Newton Method is given by:

$$\epsilon_{i+1} = - \epsilon_i^2 \frac{f''(x)}{2f'(x)} \quad 5.52$$

That is it converges quadratically in the neighborhood of a root.

The need for modification of the Newton Method arises from the fact that this method can fail in three different situations. These situations are:

- 1) inflection points
- 2) multiple zeros
- 3) local minimum

The first two situations, inflection points and multiple zeros can be compensated for using the following strategy. If the Newton Method gives a new value for a root which is not smaller than the previous value (i.e. looks like it is moving out of the interval) then this step is rejected and the previous step is halved. Thus the step size becomes:

$$\delta_{i+1} = \frac{\delta_i}{2} \quad 5.53$$

This bisection of an interval is guaranteed to converge on a zero if indeed a zero is in the interval. This halving process is continued until the new value of  $f(x)$  is smaller than the previous value. In this way inflection points and multiple roots are accommodated by this method. The convergence to a zero is stopped after the location of the root  $x_r$  is known to within a specified accuracy of typically 0.08 of a sampling interval. This resolution was determined to be an adequate compromise between resolution of relatively large sized MUAPs and smaller sized MUAPs. It should be stated here that the first and last phase durations of the MUAP may not actually cross the baseline due to the generation process of the MUAP and the effects of the windowing of the saved MUAP vector. If this is the case then the inflection point after or before the peak in that phase is

taken as the start or end of the duration of that phase. The inflection point is found by finding the zero crossing of the second derivative of  $g(k, \phi)$  as given by equation 5.39.

Local minima cause a problem only when a zero is not bracketed. The bracketing of a root is done by using the simple notion that a root of function  $f(x)$  is bracketed between  $(a, b)$  if  $f(a)$  and  $f(b)$  have opposite signs. If the function is continuous (as it is for MUAP through the interpolation formulae) then by the intermediate value theorem at least one root must lie in that interval  $(a, b)$ . Of course this method can be fooled by double roots, multiple roots or singularities. Singularities and multiple roots are not a problem with MUAPs. Double roots occur rarely in MUAP analysis and when they do occur they are defined as turns and are not defined as individual phases (this becomes evident in the determination of the other features of the MUAPs).

Thus in order to find the zero crossings of the original function  $f(x)$  the zeros are initially bracketed by an algorithm which simply looks for a change in the sign of two successive data points of the discrete sampled MUAP extracted by means described earlier. These intervals bracketing the zeros of the MUAP are stored and then passed successively to the Modified Newton Method where equations 5.31 and 5.39 are used for  $f(x)$  and  $f'(x)$ . It should be noted from these equations that the points of evaluation  $x$  are determined by  $\phi$  the phase delay. With this notation then the first data point of the length  $N$  vector of DFT coefficients is zero and the last point is  $N-1$ . Thus each zero is found successively from the bracketed intervals. The determination of a zero is stopped when the change in value of the

zero position is on the order of the ambient noise level as given by equation 5.45.

The times of the zero crossing points in terms of the sampling interval are returned from the Modified Newton Method algorithm. The real time of the zero points is found by multiplying the sampling interval by this number. This is shown in Figures 5.12a, 5.12b and 5.12c. The MUAPs in these figures were 16 point discrete sampled signals represented by the circled points. The underlying over sampled waveforms (by four times the Nyquist rate) are outlined here also for comparison. The zeros determined by the Modified Newton Method are shown by the dashed lines with the time value of occurrence written beside them. As shown the accuracy of the algorithm is demonstrated by comparing the underlying waveform zero crossings with those determined by this Modified Newton Method using the Nyquist sampled points. The individual durations can be found by simple subtraction of the times of the successive zero crossings. Overall duration can be found by subtracting the first zero crossing from the last zero crossing time.

### 5.2.3.3 Amplitude of the Peaks of a MUAP

Another very important time characteristic of MUAPs is the amplitude of the individual peaks. The amplitude of the peaks of a MUAP can easily be found using the same method as described above. The only modification required is the functions used. Instead of using  $f(x)$  and  $f'(x)$ , the function and first derivative,  $f'(x)$  and  $f''(x)$ , the first and

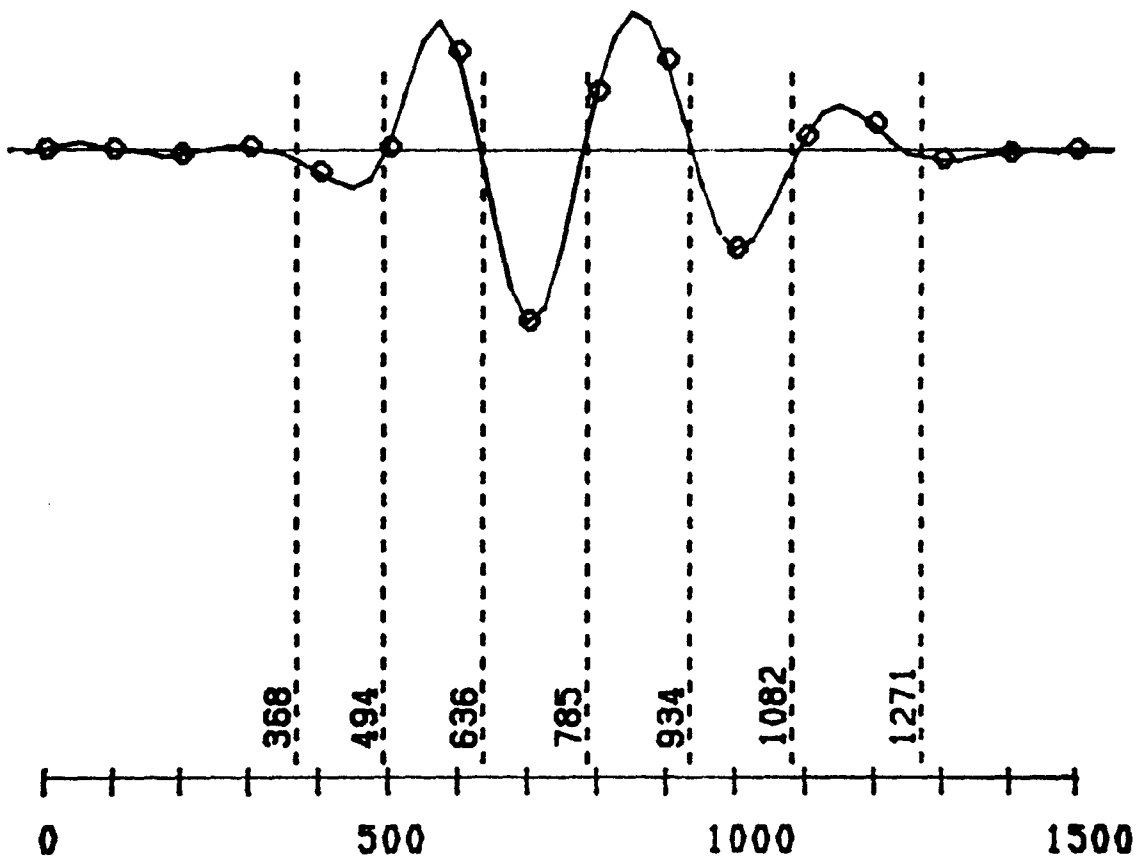


FIGURE 5.12A ZERO CROSSINGS OF A MUAP

2000  $\mu\text{V}$   
200  $\mu\text{s}$

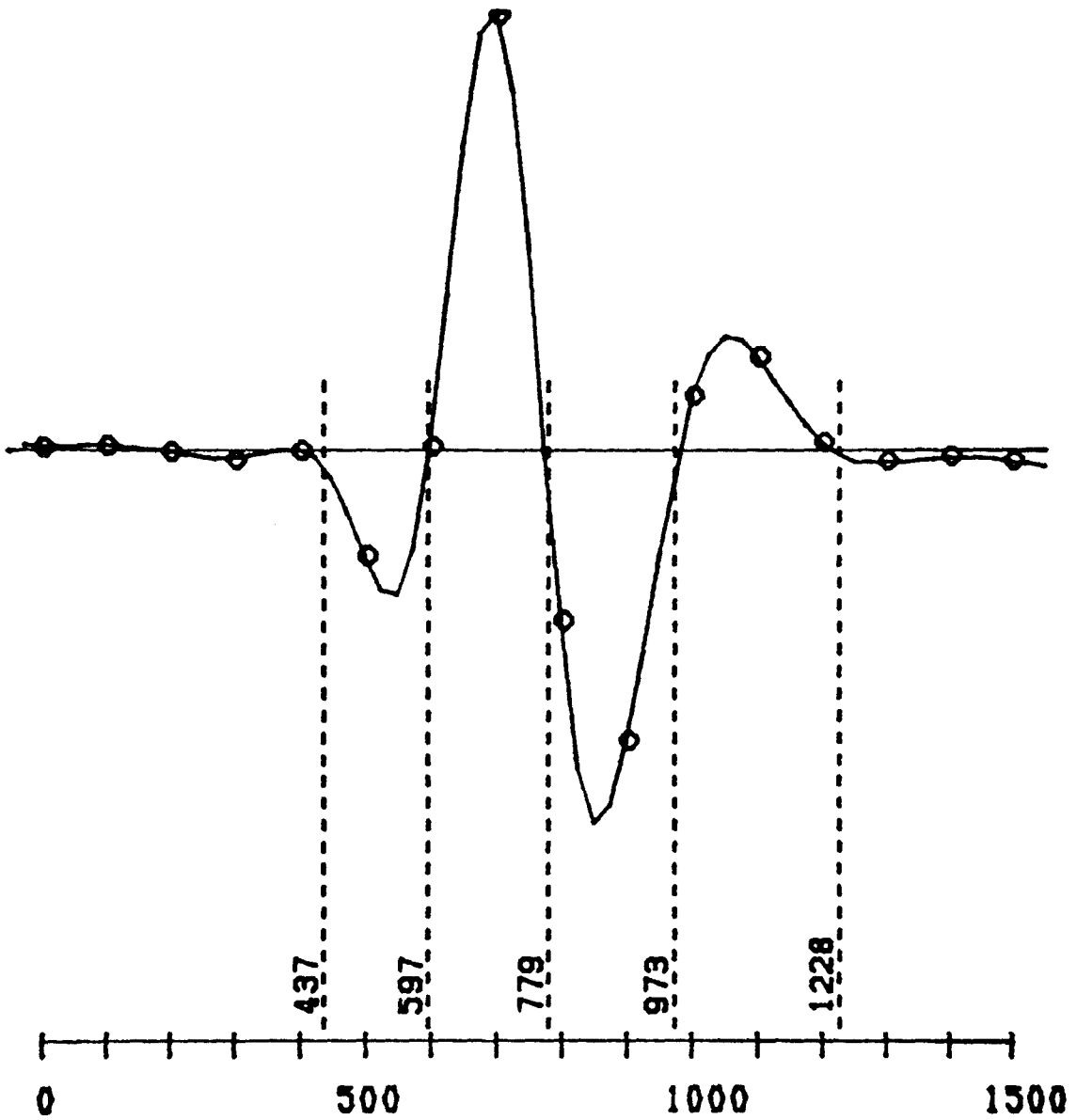
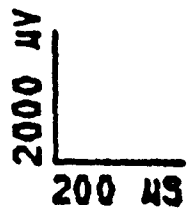


FIGURE 5.12B ZERO CROSSINGS OF A MUAP



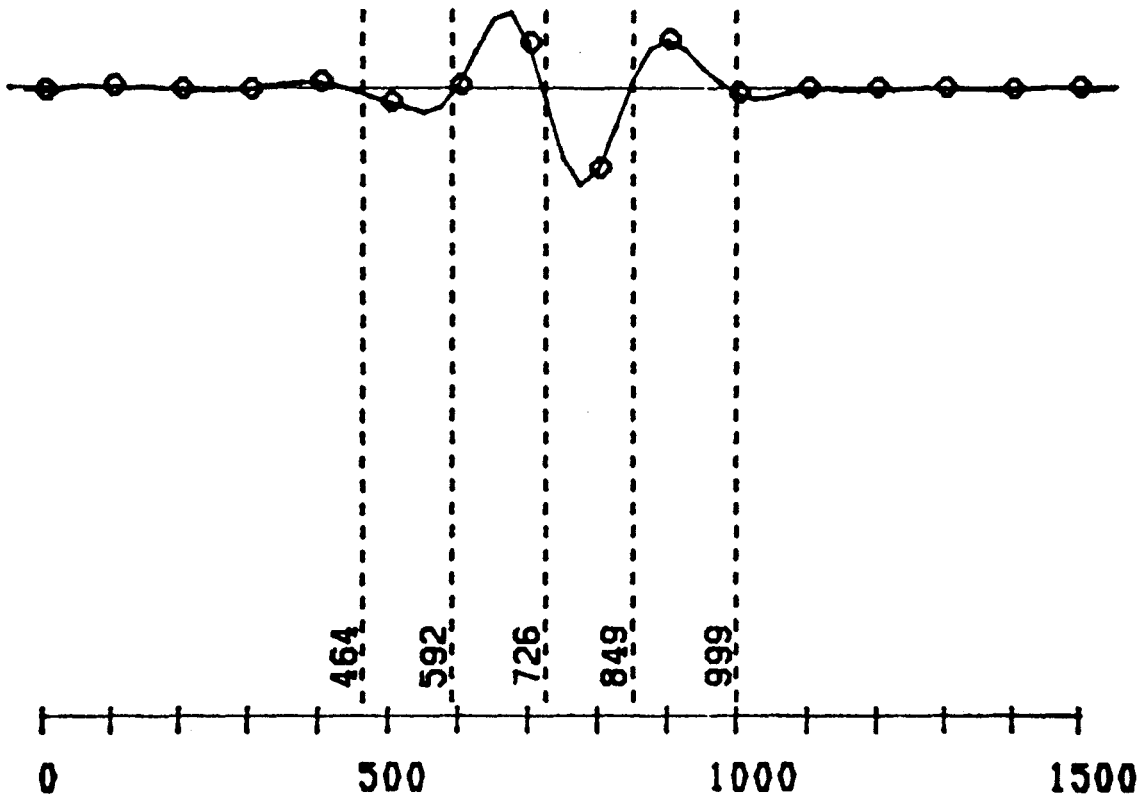
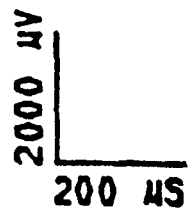


FIGURE 5.12C ZERO CROSSINGS OF A MUAP



second derivatives are used. The reason for this is that the peaks of the MUAP  $f(x)$  correspond to the zero crossings of the first derivative  $f'(x)$ .

Thus the Modified Newton Method used above can now be used without modification (except for the functions) for peak determination.

The zeros of the first derivative of the MUAP are bracketed in exactly the same manner as described above. As before, these intervals are passed successively to a Modified Newton routine. The zeros of the first derivative are returned. The determination of the time of the peak is found by multiplying the sampling interval by the number returned. The amplitude of the peak is found by inserting the value for the zero found into the original function  $f(x)$  (equation 5.31). This amplitude is then scaled for amplification and A/D gain to give actual level of the amplitude of the MUAP in  $\mu$ Volts. Therefore both the amplitude of each individual peak and the time of this peak's occurrence are found by this method.

Figures 5.13a, 5.13b and 5.13c show the determination of the peak times with this algorithm. Again, as before, the MUAPs shown are 16 point discrete sampled signals represented by the circled points. The underlying over sampled waveform (four times Nyquist rate) are outlined here also for comparison. The peaks are shown by the dashed lines with the times of occurrences beside each. The determination of the peaks using only the Nyquist sampled waveform and the the algorithms presented above results in the determination of the times and amplitude of the MUAP peaks to a high degree of accuracy when compared to the over sampled waveform.

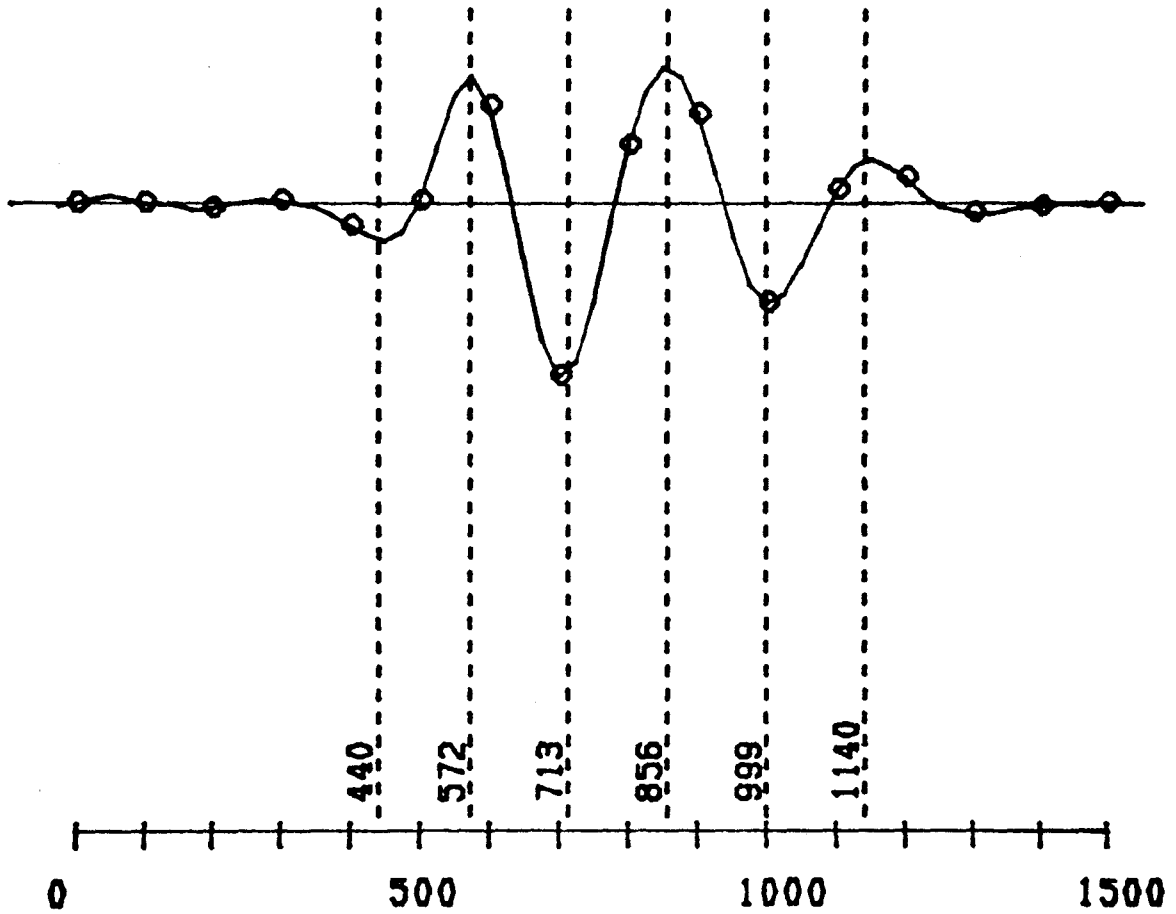


FIGURE 5.13A PEAKS OF A MUAP

2000 µV  
200 µS

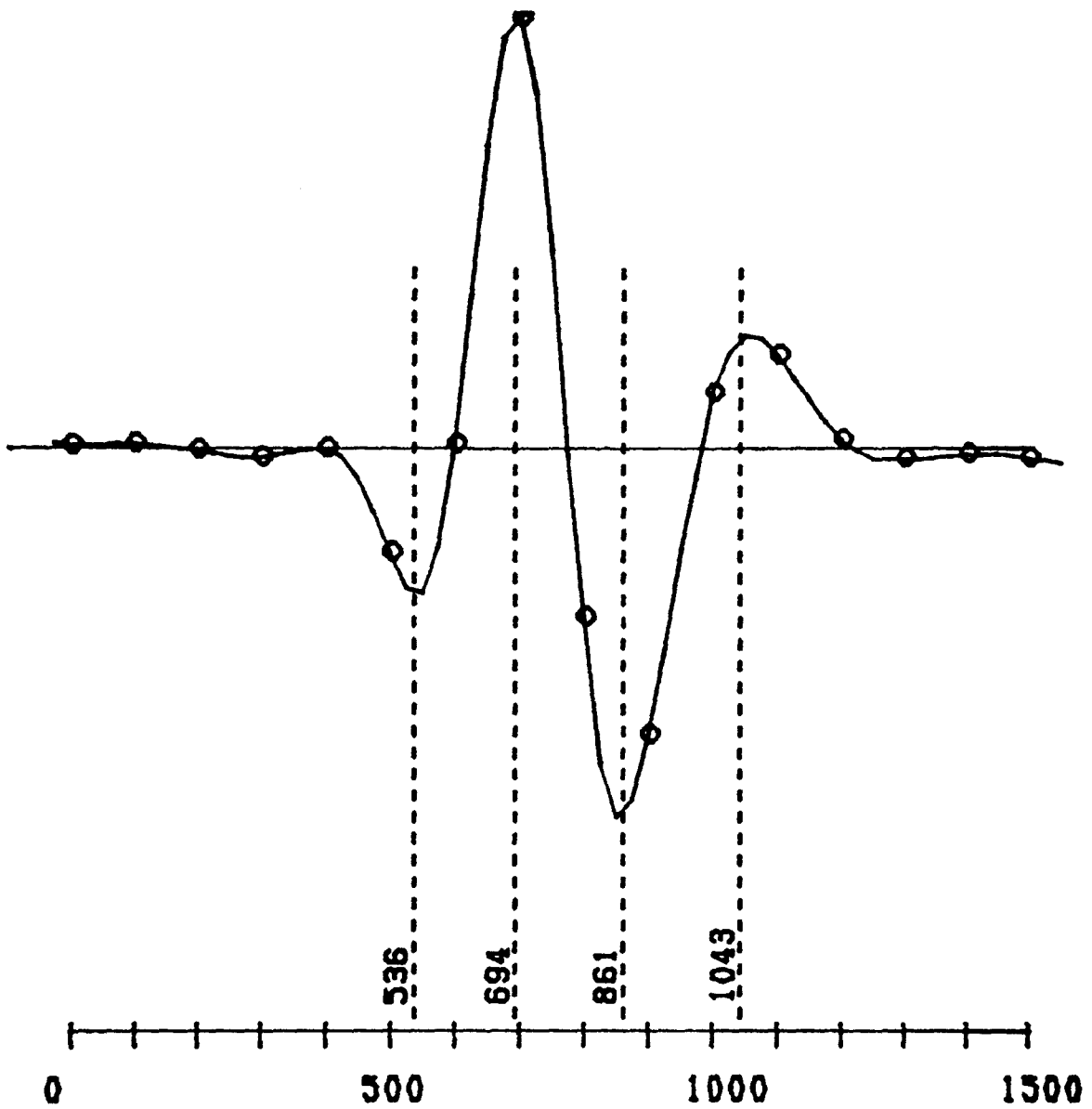


FIGURE 5.13B PEAKS OF A MUAP

2000 mV  
200 μs

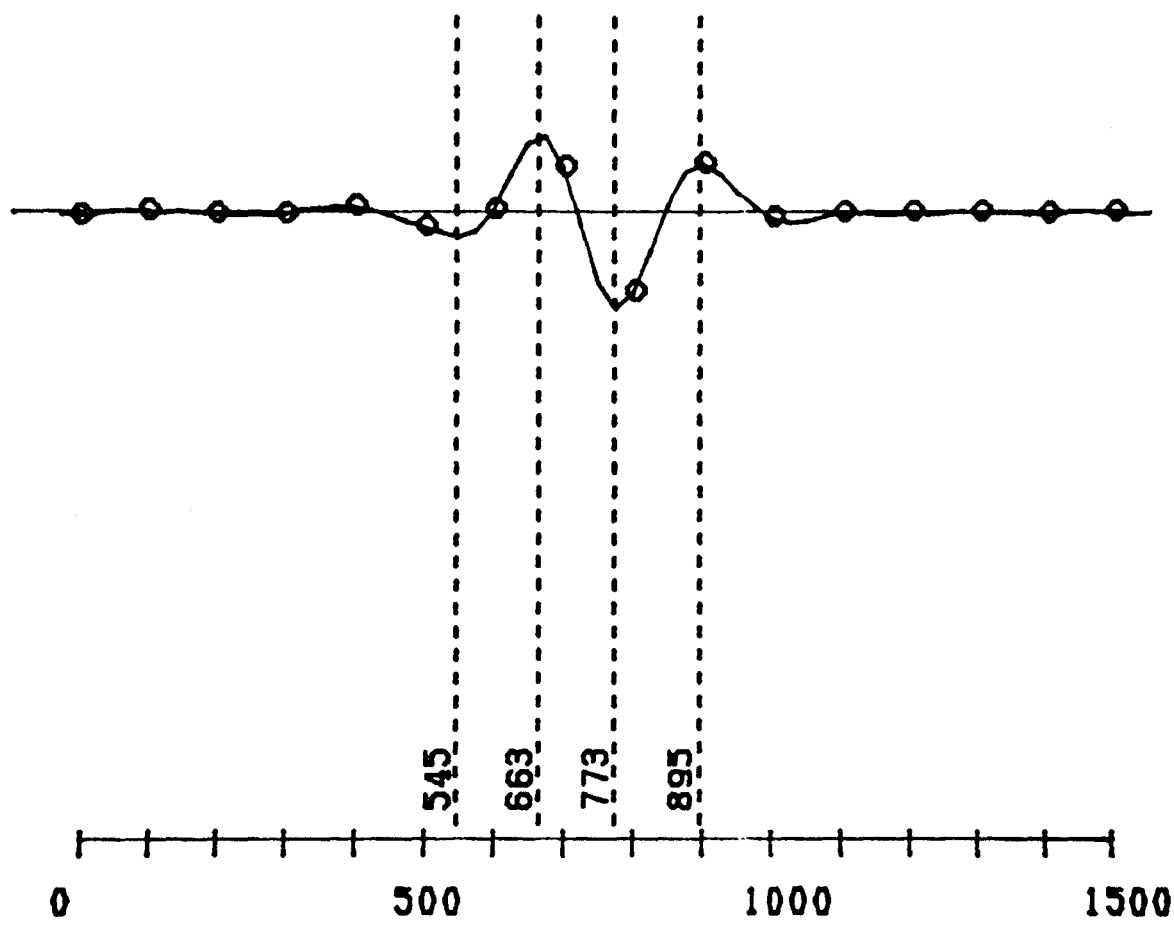


FIGURE 5.13C PEAKS OF A MUAP

2000  $\mu\text{V}$   
200  $\mu\text{s}$

#### 5.2.3.4 Overall Characteristics

Number of phases, sign of phases, number of turns and peak to peak voltages can easily be found from the aforementioned determination of the duration of the phases and the peak times and amplitudes of the MUAP under question.

The number of phases is easily determined from the number of zero crossings of the original function. The number of phases is equal to the number of zero crossings minus one (i.e. a duration must be bounded by zero crossings). It should be pointed out here that the number of zero crossings is dependent on the threshold level of detection (as discussed earlier).

The sign of the phases is determined by the sign of the MUAP function  $f(x)$  of the phase in question. It should be noted here that the sign convention followed is the convention used by the electromyographers where positive is defined as a negative voltage deflection.

One interpretation of the number of turns in a phase resulting from its definition (Chapter 3) is that it is the number of peaks within that phase. This is easily found by totaling the number of peaks found in any particular phase. The sum of the number of turns in all the phases is the total number of turns in that action potential.

Peak to peak amplitude gives an indication of the size of the action potential. It is found by searching for the maximum and minimum of the amplitudes of the peaks found. The difference of course is the maximum peak to peak amplitude. It should be noted here that the peak positive

and peak negative deflections are almost always one phase away and therefore represent the maximum peak to peak deflection. This is logical for an ac signal and the way the MUAP is generated.

One aspect of the action potential characteristics not yet covered is the area of the action potential. Since the actual area of the MUAP is zero (ac signal) the area discussed here is really the absolute area of the MUAP. Several different methods are used to calculate the area.

The first method used is a direct method using the function for the MUAP  $f(x)$  given above. The area is calculated using the trapezoid rule which states that:

$$\int_{x_1}^{x_2} f(x) dx = \delta \frac{1}{2} (f(x_1) + f(x_2)) \quad 5.54$$

where the integral of the function  $f(x)$  evaluated between points  $x_1$  and  $x_2$  is determined by a trapezoid of height  $\delta$  (step size) and sides being the amplitudes of the two values of the function  $f(x)$ . Here  $\delta$  is set to a fraction of the sampling interval and equation 5.31 as before is used for finding the value of  $f(x)$ . The points  $x_1$  and  $x_2$  are the zero crossings that begin and end a phase. Using equation 5.31 with a step size of 0.1 of the sampling interval results in a very accurate determination of the absolute value of the area of the phase. The overall absolute area of the MUAP then is the summation of the individual absolute areas.

The area of the MUAP can be calculated directly using the integral property of the DFT as described by equation 5.40. Here the area is

calculated for each phase where the limits  $x_1$  and  $x_2$  are as above. Due to the decreased computation required for computing this equation this method is quite a bit faster than the one described above. The first step again in the calculation of the area of the MUAP is to find the zero crossings. This is shown for a particular MUAP in Figure 5.14a. Figure 5.14b shows the area calculation using two methods; Method I being the trapezoid rule using equation 5.31 and Method II being the calculation of the area directly using equation 5.40. As shown the area calculation for each phase are very nearly identical and the overall sum only differs by 3 V·ms. Thus it was concluded that both methods are equal in accuracy though Method II is more efficient.

Figures 5.15a, 5.15b and 5.15c give an overall description of the MUAP characteristics found using the above methods. These characteristics are separated by phase and thus can be easily used to determine any other characteristics of the action potential, the electromyographer may wish to measure such as inter-peak intervals, maximum peak, etc. Furthermore these time characteristics may also be used as features in separation of MUAPs into their respective trains.

#### 5.2.4 Comparison Between Straightforward and Interpolation Methods

The algorithms presented in the previous sections were devised in order to obtain accurate measures from the Nyquist sampled data. If these algorithms are not able to extract characteristics which are just as accurate as those extracted directly from an over sampled waveform then the whole

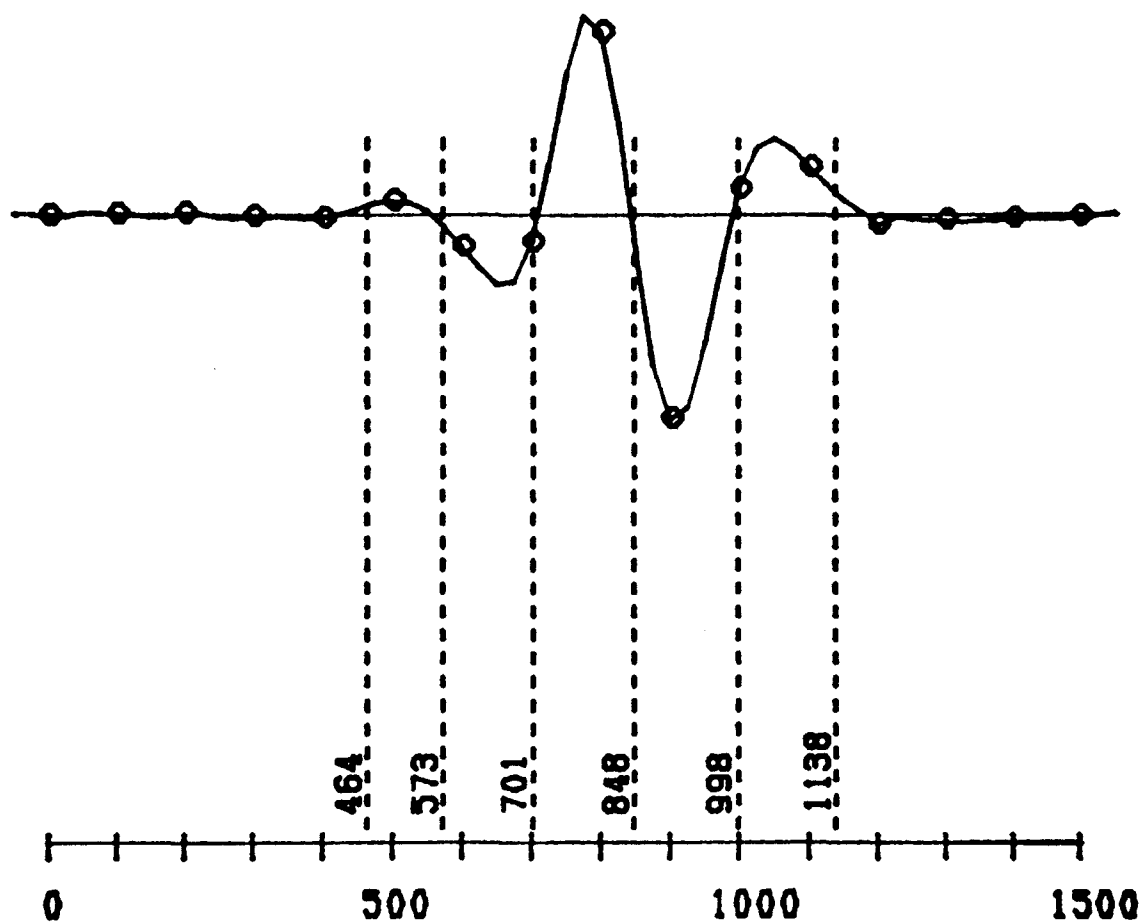
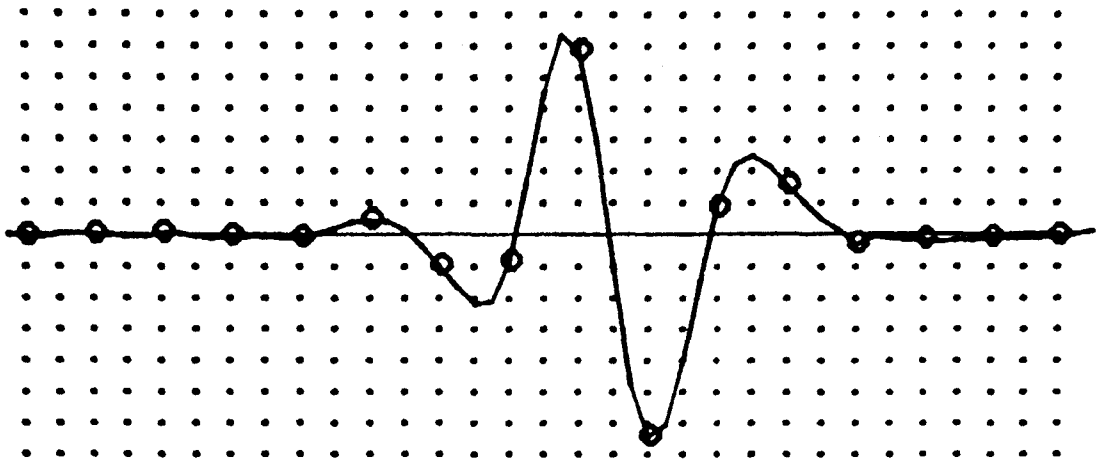


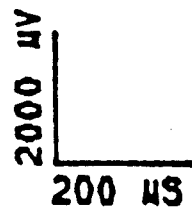
FIGURE 5.14A ZERO CROSSINGS FOR AREA

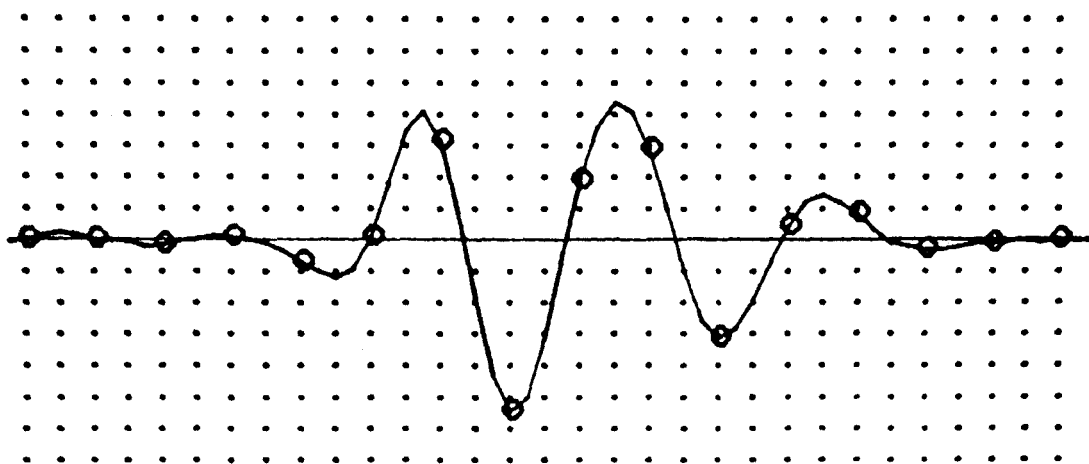
2000  $\mu\text{V}$   
200  $\mu\text{S}$



PHASE	AREA: METHOD I (V MS)	AREA: METHOD II (V MS)
1	48.91	49.10
2	127.6	127.48
3	261.94	262.14
4	290.81	291.69
5	154.89	155.54
<b>TOTAL AREA:</b>	<b>885.64</b>	<b>885.97</b>

FIGURE 5.14B MUAP AREA CALCULATIONS



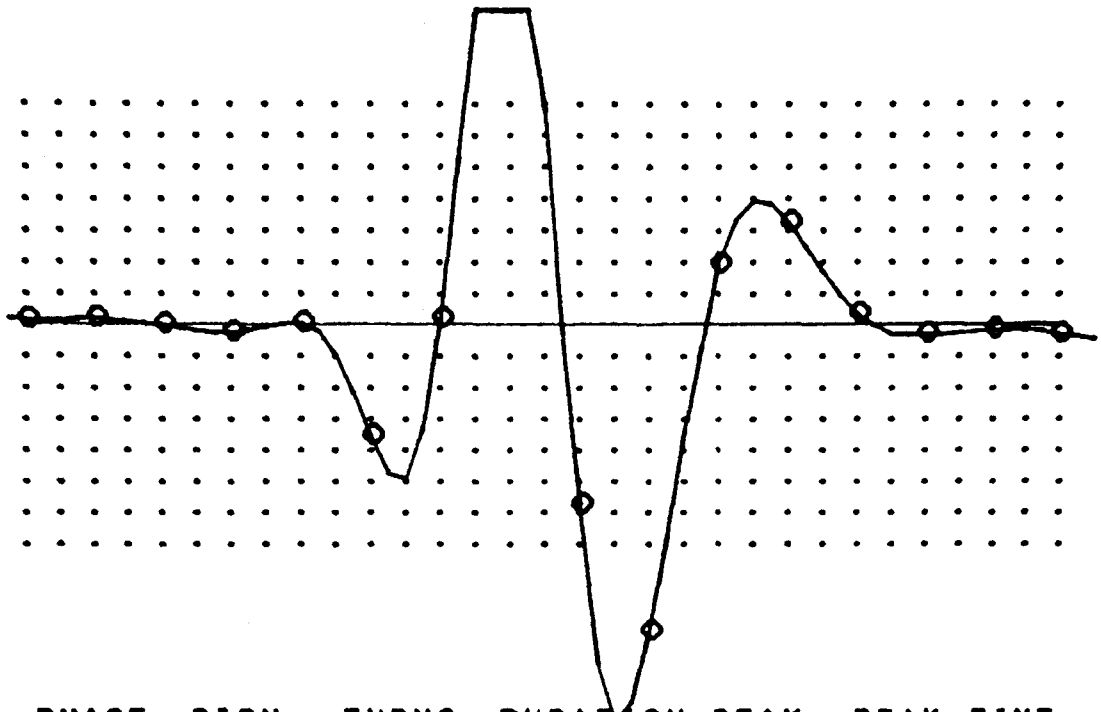


PHASE	SIGN	URNS	DURATION μS	PEAK μV	PEAK TIME μS
1	+	1	126	556	440
2	-	1	143	-1932	572
3	+	1	149	2631	713
4	-	1	149	-2119	856
5	+	1	148	1539	999
6	-	1	188	-698	1140

NUMBER OF PHASES: 6  
 NUMBER OF TURNS: 6  
 DURATION: 909 μS  
 PEAK TO PEAK VOLTS: 4750 μV  
 TOTAL AREA: 921.98 V MS

2000 μV  
 200 μS

FIGURE 5.15A INTERPOLATED CHARACTERISTIC



PHASE	SIGN	TURNS	DURATION μS	PEAK μV	PEAK TIME μS
1	+	1	160	2468	536
2	-	1	182	-7213	694
3	+	1	194	6158	861
4	-	1	255	-1935	1043

NUMBER OF PHASES: 4  
 NUMBER OF TURNS: 4  
 DURATION: 791 μS  
 PEAK TO PEAK VOLTS: 13371 μV  
 TOTAL AREA: 2055.59 V MS

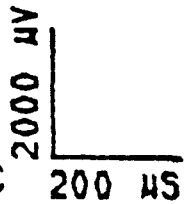
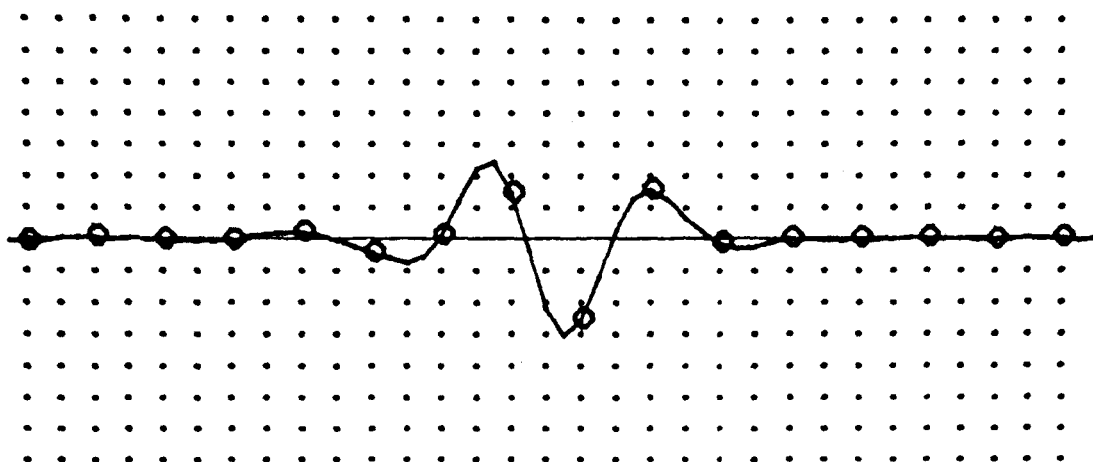


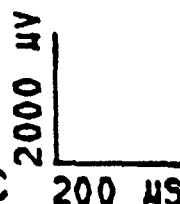
FIGURE 5.15B INTERPOLATED CHARACTERISTIC



PHASE	SIGN	TURNS	DURATION MS	PEAK MV	PEAK TIME MS
1	+	1	128	365	545
2	-	1	134	-1211	663
3	+	1	123	1453	773
4	-	1	150	-721	895

NUMBER OF PHASES: 4  
 NUMBER OF TURNS: 4  
 DURATION: 535 MS  
 PEAK TO PEAK VOLTS: 2664 MV  
 TOTAL AREA: 281.9 V MS

FIGURE 5.15C INTERPOLATED CHARACTERISTIC



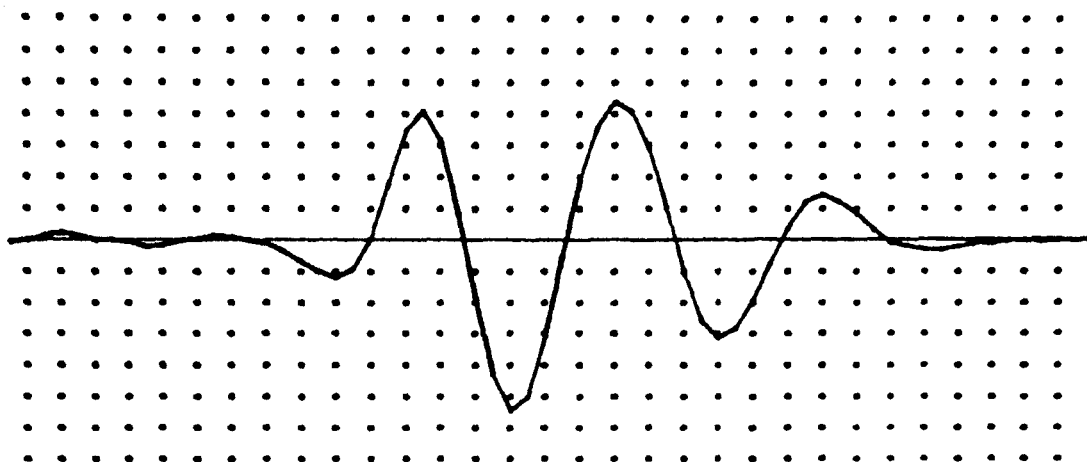
exercise is a futile waste of time. Fortunately, this is not the case. Figures 5.16a, 5.16b and 5.16c show typical MUAP characteristics found from over sampled signals. Figures 5.17a, 5.17b and 5.17c show the same Nyquist sampled signals whose characteristics are extracted in a straight forward manner. A comparison of these techniques is shown in Figure 5.18 where the absolute distance between the over sampled MUAP and the DFT technique is presented. From this comparison it is clearly seen that the DFT method used for extracting characteristics is indeed very accurate and is typically limited only by the level of the background noise. Thus the time characteristics of importance can be extracted from the Nyquist sampled waveform to a high degree of accuracy using the DFT equations presented above.

### 5.3 Preliminary MUAPT Analysis

Due to time and equipment constraints a complete MUAPT analysis could not be accomplished. However, some important preliminary analyses were done on the MUAPs so that MUAPT analysis may be done in the future. These preliminary analyses include:

- 1) alignment of MUAPs and
- 2) resolving of superpositions.

These are described below.

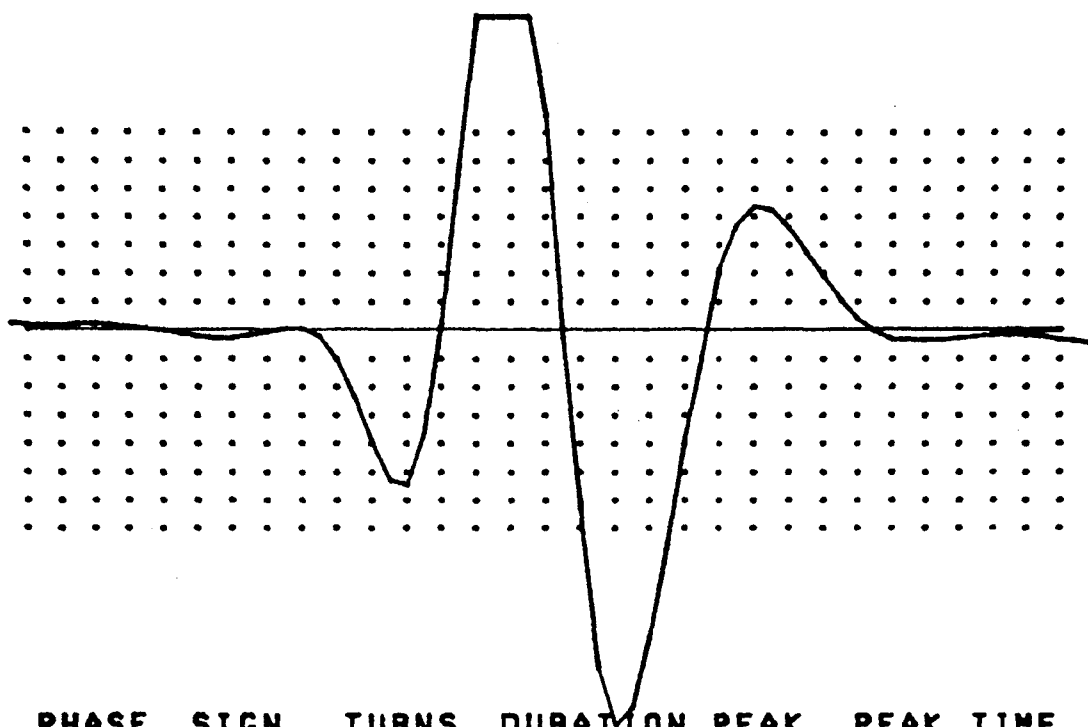


PHASE	SIGN	TURNS	DURATION μS	PEAK μV	PEAK TIME μS
1	+	1	170	573	451
2	-	1	133	-1986	573
3	+	1	147	2650	706
4	-	1	158	-2146	855
5	+	1	148	1522	1009
6	-	1	155	-709	1146

NUMBER OF PHASES: 6  
 NUMBER OF TURNS: 6  
 DURATION: 911 μS  
 PEAK TO PEAK VOLTS: 4798 μV  
 TOTAL AREA: 896.52 V MS

2000 μV  
 200 μS

FIGURE 5.16A OVERSAMPLED CHARACTERISTICS

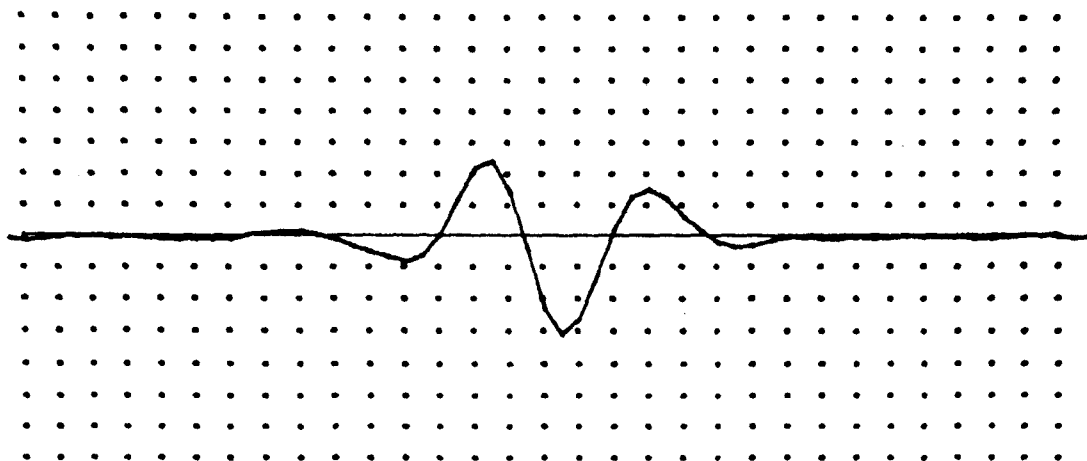


PHASE	SIGN	TURNS	DURATION μS	PEAK μV	PEAK TIME μS
1	+	1	195	2430	542
2	-	1	175	-7281	692
3	+	1	208	6164	853
4	-	1	242	-1949	1061

NUMBER OF PHASES: 4  
 NUMBER OF TURNS: 4  
 DURATION: 820 μS  
 PEAK TO PEAK VOLTS: 13444 μV  
 TOTAL AREA: 2063.56 V MS

2000 μV  
 200 μS

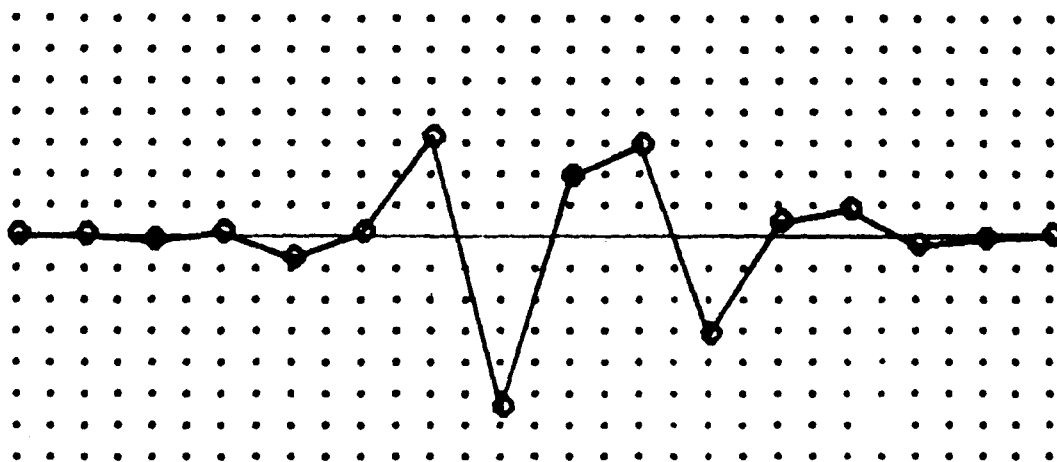
FIGURE 5.16B OVERSAMPLED CHARACTERISTICS



PHASE	SIGN	TURNS	DURATION μS	PEAK μV	PEAK TIME μS
1	+	1	159	361	550
2	-	1	123	-1206	667
3	+	1	122	1472	776
4	-	1	144	-749	897

NUMBER OF PHASES: 4  
 NUMBER OF TURNS: 4  
 DURATION: 548 μS  
 PEAK TO PEAK VOLTS: 2679 μV  
 TOTAL AREA: 303.61 V MS

FIGURE 5.16C OVERSAMPLED CHARACTERISTICS 
 2000 μV  
 200 μS

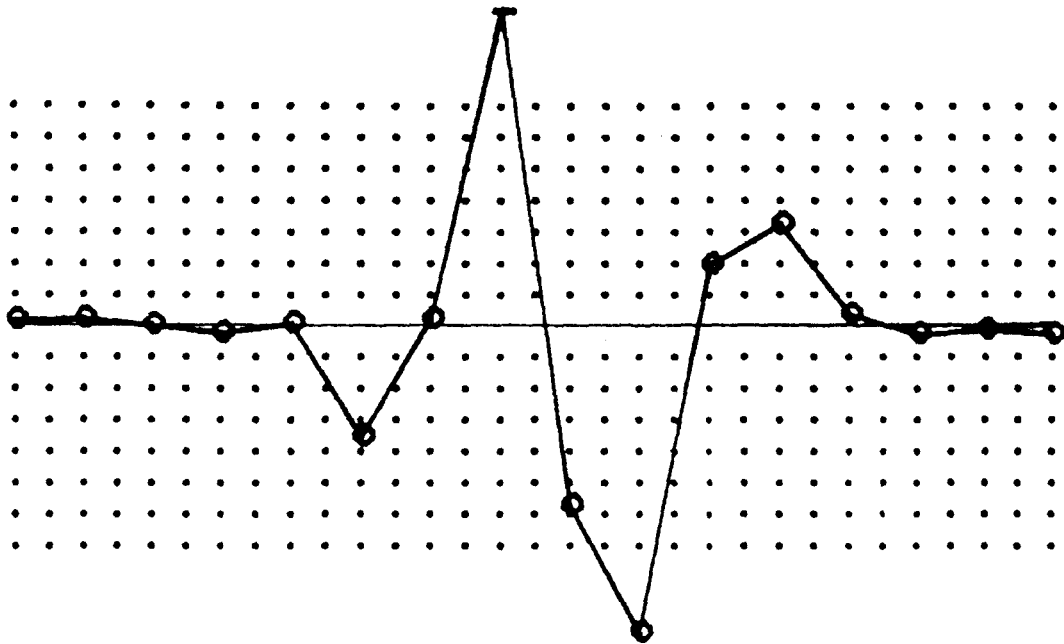


PHASE	SIGN	TURNS	DURATION μS	PEAK μV	PEAK TIME μS
1	+	1	200	500	400
2	-	1	190	-1800	600
3	+	1	145	2700	700
4	-	1	175	-1450	900
5	+	1	140	1500	1000
6	-	1	185	-450	1200

NUMBER OF PHASES: 6  
 NUMBER OF TURNS: 6  
 DURATION: 975 μS  
 PEAK TO PEAK VOLTS: 4300 μV  
 TOTAL AREA: 650.0 V MS

2000 μV  
 200 μS

FIGURE 5.17A NYQUIST CHARACTERISTICS



PHASE	SIGN	TURNS	DURATION μS	PEAK μV	PEAK TIME μS
1	+	1	200	1750	500
2	-	1	175	-5500	700
3	+	1	200	5000	900
4	-	1	225	-1500	1100

NUMBER OF PHASES: 4  
 NUMBER OF TURNS: 4  
 DURATION: 800 μS  
 PEAK TO PEAK VOLTS: 10500 μV  
 TOTAL AREA: 1800.0 V μS

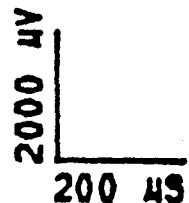
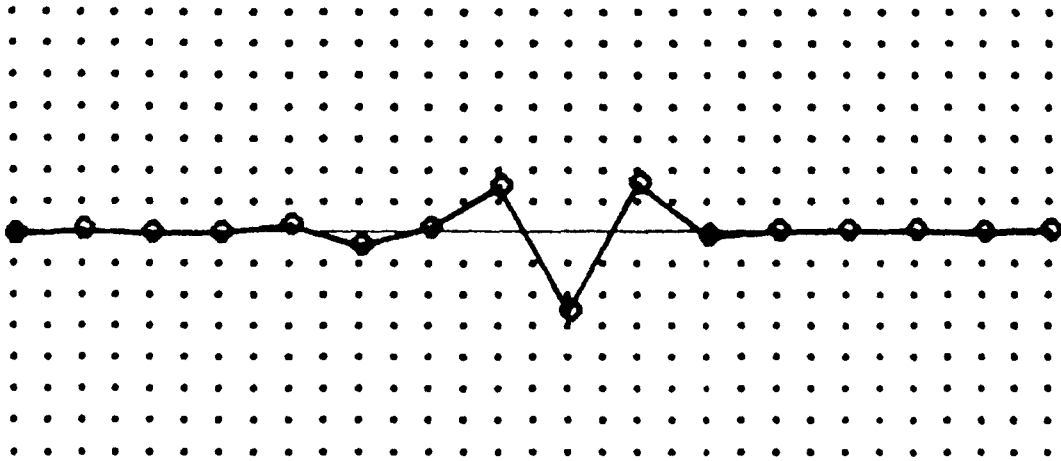


FIGURE 5.17B NYQUIST CHARACTERISTICS



PHASE	SIGN	URNS	DURATION μS	PEAK μV	PEAK TIME μS
1	-	1	125	-750	700
2	+	1	125	1250	800
3	-	1	125	-750	900

NUMBER OF PHASES: 3  
 NUMBER OF TURNS: 1  
 DURATION: 375 μS  
 PEAK TO PEAK VOLTS: 2000 μV  
 TOTAL AREA: 250.0 V MS

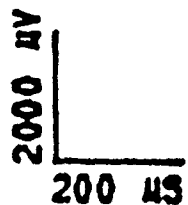


FIGURE 5.17C NYQUIST CHARACTERISTICS

	duration uS	peak-peak amplitude uV	largest peak time uS	area Vms
1 oversampled MUAP	911	4796	706	897
	820	13444	853	2064
	548	2679	776	304
2 Nyquist sampled MUAP	975	4900	700	650
	800	10500	700	1800
	375	2000	800	250
3 Interpolated MUAP	903	4750	713	921
	791	13371	861	2056
	535	2664	773	282
difference between 1-3	8	46	7	24
	29	73	8	10
	11	15	3	16

Figure 5.18 Comparison of methods

### 5.3.1 Alignment Algorithm

The whole point in MUAPT analysis is to separate MUAPs into their respective trains so that their time history of firing can be determined. This requires some form of pattern recognition technique in order to separate MUAP into different classes. The separation of a MUAP into a particular class requires the use of a difference metric. There are many such difference metrics. Probably the most widely used difference metric and consequently the simplest falls into the general euclidean distance metric defined by:

$$d_{i,j} = \frac{1}{N} \sum_{i,j=0}^{N-1} (s_i - c_{i,j})^2 \quad 5.55$$

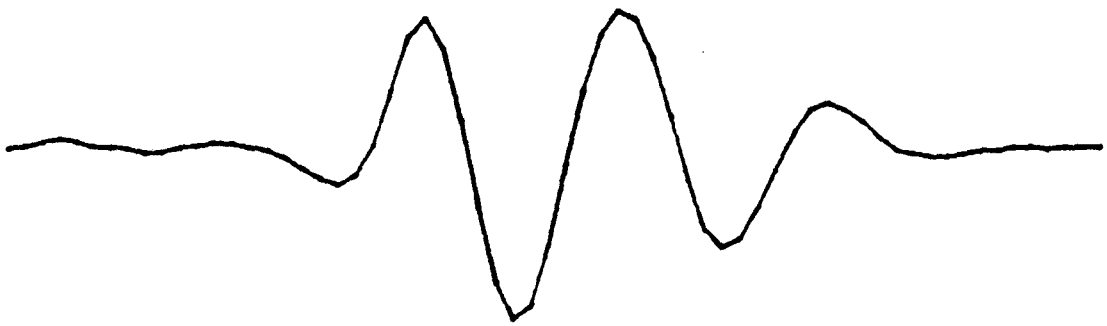
where  $d_{i,j}$  is the value which gives a measure of the separability of the class vector  $c_{i,j}$  from the signal vector  $s_i$ . A threshold level  $t$  is then set on this distance  $d$  which has the following property:

$$\begin{aligned} d_{i,j} &\leq t & s_i &\text{ belongs to class } c_j \\ d_{i,j} &> t & s_i &\text{ does not belong to class } c_j \end{aligned}$$

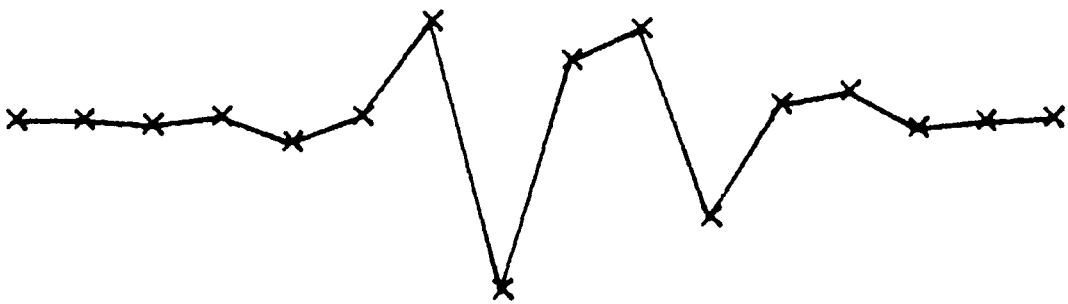
Once a signal is found to belong to a particular class then that class to which it belongs can be updated (ie averaged etc) and the threshold distance may be readjusted (only if the signal templates are non stationary). Although this simple pattern recognition technique assumes that the signals

to be classified are separable in  $N$  dimension space (they may not be) it provides an adequate basis for demonstrating the need for preliminary MUAPT analysis; namely alignment.

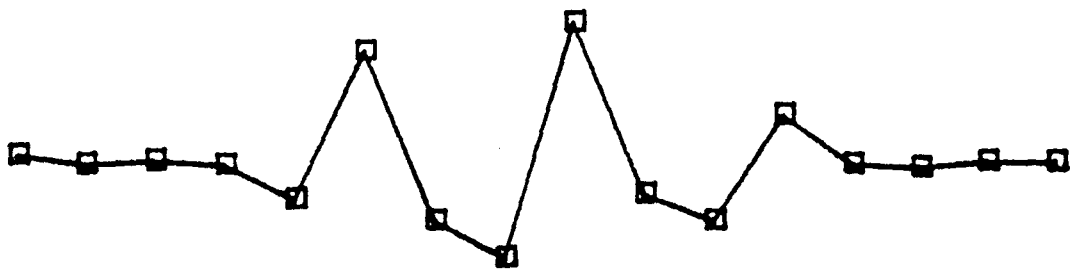
What becomes immediately apparent in this form of pattern classification presented above, is that action potentials from the same motor unit may have quite different looking shapes. This is illustrated in Figures 5.19a, 5.19b and 5.19c. The two action potentials (B) and (C) are Nyquist sampled from the same underlying (over sampled) waveform (A) but since the time an action potential occurs is unknown a priori, the sampling of that same action potential when it occurs again is never guaranteed to be in the same position. This being the case the same action potential can look quite different. Furthermore due to the method of generation, different MUAPs are inherently similar looking in nature. Any misalignment from the sampling process can cause the classifier to classify quite different MUAPs as being the same. Thus the classifier regardless of the method used is highly dependent on the sampling rate especially if Nyquist sampled signals are used as in the case for this thesis. In order to make this point clearer two different but similar looking MUAP waveforms were Nyquist sampled from their respective over sampled waveforms. The successive sampling of a MUAP was varied randomly by a value  $\phi$  up to and including  $1/2$  of the sampling interval. The distances from the original class templates (Nyquist sampled) to these misaligned signals were calculated and plotted as shown in Figure 5.20. Clearly there is some ambiguity to the determination of which samples belong to which class. The distance classifier fails for these Nyquist sampled signals.



(A)

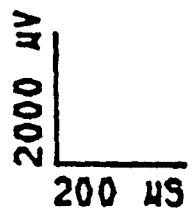


(B)



(C)

FIGURE 5.19A NYQUIST SAMPLED MUAP



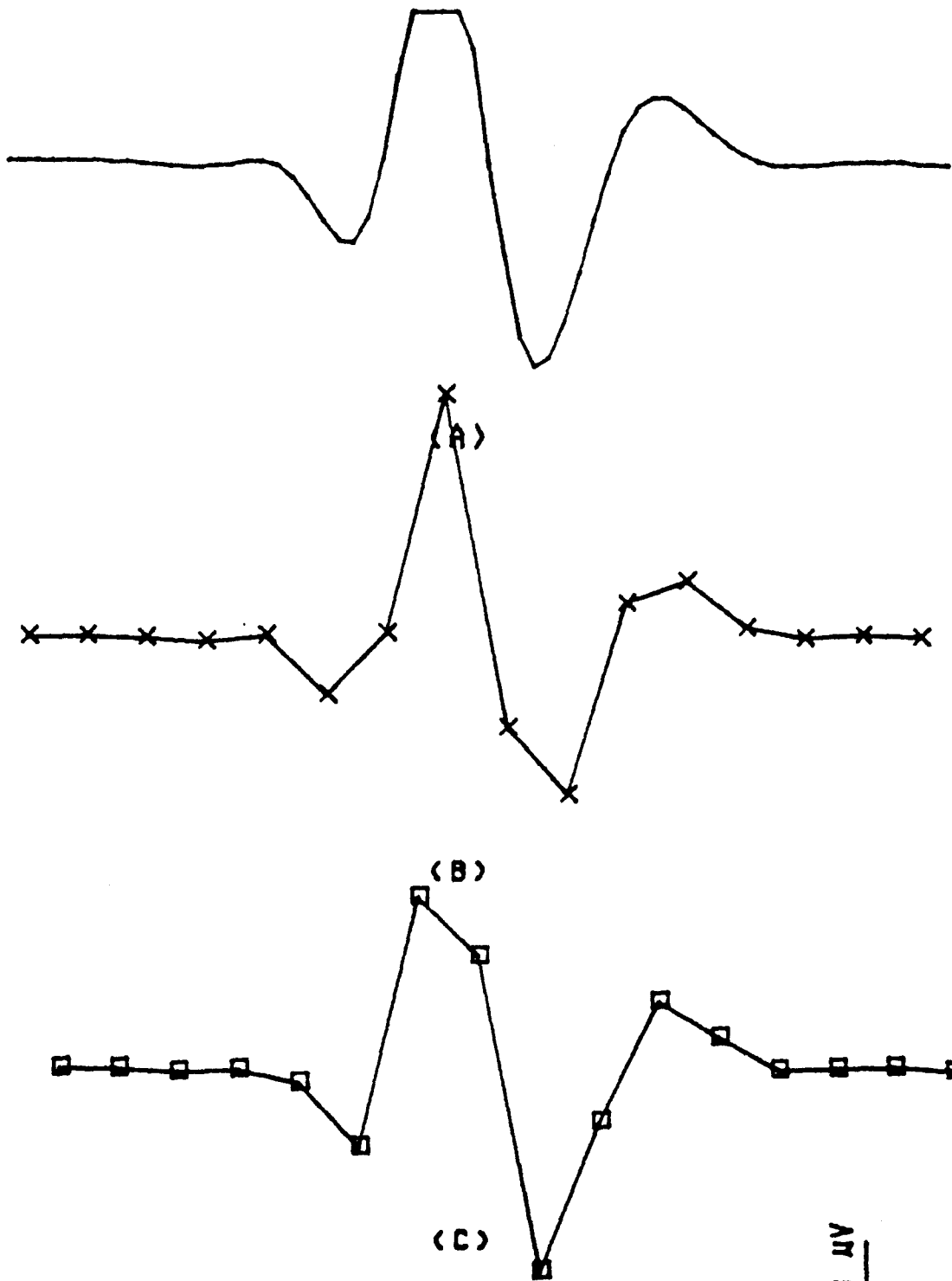
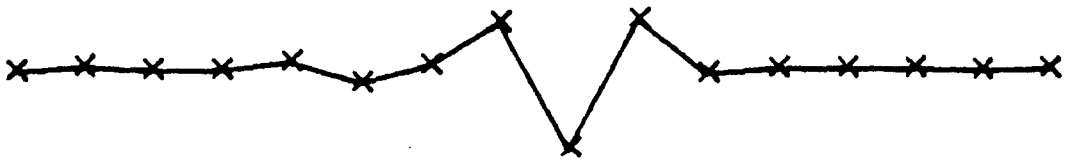


FIGURE 5.19B NYQUIST SAMPLED MUAP

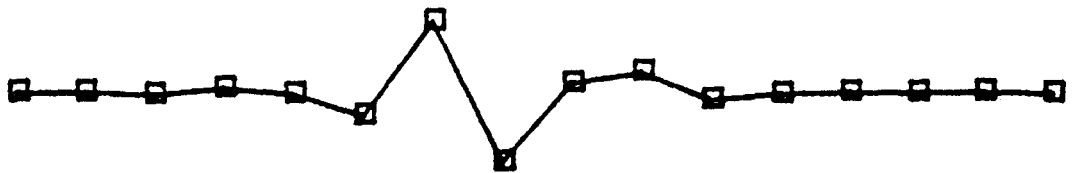
3393  $\mu\text{V}$   
200  $\mu\text{S}$



(A)

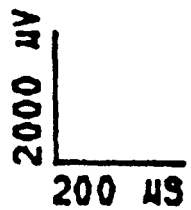


(B)



(C)

FIGURE 5.19C NYQUIST SAMPLED MUAP



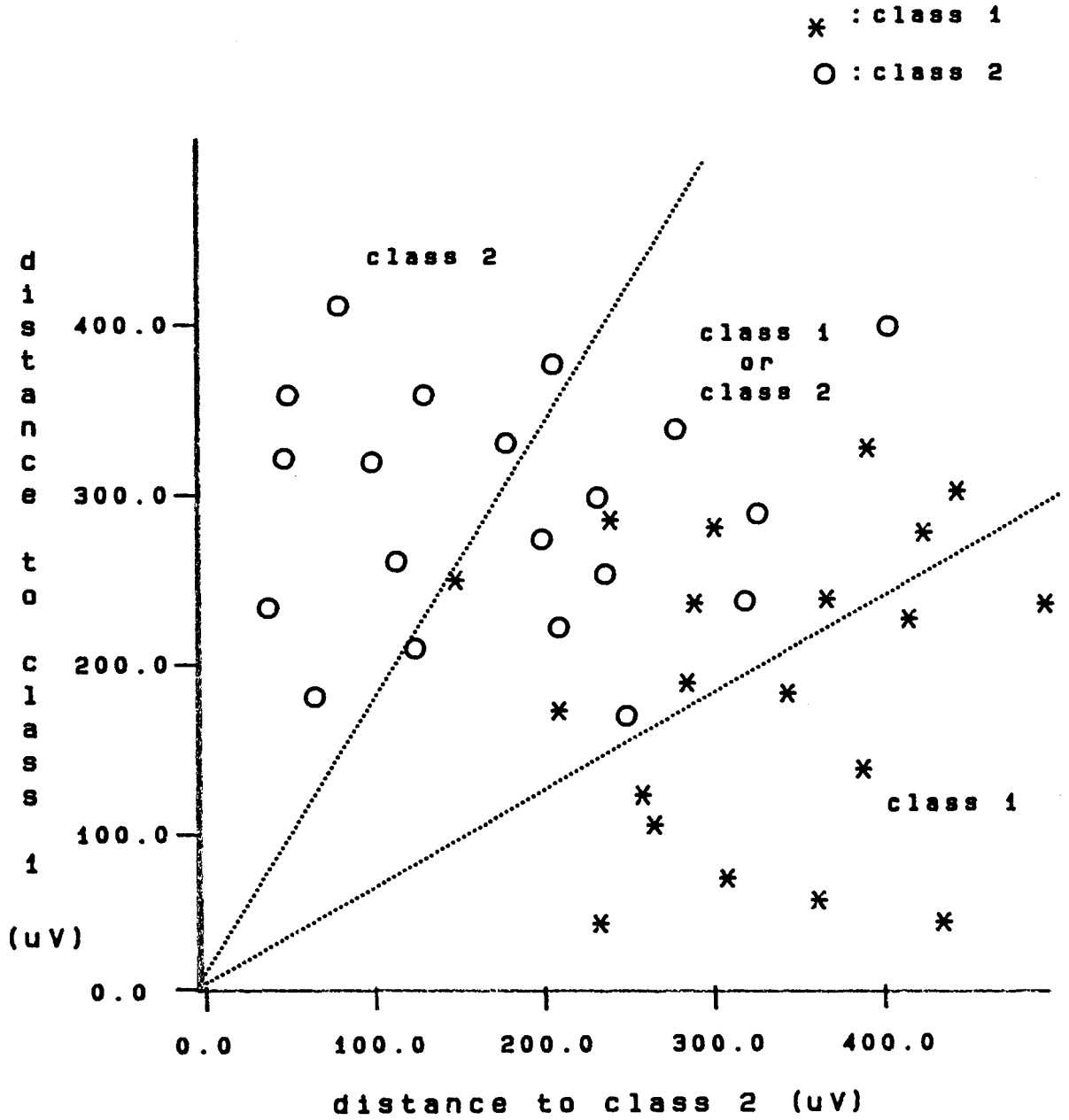


Figure 5.20 Distances between two different unaligned MUAPs

Obviously the simplest method for dealing with this classification problem is to over sample the signals so that alignment problems are reduced significantly [186]. This is a viable solution but due to the hardware constraints encountered in this thesis this was not possible. The other method for dealing with this type of problem is to try and align the MUAP signal with a class vector. This is usually accomplished by aligning MUAP signals with each other in such a way as to maximize their cross correlation. This is a particularly attractive method when dealing with Nyquist sampled signals [186]. This alignment is composed of two parts. These are:

- 1) rough alignment and
- 2) fine alignment.

These alignment schemes are explained below.

### 5.3.2 Rough Alignment

In order to accommodate a more rigorous fine alignment of a signal vector with a class vector a rough alignment must be done first. The rough alignment compares the maximum peak of the signal vector with the class vector to determine how far apart they really are in N dimensional space (N-space). This is possible in MUAPs since they characteristically have a maximum positive or negative peak. For alignment, the peak chosen is the largest one for that class whether it is positive or negative.

The similar sign peak is looked for in the signal to be aligned first and compared to the class. In order to speed up the identification process the signal is only compared to the class if the peak is of similar size  $p \pm 0.2p$ .

If these peaks are greater than one sample interval apart (an integer multiple) then the signal vector is shifted via equation 5.31 by that integer amount so that the peaks of the signal and class are roughly aligned. This rough alignment is required when comparing a class to a signal which does not belong to that class. If the signal does indeed belong in that class then this rough alignment is not too useful (though still used due to lack of any prior knowledge). This is obvious due to the fact that if the detection algorithm is not changed, then the maximum misalignment possible for identical waveforms is one half a sampling interval. That is to say if a signal is sampled with a delay of one sample period, the signal would look the same as if there were no delay since it would line up with the same sample points as the original signal. Even so, as shown by Figure 5.19a through 5.19c, even when this rough alignment is in place the same signal can be quite different looking. In order to overcome this a fine alignment scheme following the method employed by McGill and Dorfman [186] was devised.

### 5.3.3 Fine Resolution Alignment

In order to achieve fine resolution alignment it is necessary to align a MUAP signal with a class vector or template to within a particular tolerance. Since the misalignment is not known a priori the fine resolution

alignment algorithm can essentially be expressed as a minimization problem. Since the features used to represent the MUAP are the DFT coefficients, Parseval's equation can be used for this alignment algorithm. The need to do this becomes obvious once minimization is attempted, as was shown by Figure 5.20.

In order to minimize the misalignment between a class vector or template and a particular signal  $s_i$ , a measure of the difference between the aligned signal and the class is required. For this thesis the measure is defined as:

$$\epsilon_i = s_i - c_i \quad 5.56$$

where  $\epsilon_i$  is the difference between the  $i$ 'th elements of the signal  $s_i$  and class  $c_i$ . With this notation then the alignment problem can be expressed as a least means square problem where the  $i$ 'th difference element is expressed as:

$$\epsilon_i^2 = (s_i - c_i)^2 \quad 5.57$$

Thus the overall alignment error  $\epsilon^2$  can be expressed as a summation of the individual alignment errors of the corresponding data elements of the signal and class such that:

$$\epsilon^2 = \sum_{i=0}^{N-1} (s_i - c_i)^2 = \sum_{i=0}^{N-1} \epsilon_i^2 \quad 5.58$$

Furthermore since the signal vector  $s_i$  and the class vector  $c_i$  are discrete time samples in order to be consistent with previous definitions they may be represented by  $s_k$  and  $c_k$  and their DFT transformations as  $S_n$  and  $C_n$  respectively. As in any minimization problem, a degree (or several) of freedom is required. In this case the degree of freedom is the rotation of the signal with respect to the class  $c_k$  so  $s_{k,\phi}$  is used instead of  $s_k$ . The minimization then is with respect to  $\phi$ . The equation to be minimized in the least square sense then becomes:

$$\epsilon^2 = \sum_{k=0}^{N-1} (s_{k,\phi} - c_k)^2 \quad 5.59$$

Again, due to the efficiency of the FFT it is more advantageous to express the above equation in terms of the DFT coefficients. This can be done by using Parseval's equation described previously to get:

$$\epsilon^2 = \frac{1}{N} \sum_{n=0}^{N-1} |S_{n,\phi} - C_n|^2 \quad 5.60$$

where  $S_{n,\phi}$  and  $C_n$  are the discrete fourier coefficients of  $s_{k,\phi}$  and  $c_k$  respectively. Thus minimization of  $\epsilon^2$  in the least mean square sense is equivalent to rotating a signal vector until it lines up with the class vector in the best possible way. In short it maximizes their cross correlation and equation 5.59 can be thought of as a correlation maximizer.

Furthermore, since the original discrete signal is real and has zero mean a further simplification of the above equation is possible. Due to the symmetry of the DFT for real sequences (ie  $F_{N-n} = F_n$ ) equation 5.60 can be rewritten as:

$$\epsilon^2 = \frac{2}{N} \sum_{n=1}^{N/2-1} | S_{n,\phi} - C_n |^2 \quad 5.61$$

where only the positive half of the DFT coefficients are required. This greatly reduces the computation load required (especially on a PDP 11/34).

There are a variety of methods available for minimizing equation 5.61. The method employed in this thesis was that describe by Brent [192].

### 5.3.4 Minimization Method

The minimization method employed by Brent requires the following properties of the function to be minimized. These properties are:

- 1) that the minimum be bracketed,
- 2) that the first derivative of the function to be minimized be known and
- 3) the function is essentially smooth near the minimum.

The first property is guaranteed by the rough alignment method

described in the previous section. Whether the signal belongs to a particular class or not the rough alignment guarantees that a minimum is located between two successive sample points  $(a, b)$  of the signal to be aligned. Thus the minimum is bracketed in the interval  $(a, b)$  where  $f(c)$  is a point within the interval  $(a, b)$  with the property that  $f(a) < f(c) > f(b)$ . This can be expressed in terms of the least mean square error as  $\epsilon_a \geq \epsilon_c \leq \epsilon_b$  where  $\epsilon_a$ ,  $\epsilon_b$  and  $\epsilon_c$  are the error measurements at points  $a$ ,  $b$  and  $c$  respectively. The first derivative of equation 5.61 is required for minimization. This can be found by differentiating equation 5.61 with respect to  $\phi$  to get:

$$\frac{d\epsilon^2}{d\phi} = \frac{4}{N} \sum_{n=1}^{N/2-1} \left[ \frac{2\pi n}{N} \right] \text{Im} \{ S_{n, \phi}, C_n^* \} \quad 5.62$$

where  $\text{Im}$  stands for the imaginary part of the quantity in the brackets and  $C_n^*$  represents the complex conjugate of the quantity  $C_n$ .

The equation 5.60 is essentially smooth around the minimum due to the continuous shape of the MUAP around the minimum. In fact this function is parabolic in nature. The parabolic nature of the least mean squares alignment function given in equation 5.60 can be rewritten as:

$$\epsilon^2 = \sum_{k=1}^{N/2-1} ( s_{k, \phi}^2 - 2s_{k, \phi} c_k + c_k^2 ) \quad 5.63$$

where  $s_{k, \phi}$  is the independent variable and  $\epsilon^2$  is the dependent

variable. This above equation has the general form of a N-dimensional parabola given by:

$$y = ax^2 + bx + c \quad 5.64$$

This equation therefore is suitable for minimization by parabolic interpolation. This is shown in Figure 5.21 a plot of the minimization function as a function of the sampling interval.

Now Brent's method can be exploited for the minimization of equation 5.60. Brent's method is basically an inverse parabolic interpolation (ie looking for the abscissa rather than the ordinate). The minimum is initially bracketed in the interval  $(a, b)$ . Within this bracket a parabolic interpolation is attempted if possible and fitted through three points (three nonlinear points specify a parabola). The if possible refers to the fact that the parabola must:

- i) fall within the boundary interval  $(a, b)$  and
- ii) imply a movement from the best current minimum found that is less than half the movement of the last step.

The first criterion is required for convergence while the second criterion ensures that the minimum is smoothly converging to a point.

The sign of the first derivative is used in determining the next test interval  $(a, x)$  or  $(b, x)$  where  $x$  is in  $(a, b)$ . The value of this derivative at this point and the previous point is extrapolated to zero by the secant

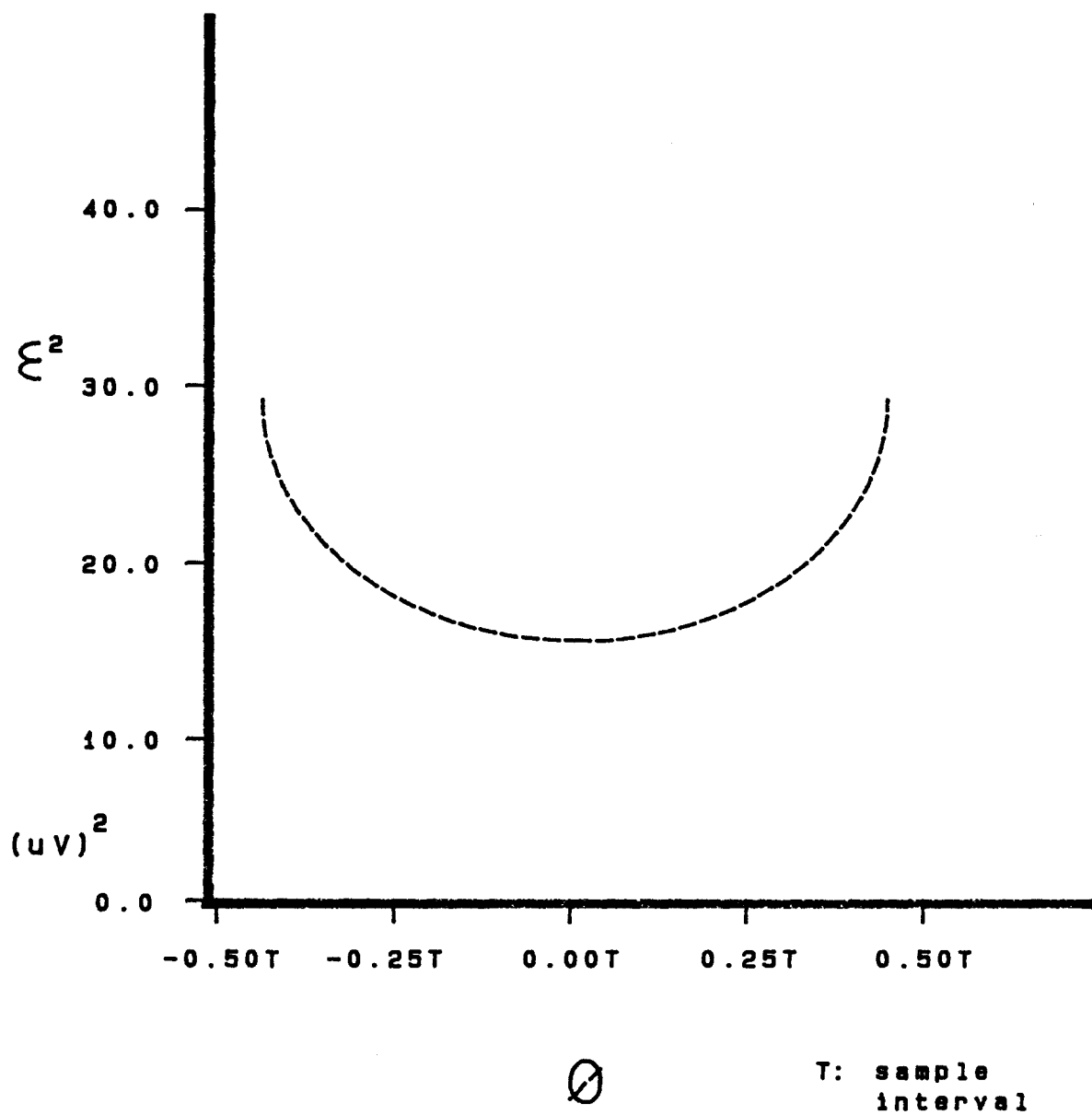


Figure 5.21 Minimization function

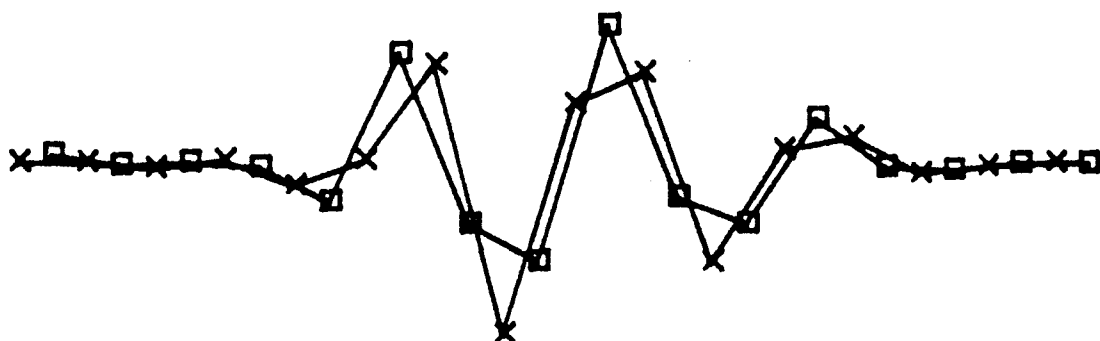
method to find the next point. Again, as in the case of Newton's Method if this interval is jumped out of then bisection is done and the whole process is continued.

The minimization essentially then varies the parameter  $\phi$  of the DFT of the signal  $s_{k,\phi}$  to find the least mean square error. The minimization continues until a tolerance of approximately 0.08 of a sampling interval is accomplished. The alignment of a signal with a class template regardless of whether or not they are identical takes approximately 2 – 3 iterations for this alignment resolution. In essence then the result of the minimization of equation 5.60 is to find the value of the rotation  $\phi$  of the signal  $s_k$  which minimizes the distance between the signal and the class. Thus when the value of  $\phi$  is determined then the signal is shifted by that amount via equation 5.31 and the overall euclidean distance is calculated again.

The results of the alignment algorithm are shown in Figures 5.22a, 5.22b and 5.22c. In each figure two identical MUAPs are shown. In the top half of Figure 5.22a the two MUAPs are unaligned and the euclidean distance calculated for the distances between the individual points is shown to be  $252\mu V^2$ . In the bottom half of the figure the two MUAPs are aligned and the euclidean distance is calculated to be  $58.1\mu V^2$ . From visual inspection of the signal it can be seen that aligned MUAPs look like they are from the same underlying waveform which they are indeed.

For the sake of demonstration to show that the above alignment algorithm works not only for MUAPs coming from the same underlying waveform but also for different MUAPs as is the case when pattern recognition techniques are applied, several different MUAPs were aligned

## UNALIGNED MUAPS

EUCLIDEAN DISTANCE:  $252.21 \mu\text{V}^2$ 

## ALIGNED MUAPS

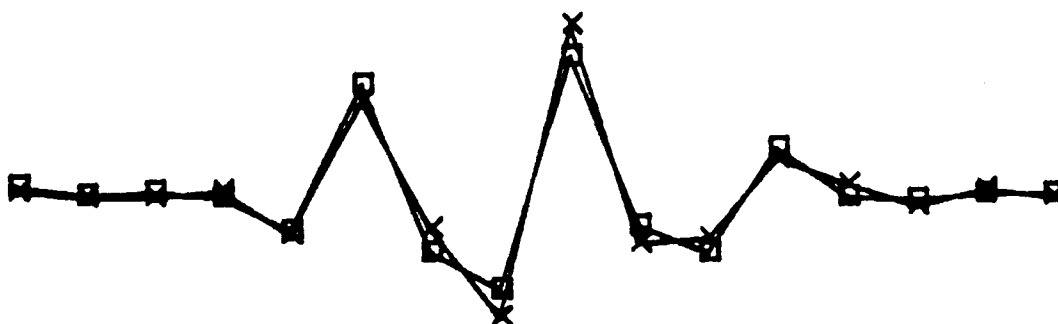
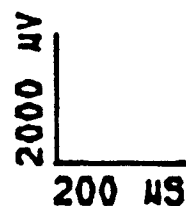
EUCLIDEAN DISTANCE:  $58.18 \mu\text{V}^2$ 

FIGURE 5.22A ALIGNMENT OF A MUAP



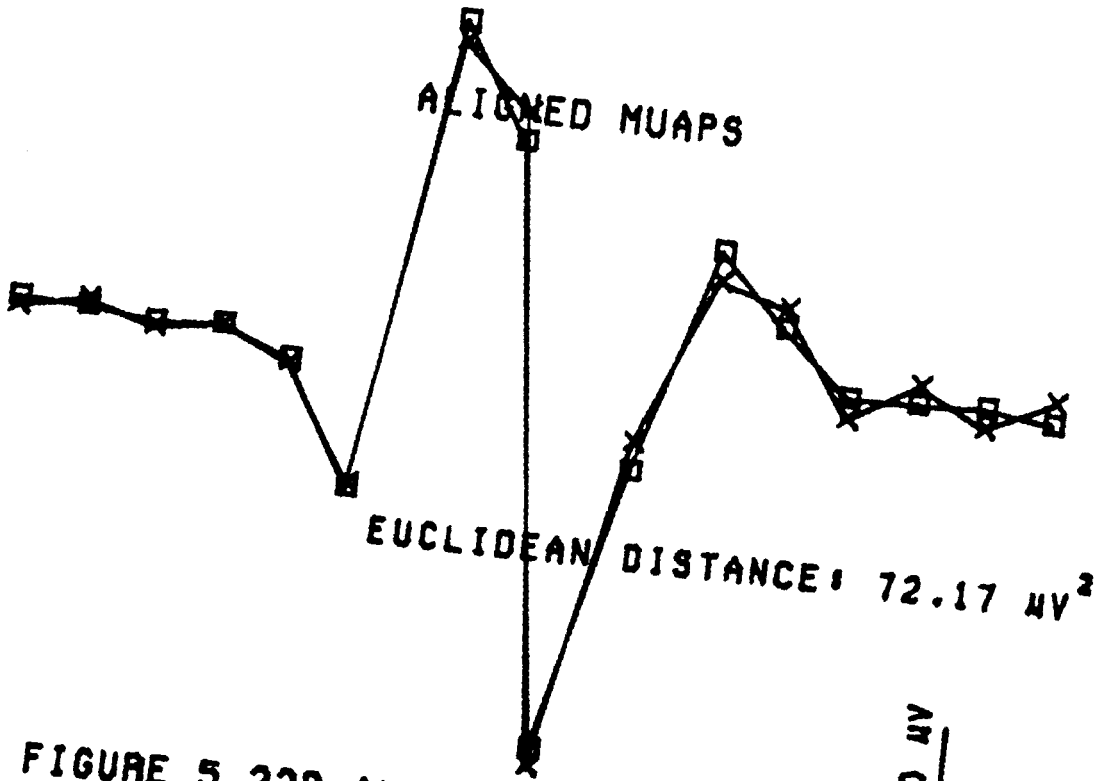
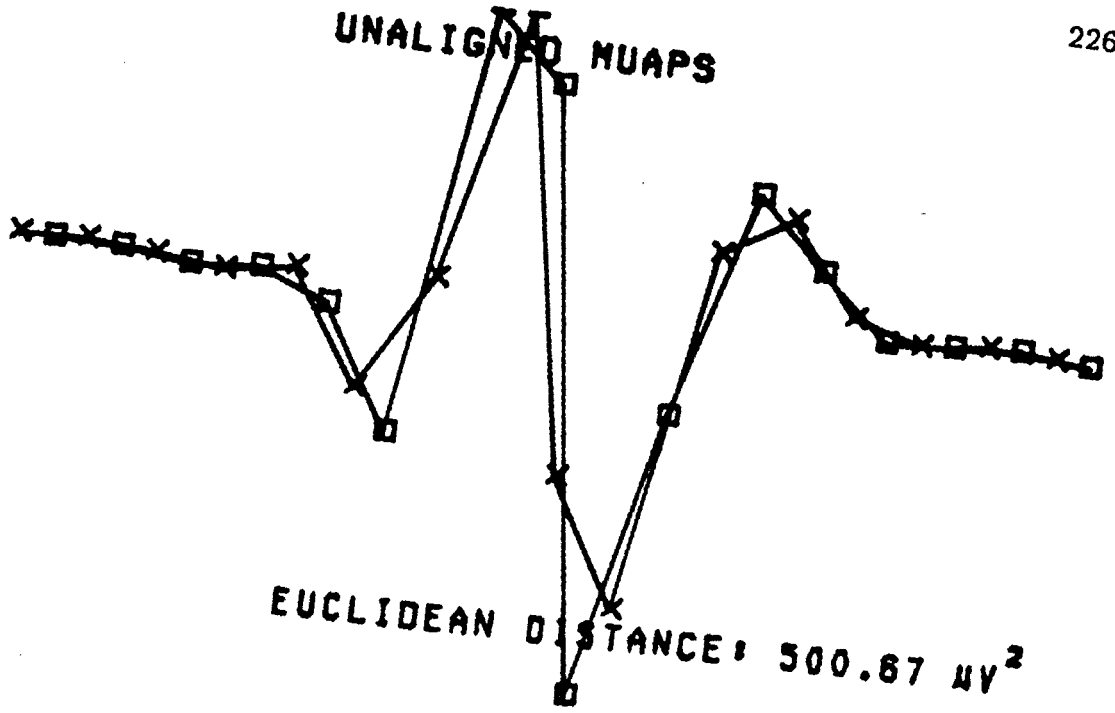
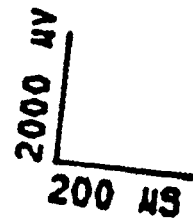
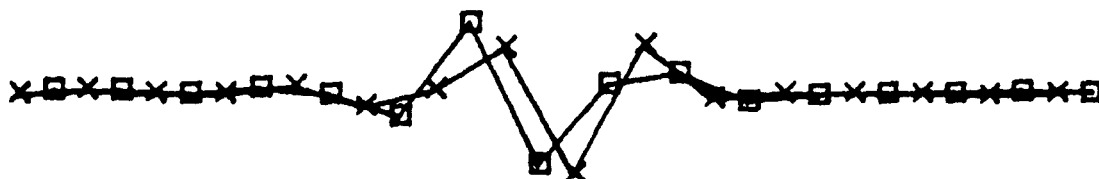


FIGURE 5.22B ALIGNMENT OF A MUAP

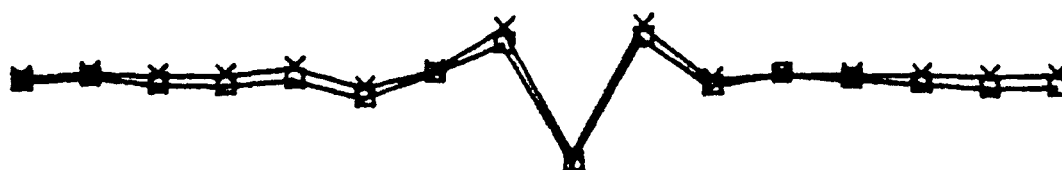


## UNALIGNED MUAPS



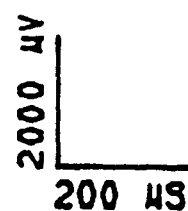
EUCLIDEAN DISTANCE:  $159.98 \mu\text{V}^2$

## ALIGNED MUAPS



EUCLIDEAN DISTANCE:  $38.69 \mu\text{V}^2$

FIGURE 5.22C ALIGNMENT OF A MUAP

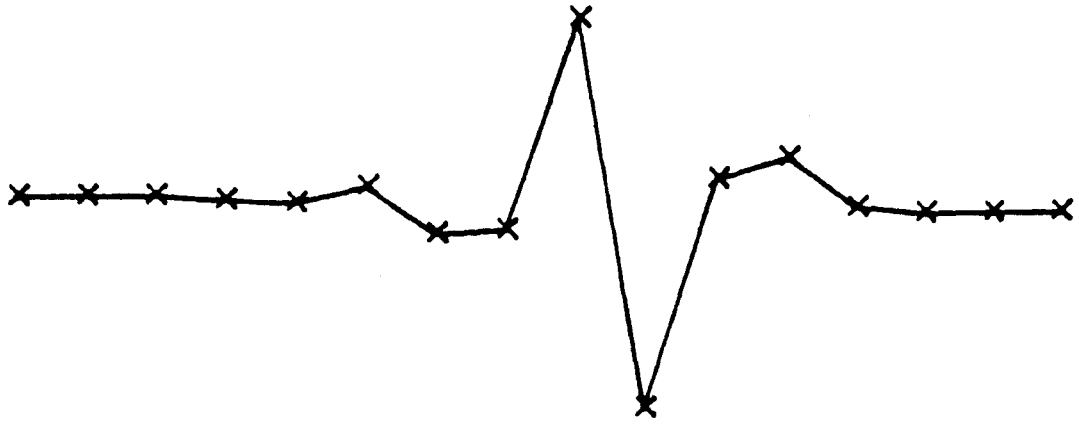


with each other. A typical alignment is shown in Figures 23a and 23b. As shown the alignment does work though due to the different peak times of the individual MUAPs the alignment can be quite rough at best.

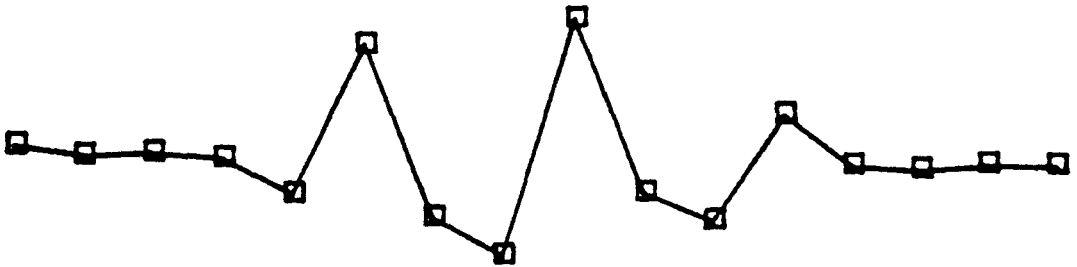
The same two MUAP classes used to generate Figure 5.20 were used to show the effect of the alignment algorithm on the MUAPs sampled with different phase shifts. The two MUAPs were sampled with random shifts and then aligned with the alignment algorithm. The results are presented in Figure 5.24. Clearly the two classes of MUAPs are distinct and can therefore be correctly classified.

### 5.3.5 Superpositions

For the resolution of superpositions the equation presented for the high resolution alignment of a signal vector to a class can be used with several modifications. First of all the superpositioned complex extracted earlier may be composed of two or more single MUAP signals. Exactly how many is not known but a rough estimate can be obtained from the number of peaks in the detection level output. This requires equation 5.60 to account for more than one MUAP at a time. Hence the equation must be extended to higher dimensions. Secondly, whereas equation 5.60 rotated the signal vector to obtain maximum alignment, this can no longer be done with the signal complex vector. The class vectors of single MUAPs must be rotated or shifted with respect to the MUAP complex vector. If  $\epsilon_m^2$  is the mean square error of the complex MUAP vector aligned with  $m$  class templates then equation 5.60 may be expressed as:

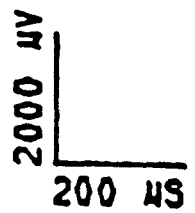


(A)

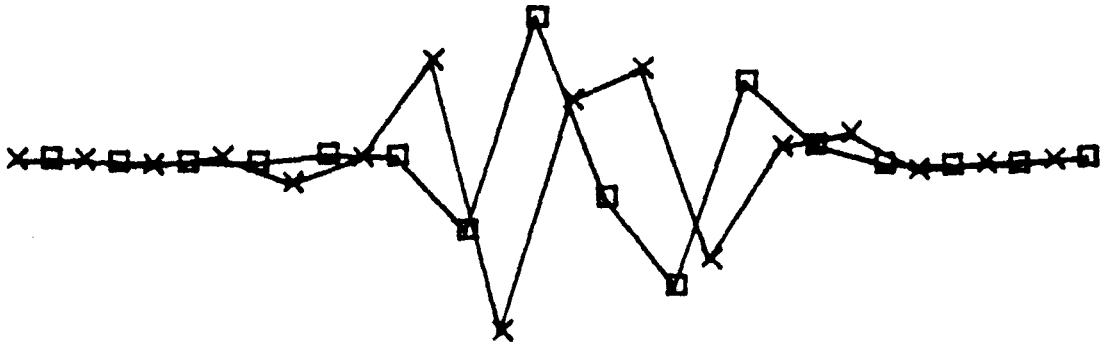


(B)

FIGURE 5.23A DIFFERENT MUAPS

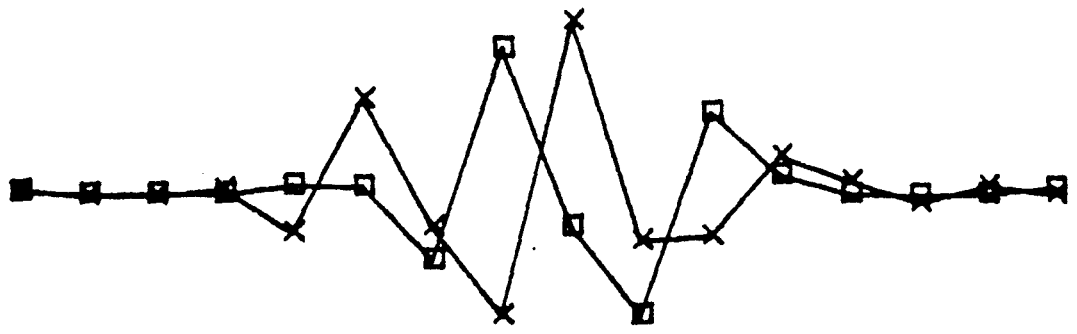


### UNALIGNED MUAPS



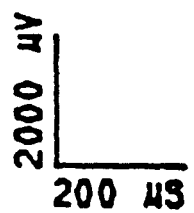
EUCLIDEAN DISTANCE: 451.84  $\mu\text{V}^2$

### ALIGNED MUAPS



EUCLIDEAN DISTANCE: 373.07  $\mu\text{V}^2$

FIGURE 5.29B ALIGNMENT OF MUAPS



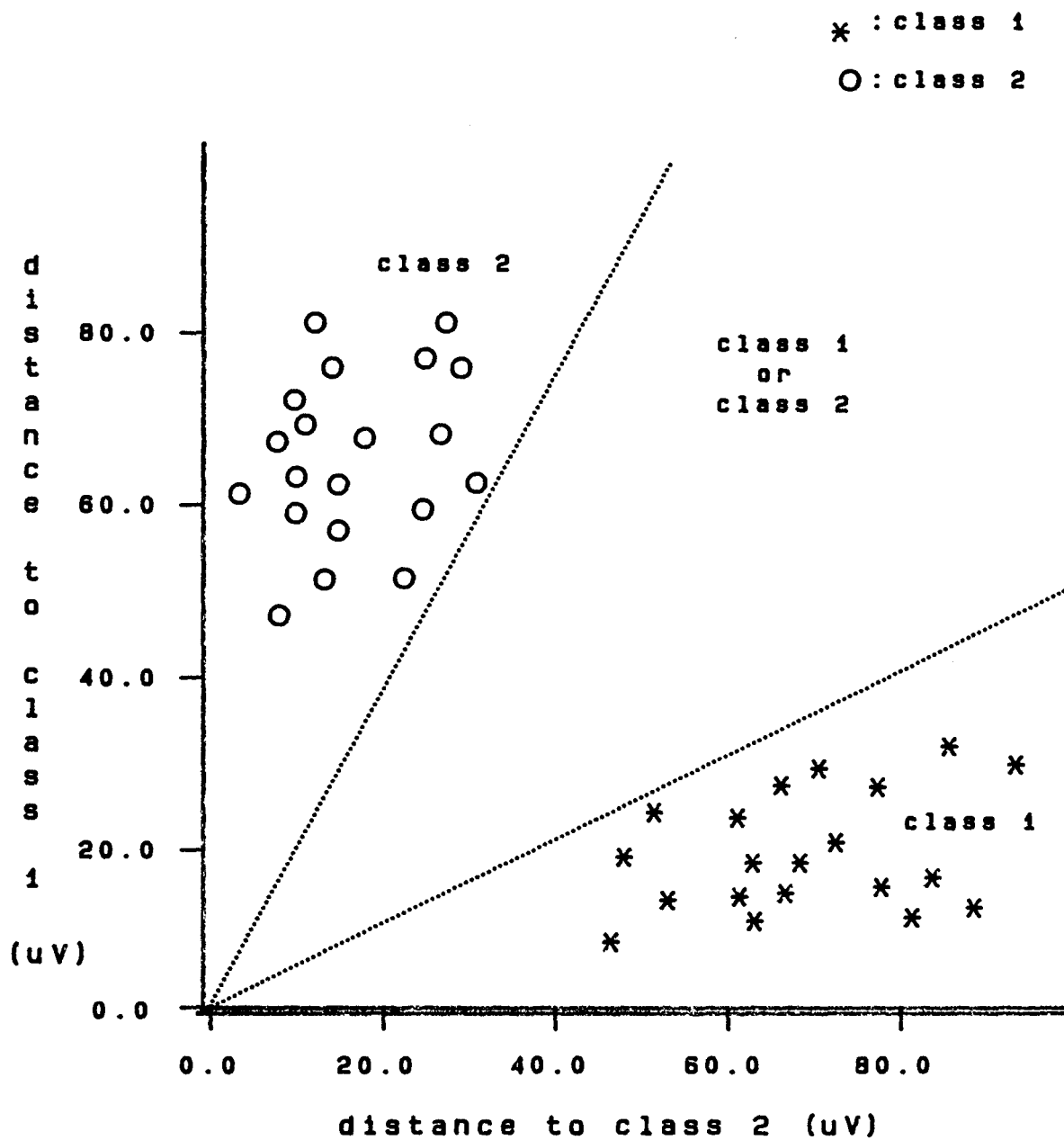


Figure 5.24 Distances between two different aligned MUAPs

$$\epsilon_m^2 = \frac{1}{N} \sum_{n=0}^{N-1} | S_n - C_{1,n,\phi_1} \cdot \cdot \cdot - C_{m,n,\phi_m} |^2 \quad 5.65$$

where  $S_n$  is the signal complex vector and  $C_{m,n,\phi_m}$  is the m'th class vector shifted by the value  $\phi_m$ .

There are several assumptions made by this equation. First, the above equation assumes that MUAPs superimpose algebraically. This is a very good assumption since there is no evidence of multiplicative interference. Secondly the above equation can only work if the complex vector is composed of some linear shift of class vectors which have already been extracted from the IP. If this is not the case then MUAP complexes cannot be resolved into their individual MUAPs. It should be pointed out here that with higher contraction levels there is more superpositioning. However, to overcome this resolution problem a low contraction to a high contraction protocol of the muscle is performed; thus the MUAPs recruited at lower contraction levels would likely be present at higher contraction levels and would likely be involved in superpositioning. Currently if the resolution of superimposed MUAPs is deemed undetermined (i.e.  $\epsilon_m^2$  too large) it is left unclassified. Furthermore in order to increase the probability of the individual classes occurring prior to superpositioning the resolution of superpositions is done after all single MUAPs have been extracted. As before a two step approach is taken for resolution of MUAPs, a rough resolution and a fine resolution.

### 5.3.6 Rough Alignment

In order to resolve superimposed MUAPs into single MUAPs a rough alignment is first done which attempts to indirectly deduce the number of MUAPs superimposed. This is done simply from the detection envelope as described earlier. Two or more superimposed MUAPs tend to produce two or more peaks in the MUAP detection complex. Again it should be noted here that the peaks are brief in occurrence and rarely superimpose. Thus the number of peaks gives an indication of the number of MUAPs superimpose and where they are superimposing in terms of the peak occurrence and the height of the action potential. Thus the first step in decomposing the MUAP complex is to determine if possible the following parameters of the detection complex. These are:

- 1) determining the probable number of peaks in the MUAP complex,
- 2) determining the time occurrence of these peaks and
- 3) determining the relative amplitude of these peaks.

With this information then the following analysis can be done. The number of peaks is assumed to equal the number of MUAPs superimposed. Thus this also equals the number of classes used in equation 5.65. Determining the time occurrences of these peaks provides a means for initially aligning the classes to the MUAP complex. Thus a local minimum is ensured for convergence and this greatly reduces the amount of computation time required by the fine resolution algorithm employed later.

The last specification of the amplitude is less reliable. The idea here is to choose the number of templates  $m$  whose height corresponds to the height of the peaks. Unfortunately since these signals are superimposed in the first place the MUAPs peaks can vary widely. This stipulation for rough alignment is rarely used. The rough alignment algorithm outputs are shown in Figures 5.25b and 5.26b.

The number of MUAPs is determined and placed in a comparison vector of length equal to the complex to be resolved. The peaks are aligned as best as possible to correspond to the peaks of the complex.. The next step which can be done therefore is the high resolution of these signals. It should be pointed out here that when the rough alignment is done, a distance measure is computed for (i.e. same cross correlation method) and if this is found to exceed a certain threshold then no further analysis is done on this class pair and a new pair of classes is chosen. Thus not all classes are aligned with the MUAP complex in a high resolution sense; rather only the ones which are relatively similar in a macro sense.

Of course for  $m$  different classes there are  $m!$  different ways they can be combined since order is important (i.e. MUAP complex may be composed of classes 1, 2 or 2, 1 since both are different).

### 5.3.7 Fine Resolution

The resolving of a superimposed complex is equivalent to the minimization of an  $N$  dimensional function. The minimization of a function

$f(x)$  of  $N$  dimensions along some direction  $u$  requires the gradient of the function to be perpendicular to  $u$  along that line minimum. Any particular point  $p$  of the function  $f(x)$  can be approximated by its Taylor series expansion of the form:

$$f(x) = f(p) + \sum_i \frac{\delta f}{\delta x_i} x_i + \frac{1}{2} \sum_{i,j} \frac{\delta^2 f}{\delta x_i \delta x_j} x_i x_j + \dots \quad 5.66$$

where the terms after the second partial derivative are assumed to be negligible. Adopting the following representations:

$$c \equiv f(p) \quad 5.67$$

$$b \equiv - \nabla f|_p \quad 5.68$$

$$[A]_{ij} \equiv \left. \frac{\delta^2 f}{\delta x_i \delta x_j} \right|_p \quad 5.69$$

then  $f(x)$  may be approximated by the quadratic equation (in  $N$  dimensions):

$$f(x) \approx c - b \cdot x + \frac{1}{2} x \cdot A \cdot x \quad 5.70$$

The gradient of the function  $f$  can be calculated from the equation:

$$\nabla f = A \cdot x - b \quad 5.71$$

The condition that a minimum in a line direction  $\mathbf{u}$  be obtained and then a new direction  $\mathbf{v}$  not destroy the minimum obtained is given by:

$$0 = \mathbf{u} \cdot \mathbf{A} \cdot \mathbf{v} \qquad 5.72$$

The two direction vectors  $\mathbf{u}$  and  $\mathbf{v}$  are said to be conjugate. Thus minimization along any particular line is preserved.

Of course this minimization assumes that the function to be minimized is of a quadratic form. If it is not then this will converge quadratically to the minimum.

### 5.3.8 Multidimensional Minimization Method

There are a variety of methods which can be used to minimize a function in  $m$  dimensions. The method employed in this thesis was the method presented by Polak and Ribiere (PR).

The method of PR requires the following properties of the function to be minimized. These properties are:

- 1) that the gradient of the function to be minimized is known and
- 2) the function is essentially smooth near the minimum.

The gradient of the function to be minimized is the vector of the first partial derivatives of the function. This is found by taking the partial

derivatives of equation 5.65 with respect to  $\phi_1, \dots, \phi_m$  to get the gradient vector  $\mathbf{g}$  of the form:

$$\left[ \frac{\delta \epsilon^2}{\delta \phi_1}, \frac{\delta \epsilon^2}{\delta \phi_2}, \dots, \frac{\delta \epsilon^2}{\delta \phi_m} \right]^T \quad 5.73$$

where the vector:

$$(\phi_1, \phi_2, \dots, \phi_m)^T \quad 5.74$$

is the vector of the individual class offsets used to align a particular superposition MUAP complex to  $m$  classes. The partial derivatives used in 5.73 can be found by taking the partial derivatives of equation 5.65. Differentiating equation 5.65 with respect to  $\phi_i$  gives:

$$\frac{\delta \epsilon^2}{\delta \phi_i} = \frac{4}{N} \sum_{n=1}^{N/2-1} \left( \frac{2\pi n}{N} \right) \text{Im} \left\{ C_{i,n,\phi_i} A_n^* \right\} \quad 5.75$$

where the value  $A_n$  is given by the expression:

$$A_n = S_n - C_{1,n,\phi_1} - \dots - C_{m,n,\phi_m} \quad 5.76$$

and  $\text{Im}$  is the imaginary part of the quantity in the brackets.

Therefore the general gradient vector can be found

The method of PR essentially is a line minimization routine which

does not require the use of the Hessian matrix in order to find the minimum. Essentially this method is a conjugate gradient method where the direction taken to the minimum is the conjugate of the gradient of the last step. The basic algorithm is as follows. Let  $A$  be an  $n \times n$  positive definite symmetric matrix and  $g_0$  and  $h_0$  arbitrary vectors such that  $g_0 = h_0$  then two sequences of vectors may be defined as:

$$g_{i+1} = g_i - \lambda_i A \cdot h_i \quad \text{and} \quad 5.77$$

$$h_{i+1} = g_{i+1} + \gamma_i \cdot h_i \quad 5.78$$

where  $\lambda_i$  and  $\gamma_i$  are chosen such that  $g_{i+1} \cdot g_i = 0$  and  $h_{i+1} \cdot A \cdot h_i = 0$ .

It should be noted here that if  $g_i \cdot A \cdot h_i = 0$  and or  $h_i \cdot A \cdot h_i = 0$  then take  $\lambda_i = 0$  and  $\gamma_i = 0$ . Thus the condition for:

$$g_i \cdot g_j = 0 \quad 5.79$$

and

$$h_i \cdot A \cdot h_j = 0 \quad 5.80$$

is satisfied.

Therefore all  $g_i$ 's are mutually orthogonal and all  $h_i$ 's are mutually

conjugate. The values for  $\gamma_i$  and  $\lambda_i$  can be found from the equations:

$$\gamma_i = \frac{(g_{i+1} - g_i) \cdot g_{i+1}}{g_i \cdot g_j} \quad 5.81$$

and

$$\lambda_i = \frac{g_i \cdot h_i}{h_i \cdot A \cdot h_i} \quad 5.82$$

which can be used to minimize the function of a quadratic form which of course equation 5.74 is. Now for the minimization routine from equation 5.74 it is required that at some point  $p_i$  then:

$$g_i = -\nabla f(p_i) \quad 5.83$$

Now for a local minimum in direction  $h_i$  at point  $p_{i+1}$  then:

$$g_{i+1} = -\nabla f(p_{i+1}) \quad 5.84$$

and

$$g_{i+1} = -A \cdot (p_i + \lambda h_i) - b = g_i - \lambda A \cdot h_i \quad 5.85$$

where  $\lambda_i$  is chosen such that the minimum condition is given by:

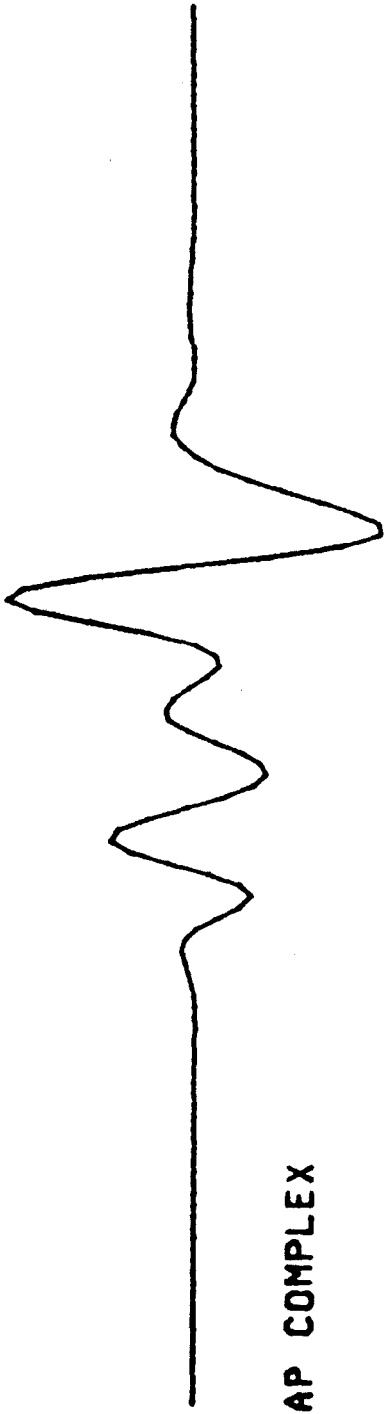
$$h_i \cdot \nabla f = -h_i \cdot g_{i+1} = 0 \quad 5.86$$

where equations 5.86 and 5.85 can be combined to solve for  $\lambda$  without knowledge of the hessian matrix  $A$ .

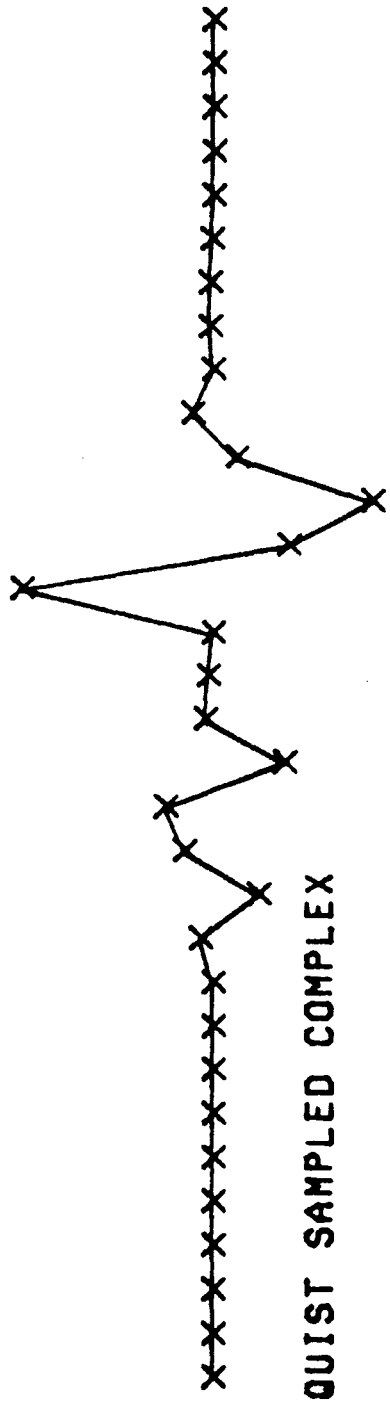
Essentially then the minimization routine finds the values of  $\phi_1$  through  $\phi_m$  which are required to rotate  $m$  classes of MUAP vectors such that  $\epsilon_m^2$  is a minimum. A typical superimposed MUAP complex is shown in Figures 5.25a and 5.26a. The over sampled MUAP complex is shown in the top half of the figure and the Nyquist sampled complex is shown below it. These particular complexes are composed of two individual MUAPs. Figures 5.25b and 5.26b show the initial alignment of the MUAP classes selected for each complex signal.

The results of the resolution of the superimposed MUAP complexes are shown in Figures 5.25c and 5.26c. In these figures the top half of the figure shows the rough alignment of the two classes to the superimposed signal. As shown in Figure 5.25c, the euclidean distance calculated for the distances between the individual points is shown to be  $58\mu V^2$ . In the bottom half of the figure the result of the multidimensional alignment routine is shown. The euclidean distance for this case is calculated to be  $17.06\mu V^2$ . Clearly then, the superimposed MUAP complex is composed of these two MUAP classes. Thus MUAP complexes can be resolved to some degree.

Once MUAPs are detected in the IP then both MUAP and MUAPT analysis can be done. As shown in this chapter, once the MUAP vector is



MUAP COMPLEX



NYQUIST SAMPLED COMPLEX

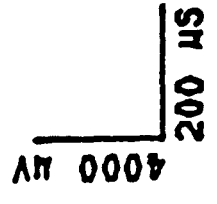


FIGURE 5.25A SUPERPOSITIONED MUAPS

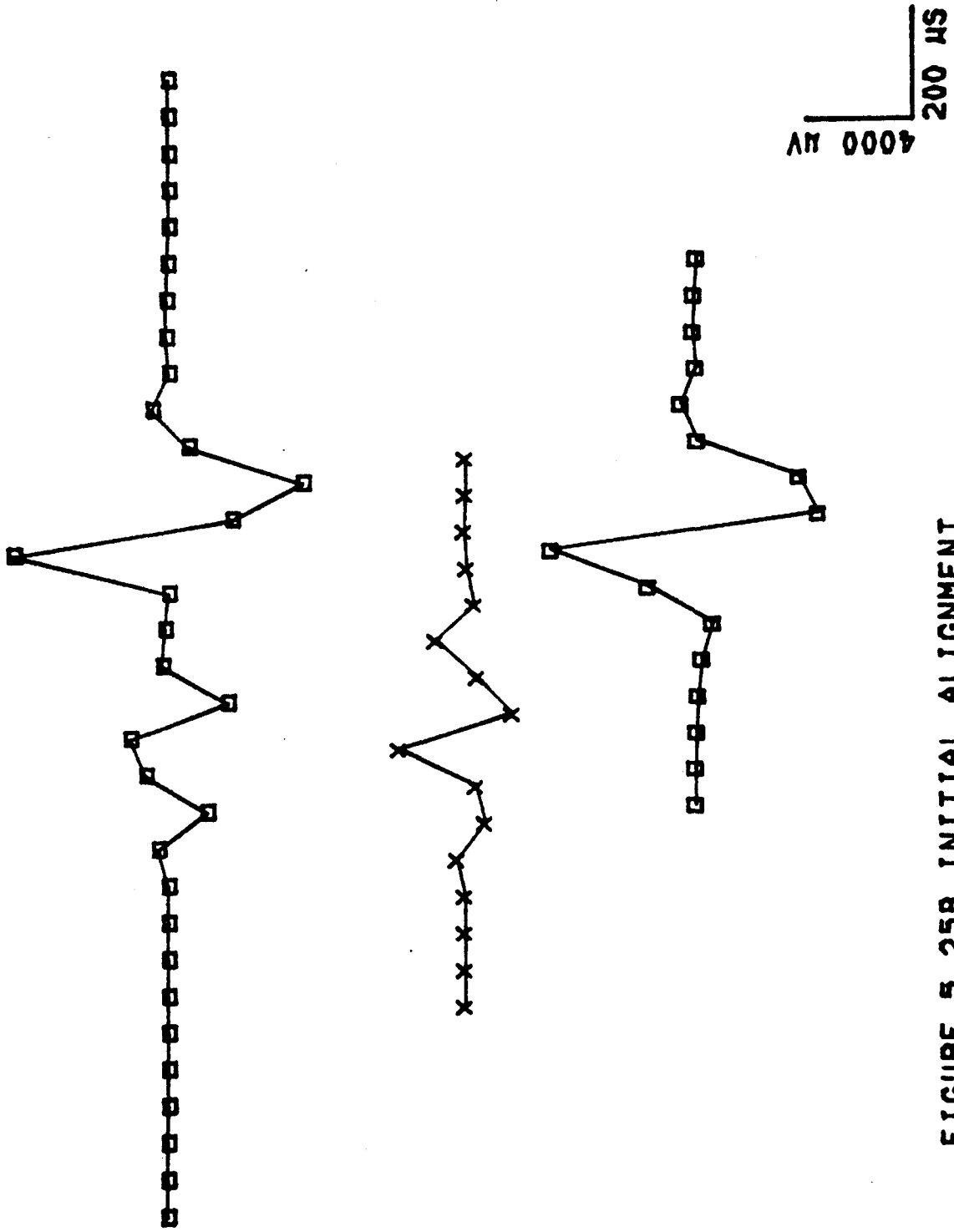
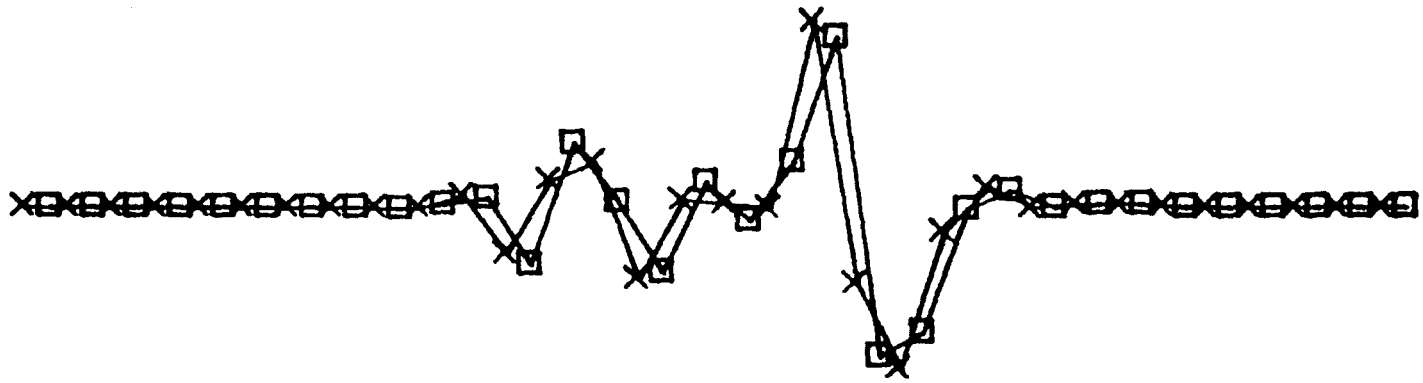
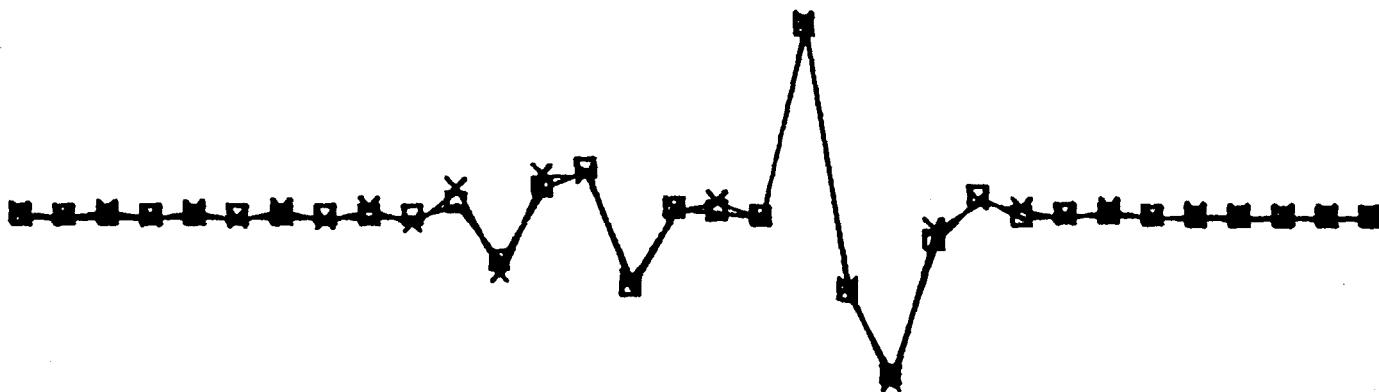


FIGURE 5.25B INITIAL ALIGNMENT



UNALIGNED MUAP COMPLEX

EUCLIDEAN DISTANCE: 56.02  $\mu\text{V}^2$



ALIGNED MUAP COMPLEX

EUCLIDEAN DISTANCE: 17.06  $\mu\text{V}^2$

FIGURE 5.25C ALIGNMENT OF MUAPS TO MUAP COMPLEX

4000  $\mu\text{V}$   
 200  $\mu\text{S}$   
 243

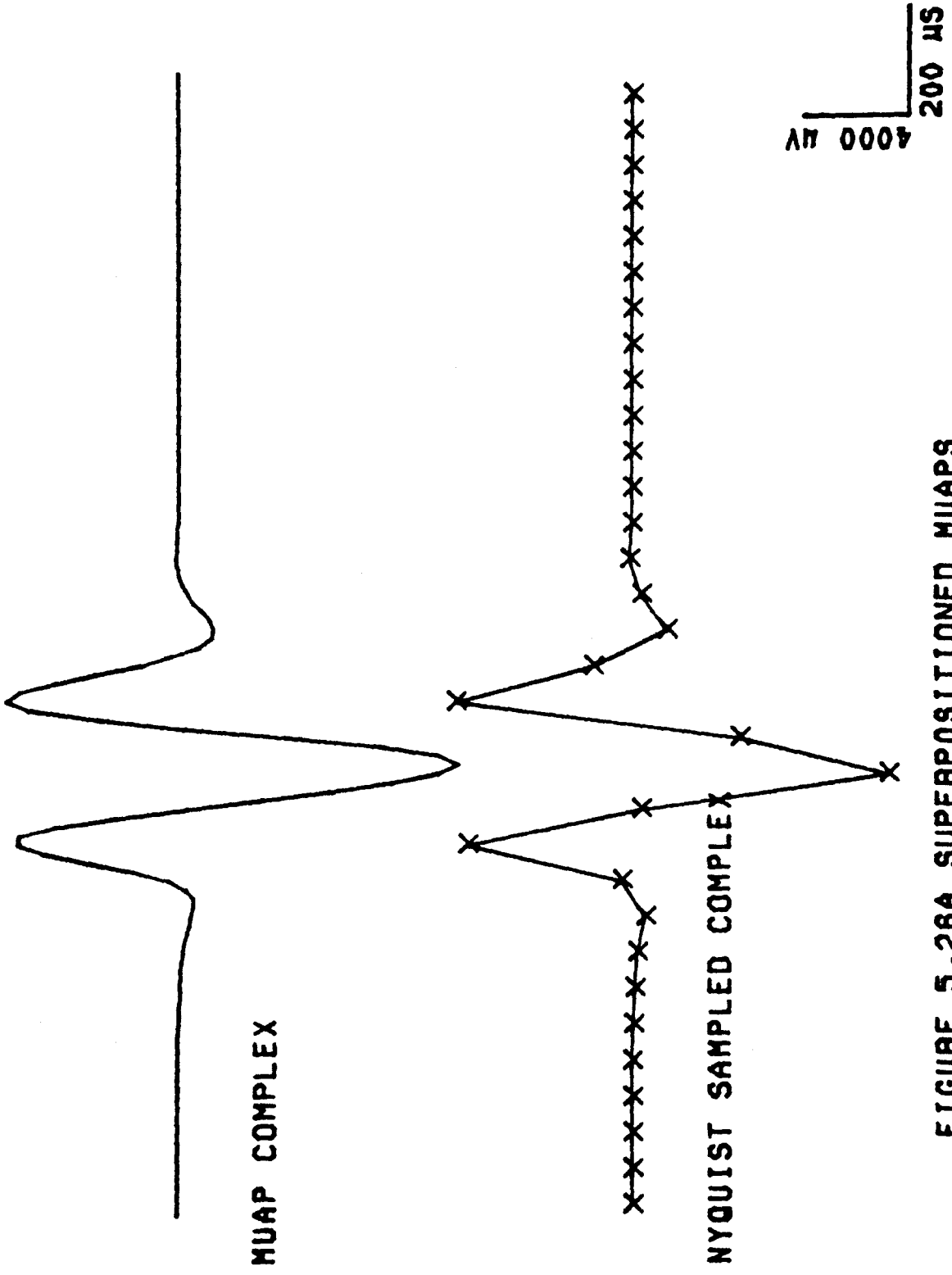


FIGURE 5.26A SUPERPOSITIONED MUAPS

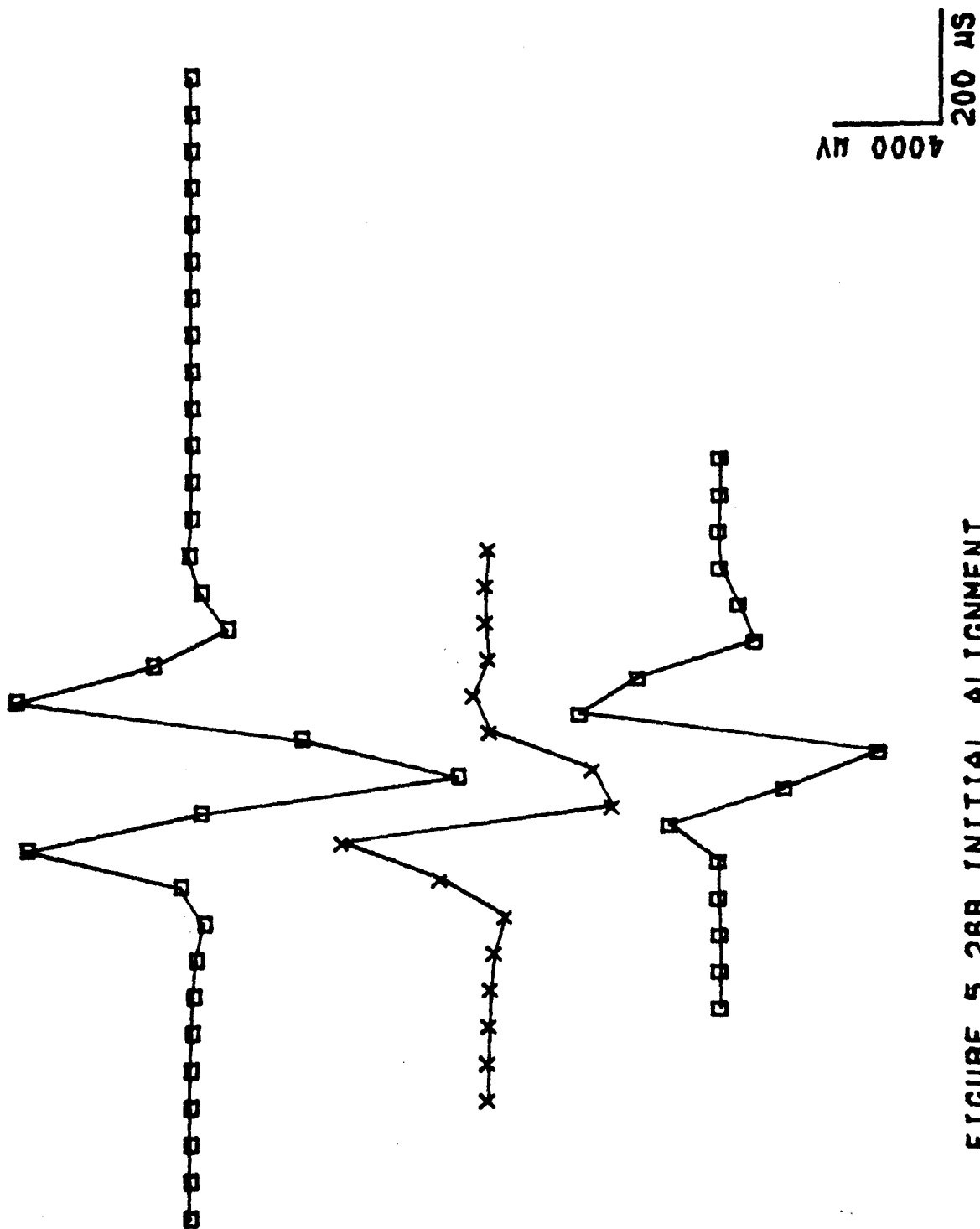


FIGURE 5.26B INITIAL ALIGNMENT

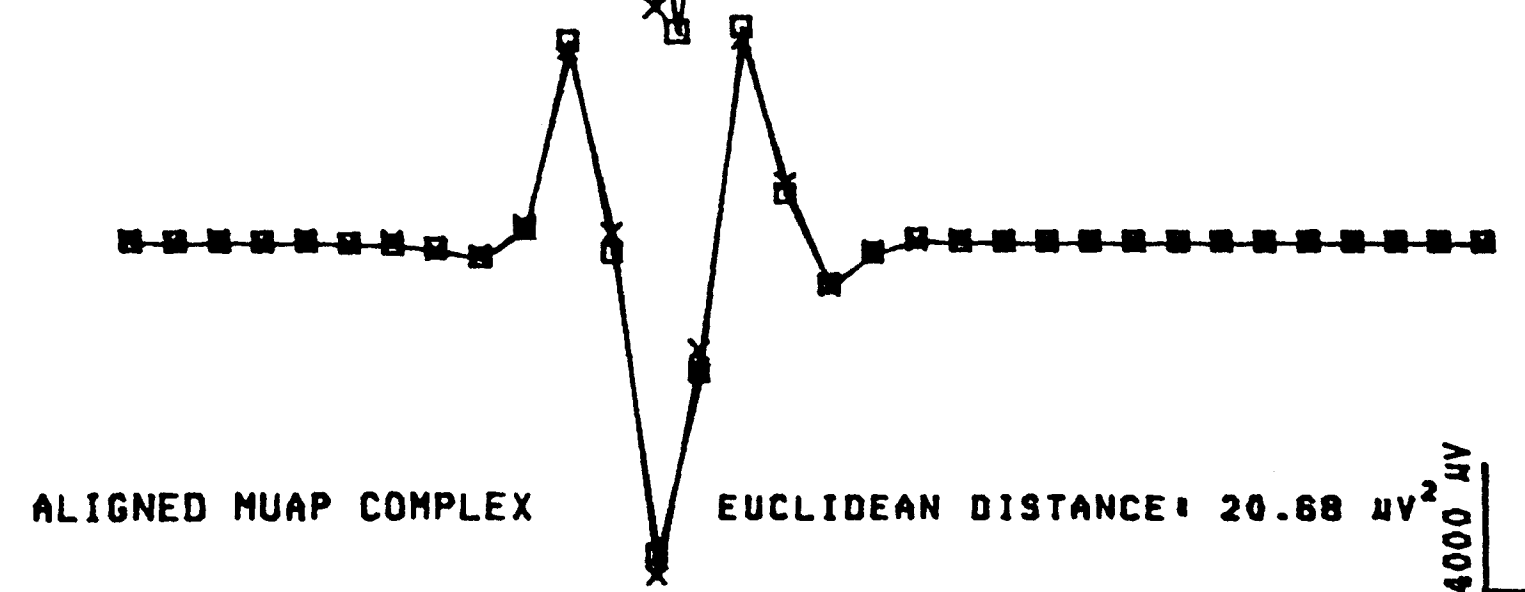
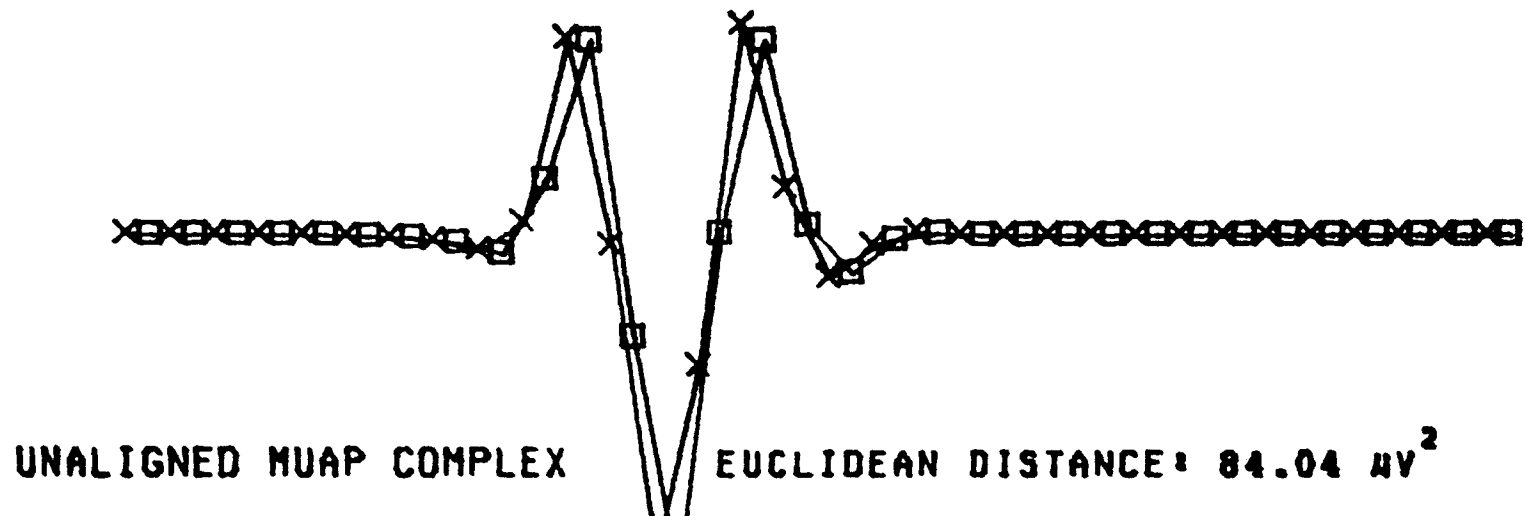


FIGURE 5.28C ALIGNMENT OF MUAPS TO MUAP COMPLEX

4000  $\mu\text{V}$   
200  $\mu\text{S}$   
246

represented by its discrete Fourier coefficients then the full brunt of the DFT properties can be brought to bear on the problems of classifying MUAPs, extracting MUAP characteristics and resolving MUAP superpositions.

## Chapter Six

### Conclusions and Recommendations

The purpose of this thesis was to describe the generation, recording and subsequent analysis of the electromyogram (EMG) produced by skeletal muscle. As pointed out in Chapter One and shown in Chapter Four the means by which this analysis was accomplished was through the use of a multichannel single fiber recording electrode. Supporting hardware and software systems were developed in order that the EMG signals recorded from the first dorsal interosseus (FDI) muscle could be analyzed. In order to develop a viable multichannel recording system a thorough understanding of the generation, recording and subsequent analysis of EMG signals was required. Essentially this led to an understanding of the intricate relationships regarding generation, recording and analysis, and highlighted the tremendous variability that can occur in the EMG characteristics depending on how and where this signal is recorded. Conclusively, as was demonstrated in Chapter Two an understanding of MUAP generation is required for the recording of EMG signals.

Chapter Three presented a variety of ways in which the EMG signals have been analyzed. These methods basically fall into three main categories; interference pattern analysis, MUAP analysis and MUAPT analysis. A description of each analysis method was done. Along with these descriptions, some idea as to what type of information regarding muscle control could be gained from each of these analyses was presented. The necessary and sufficient information present in the EMG signal from a muscle control point of view is manifested by MUAPs located in

that signal. Particular emphasis was therefore placed on the physiological characteristics, as defined by electromyographers, that are used to describe MUAPs. Needless to say this was also done through the belief that any viable multichannel recording system must eventually be used by electromyographers (not only engineers) and therefore should be compatible with the current knowledge and expertise. Finally, it was concluded from this chapter that in order to successfully develop an understanding of muscle control, not only must MUAP analysis be done but MUAPT analysis as well. It is in these two types of analysis that the concept of pattern recognition comes about and indeed is required for separation of MUAPs into MUAPTs. The methods and means by which MUAPs are separated into MUAPTs are as varied and complex as there are ways to classify data. Many such classification methods have been used in the past and several were presented in this chapter. This survey of classification methods that have been applied to EMG analyses provided the necessary groundwork from which a classification system involving the multichannel recorded EMG signals could be developed.

With an understanding of the generation, recording and analysis of EMG activity, a multichannel single fiber recording system was then designed. The implementation of this recording system included both hardware and software interfacing. These implementations were presented in Chapter Four; the collection of motor unit action potentials. The details of the hardware preprocessor were presented in Appendix A while the functionality of the preprocessor was presented in Appendix C. The design of the instrumentation amplifier and filtering circuits was done with the knowledge previously obtained from the study of the generation and recording processes. Continuous recordings of EMG signals to FM tape via the hardware preprocessor and multichannel single fiber recording electrode were

possible. With the aid of supporting software, contiguous records of three fine wire EMG signals, the cannula EMG signal and the force produce by the FDI muscle could be digitized on a PDP 11/34 via an LPS11 A/D front end. Even though a fast double buffer collection algorithm was written in PDP 11/34 assembler the collection and analysis of the MUAPs could not be done on line due to both the speed and memory limitations of the PDP 11/34 computer. Enhancement of the single fiber EMG recordings was accomplished by taking the difference between successive single fiber channels enabling the elimination of low frequency background MUAPs in the EMG signal.

Using the digitized recordings of EMG activity, preliminary detection and analysis techniques were performed in order to extract MUAPs from the EMG signal. As described in Chapter Five, Nyquist sampled EMG signals had to be used for analysis due to the limited collection rates and memory storage available with the present computer system. This lead to several problems when trying both to extract MUAPs from ambient EMG activity and determining the characteristic features of a MUAP. The only way to alleviate these problems was to perform some sort of interpolation on the Nyquist sampled signals. The method chosen to do this interpolation involved determining the DFT coefficients of the discretely sampled signals. In essence then these DFT coefficients were the features used to describe MUAPs. As shown in the chapter, the properties associated with the discrete Fourier transform were used extensively for extraction of MUAPs from the EMG record, interpolation (rotation), determining peaks and zeros of the MUAPs analyzed and deciding whether or not a particular MUAP identified, belonged to one motor unit or another. Algorithms were developed for implementing each of the above procedures. Furthermore, this representation of the MUAP allowed the

resolution of superimposed MUAPs into individual MUAPs as long as the MUAPs comprising the superimposed signal were identified as having occurred separately at some other point in time. With these DFT techniques in place then the process of MUAP analysis (and to some extent MUAPT analysis) was essentially reduced to arithmetic computation. Preliminary analysis demonstrated the validity and accuracy of using the DFT coefficients in determining both MUAP characteristics and classes of MUAPs.

Further development of a MUAPT analysis system must be done in order to make the multichannel single fiber recording system a usable diagnostic tool. The basic recording and collection systems are in place. The implementation of such a system to a new computer system is a relatively straight forward task due to the modularity of the designed system. Furthermore, the installation of the multichannel recording system to a computer with greater speed, larger memory and faster A/D front end will alleviate many of the the problems encountered in the EMG analysis. Apart from future computational considerations, further improvements could be made in the hardware preprocessor. An isolated front end, more adaptable force signal generator and a direct interface to an A/D collection system are just a few of the suggested hardware preprocessor changes. Further improvements could also be made in the multichannel single fiber recording electrode. The current design of the electrode is linear regarding its recording volume within the muscle. This limits the interpretation of the MUAP to a plane parallel to this linear array of electrodes. Future designs involving three dimensional recording electrodes should be considered not only to develop a better understanding of the shape of the MUAP in a volume of muscle but also to be used in determining the location of the motor unit which is firing.

Of course the algorithms designed and implemented for MUAP analysis can be improved. Future considerations involve looking at different representations of MUAPs (such as principal curves) and new ways of classifying MUAPs (i.e. with neural networks). Many of the software problems encountered in the development of the algorithms will be alleviated when higher sampling rates and greater memory storage are available.

The goal of this thesis was to do the preliminary groundwork required for the functional analysis of skeletal muscle. This required the understanding of the generation and recording of EMG activity and lead to an initial attempt at MUAP analysis. The results of this preliminary groundwork and analysis demonstrate that this goal has been achieved.

## Appendix A

### Hardware Preprocessor Design

#### A.0 Introduction

The purpose of this appendix is to describe in detail the hardware designed to collect both multichannel fine wire and cannula EMG and force signals produced by the muscle under study.

#### A.1 Instrumentation Amplifier

The input stage of the data acquisition hardware is an instrumentation amplifier. The configuration of the instrumentation amplifier is shown in Figure A.1. This figure shows both the instrumentation amplifier and the preamplifier used. The instrumentation amplifier has a typical configuration where the first two operational amplifiers are voltage followers and the third operational amplifier is a differencing amplifier. For the multichannel single fiber electrode there are four instrumentation amplifiers; three for the single fiber electrodes and one for the cannula. For each instrumentation amplifier there are three inputs; one for the single fiber or cannula recording surface, one for signal reference and one for the ground (shown in the figure). Parameters which characterize the instrumentation

amplifier are:

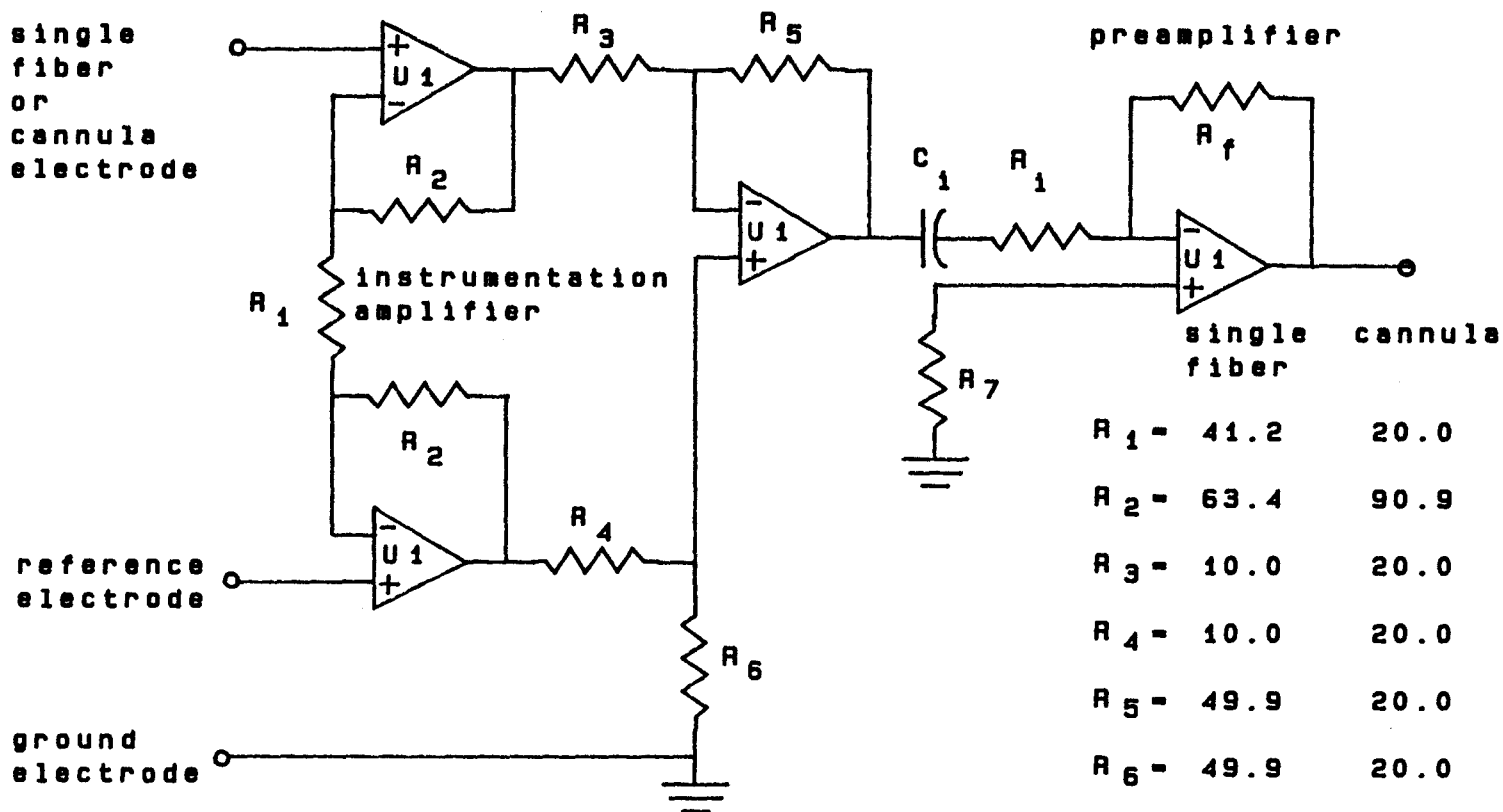
- (1) input impedance,
- (2) common mode rejection ratio and
- (3) gain.

The input impedance of the amplifier,  $Z_{in}$ , is the input impedance of the operational amplifiers used. In this case it is on the order of  $10^{12}$  ohms. The actual input amplitude of the recorded signal then is basically the ratio of the input impedance of the amplifier divided by the summation of this impedance with the impedance of the needle electrode  $Z_n$ . For the multichannel fine wire needle of  $10\text{k}\Omega$  (calculated in chapter four), the reduction in the recorded signal as a percentage of the input amplitude of the signal is given by:

$$\% \text{ Reduction} = 100 \left[ 1 - \frac{Z_n}{Z_n + Z_{in}} \right] \quad \text{A.1}$$

Thus the reduction in the EMG signal recorded by the instrumentation front end is approximately 0.00001%, therefore there is little input signal attenuation.

The common mode rejection ratio is defined as the differential gain of the amplifier divided by the common mode gain of the amplifier. For the instrumentation amplifier shown in Figure A.1 the common mode rejection ratio is on the order of 120db at 60 Hz. Thus the common mode noise present at the inputs of the amplifier is rejected.



$R_1 =$	41.2	20.0
$R_2 =$	63.4	90.9
$R_3 =$	10.0	20.0
$R_4 =$	10.0	20.0
$R_5 =$	49.9	20.0
$R_6 =$	49.9	20.0
$R_7 =$	1.0	1.0
$R_f =$	100.0	100.0
$C_1 =$	2.0	1000.0

U1: CA3240 op amp

note: resistance values in  $k\Omega$   
capacitance values in  $\mu F$

Figure A.1 Input amplifier

The gain,  $G$  of the instrumentation amplifier used is given by the equation:

$$G = \left[ \frac{2R_2}{R_1} + 1 \right] \left[ \frac{R_5}{R_3} \right] \quad \text{A.2}$$

where the resistance values are as shown in Figure A.1. The gains for the instrumentation amplifiers were chosen to be 20 times for single fiber EMG activity and 10 times for cannula activity.

The instrumentation amplifier is ac coupled to the preamplifier. This ac coupling is required in order to eliminate any dc offset resulting from electrode half cell potentials present at the electrode/electrolyte interfaces (chapter two) and the instrumentation amplifiers. It is justifiable to do this since the EMG signals are inherently ac to begin with (chapter two). The capacitor  $C_i$  is called the decoupling capacitor. The preamplifier along with this capacitor forms a high pass filter with a transfer function of the form:

$$H(j\omega) = - \frac{R_f}{\frac{1}{j\omega C_i} + R_i} \quad \text{A.3}$$

giving:

$$H(j\omega) = \frac{V_o(j\omega)}{V_i(j\omega)} = - \frac{R_f}{R_i} \left[ \frac{j\omega\tau}{1 + j\omega\tau} \right] \quad \text{A.4}$$

:where  $\tau = R_i C_i$ ,  $V_o$  is the output voltage and  $V_i$  is the input voltage and  $R_i$  and  $R_f$  are as shown in Figure A.1.  $\tau$  is the time constant of the filter. From this it

is clearly seen that for frequencies much less than  $\frac{1}{2\pi\tau}$  the circuit behaves like a differentiator ( the impedance of the capacitor is greater than the impedance of the resistor) and for frequencies much greater than  $\frac{1}{2\pi\tau}$  it acts like an inverter ( the impedance of  $R_i$  is large compared to the impedance of  $C_i$ ). For this implementation  $f_c$  was chosen to be 250 Hz for single fiber and 0.5 Hz for cannula recorded EMG. If  $R_i$  is chosen to be 10 k $\Omega$  then the value of the capacitance can be found by the equation:

$$C_i = \frac{\tau}{R_i} = \frac{2\pi}{fR_i} \quad \text{A.5}$$

The values of  $C_i$  for the fine wire and cannula EMG recording channels are approximately 2.2 and 1000  $\mu\text{F}$  respectively. For frequencies greater than those those specified above the EMG activity is amplified by 50 times. Thus the overall gain at the preamplifier stage is 1000 for the single fiber and 500 for the cannula recorded EMG activities.

## A.2 Amplifier

Further amplification is provided by an amplifier stage following the preamplifier. A simple voltage inverter amplifier is used. The amplifier is shown in Figure A.2. The gain  $G$ , is given by:

$$G = -\frac{R_f}{R_i} \quad \text{A.6}$$

where  $R_{f_x}$  and  $R_i$  are given in Figure A.2. The amplifier has selectable gain settings of 1, 2, 5 or 10. The gain switching is achieved through the use of analog switches shown as  $S_1$  through  $S_4$ . Therefore the overall gain of single fiber EMG is 1000 to 10,000 times and for cannula EMG from 500 to 5000 times. As previously pointed out (chapter two) the typical range for needle recorded EMG signals is on the order of 1 millivolt. Since the LPS-11 A/D converter used has a range of  $\pm 5$  volts these amplifications are adequate for utilizing the full range of the A/D converter.

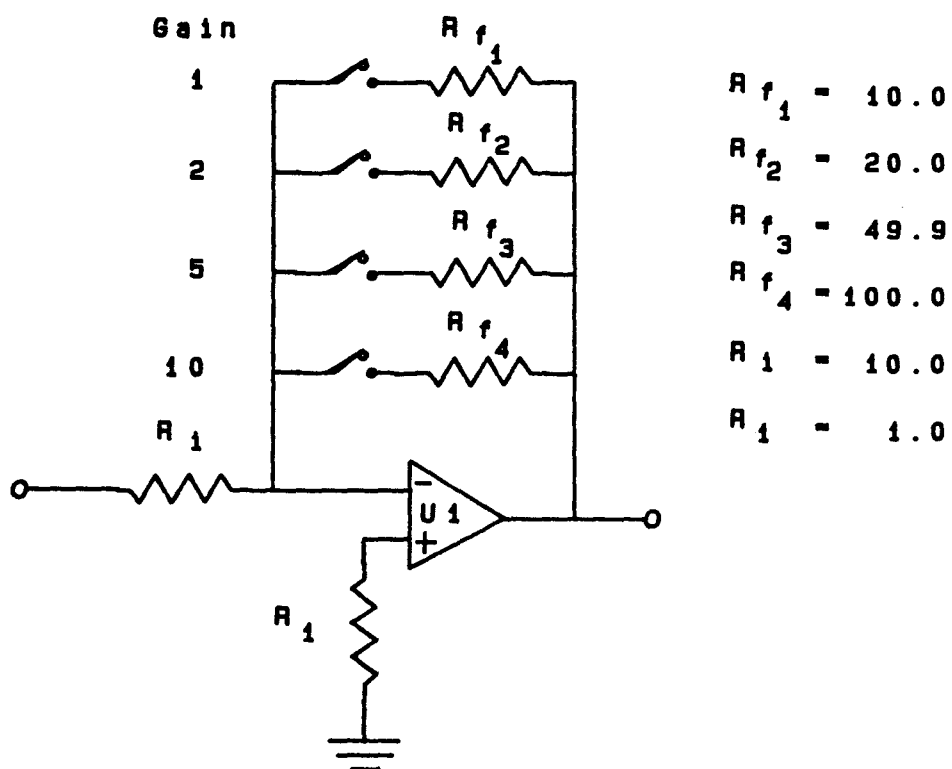
### A.3 Filtering

Filtering of the EMG signals is accomplished by active fourth order Butterworth filters. The butterworth filters are used to ensure constant amplitude and linear phase delay in the pass band. In fact their amplitude response is called a maximally flat response [194][195].

The design of the filters included a fourth order low pass Butterworth filter and a fourth order high pass Butterworth filter in order to create a band pass filter. The fourth order (low pass and high pass) Butterworth filters were implemented by using two second order filter stages. The design of these filters follows from the equations is given below.

The equation for the low pass amplitude function of a Butterworth filter of  $n$ th order is of the form:

$$|H(j\omega)| = \frac{A}{\sqrt{1 + (\omega/\omega_c)^{2n}}} \quad \text{A.7}$$



U1: 34001 Bifet input op amp

note: resistance values in  $k\Omega$

Figure A.2 Amplifier

where  $|H(j\omega)|$  is the magnitude of the response,  $A$  is the gain coefficient,  $\omega$  is the frequency  $\omega_c$ , is the cutoff frequency and  $n$  has the values 1, 2, ... ,  $N$ . This type of filter is an all pole filter which can therefore be expressed as a transfer function in the  $s$  plane as:

$$\frac{V_o}{V_i}(s) = \frac{Kb_o}{S^n + b_{n-1}S^{n-1} + \dots + b_1S + b_o} \quad \text{A.8}$$

where  $b_o \dots b_n$  are constants,  $K$  is a gain constant and  $V_o$  and  $V_i$  are the output and input signal voltages respectively. Further simplification may be made by normalizing the frequency ( $\omega=1$ ) and factoring for even ordered filter lengths:

$$\frac{V_o}{V_i}(s) = \prod_{k=1}^{N/2} \frac{A_k}{s^2 + a_k s + 1} \quad \text{A.9}$$

where  $A_k$  is the gain of the  $k$ 'th second order stage and  $a_k$  is a constant given by the equation:

$$a_k = 2 \text{ SIN} \left[ \frac{(2k - 1)\pi}{2n} \right] \quad \text{A.10}$$

for  $k = 1, \dots, n$  and where  $n$  is the even order of the filter.

Since filter equations may be described as functions in the  $s$ -plane they may therefore be constructed from operational amplifiers. There are a variety of configurations which may be used. The structure chosen for this hardware

implementation of a low pass Butterworth filter is a voltage controlled voltage source (VCVS) as shown in Figure A.3. From the figure, the choice of  $C_2$  ( $C_4$ ) is preferably near  $10/f_c \mu\text{F}$  where  $f_c$  is the cutoff frequency desired for the low pass filter. Then  $C_1$  ( $C_3$ ) is found according to the equation:

$$C_1 \leq \frac{a_k^2 C_2}{4} \quad \text{A.11}$$

which ensures  $R_1$  ( $R_3$ ) has a real value. The resistance value for  $R_1$  may be found by solving the equation:

$$R_1 = \frac{2}{\left[ a_k C_2 + \sqrt{(a_k^2 + 4(K-1))C_2^2 - 4C_1 C_2} \right] \omega_c} \quad \text{A.12}$$

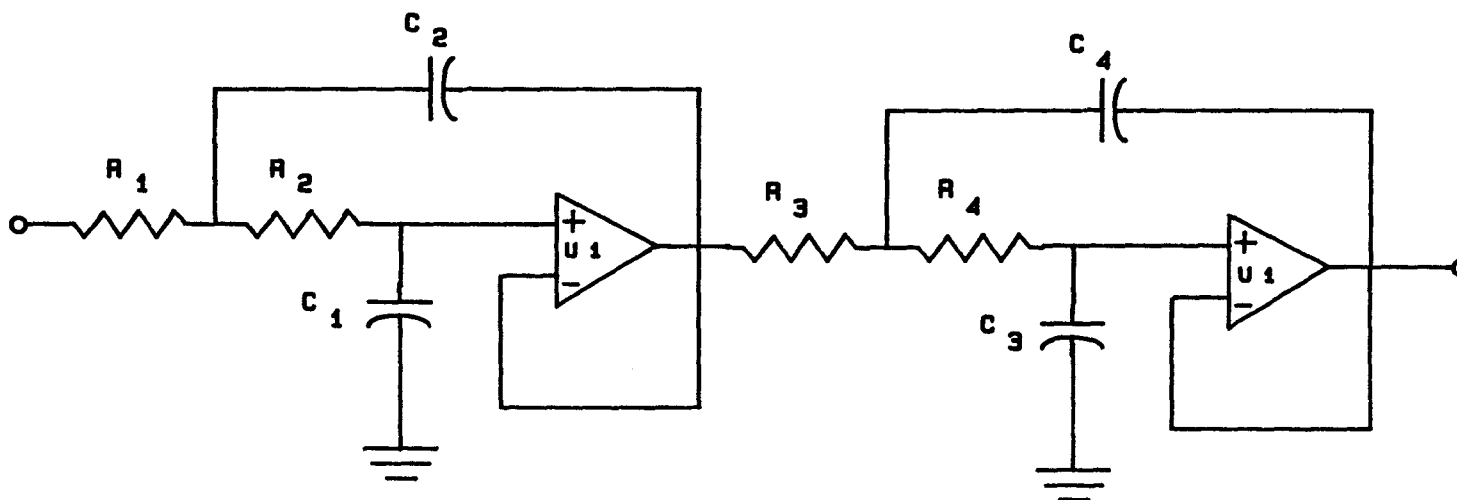
where again  $K$  is the gain of the filter,  $\omega_c$  is the cutoff frequency and  $C_1$  and  $C_2$  are as specified above. For this implementation the gain  $K$  was set at 1 thus the middle term of equation A.12 drops out and the equation becomes:

$$R_1 = \frac{1}{\left[ a_k C_2 + \sqrt{a_k^2 - 4C_1 C_2} \right] \omega_c} \quad \text{A.13}$$

The resistance value for  $R_2$  may be found similarly by solving the equation:

$$R_2 = \frac{1}{C_1 C_2 R_1 \omega_c^2} \quad \text{A.14}$$

Thus the resistance and capacitance values specifying a low pass Butterworth



$$F_c = 5.000 \text{ Hz}$$

$$C_1 = 0.0001$$

$$R_1 = 0.0001$$

$$C_2 = 0.001$$

$$R_2 = 0.001$$

$$C_3 = 0.00068$$

$$R_3 = 0.00068$$

$$C_4 = 0.001$$

$$R_4 = 0.001$$

U1: 34001 Bifet input op amp

note: resistance values in  $k\Omega$   
 capacitance values in  $\mu F$

Figure A.3 Fourth order low pass Butterworth filter

filter of even order  $n$  may be found for a particular cutoff frequency  $\omega_c$  for the VCVS. The low pass filter settings for the fourth order Butterworth filter were 5,000 Hz for both the cannula and single fiber EMG signals. The values of the resistances and capacitances resulting from the cutoff frequencies are shown in Figure A.3.

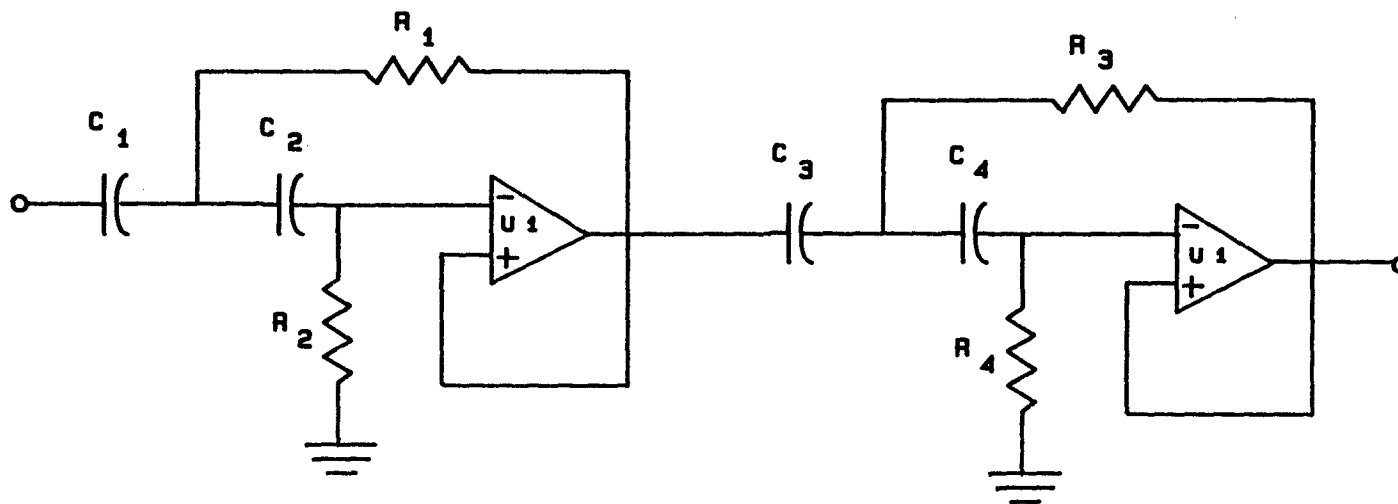
A general second order high pass Butterworth filter can be described in the  $s$ -plane by the equation:

$$\frac{V_o}{V_i}(s) = \frac{Ks^2}{(s^2 + a_k\omega_c s + \omega_c^2)} \quad \text{A.15}$$

where again  $\omega_c$  is the cutoff frequency,  $K$  is the gain and  $a_k$  is a constant given by equation A.10. The implementation of the high pass Butterworth filter was a fourth order design implemented in two second order stages. Furthermore, the structure of the filter in hardware terms was a voltage controlled voltage source much like that used for the low pass Butterworth filter. This is shown in Figure A.4. Again the same criteria used for the low pass filter design are used for selecting the capacitance values  $C_1$  ( $C_3$ ) and  $C_2$  ( $C_4$ ) in the high pass design. The resistance values  $R_1$  ( $R_3$ ) and  $R_2$  ( $R_4$ ) are given by the equations:

$$R_2 = \frac{4}{(2a_k\omega_c C_1)} \quad \text{A.16}$$

$$R_1 = \frac{1}{\omega_c^2 C_1^2 R_2} \quad \text{A.17}$$



single fiber		cannula		single fiber		cannula		single fiber		cannula	
$F_c = 250 \text{ Hz}$		$0.8 \text{ Hz}$		$C_1 = 0.0001$	10.0	$R_1 = 6.30$	7.68	$C_2 = 0.001$	10.0	$R_2 = 42.02$	51.02
		$C_3 = 0.00068$	10.0	$R_3 = 15.05$	18.20	$C_4 = 0.001$	10.0	$R_4 = 17.38$	21.53		

U1: 34001 Bifet input op amp

note: resistance values in  $k\Omega$   
 capacitance values in  $\mu F$

Figure A.4 Fourth order high pass Butterworth filter

where  $a_k$  is again found by Equation A.10. The high pass filter settings for the cannula and the single fiber EMG were 0.5 and 250 Hz respectively. The resistance and capacitance values for these cutoff frequencies are shown in Figure A.4.

The overall band pass frequencies for the cannula and single fiber recorded EMG signals are 0.5 – 5,000 Hz and 250 – 5,000 Hz respectively. The magnitude response of the band pass filtering done on the single fiber EMG signals was measured using a frequency generator and oscilloscope and the results shown in Figure A.5. As shown, this is the result of a fourth order Butterworth low pass filter cascaded with a fourth order Butterworth high pass filter.

## A.4 Action Potential Detector

### A.4.1 Amplitude Detection

Figures A.6a and A.6b show the amplitude detection circuit designed to detect action potentials by the use of level detection. The raw EMG data is compared to two preset levels set on a couple of voltage comparators. Two voltage comparators are used; one for positive amplitude detection and one for negative amplitude detection. Similarly two amplitude set circuits are used to set the voltage levels. These include 1.2 volt references. The levels of the voltage references are set by a 10 k $\Omega$  ten turn potentiometer and are connected to a voltage display circuit so that the voltage level may be set. The positive amplitude detect is directly tied to the incoming single fiber signal whereas the negative amplitude detection circuit detects amplitudes that are first inverted. The outputs of both

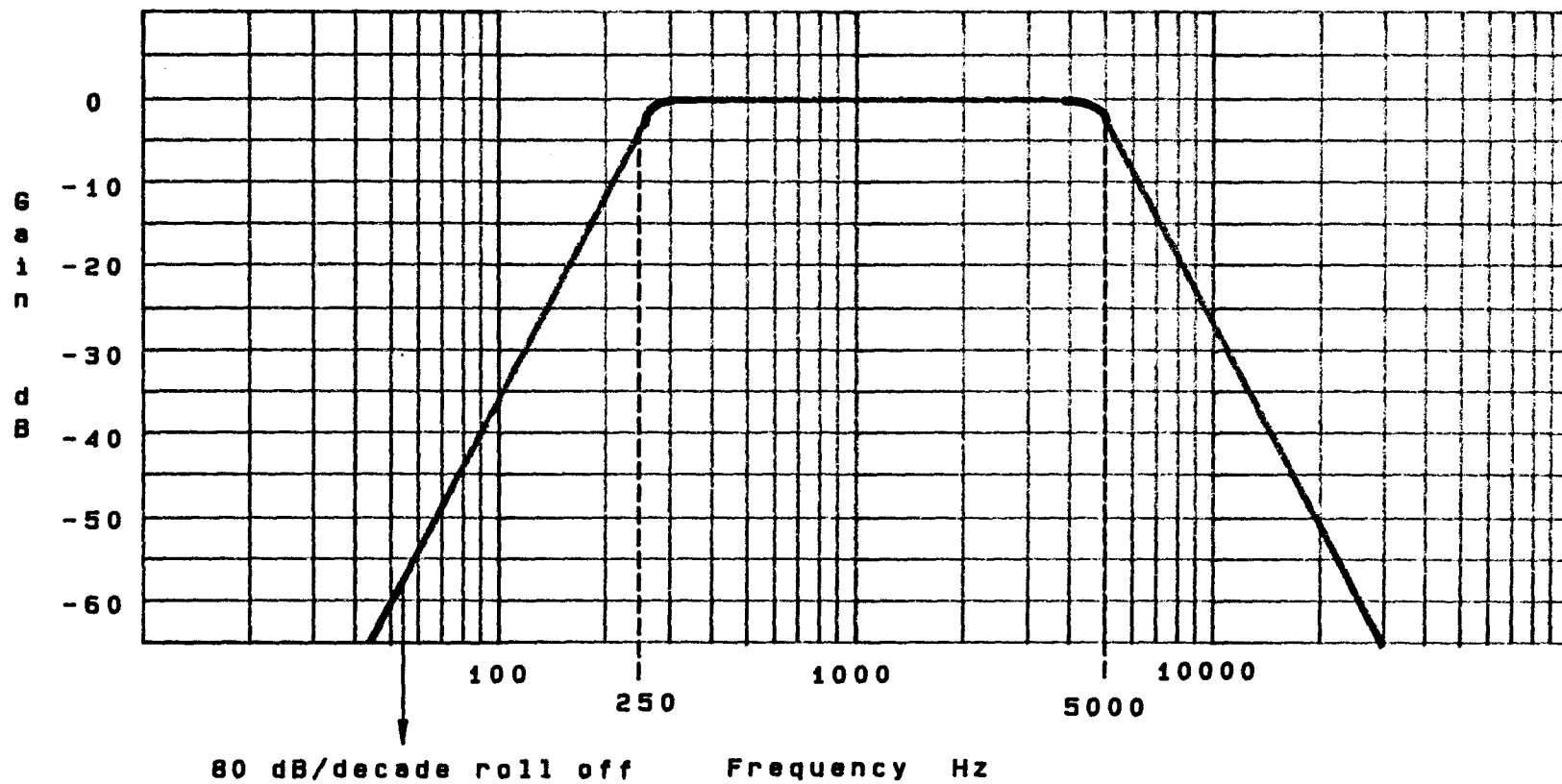
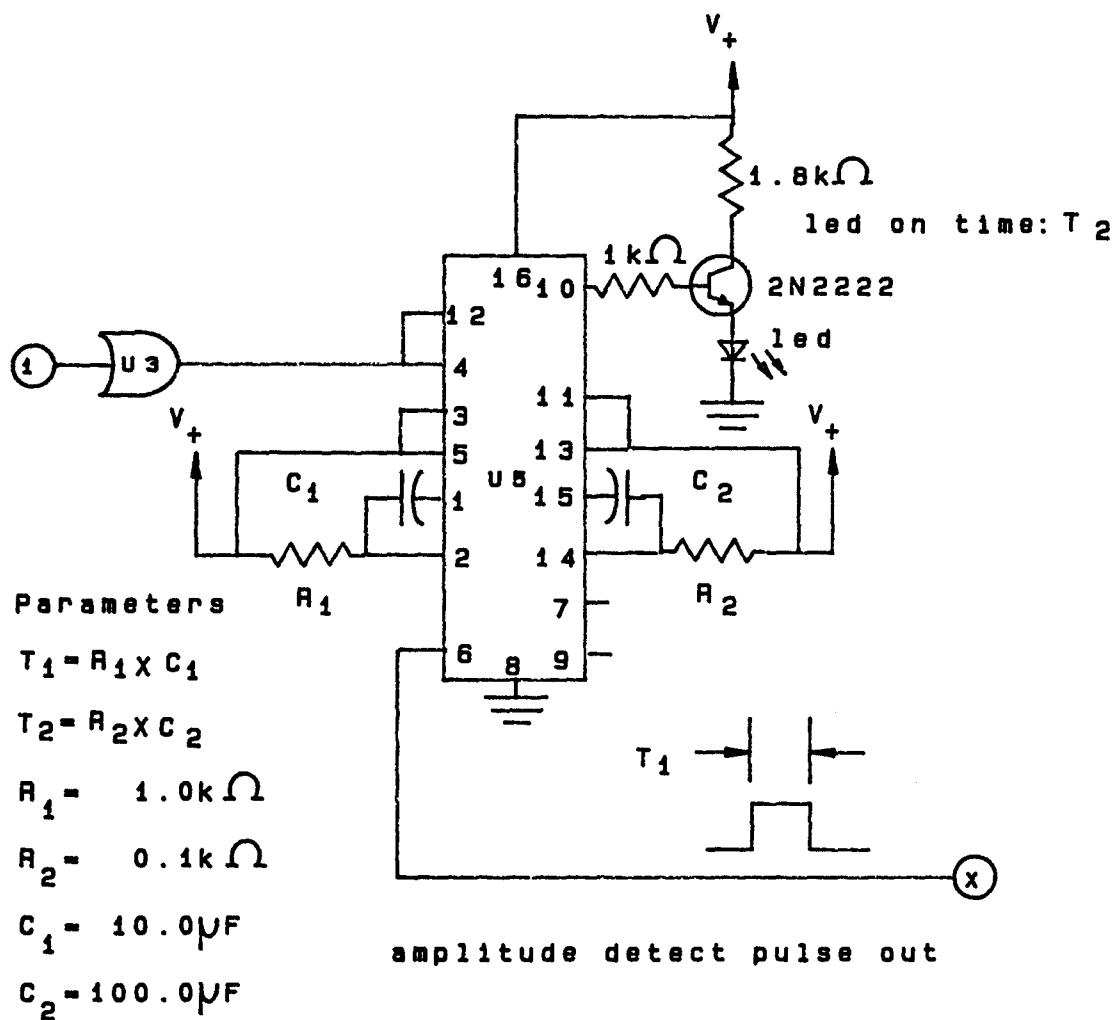


Figure A.5 Bandpass filter response of single fiber channel





U1: 34004 Bifet Opamp

U2: 4081 Quad 2 input AND gate

U3: 4071 Quad 2 input OR gate

U4: 4538 Dual monostable multivibrator

U5: 311 Comparator

D1, D2: 8069 1.2 Volt reference

Figure A.6b Amplitude detection circuit

comparators are ANDED with a high/low switch which is used to either turn the positive or negative amplitude detect circuit on or off. In this way either positive or negative amplitudes or both amplitude criteria may be used to detect MUAPs.

The output of this detection circuit is passed through an OR gate to a pulse generator circuit composed of a 4538 dual monostable multivibrator. This part of the circuit generates two pulses. One pulse turns on an amplitude detect LED while the other pulse is used by the MUAP detection circuit. The pulse width of the multivibrator pulse output is given by  $T=RC$ . The amplitude detect light is pulsed on for a time of approximately one second. The generated amplitude detect pulse has a width of  $100\mu\text{S}$ . The values of the resistances and capacitances required for these pulse widths are shown in Figure A.6b.

#### A.4.2 Slope Detection

The slope detection circuit is shown in Figures A.7a through A.7c. The same single fiber EMG signal selected for amplitude detection is used in the slope detect circuit. Slope is basically a measure of the rise time of the MUAP. Thus the higher the slope the smaller the rise time of the signal. Ideally, the slope is measured by taking the difference of the amplitude of the signal at two different instances of time and dividing by the time delay between these points. One way to accomplish this in analog circuitry is to delay the signal by a preset time  $T$  and subtract this from the original signal. In this way the resulting difference will be proportional to the slope of the signal. To accomplish the analog delay of time  $T$  an all pass constant time delay filter was designed. This is shown in Figure A.7a of the slope detection circuit. These phase shift filters have the property that the frequencies in the

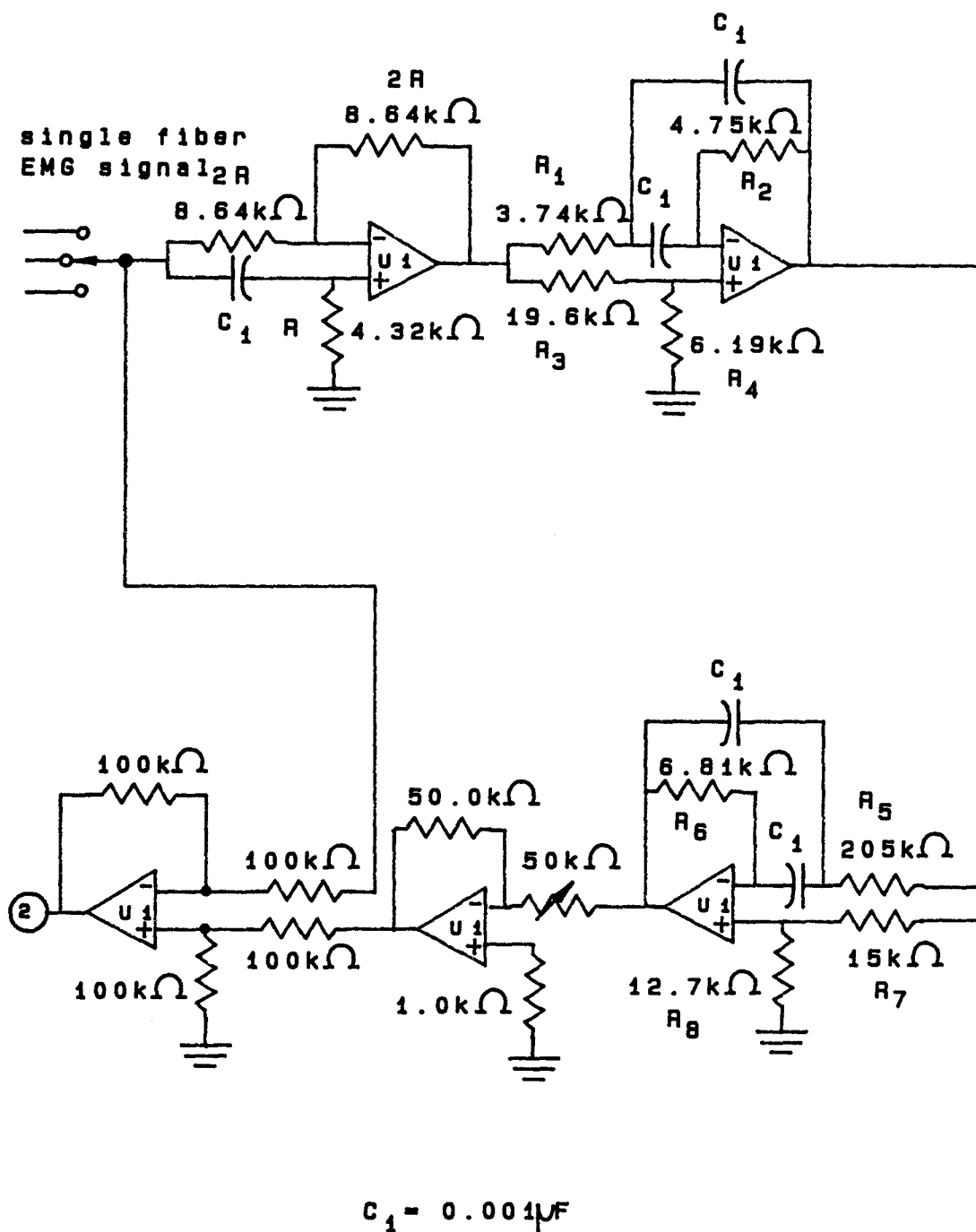


Figure A.7a Slope detection circuit

passband are delayed by the same constant time. The constant all pass time delay filter is defined by the transfer function in the  $s$ -plane by the equation:

$$\frac{V_o}{V_i}(s) = \frac{KB_n(-s/2)}{B_n(s/2)} \quad \text{A.18}$$

where  $K$  is the gain of the filter (set equal to one in this case) and  $B_n$  is the  $n$ 'th order Bessel function given by the equation:

$$B_n(s) = s^n + b_{n-1}s^{n-1} + \dots + b_1s + b_0 \quad \text{A.19}$$

with  $w_c$  the cutoff frequency,  $b_k$  is found using the equation:

$$b_k = \frac{(2n - k)}{k!(n - k)!} \left[ \frac{w_c}{2} \right]^{n-k} \quad \text{A.20}$$

A fifth order constant time delay all pass filter is composed of two second order filter sections cascaded with a first order filter. The second order filter may be expressed as:

$$\frac{V_o}{V_i}(s) = K_1 \left[ \frac{s^2 - 2bw_c s + 4cw_c^2}{s^2 + 2bw_c s + 4w_c^2} \right] \quad \text{A.21}$$

and a first order term as:

$$\frac{V_o}{V_i}(s) = K_2 \left[ \frac{s - 2cw_c}{s + 2cw_c} \right] \quad \text{A.22}$$

where  $K_1$  and  $K_2$  are the gains of the respective stages of the filter and  $b$  and  $c$  are the coefficients found from factoring equation A.18.

A multiple feedback operational amplifier for implementing a constant time delay all pass filter was used as shown in Figure A.7a through A.7c. The value for the capacitance  $C_1$  is chosen to be  $10/f_c \mu\text{F}$  where  $f_c$  is the cutoff frequency. The value of  $f_c$  is given by the equation:

$$f_c = \frac{0.15915}{\tau} \quad \text{A.23}$$

where  $\tau$  is the time delay of the filter. The resistance  $R$  for the first order stage of the filter is given by the equation:

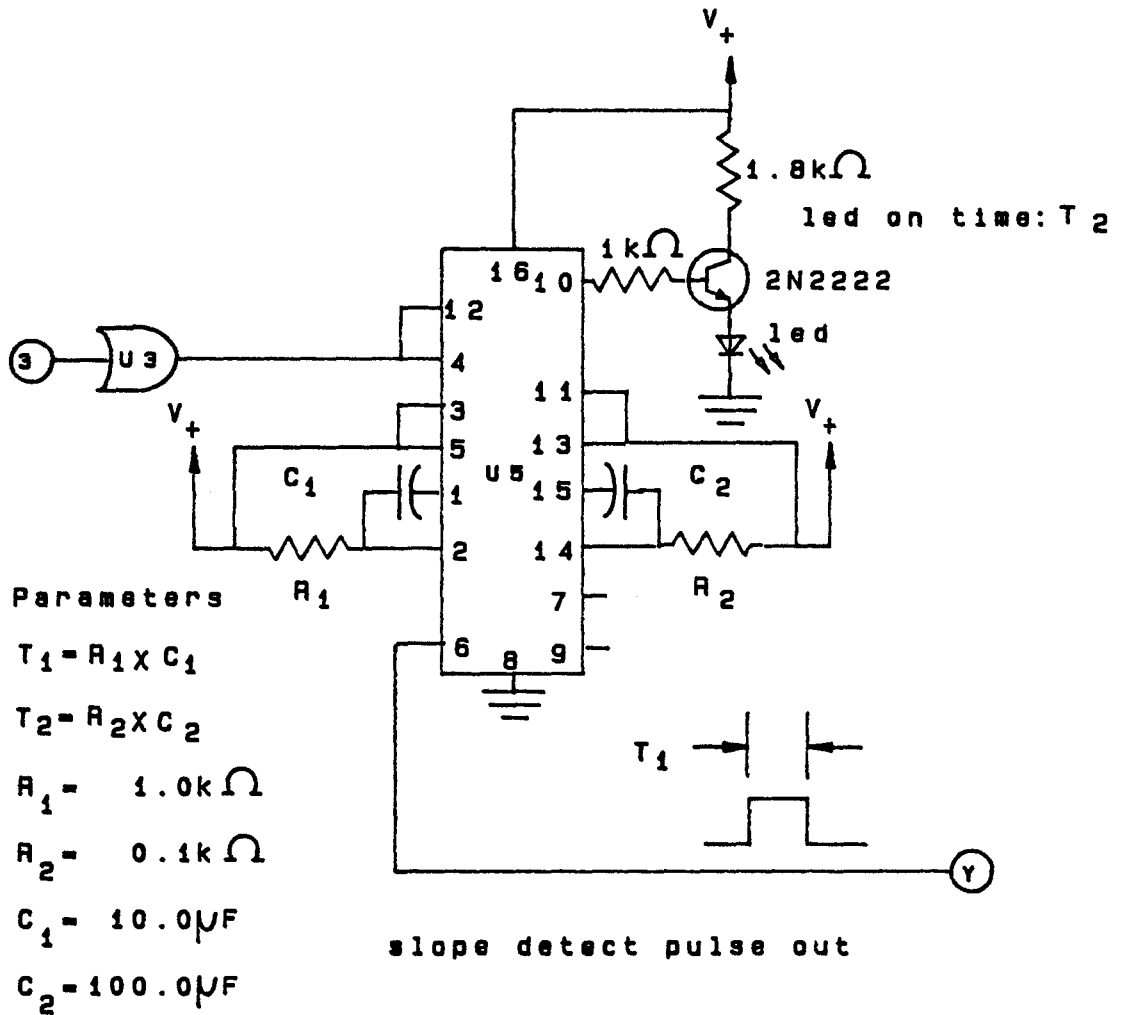
$$R = \frac{1}{2c\omega_c C_1} \quad \text{A.24}$$

The gain of this first order stage is negative one. The capacitance values in the second order stages  $C_2$  is chosen to be the same as for  $C_1$  as calculated above. The values of the resistances for the two second order stages are given by the following equations:

$$R_2, R_6 = \frac{1}{b\omega_c C_2} \quad \text{A.25}$$

$$R_1, R_5 = \frac{b^2}{4c} R_2 \quad \text{A.26}$$





U1: 34004 Bifet Opamp

U2: 4081 Quad 2 input AND gate

U3: 4071 Quad 2 input OR gate

U4: 4538 Dual monostable multivibrator

U5: 311 Comparator

D1, D2: 8069 1.2 Volt reference

Figure A.7c Slope detection circuit

$$R_9, R_7 = \frac{R_2}{K} \quad \text{A.27}$$

$$R_4, R_8 = \frac{c}{b^2 K} R_2 \quad \text{A.28}$$

where the values of  $b$  and  $c$  are as stated previously and  $K$  is the gain of the filter stage given by:

$$K = \frac{c}{c + b} \quad \text{A.29}$$

The overall gain of the filter is adjusted to unity gain with the inclusion of a simple inverting amplifier located at the end of the filtering circuit.

The phase response of this constant time delay filter was measured using a signal generator and a dual channel oscilloscope. This is presented in Figure A.8. The ideal phase response is shown with the actual phase response. As seen the actual phase response is very close to the ideal. The magnitude of the response although not presented was also measured and found to be for all intents and purposes constant (i.e. gain of one) in the band pass (0 – 5000 Hz).

The time delay of this particular filter is on the order of 0.1 milliseconds. The resistance and capacitance values for the constant time delay all pass filter are shown in Figure A.7a. The approximate slope may be calculated by using a difference amplifier. Typical values for the slope are on the order 10–40 volts/sec. The output of the difference amplifier therefore is an approximate measure of the slope of the signal at any particular point in time.

The output of the difference amplifier is put through a circuit similar to the one used for amplitude detection. This is shown in Figures A.7b and A.7c. Again

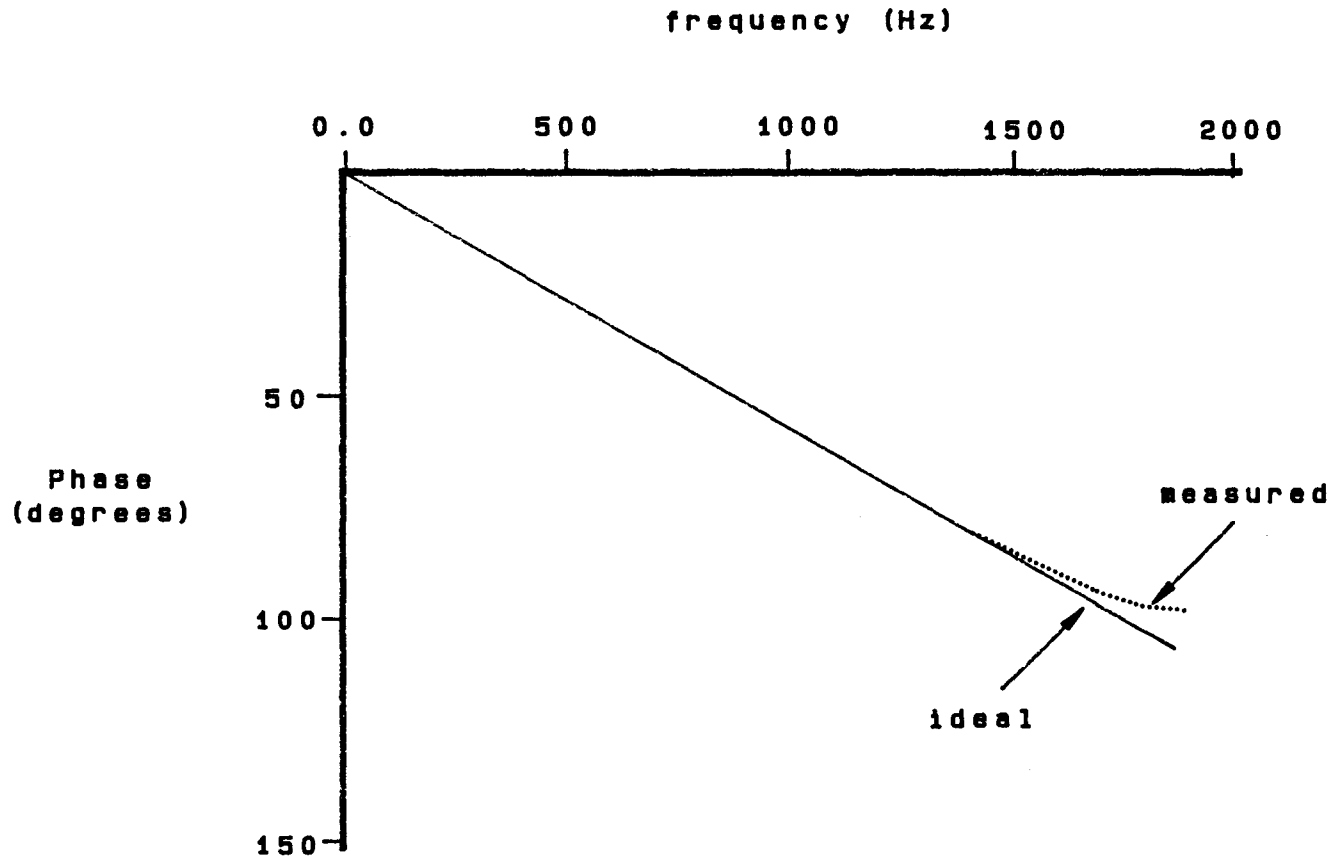
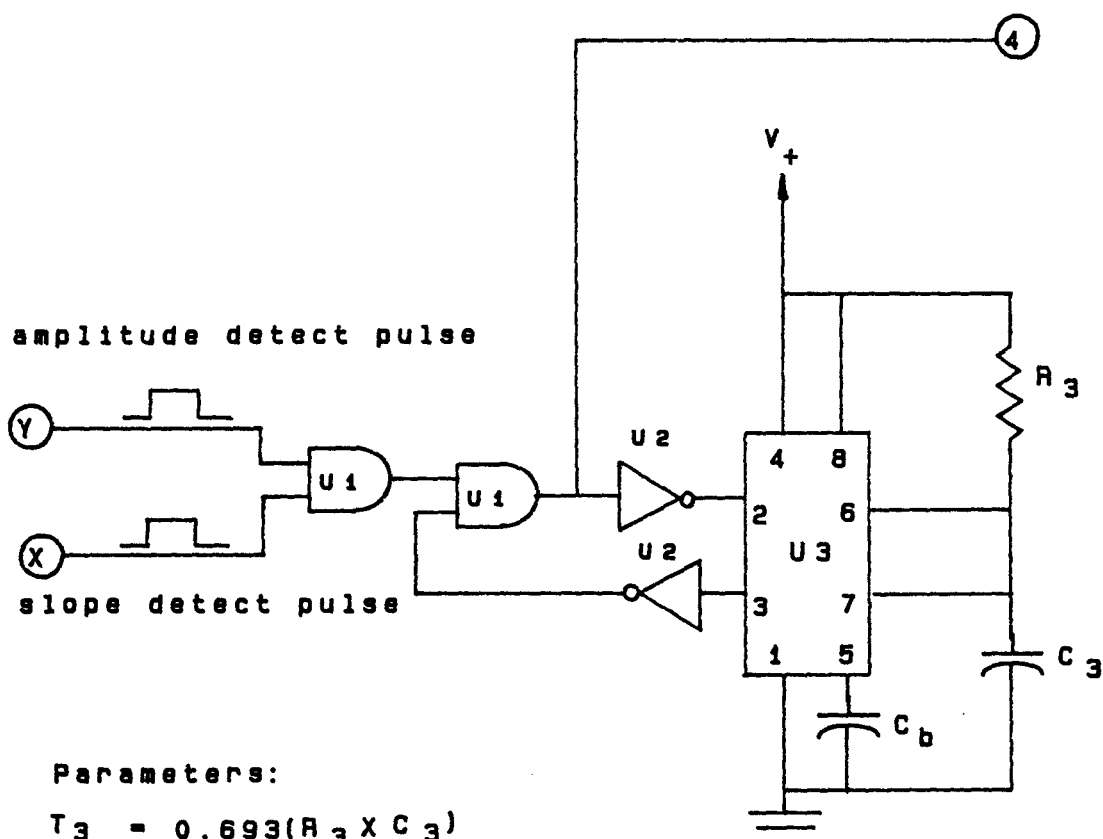


Figure A.8 Phase response of constant time delay filter

as before, positive, negative or both positive and negative slope can be used for the slope criteria with the levels of the slopes adjustable. Pulse generation is accomplished in exactly the same manner as done in the amplitude detection circuit. Two pulses are generated; one for driving the slope detect LED and one for producing a slope detect pulse which is used in the MUAP detect circuit. Again, the timing of these pulses is the same as those for amplitude detection. The values for the resistances and capacitances for these pulse times are shown in Figure A.7c.

#### A.4.3 Detection Circuit

Now that both amplitude and slope pulses have been generated the criteria for determining a valid MUAP can be implemented. This is done by simply determining if the valid amplitude and slope occur at approximately the same moment in time. (Actually the width of either pulse is the time constraint.) The MUAP pulse generation circuit is shown in Figures A.9a and A.9b. The slope and amplitude detect pulses are passed through an AND gate. Thus a pulse is generated if and only if a slope detect pulse and an amplitude detect pulse occur at relatively the same time. The output pulse from the AND gate goes into another gate which has the other input tied to a timer circuit. The output of this AND gate triggers a dual monostable multivibrator which generates as before two pulses; one for the MUAP detect LED and the other a MUAP detect pulse. Again, these pulse widths are the same as before and the values for the resistances and capacitances are shown in the figure. This MUAP detect pulse is used by another circuit to count the aggregate number of action potentials for a particular channel. However, in order to prevent multiple detection of the same MUAP, a lock out circuit is added which



Parameters:

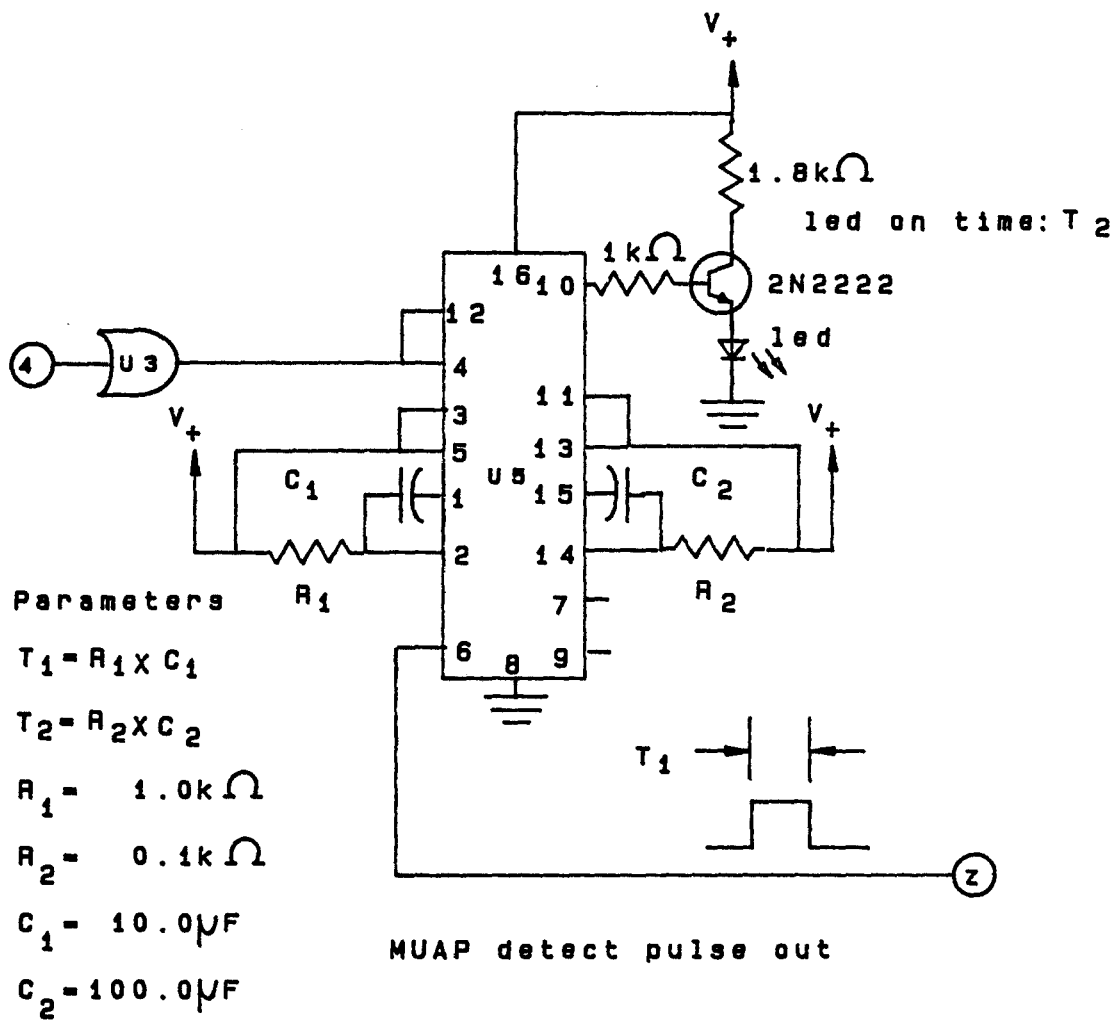
$$T_3 = 0.693(R_3 \times C_3)$$

$$C_3 = 0.10 \mu\text{F}$$

$$C_b = 0.01 \mu\text{F}$$

$$R_3 = 72.1 \text{k}\Omega$$

Figure A.9a MUAP detection circuit



U1: 4081	Quad 2 input AND gate
U2: 4009	Hex Inverter Buffer
U3: 1455	Programmable Timer
U4: 4538	Dual monostable multivibrator

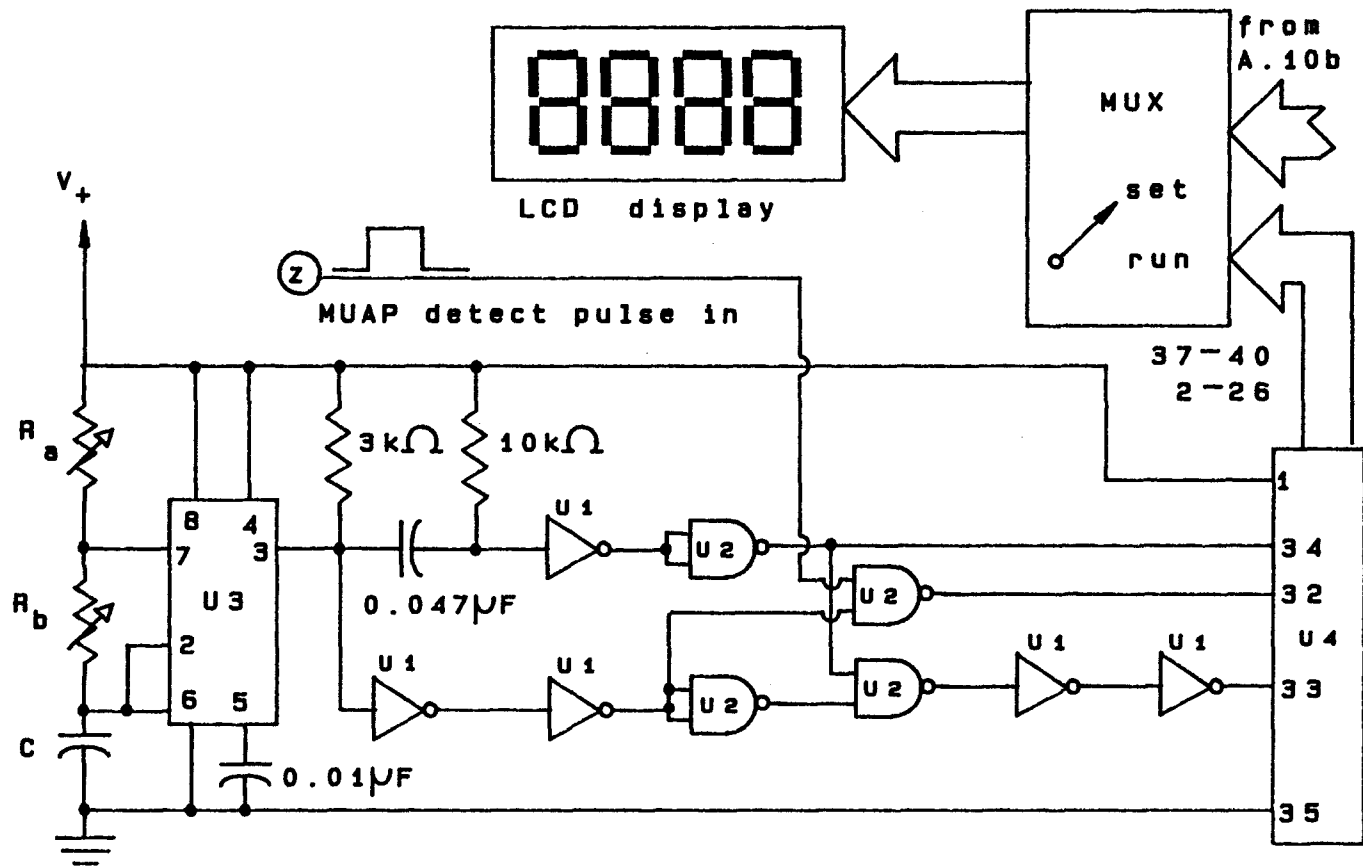
Figure A.9b MUAP detection circuit

simply times when a MUAP occur and will not allow the detection of another MUAP until after a certain amount of time. This period of time is created by the 455 timer with the pulse width set at five milliseconds. This value then sets the maximum firing rate that can be recorded at 200 per second. This is assumed to be adequate since firing rates of motor units in the first dorsal interosseus are between 10 and 50 times per second. The purpose of this lock out circuit then is to prevent multiple generation of MUAP detection pulses for the same MUAP.

#### A.4.4 Aggregate Display Counter

Now that the MUAP has been detected and a pulse has been generated the aggregate number of action potentials detected per second is displayed to the electromyographer. This is accomplished by the display generating circuit presented in Figures A.10a and A.10b. Figure A.10a is the MUAP counter display. When a detection pulse is generated it is counted by IC U4, a 4 1/2 digit cmos counter LCD display driver. The purpose of U1 a 555 timer is to generate the time window for the counts so that the aggregate MUAP count is updated every second. Thus an aggregate MUAP firing rate per second is displayed by the LCD.

Figure A.10b shows U5, an A/D converter with LCD driver. The purpose of this circuit is to display the voltage levels of both positive and negative amplitude and slope settings in the previously described circuits. This gives some idea of how these parameters are set and thus may be adjusted in order to achieve a viable aggregate action potential count. In order for these two circuits to use the same LCD display, a multiplexer was constructed out of quad bilateral switches (4066's). In set up mode the LCD display is switched to level set adjust, and with the aid of a



Parameters

$T_n = 0.693 (R_a + R_b) C$	$C = 0.47 \mu F$
$T_p = 0.693 R_b C$	$R_a = 1.0 k\Omega$
	$R_b = 5.0 M\Omega$

Figure A.10a Display circuit

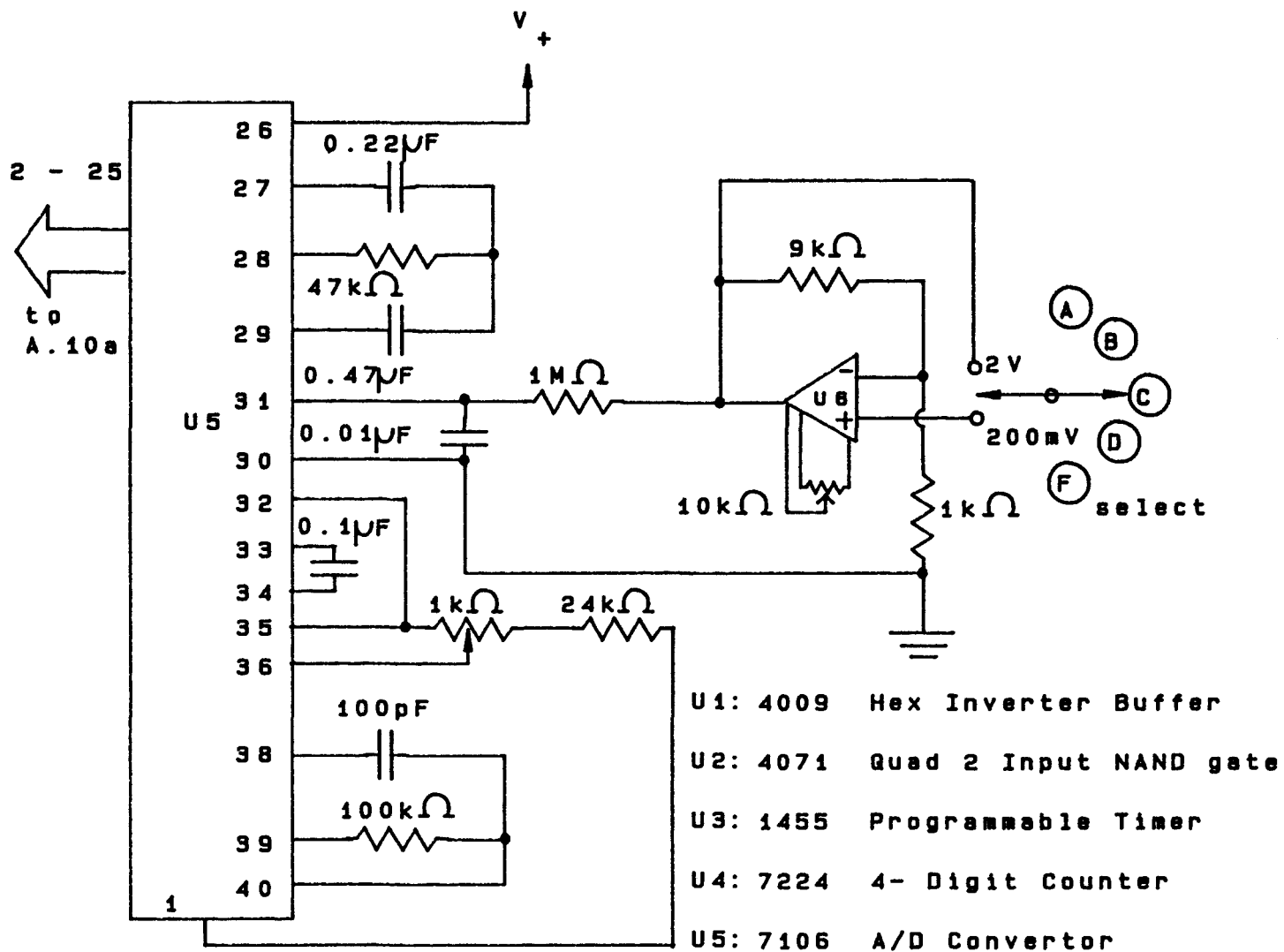


Figure A.10b Display circuit

selection switch to select any combination of positive and negative parameters of slope or amplitude, the analog levels of these parameters being presented on the LCD display. The A/D circuit has a range switch of either 2 volts or 200 millivolt. In this way small and large voltage levels may be accurately obtained. Thus both aggregate count of action potentials detected in a particular channel and level set are presented to the experimenter.

#### **A.5 Force Signal Amplification/Filtering and Target Generation**

The force signal amplification/filtering and target generation circuit is shown in Figures A.11a and A.11b. It consists of a common mode rejection amplifier that is dc coupled to a filter/amplifier stage. The low pass filter used was a fourth order Butterworth filter. The cut off frequency was designed for 10hz. This was judged to be adequate for the low rate of force contractions studied. The development of the preamplifier and filter was identical to those designed for the EMG signal processing.

Along with the processing of the force signal, a force target signal is created and displayed on an oscilloscope. The force generated by the muscle, converted to an electrical signal via the force transducers arranged in a wheatstone bridge, can then be made to follow the target signal on the oscilloscope. The signal generator used was a 8038 integrated circuit with a triangle wave period of either 10, 20 or 30 seconds (equivalent to a ramp time of 5, 10 and 15 seconds respectively). In order to present an error boundary within which generated force of the muscle must fall during a collection of data , an error signal was added to the generated waveform. The error signal is developed by a 555 timer in the form of a square wave which was

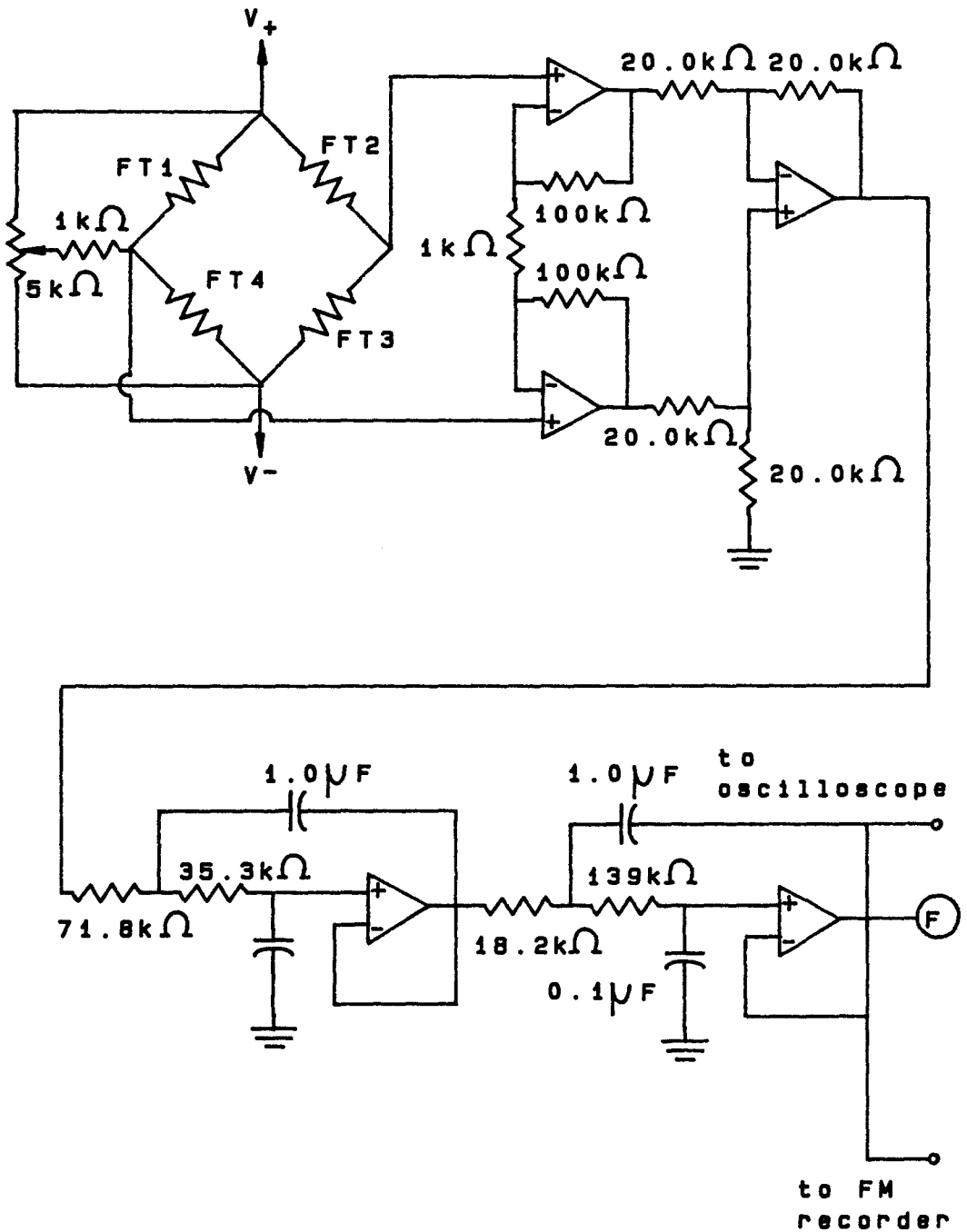
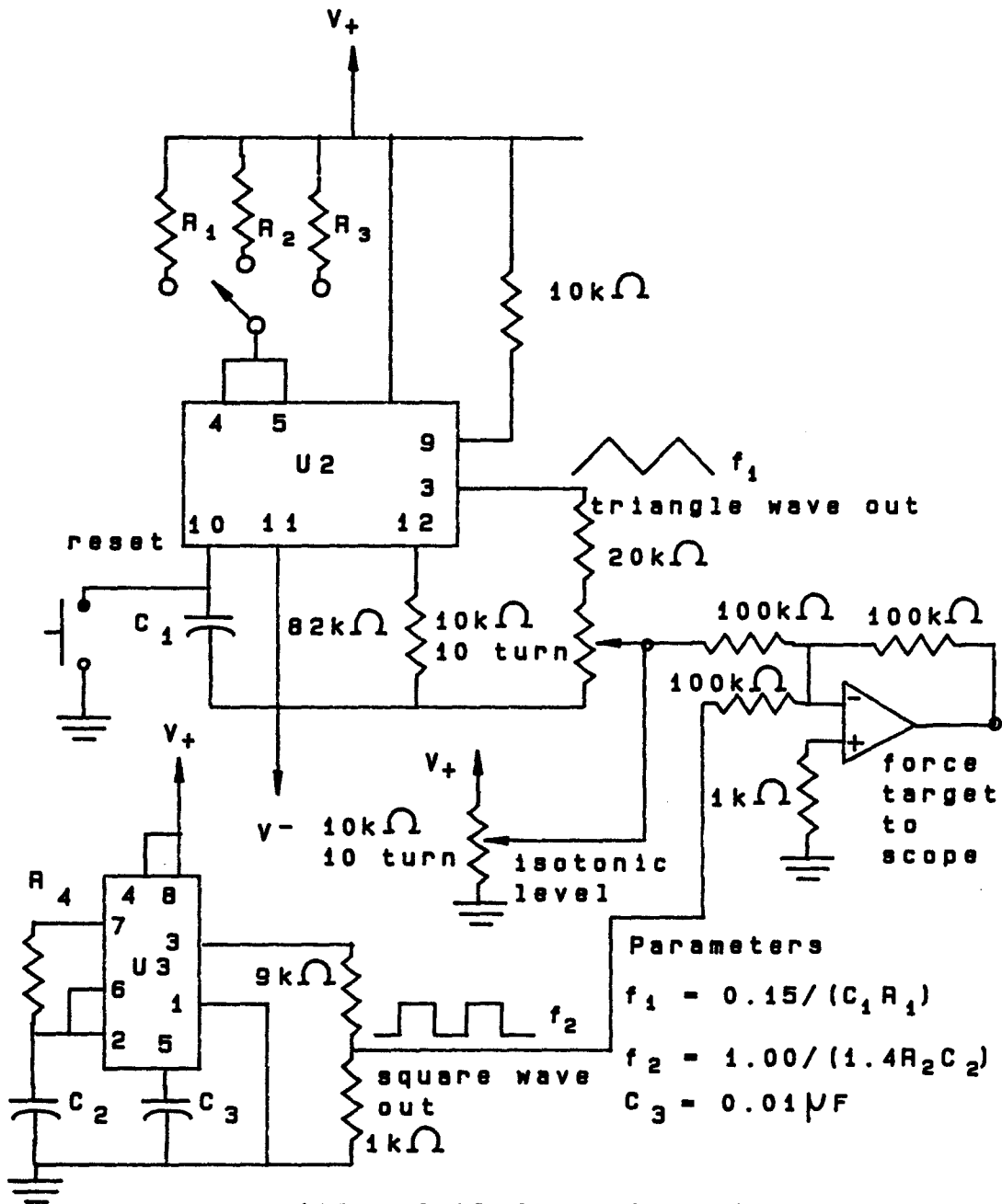


Figure A.11a Force signal amplification and filtering circuit



FT1 - FT4 120 foil force transducers

U1 34004 Bifet Opamp

U2 8038 Signal Generator

U3 1455 Programmable Timer

Figure A.11b Force target signal generation circuit

1/9th the amplitude of the generated signal. Both of these signals are added to form the output which goes to one oscilloscope channel. Furthermore, the triangle wave generator can be switched to a separate level adjustment for isotonic contractions. The actual force signal generated by the muscle is put into the other channel of the oscilloscope. With the oscilloscope on alternate display then both signals may be seen on the display at the same time and thus the generated signal can be used as the target to be followed by the muscle under contraction.

## Appendix B

### Power Spectral Density of Motor Unit Action Potentials

#### B.0 Introduction

The purpose of this appendix is to determine the significant frequencies present in both single fiber and cannula EMG signals. Knowing the frequency content of these EMG signals is required in determining both the analog filter cut off frequencies used in the hardware preprocessor and the required sampling rates used to digitize these signals. It must be pointed out again that the frequency content of the EMG signals recorded is highly dependent on the filtering characteristics of the recording electrode (Chapter Two). Since this multichannel single fiber recording electrode has never been used before, there is an inherent need to find out the frequency ranges of the EMG signals recorded with it.

#### B.1 Calculating the Power Spectral Density

In order to calculate the power spectral density (PSD) of the EMG signals, raw or unfiltered EMG signals were recorded from one of the single fiber channels and the cannula channel. This raw EMG signal was recorded to FM tape using the hardware pre-processor described in chapter four (and appendix A). These signals were then played back at 1/16th tape speed to the LPS-11 A/D converter and a data collection routine similar to the one described in chapter four was used to sample and then store this sampled data to hard disk. Due to the slower playback

speed of the FM tape recorder an effective sampling rate of 32 kHz was obtained. Thus at this sampling rate, the Nyquist frequency was assumed to be just less than 16 kHz.

From the sampled data recorded on hard disk, the PSD was calculated. This was done in the following way. In the single fiber EMG signal the important event is the occurrence of a MUAP. Therefore it was the frequency content of the MUAP which was looked at. In the cannula EMG signal, MUAPs are also be present (but with a lower frequency content(chapter two)) and it is these which are looked at. The calculation of the PSD is estimated in this thesis by the mean square amplitude given by the equation:

$$\frac{1}{T} \int_0^T |s(t)|^2 dt \simeq \frac{1}{N} \sum_{n=0}^{N-1} |s(n\tau)|^2 \quad \text{B.1}$$

where the signal  $s(t)$  is sampled at a rate  $1/\tau$  (32 kHz) to produce  $N$  discrete values [192]. In order to lessen the effects of frequency leakage the data vector describing the MUAP (single fiber and cannula) was windowed according to the formula given by Welch as:

$$W(n) = 1 - \left[ \frac{n - 0.5(N - 1)}{0.5(N + 1)} \right]^2 \quad \text{B.2}$$

where  $W(n)$  is the  $n$ 'th window coefficient and  $n$  has the range of one to  $N$  [192]. In order to obtain the smallest variance in the PSD estimates at any particular frequency, the sampled signal must be segmented into overlapping windows. The amount of overlapping required for the least variance turns out to be

approximately one half of the length of a segment. In this case, the length of the discrete vector describing the EMG signals was 2048 points. The  $M$  periodograms used to calculate the PSD of the cannula and single fiber EMG signals are averaged to obtain the PSD estimate of the MUAP signal at the frequencies given by the formula:

$$f_n = \frac{n}{(2M)\tau} \quad \text{B.3}$$

where  $n = 0, \dots, M-1$  and again  $\tau$  is the sampling interval.

## B.2 Results

Several PSD calculations for the single fiber and cannula EMG were done. These are presented in Figures B.1a through B.1c. As shown, the majority of the power is located in the bandwidth of 250 Hz to 4,000 Hz for the single fiber recording and 100 Hz to 3,000 Hz for the cannula recording. In actuality since these are real signals that are being used, the bandwidth chosen for the single fiber EMG recording was between 250 to 5,000 Hz and the bandwidth chosen for the cannula EMG recording was between 0.5 to 5,000 Hz. These are therefore the cut off frequencies used by the high and low pass Butterworth filters in the hardware preprocessor. With these bandwidths then, a sampling rate of 10,000 Hz meets the Nyquist sampling criterion for either single fiber or cannula recorded EMG signals. This is therefore the sampling frequency used by the collection routines in this thesis.

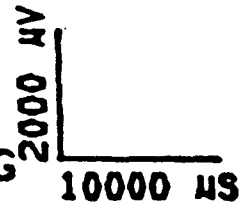
CANNULA EMG



SINGLE FIBER EMG



FIGURE B.1A CANNULA AND SINGLE FIBER EMG



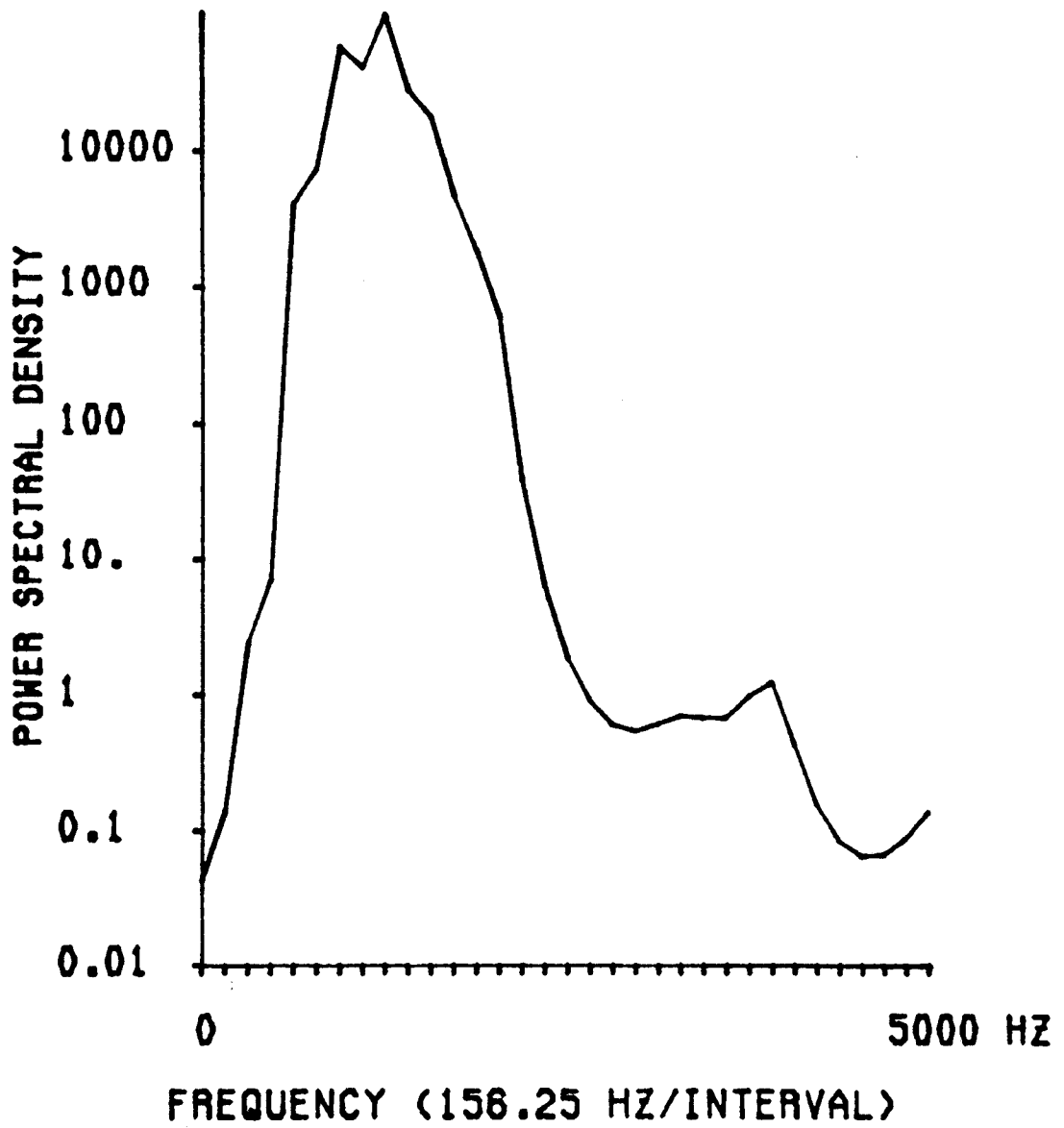


FIGURE B.1B CANNULA PSD

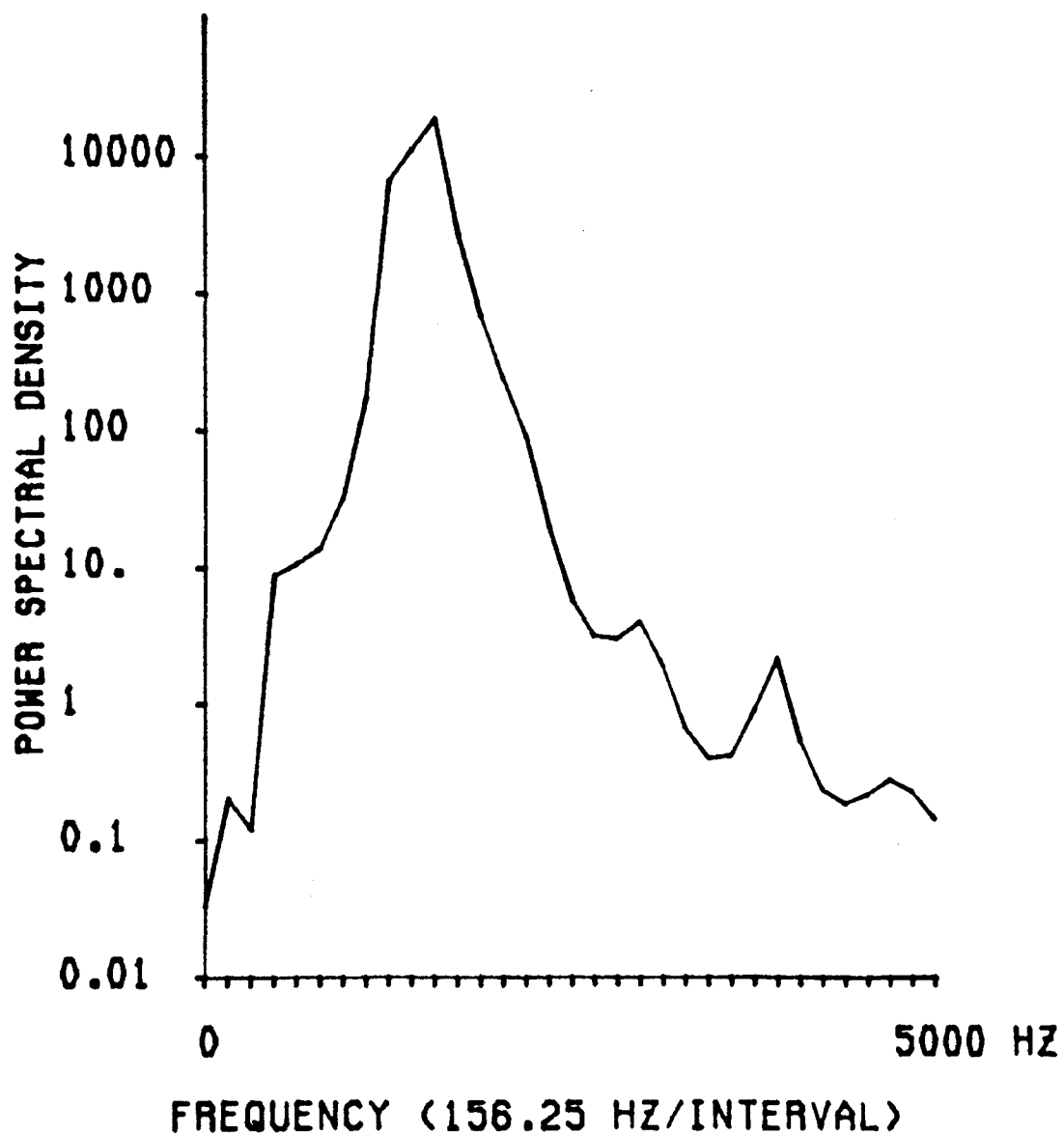


FIGURE B.1C SINGLE FIBER PSD

## Appendix C

### Hardware Preprocessor Functions

#### C.0 Introduction

The purpose of this appendix is to describe in brief the switch settings and functions of the hardware preprocessor. The front and back panels referred to in this appendix are in reference to the front and back panels of the hardware preprocessor and are shown in Figures C.1 and C.2 respectively. The labelled switch settings shown in these diagrams are explained below.

#### C.1 Front Panel

##### C.1.1 EMG Preprocessor Switch Settings

1. SLOPE
  - A. Negative slope select and level adjust for MUAP detection circuit.
  - B. Positive slope select and level adjust for MUAP detection circuit.
2. AMPLITUDE
  - C. Negative amplitude select and level adjust for MUAP detection circuit.
  - D. Positive amplitude select and level adjust for MUAP detection circuit.
3. GAIN

Amplifier gain of the EMG signals (single fiber and cannula).

Switch selectable for gains of 1, 2, 5, or 10 times the gain of the preamplifier.

Preamplifier has a gain of 1000 for the single fiber and 500 for the cannula.

4. T. CHANNEL

Trigger channel select switch.

Any of the three single fiber EMG or cannula EMG channels may be selected for the MUAP detection circuit. Usual procedure is to select the channel with the most prominent EMG activity.

5. T. GAIN

Trigger channel gain.

Additional gain to the trigger channel selected above may be added here for better detection of MUAPs used in aggregate MUAP count.

6. COUNT / SET

Selects either the counting mode or level set mode for the LCD display.

In COUNT mode the aggregate number of MUAPs detected per second is displayed.

In SET mode the levels of the detection parameters (Slope, Amplitude) calibrated in millivolts are displayed.

7. 1X / 10X

Selects either a 1200 millivolt or 120 millivolt full range scale when in SET mode.

8. 1/4 SPEED / NORMAL

Corresponds to the speed of the FM tape when playing back a FM tape

through the preprocessor.

At 1/4 SPEED it effectively reduces the slope parameters set by one quarter of their original values.

At Normal all parameters remain the same.

9. SELECT

Selects the parameter to be displayed on the LCD display.

Not only can the detection parameters (slope and amplitude) be displayed but also the force level of contraction.

10. LCD DISPLAY

Displays both the level settings of the detection parameters (along with force level) and the aggregate MUAP count.

11. MUAP DETECT LED

LED turns on when one MUAP is detected.

12. S. DETECT LED

LED turns on when the slope detection parameter is satisfied for a MUAP detection.

### C.1.2 Force Preprocessor Switch Settings

1. RAMP / ISOMETRIC

Selects type of force target to be generated on the oscilloscope.

In RAMP mode the force target generated is a triangle wave with a user selectable period. A dc offset may be added to this force target.

In ISOMETRIC mode the force target generated is a constant level which is user adjustable.

**2. RAMP TIME**

Selects the period of the RAMP or triangle wave.

A ramp time of 5, 10, or 15 seconds can be selected.

**3. F. LEVEL**

Sets the amplitude of the RAMP target signal.

**4. DC OFFSET**

Sets the level of the isometric force target or the dc offset of the ramp force target.

**5. RESET**

Resets the ramp force target signal to zero volts dc output.

**C.2 Back Panel****C.2.1 EMG Preprocessor Inputs/Outputs****1. NEEDLE**

Single fiber and Cannula EMG input.

**2. REF.**

Reference electrode input.

**3. GND**

Ground or common electrode input.

**4. AUXILIARY INPUT**

Inputs used when using prerecorded FM tape EMG activity.

Channels 1 through 5 are single fiber signal inputs and channel 6 is the cannula signal.

**5. OUTPUT**

Single fiber and Cannula EMG signal output.

Channels 1 through 5 are single fiber signal outputs and channel 6 is the cannula signal.

Although only three single fiber EMG channels are used by the present needle, an additional two channels are provided for future use.

6. T. TRIGGER

Trigger channel output.

Output of trigger channel selected on front side.

7. TRIGGER

Output of MUAP detection circuit.

### C.2.2 Force Preprocessor Inputs/Outputs

1. FORCE INPUT

Force signal recorded from the muscle under study by means of force transducers arranged in a wheatstone bridge.

2. BALANCE

Potentiometer adjustment used to balance the wheatstone bridge.

3. FORCE OUTPUT

A. Force signal generated by muscle.

This force is recorded to FM tape.

B. Force signal generated by muscle.

This force is output to channel one of the oscilloscope.

C. Force target signal generating circuit output.

This signal is either the RAMP or ISOMETRIC signal generated and

is output to channel two of the oscilloscope.

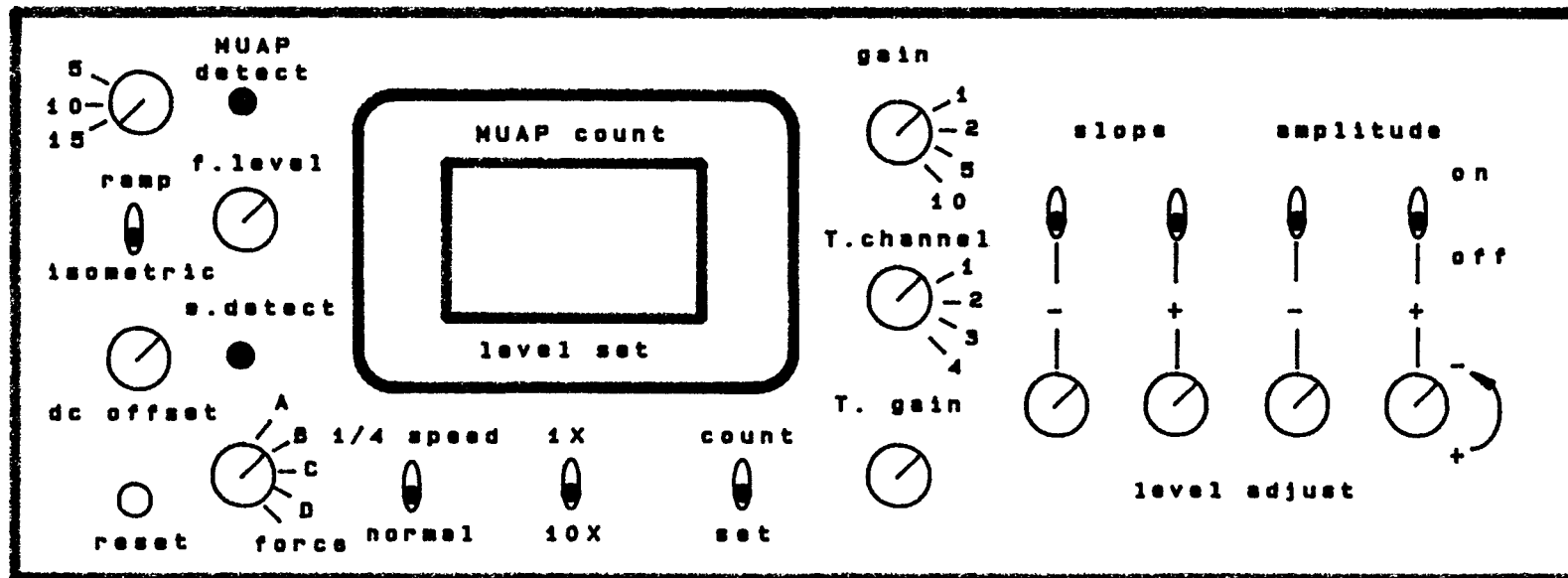


Figure C.1 EMG preprocessor - front panel

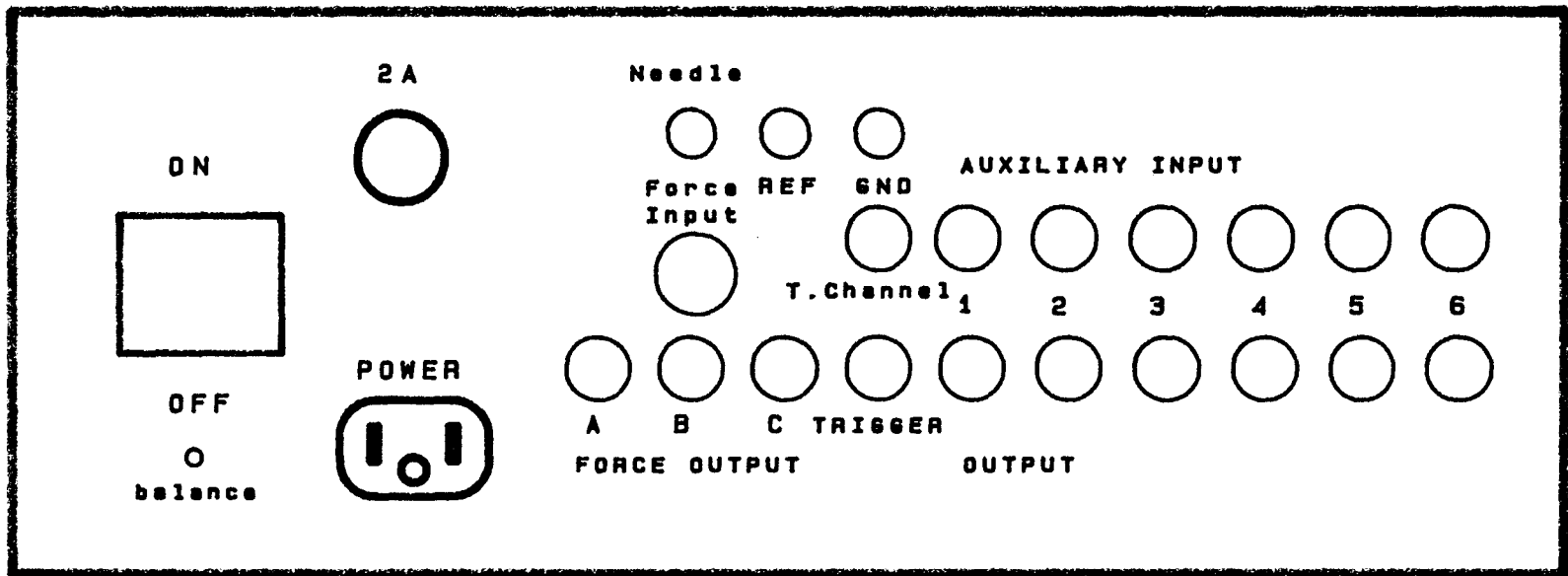


Figure C.2 EMG preprocessor - back panel

## **Appendix D**

### **Reference Electrode Placement**

#### **D.0 Introduction**

Of primary interest in the recording of multichannel EMG signals is the positioning of the electrodes. As stated previously (Chapter Three), there are three electrode inputs into the instrumentation amplifier designed. These are:

- 1) the multichannel fine wire recording electrode,
- 2) the reference electrode and
- 3) the common electrode.

The position of the multichannel fine wire recording electrode is fixed since it is inserted into the muscle under study, the first dorsal interosseus muscle (FDI). Both the common and reference electrodes are silver disc surface electrodes (Chapter Four). The positioning of the common electrode is not critical since its sole purpose is to provide a common ground between the subject from which the EMG activity is recorded and the hardware preprocessor. For the collection of EMG signals from the FDI muscle the common electrode was placed on the elbow. The positioning of these electrodes is shown in Figure D.1.

The positioning of the reference electrode is critical in the recording of EMG signals from the FDI muscle. The primary reason for this is related to the way the instrumentation amplifier is constructed. The reference electrode and the recording

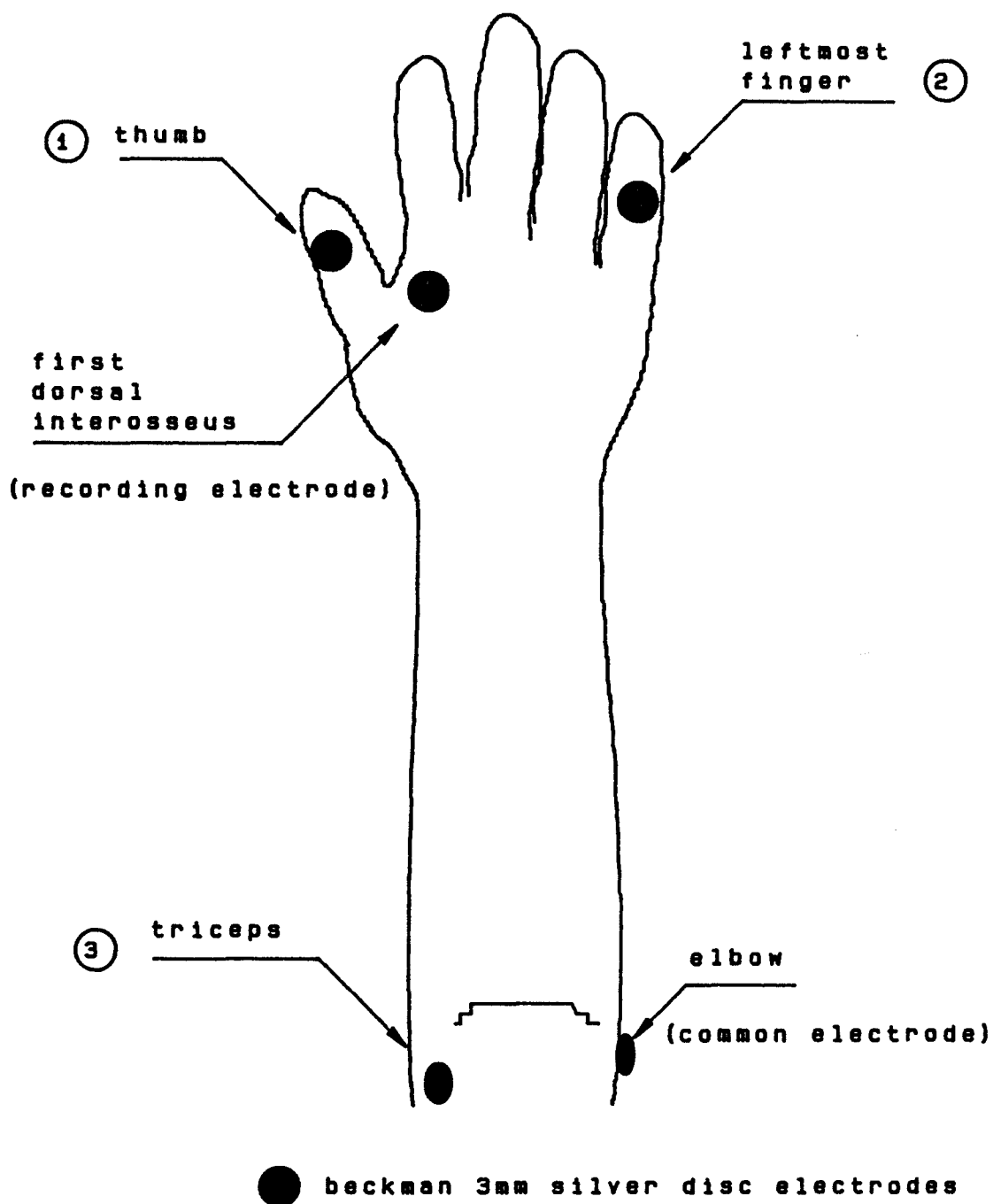


Figure D.1 Reference electrode positions

electrode are the differential inputs to the instrumentation amplifier, thus common mode signals on both of these inputs are rejected. Since the recording and reference electrodes are different types and the distance between them is large compared to the recording volume of the electrode, the commonality in the signals at each electrode is reduced. It should be noted that the low frequency noise (60 Hz) will still be rejected since it has the same amplitude and phase at each electrode site and thus will be differenced out of the overall EMG signal recorded by multichannel single fiber electrode.

Nevertheless, in order to ensure a low noise differential recording then the EMG activity recorded by the reference electrode must be as low as possible. Here low noise refers to a low background ambient activity since the actual noise of the hardware can be at least an order of magnitude lower than this activity.

#### D.1 Reference Electrode Placement

Under normal EMG recording conditions the recording electrode used was a multichannel single fiber electrode and the reference electrode was a Ag–AgCl disc electrode. In determining the best location for the reference electrode, the recording electrode used was also a Ag–AgCl disc electrode similar to those normally used by the reference and common electrodes. Although the substitution of this type of electrode for the multichannel electrode tends to bias the results of the study undertaken to determine the best location of the reference electrode, the overall conclusions will be the same.

In order to determine the best location of the reference electrode several different positions were tried. These positions, shown in Figure D.1, are:

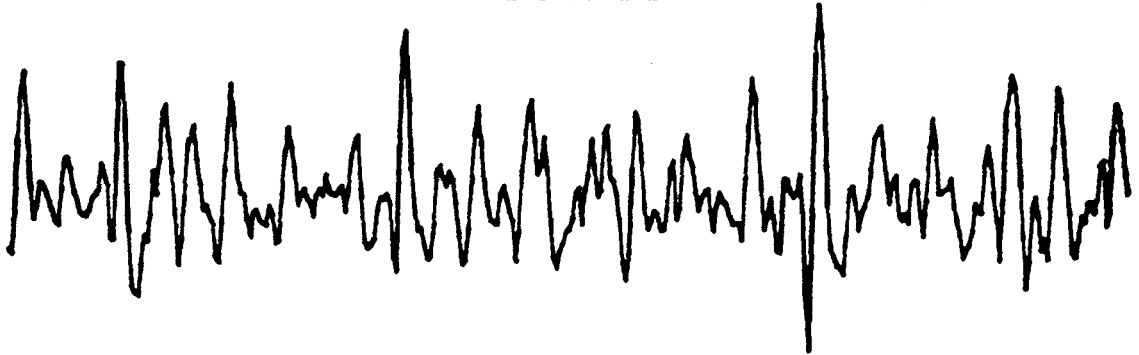
- 1) thumb,
- 2) leftmost finger and
- 3) triceps.

To determine which position was best for the reference electrode the following study was performed. The arm was placed in the arm jig as previously described in chapter four. Surface recorded EMG was then simultaneously recorded from the various electrode positions, using pairs of Ag–AgCl electrodes as the first dorsal interosseus was undergoing contraction. The FDI muscle was contracted at several different levels (i.e. low, medium or high) of the maximum voluntary contraction (MVC). Typical recordings of the surface recorded EMG from each position are shown in Figures D.2 and D.3. In these figures the first EMG signal is the FDI while the second, third and fourth signals are the EMG signals recorded from the thumb, the leftmost finger and the triceps respectively. The largest EMG signal present is indeed that recorded from the FDI which makes sense since it is the muscle undergoing contraction. As shown in the figures, the root mean square (RMS) value for each of the EMG signals is calculated and recorded alongside the corresponding signal.

#### D.1.1 Comparison Measures

In order to compare the different reference electrode placements a measure(s) of relative merit of that position must be made. The two measurements of merit used in this study were:

FIRST DORSAL INTEROSSEUS      RMS = 758  $\mu$ V



THUMB      RMS = 343  $\mu$ V



LEFTMOST FINGER      RMS = 160  $\mu$ V



TRICEPS      RMS = 87  $\mu$ V

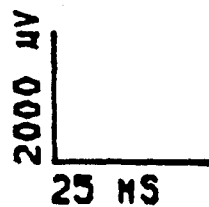
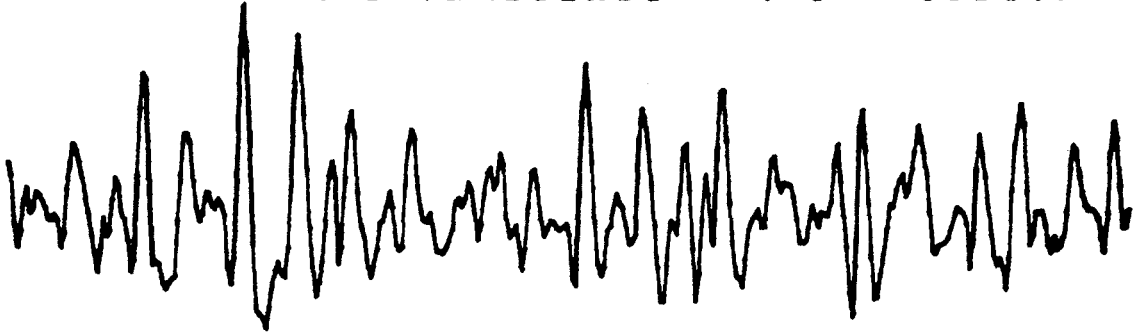
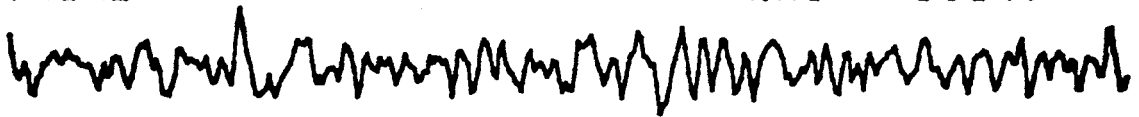


FIGURE D.2 MODERATE CONTRACTION

FIRST DORSAL INTEROSSEUS      RMS = 1004 $\mu$ V



THUMB      RMS = 313 $\mu$ V



LEFTMOST FINGER      RMS = 154 $\mu$ V



TRICEPS      RMS = 77 $\mu$ V



FIGURE D.9      HIGH CONTRACTION      25 MS

- 1) the normalized RMS values and
- 2) the cross correlation.

It is important to note that these measures are made relative to the EMG activity recorded on the FDI and then compared between each other in order to find the best reference electrode placement.

The normalized RMS value of a EMG signal is simply the RMS value of that signal divided by the RMS value of the EMG signal recorded by the electrode at the FDI position. This is given by the equation:

$$RMS = \frac{\sqrt{\frac{1}{N} \sum_{i=1}^N s_i^2}}{RMS_{fdi}} \quad D.1$$

where  $N$  is the length of the recorded signal  $s_i$  and  $RMS_{fdi}$  is the root mean square value of the EMG signal recorded from the FDI muscle. Therefore, this gives a relative measure of the amplitude of the EMG signals recorded at the various points tested.

The EMG signals recorded from the thumb, small finger and triceps can be composed of some of the EMG signals produced by the FDI muscle. This is possible through the process of volume conduction. A better indicator of volume conduction can be made by determining whether or not the EMG signal recorded at the FDI muscle is correlated to the EMG signals recorded at the other positions. This can be measured by finding the individual cross correlations between the EMG signal at

the FDI muscle location and the EMG signals recorded at the other positions. The  $j$ 'th value of the cross correlation between two sequences  $s_1$  and  $s_2$  is defined as:

$$corr(s_1, s_2)_j = \sum_{k=0}^{N-1} s_{1_{j+k}} s_{2_k} \quad D.2$$

where again  $N$  is the length of the sequences [192]. A particularly convenient way of calculating the above equation is given by the discrete convolution theorem. This theorem is given by the relation:

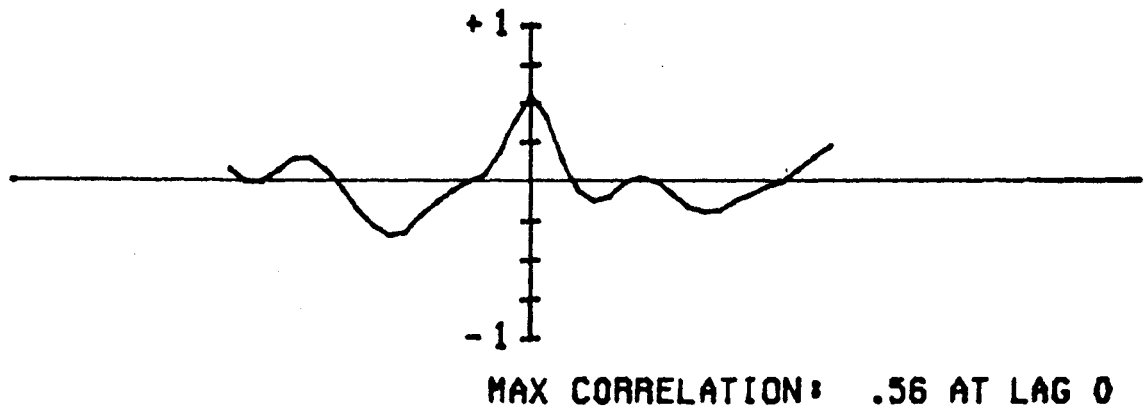
$$corr(s_1, s_2)_j \Leftrightarrow S_{1_k} S_{2_k}^* \quad D.3$$

where  $S_{1_k}$  and  $S_{2_k}$  are the discrete Fourier Transforms (chapter five) of  $s_1$  and  $s_2$  respectively and  $*$  denotes the complex conjugation. Thus equation D.3 can be computed efficiently using the fast Fourier Transform (FFT). The two sequences are normalized with respect to their standard deviations. The cross correlations for  $\pm 20$  lags between the EMG signals shown in Figures D.2 and D.3 are presented in Figures D.4 and D.5 respectively. As seen the cross correlation is significant for the thumb and small finger locations especially in Figure D.5.

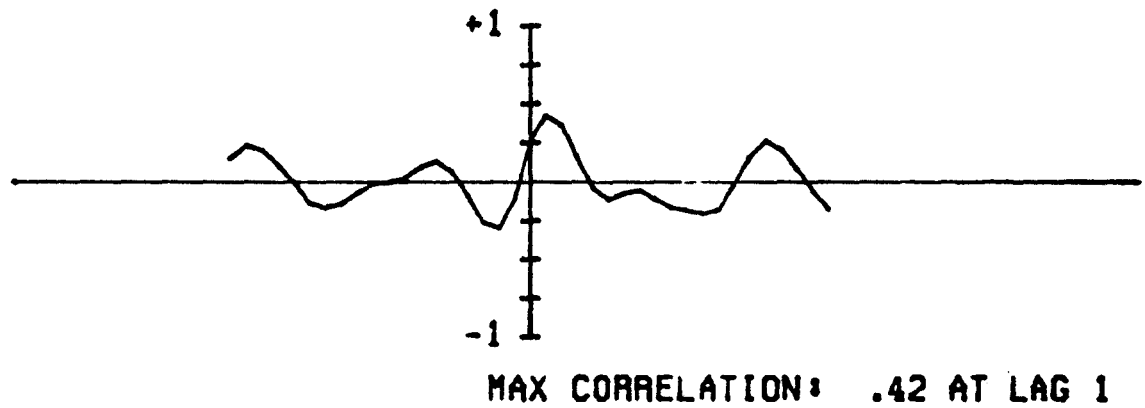
### D.1.2 Results

The results of several recordings were compiled and recorded in Figure D.6. This figure is a plot of the normalized RMS amplitudes of the recorded signals from the various reference points plotted against their cross correlation with the FDI

## FDI VS THUMB



## FDI VS FINGER



## FDI VS TRICEPS

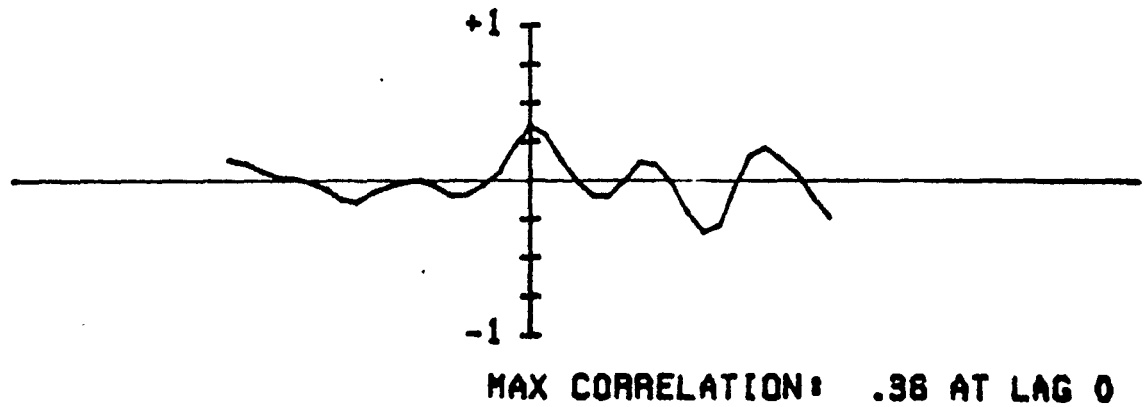
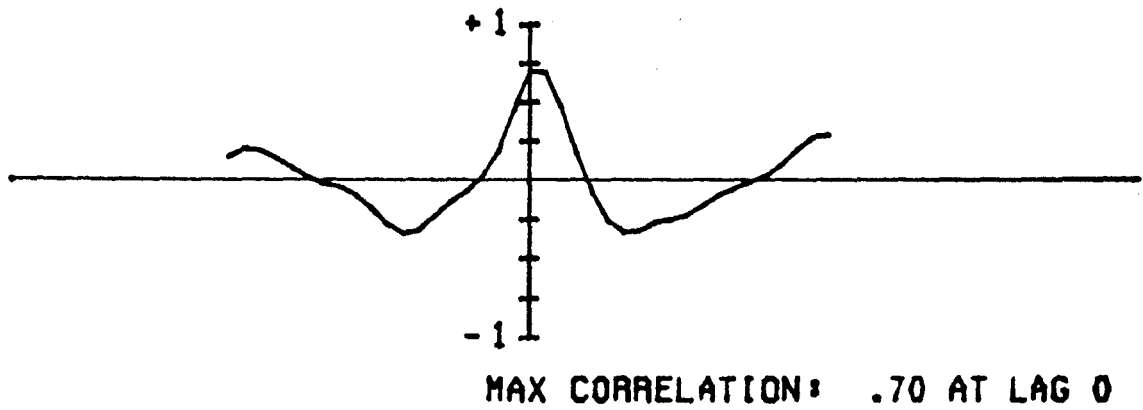
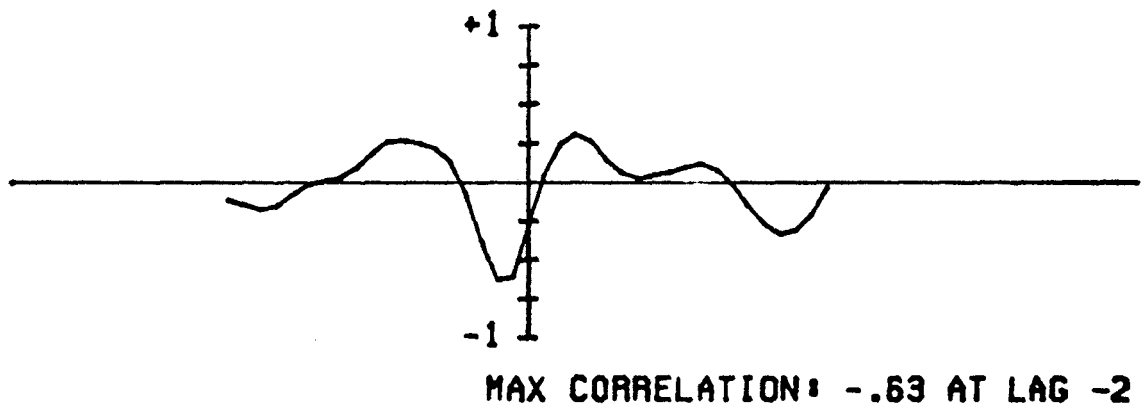


FIGURE D.4 CROSS CORRELATIONS

## FDI VS THUMB



## FDI VS FINGER



## FDI VS TRICEPS

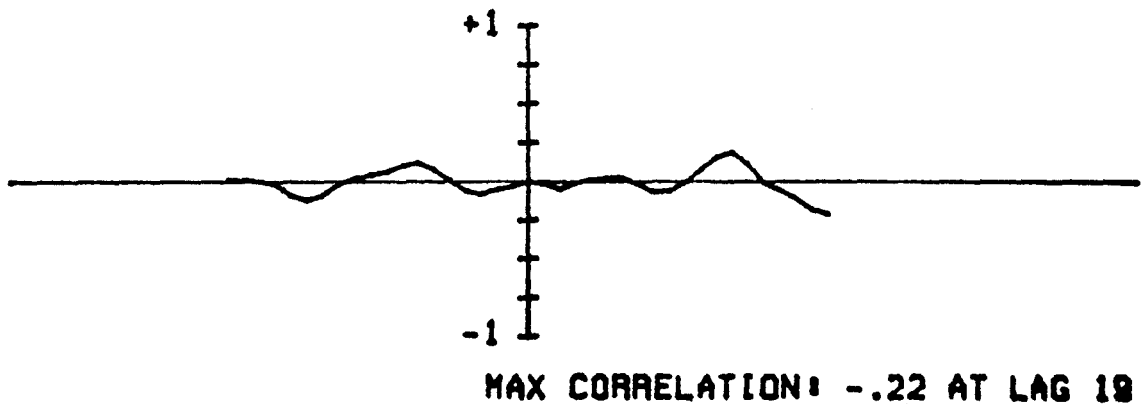
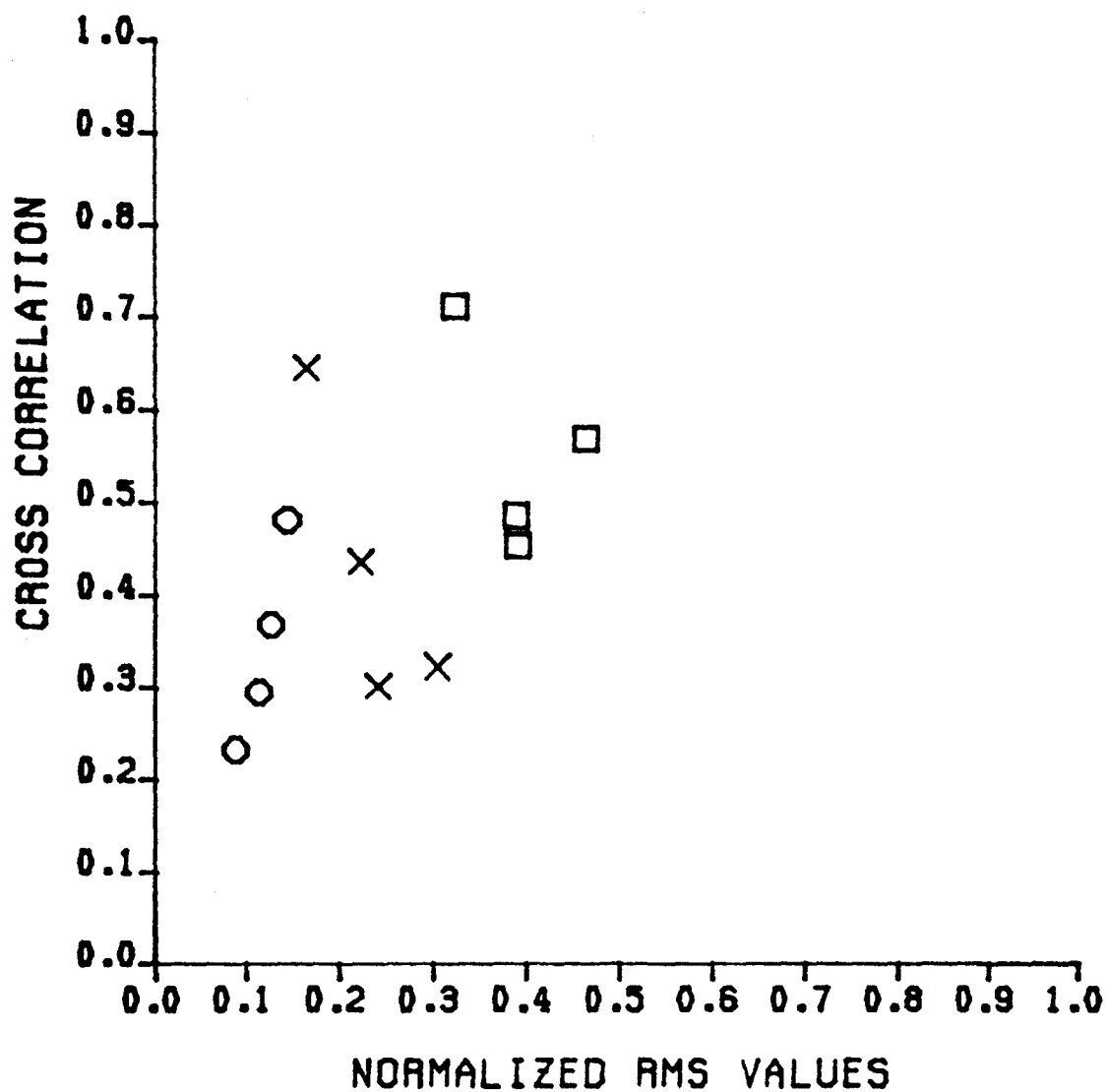


FIGURE D.5 CROSS CORRELATIONS



□ ELECTRODE PLACED ON THUMB  
× ELECTRODE PLACED ON FINGER  
○ ELECTRODE PLACED ON TRICEPS

FIGURE D.6 RMS VS CROSS CORRELATION

signal. As seen from the figure the least RMS activity and cross correlation on average comes about when the reference electrode is placed on the triceps. This result is pleasing for two reasons. First of all the distance from the first dorsal interosseus to the triceps location is greatest of all the locations looked at, so little if any cross correlation due to volume conduction would be expected (i.e. signals are attenuated greatly by the low pass filter characteristics of tissue). Secondly, the way the arm jig is constructed, there is little if any activity in the triceps when the first dorsal interosseus is active. It should be pointed out from Figure B.6 that the cross correlation calculated for the triceps in some instances is higher than that for the the small finger. This can be misleading since the cross correlation function will give an exaggerated value if an EMG record has several large peaks relative to the overall level of activity. These relatively large peaks can inflate the cross correlation values if they line up with peaks in the other sequence even though they are in no way related. Due to the inherent peaky nature of any EMG recording this can occur quite often. This is what is probably happening in a few of the cross correlation values shown in Figure D.6.

In conclusion then the best position of the reference electrode was determined to be the triceps.

## Appendix E

### Proof of Theorems

The purpose of this appendix is to present the derivations of the equations presented in Chapter Five. These derivations are separated into the continuous time and discrete time derivations.

#### E.1.1 Continuous Time

The continuous time Fourier transform is given by the equation

$$G(\omega) = \int_{-\infty}^{+\infty} g(t) e^{j\omega t} dt$$

and the inverse by equation

$$g(t) = \frac{1}{2\pi} \int_{-\infty}^{+\infty} G(\omega) e^{-j\omega t} d\omega$$

Both equations are presented in Chapter Five as equations 5.10 and 5.11 respectively. This transform pair is represented by the convention

$$g(t) \Leftrightarrow G(\omega)$$

which is given in Chapter Five as relation 5.12.

### E.1.2 Time Shifting

The Fourier transform of a time shifted signal  $g(t-t_0)$  may be found by direct application of equation 5.10 such that

$$F[g(t-t_0)] = \int_{-\infty}^{+\infty} g(t-t_0) e^{j\omega t} dt$$

Let  $x = t-t_0$

$$F[g(t-t_0)] = \int_{-\infty}^{+\infty} g(x) e^{j\omega(x+t_0)} dx$$

$$F[g(t-t_0)] = \int_{-\infty}^{+\infty} g(x) e^{j\omega x} e^{j\omega t_0} dx$$

$$F[g(t-t_0)] = G(\omega) e^{j\omega t_0}$$

Therefore the Fourier transform of a time shifted signal may be expressed as

$$g(t-t_0) \Leftrightarrow G(\omega) e^{j\omega t_0}$$

which is relation 5.13 in Chapter Five.

### E.1.3 Differentiation

The Fourier transform of the derivative of a continuous signal may be found by integrating the right hand side of equation 5.10. Integration by parts yields

$$G(w) = - \frac{1}{jw} g(t) e^{j\omega t} \Big|_{-\infty}^{+\infty} + \frac{1}{jw} \int_{-\infty}^{+\infty} \frac{dg}{dt} e^{j\omega t} dt$$

Since  $g(t)$  is Fourier transformable then  $\lim_{t \rightarrow \pm\infty} g(t) = 0$  then

$$jwG(w) = \int_{-\infty}^{+\infty} \frac{dg}{dt} e^{j\omega t} dt$$

The right hand side of the equation is just the Fourier transform of  $\frac{dg}{dt}$  thus

$$F\left[\frac{dg}{dt}\right] = jwG(w)$$

This result can be generalized for finding the  $m$ 'th derivative as

$$F\left[\frac{d^m g}{dt^m}\right] = (jw)^m G(w)$$

Therefore this may be written as

$$\frac{d^m g}{dt^m} \Leftrightarrow (jw)^m G(w)$$

which is given in Chapter Five as relation 5.15.

### E.1.4 Integration

The Fourier transform of the integration of a continuous signal may be found by direct evaluation of the integral of  $g(t)$  such that

$$\int_{-\infty}^{+\infty} g(x) dx = \int_{-\infty}^t g(x) u(t-x) dx$$

where

$$u(t-x) = \begin{cases} 1, & x \leq t \\ 0, & x > t \end{cases}$$

Taking the Fourier transform of the integral yields

$$F\left[\int_{-\infty}^{+\infty} g(x) dx\right] = \int_{-\infty}^{+\infty} e^{j\omega t} \left[\int_{-\infty}^t g(x) u(t-x) dx\right] dt$$

Using Fubini's theorem, the order of integration can be changed so that

$$F\left[\int_{-\infty}^{+\infty} g(x) dx\right] = \int_{-\infty}^{+\infty} g(x) \left[\int_{-\infty}^{+\infty} u(t-x) e^{j\omega t} dt\right] dx$$

Since

$$u(t) \Leftrightarrow \frac{1}{j\omega} + \pi\delta(\omega)$$

then

$$F\left[\int_{-\infty}^{+\infty} g(x) dx\right] = \int_{-\infty}^{+\infty} g(x) \left[\frac{1}{jw} + \pi \delta(w)\right] e^{jwx} dx$$

$$F\left[\int_{-\infty}^{+\infty} g(x) dx\right] = G(w) \left[\frac{1}{jw} + \pi \delta(w)\right]$$

$$F\left[\int_{-\infty}^{+\infty} g(x) dx\right] = \frac{G(w)}{jw} + \pi G(0) \delta(w)$$

therefore

$$\int_{-\infty}^t g(x) dx \Leftrightarrow \frac{G(w)}{jw} + \pi G(0) \delta(w)$$

which is given by relation 5.16 in Chapter Five. If the area under the signal  $g(t)$  is zero the above relation can be represented as

$$\int_{-\infty}^t g(x) dx \Leftrightarrow \frac{G(w)}{jw}$$

which is relation 5.17 in Chapter Five.

## E.2 Discrete Time

The discrete time Fourier transform is given by equation

$$G_n = \sum_{k=0}^{N-1} g_k e^{j2\pi kn/N}$$

and its inverse by equation

$$g_k = \frac{1}{N} \sum_{n=0}^{N-1} G_n e^{-j2\pi kn/N}$$

which are given in Chapter Five as equations 5.22 and 5.23 respectively. As in the case of the continuous Fourier transform, this discrete transform pair is represented by the convention

$$g_k \Leftrightarrow G_n$$

which is given in Chapter Five as relation 5.28.

### E.2.1 Discrete Time Shifting

The discrete Fourier transform of the time shifted discrete signal  $g(t_k - t_\phi)$  where  $t_\phi$  is some non-integer time shift from  $t_k$  can be found by direct application of equation 5.22.

Let  $g(t_k - t_\phi) = g_{k-\phi}$  then

$$DFT[g_{k-\phi}] = \sum_{k=0}^{N-1} g_{k-\phi} e^{j2\pi kn/N}$$

Let  $x = k - \phi$  then

$$DFT[g_{k-\phi}] = \sum_{x=k-\phi}^{N-1} g_x e^{j2\pi n(x+\phi)/N}$$

$$DFT[g_{k-\phi}] = \sum_{x=k-\phi}^{N-1} g_x e^{j2\pi xn/N} e^{j2\pi \phi n/N}$$

$$DFT[g_{k-\phi}] = G_n e^{j2\pi \phi n/N}$$

Therefore the time shifted discrete Fourier transform may be represented by the relation

$$g_{k-\phi} \Leftrightarrow G_n e^{j2\pi \phi n/N}$$

which is relation 5.29 in Chapter Five. Making the simplification

$$G_{n,\phi} = G_n e^{j2\pi \phi n/N}$$

then the discrete time shift of a discretely sampled signal may be found by using

$$g_{k-\phi} = \frac{1}{N} \sum_{n=0}^{N-1} G_{n,\phi} e^{-j2\pi kn/N}$$

which is equation 5.31 in Chapter Five.

### E.2.2 Discrete Differentiation

The discrete Fourier transform of the derivative with respect to  $\phi$  of a discrete signal shifted by time  $t_\phi$  may be found by direct application of the above result where

$$g_{k-\phi} = \frac{1}{N} \sum_{n=0}^{N-1} G_{n,\phi} e^{-j2\pi kn/N}$$

Taking the  $m$ 'th derivative with respect to  $\phi$  of the above equation yields

$$\frac{d^m g_{k-\phi}}{d\phi^m} = \frac{d}{d\phi^m} \left[ \frac{1}{N} \sum_{n=0}^{N-1} G_{n,\phi} e^{-j2\pi kn/N} \right]$$

where the derivative operation may be taken inside the summation giving

$$\frac{d^m g_{k-\phi}}{d\phi^m} = \frac{1}{N} \sum_{n=0}^{N-1} \frac{d}{d\phi^m} \left[ G_{n,\phi} e^{-j2\pi kn/N} \right]$$

resulting in equation 5.39 as presented in Chapter Five as

$$\frac{d^m g_{k-\phi}}{d\phi^m} = \frac{1}{N} \sum_{n=0}^{N-1} \left[ \frac{j2\pi n}{N} \right]^m \left[ G_{n,\phi} e^{-j2\pi kn/N} \right]$$

This equation can be simplified further by representing the discrete Fourier transform of a real signal by the equation

$$g_{k-\phi} = \frac{G_0}{N} + \frac{1}{N} \sum_{n=1}^{N/2-1} ( G_{n,\phi} e^{-j2\pi kn/N} + G_{n,\phi}^* e^{j2\pi kn/N} )$$

where  $G_{n,\phi}^*$  denotes the complex conjugate of  $G_{n,\phi}$  and the negative frequency coefficients equal the complex conjugates of the positive frequency coefficients. Furthermore,  $G_0$  is the dc offset of the signal. This equation assumes that the coefficient  $G_{N/2}$  is zero which it should be if the Nyquist sampling criteria is satisfied. Making the substitution  $\theta = \phi - k$  where  $\theta$  represents the phase delay at any particular point in time where the discrete signal is defined the above equation can then be written as

$$g_\theta = \frac{G_0}{N} + \frac{1}{N} \sum_{n=1}^{N/2-1} ( G_n e^{j2\pi\theta n/N} + G_n^* e^{-j2\pi\theta n/N} )$$

Now let  $G_{n,\theta} = G_n e^{j2\pi\theta n/N}$  and  $G_{n,\theta}^* = G_n^* e^{-j2\pi\theta n/N}$  then

$$g_\theta = \frac{G_0}{N} + \frac{1}{N} \sum_{n=1}^{N/2-1} ( G_{n,\theta} + G_{n,\theta}^* )$$

taking the derivative results in

$$\frac{dg_{\theta}}{d\theta} = \frac{1}{N} \sum_{n=1}^{N/2-1} \left[ \left[ \frac{j2\pi n}{N} \right] G_{n,\theta} + \left[ -\frac{j2\pi n}{N} \right] G_{n,\theta}^* \right]$$

which can be generalized for the m'th derivative as

$$\frac{d^m g_{\theta}}{d\theta^m} = \frac{1}{N} \sum_{n=1}^{N/2-1} \left[ \left[ \frac{j2\pi n}{N} \right]^m G_{n,\theta} + \left[ -\frac{j2\pi n}{N} \right]^m G_{n,\theta}^* \right]$$

The significant part of the above equation is the expression within the summation sign. This can further be simplified as shown below. Let  $X$  equal this expression such that

$$X = \left[ \left[ \frac{j2\pi n}{N} \right]^m G_{n,\theta} + \left[ -\frac{j2\pi n}{N} \right]^m G_{n,\theta}^* \right]$$

Factoring the above equation yields

$$X = \left[ \frac{j2\pi n}{N} \right] \left[ \left[ \frac{j2\pi n}{N} \right]^{m-1} G_{n,\theta} - (-1)^{m-1} \left[ \frac{j2\pi n}{N} \right]^{m-1} G_{n,\theta}^* \right]$$

$$X = \left[ \frac{j2\pi n}{N} \right] \left[ \left[ \frac{j2\pi n}{N} \right]^{m-1} ( G_{n,\theta} - (-1)^{m-1} G_{n,\theta}^* ) \right]$$

Separation into Real ( $Re$ ) and Imaginary ( $Im$ ) parts gives

$$X = \left[ \frac{2\pi n}{N} \right] \left[ \left[ \frac{j2\pi n}{N} \right]^{m-1} (jRe(G_{n,\theta}) + jIm(G_{n,\theta}) + (-1)^m (jRe(G_{n,\theta}^*) + jIm(G_{n,\theta}^*))) \right]$$

The quantity within the square brackets is of interest here. In particular how this quantity varies with  $m$  is shown below.

When  $m$  is an odd integer then

$$\left[ \frac{j2\pi n}{N} \right]^{m-1} = \pm \text{Real number and,}$$

$$jRe(G_{n,\theta}) + jIm(G_{n,\theta}) + (-1)^m (jRe(G_{n,\theta}^*) + jIm(G_{n,\theta}^*)) = 2jIm(G_{n,\phi}^*)$$

When  $m$  is an even integer then:

$$\left[ \frac{j2\pi n}{N} \right]^{m-1} = \pm \text{Imaginary number and,}$$

$$jRe(G_{n,\theta}) + jIm(G_{n,\theta}) + (-1)^m (jRe(G_{n,\theta}^*) + jIm(G_{n,\theta}^*)) = j2Re(G_{n,\phi})$$

Although it may not be immediately obvious, the expression represented by  $X$  is equal to  $-2Im \left\{ G_{n,\phi} \left[ \frac{j2\pi n}{N} \right]^{m-1} \right\}$  for  $m$  equal to any positive integer. Thus the  $m$ 'th derivative of a discretely sampled signal may be represented by the equation

$$\frac{d^m g_\theta}{d\theta^m} = -\frac{2}{N} \sum_{n=1}^{N/2-1} Im \left\{ G_{n,\phi} \left[ \frac{j2\pi n}{N} \right]^{m-1} \right\}$$

which is given by equation 5.40 in Chapter Five.

### E.2.3 Discrete Integration

The discrete Fourier transform of the integral of a discrete signal shifted by time  $t_\phi$  may be found by directly integrating the result obtained in the discrete time shifted section where the dc component is separated from the rest of the frequency components such that

$$g_{k-\phi} = \frac{G_0}{N} + \frac{1}{N} \sum_{n=1}^{N-1} G_{n,\phi} e^{-j2\pi kn/N}$$

Integrating with respect to  $\phi$  in the interval  $(a, b)$  gives

$$\int_a^b g_{k-\phi} d\phi = \int_a^b \left[ \frac{G_0}{N} + \frac{1}{N} \sum_{n=1}^{N-1} G_{n,\phi} e^{-j2\pi kn/N} \right] d\phi$$

Bringing the integral sign inside the summation sign gives

$$\int_a^b g_{k-\phi} d\phi = \int_a^b \frac{G_0}{N} d\phi + \frac{1}{N} \sum_{n=1}^{N-1} \int_a^b G_{n,\phi} e^{-j2\pi kn/N} d\phi$$

$$\int_a^b g_{k+\phi} d\phi = \frac{G_0}{N}(b-a) + \frac{1}{N} \sum_{n=1}^{N-1} \frac{G_{n,\phi}}{(j\frac{2\pi n}{N})} \Big|_{\phi=a}^{\phi=b} e^{-j2\pi kn/N}$$

$$\int_a^b g_{k-\phi} d\phi = \frac{G_0}{N}(b-a) + \frac{1}{N} \sum_{n=1}^{N-1} \left[ \frac{G_{n,b}}{(j2\pi n/N)} - \frac{G_{n,a}}{(j2\pi n/N)} \right] e^{-j2\pi kn/N}$$

This last result is given as equation 5.41 in Chapter Five. Of course if the dc area under the discrete function  $g_{k-\phi}$  is zero then the above equation may be written as

$$\int_a^b g_{k-\phi} d\phi = \frac{1}{N} \sum_{n=1}^{N-1} \left[ \frac{G_{n,b}}{(j2\pi n/N)} - \frac{G_{n,a}}{(j2\pi n/N)} \right] e^{-j2\pi kn/N}$$

which is given as equation 5.42 in Chapter Five.

### E.2.4 Discrete Minimization

Chapter five presented both a one dimensional and a multidimensional minimization equation which were used to find MUAP features and to resolve superimposed MUAPs respectively. The derivation of both of these equations is identical with the only difference being the use of a partial derivative in the multidimensional case as opposed to an ordinary derivative in the one dimensional case. In the one dimensional case, the least means square equation was given in Chapter Five (equation 5.61) as

$$\epsilon^2 = \frac{1}{N} \sum_{n=0}^{N-1} |S_{n,\phi} - C_n|^2$$

Further simplification can be made to the above equation due to the symmetry of the real sequence since  $G_{N-n} = G_N$  therefore

$$\epsilon^2 = \frac{1}{N} |S_0 - C_0|^2 + \frac{2}{N} \sum_{n=1}^{N/2-1} |S_{n,\phi} - C_n|^2$$

where  $S_{n,\phi}$  is the MUAP vector that is matched to the class vector given by  $C_n$ . Separating the dc value from the rest of the frequencies yields

$$\epsilon^2 = \frac{1}{N} |S_0 - C_0|^2 + \frac{2}{N} \sum_{n=1}^{N/2-1} |S_{n,\phi} - C_n|^2$$

Taking the derivative of  $\epsilon^2$  with respect to  $\phi$  gives

$$\frac{d\epsilon^2}{d\phi} = \frac{d}{d\phi} \left[ \frac{1}{N} |S_0 - C_0|^2 + \frac{2}{N} \sum_{n=1}^{N/2-1} |S_{n,\phi} - C_n|^2 \right]$$

Where the derivative of the dc term is zero and the derivative of the summation can be written as the summation of derivatives such that

$$\frac{d\epsilon^2}{d\phi} = \frac{2}{N} \sum_{n=1}^{N/2-1} \frac{d}{d\phi} \left[ |S_{n,\phi} - C_n|^2 \right]$$

The term of interest then is  $|S_{n,\phi} - C_n|^2$  which in turn can be evaluated as

$$|S_{n,\phi} - C_n|^2 = \left[ ((\operatorname{Re}(S_{n,\phi}) - \operatorname{Re}(C_n))^2 + (\operatorname{Im}(S_{n,\phi}) - \operatorname{Im}(C_n))^2)^{1/2} \right]^2$$

$$|S_{n,\phi} - C_n|^2 = S_{n,\phi} S_{n,\phi}^* + C_n C_n^* - S_{n,\phi} C_n^* - S_{n,\phi}^* C_n$$

Now differentiating with respect to  $\phi$  gives

$$\frac{d}{d\phi} [|S_{n,\phi} - C_n|^2] = \frac{d}{d\phi} [S_{n,\phi} S_{n,\phi}^* + C_n C_n^* - S_{n,\phi} C_n^* - S_{n,\phi}^* C_n]$$

Given that  $S_{n,\phi} = S_n e^{j2\pi n\phi/N}$  then the differentiation yields

$$\frac{d}{d\phi} [|S_{n,\phi} - C_n|^2] = -C_n^* \left[ \frac{j2\pi n}{N} \right] S_{n,\phi} - C_n \left[ -\frac{j2\pi n}{N} \right] S_{n,\phi}^*$$

$$\frac{d}{d\phi} [|S_{n,\phi} - C_n|^2] = -\left[ \frac{2\pi n}{N} \right] [j(C_n^* S_{n,\phi} - S_{n,\phi}^* C_n)]$$

Although it may not seem immediately obvious, the term  $j(C_n^* S_{n,\phi} - S_{n,\phi}^* C_n)$  reduces to the form  $2\operatorname{Im}\{S_{n,\phi} C_n^*\}$ , therefore the above equation can be written as

$$\frac{d}{d\phi} [|S_{n,\phi} - C_n|^2] = 2 \left[ \frac{2\pi n}{N} \right] \operatorname{Im}\{S_{n,\phi} C_n^*\}$$

and the overall error squared function may be expressed as

$$\frac{d\epsilon^2}{d\phi} = \frac{4}{N} \sum_{n=1}^{N/2-1} \left[ \frac{2\pi n}{N} \right] \operatorname{Im}\{S_{n,\phi} C_n^*\}$$

which is equation 5.62 in Chapter Five.

As stated previously the derivation of of the multidimensional minimization equations (equations 5.65 and 5.75 in Chapter Five) are identical to the derivation above and are not presented here.

## References

- [1] AAEE Glossary of Terms in Electromyography, Supplement to Muscle and Nerve, 10, October 1987.
- [2] Cavasin, R., "An Automated Muscle Motor Unit Counting System", Masters Thesis, McMaster University, Hamilton, Ontario, 1989.
- [3] Ritchfield, H., B. Cohen and J. Albers, "Review of quantitative automated needle electromyography", IEEE Transactions Biomedical Engineering, 18, 155–157, 1971.
- [4] DeLuca, C., "Physiology and mathematics of myoelectric signals", IEEE Transactions Biomedical Engineering, 26, 313–325, 1979.
- [5] Stashuk, D., "Automatic Quantitative Analysis of Needle Recorded EMG Signals", PhD Thesis, McMaster University, Hamilton, Ontario, Canada, 1985.
- [6] Geddes, L. and L. Baker, "Principles of Applied Biomedical Instrumentation", second edition, John Wiley and Sons, Toronto, 1975.
- [7] Katz, B., "Nerve, Muscle and Synapse", McGraw–Hill, Toronto, 1966.
- [8] Stalberg, E. et al, "The normal motor unit in man", Journal of Neurological Science, 27, 291–301, 1976.
- [9] Stein, R., "Nerve and Muscle: membranes, cells and systems", Plenum Press, New York, 1980.
- [10] Webster, J. (editor), "Medical Instrumentation: Application and Design", Houghton Mifflin Company, Boston, 1978.

- [11] Masterton, W. L., E. J. Slowinski and C. L. Stanitski, "Chemical Principles", Saunders College Publishing, Philadelphia, 1981.
- [12] Piotrkiewicz, M. and A. Millner-Larsson, "A method of description of single fiber action potential by an analytical function  $V(t,r)$ ", Biological Cybernetics, 56, 237-245, 1987.
- [13] Plonsey, R. and R. Barr, "Bioelectricity", Plenum Press, New York, 1988.
- [14] Plonsey, R., "Bioelectric Phenomena", McGraw-Hill, Toronto, 1969.
- [15] Plonsey, R., "The active fiber in a volume conductor", IEEE Transactions Biomedical Engineering, 21, 371-381, 1974.
- [16] Gath, I. and E. Stalberg, "On the volume conduction in human skeletal muscle in situ", Electroencephalography and Clinical Neurophysiology, 43, 106-110, 1977.
- [17] Bigland, B. and O. Lippold, "Motor unit activity in the voluntary contraction of human muscle", Journal of Physiology, 125, 322-335, 1954.
- [18] Buchthal, F., P. Pinelli and P. Rosenflack, "Action potential parameters in normal human muscle and their physiological determinants", Acta Physiologica Scandinavia, 32, 219-229, 1954.
- [19] Brody, G. et al, "A model for myo-electric signal generation", Med. Biol. Eng., 12, 29-41, 1974.
- [20] Paul, C. R. and S. A. Nasar, "Introduction to Electromagnetic Fields", McGraw-Hill, Toronto, 1982.
- [21] Buchthal, F., C. Gould and P. Rosenflack, "Action potential parameters in normal human muscle and their dependence on physical variables", Acta Physiologica Scandinavia, 32, 200-218.

- [22] Gath, I. and E. Stalberg, "The calculated radial decline of the extracellular action potential compared with in situ measurements in human brachial biceps", *Electroencephalography and Clinical Neurophysiology*, 44, 547–552, 1978.
- [23] Gath, I. and E. Stalberg, "Measurement of uptake area of small-size electromyographic electrodes", *IEEE Transactions Biomedical Engineering*, 26, 374–376, 1979.
- [24] Basmajian, J., "Muscles Alive: their functions revealed through electromyography", fourth edition, Williams and Wilkins Company, Baltimore, 1979.
- [25] Ekstedt, J. and E. Stalberg, "How the size of the needle electrode leading off surface influences the shape of the single muscle fibre action potential in electromyography", *Computer Programs in Medicine*, 3, 204–212, 1973.
- [26] Buchthal, F., F. Erminio and P. Rosenflack, "Motor unit territory in different human muscles", *Acta Physiologica Scandinavia*, 45, 72–87, 1959.
- [27] Burke, R., and P. Tsairs, "Anatomy of innervated rations in motor units of cat gastronemius", *Journal of Physiology*, 234, 749–765, 1973.
- [28] Lang, A. and H. Tuomola, "The time parameters of motor unit potentials recorded with multi-electrodes and the summation technique", *Electroencephalography and Clinical Neurophysiology*, 14, 513–525, 1974.
- [29] Lindstrom, L. and R. Magnusson, "Interpretation of the myoelectric power spectra: a model and it's application", *Proceedings IEEE*, 65, 653–662, 1977.

- [30] Willison, R., "A method of measuring motor unit activity in human muscle", *Journal of Physiology*, 168, 35–36, 1963.
- [31] Lindstrom, L., R. Magnusson and I. Petersen, "Muscular fatigue and action potential conduction velocity changes studied with frequency analysis of EMG signals", *Electromyography*, 4, 341–353, 1970.
- [32] DeLuca, C. and W. Forrest, "An electrode for recording single motor unit activity during strong muscle contractions", *IEEE Transactions Biomedical Engineering*, 19, 367–372, 1972.
- [33] Basmajian, J. and G. Cross, "Duration of motor unit potentials from fine-wire electrodes", *American Journal Phys. Med.*, 50, 144–148, 1971.
- [34] Dorfman, L., K. McGill and K. Cummins, "Clinical properties of commercial concentric EMG electrodes", *Muscle and Nerve*, 8, 1–9, 1985.
- [35] Howard, J., K. McGill and L. Dorfman, "Properties of MUAP recorded with concentric and monopolar needle electrodes", *Muscle and Nerve*, 11, 1051–1055, 1988.
- [36] Parker, P., and R. Scott, "Statistics of the myoelectric signal from monopolar and bipolar electrodes", *Med. Biol. Comput.*, 11, 591, 1978.
- [37] Geddes, L., "Electrodes and Measurement of Bioelectric Events, Wiley, New York, 1972.
- [38] Gath, I. and E. Stalberg, "Techniques for improving selectivity of electromyographic recordings", *IEEE Transactions Biomedical Engineering*, 23, 467–472, 1976.
- [39] Basmajian, J. and G. Stecko, "A new bipolar electrode for electromyography", *Journal of Applied Physiology*, 17, 849, 1962.

- [40] Masland, W., D. Sheldon and C. Hershey, "The stochastic properties of individual motor unit interspike intervals", *American Journal Physiology*, 217, 1384–1388, 1969.
- [41] Milner–Brown, H., R. Stein and B. Lee, "Contractile and electrical properties of human motor units in Neuropathies and motor neuron disease", *Journal Neurol., Neurosurg and Psychiat*, 37, 670–676, 1974.
- [42] Gerstein, G. and W. Clark, "Simultaneous studies of firing patterns in several neurons", *Science*, 143, 1325–1327, 1964.
- [43] Gath, I., "On the separation of semi–periodic superimposed point processes: application to electromyographic signals", *Computer Programs in Biomedicine*, 4, 137–143, 1975.
- [44] Goldberg, L. and B. Derfler, "Relationship among recruitment order, spike amplitude and twitch tension of single motor units in human masseter muscle", *Journal Neurophysiology*, 40, 879–890, 1977.
- [45] Guber, A. et al, "A new framework and computer program for quantitative EMG signal analysis", *IEEE Transactions Biomedical Engineering*, 3, 19–28, 1966.
- [46] Hirose, K., "Quantitative electromyography, a method of computer analysis", *Electroencephalography and Clinical Neurophysiology*, 12, 421–429, 1972.
- [47] Keehn, D., "An iterative spike separation technique", *IEEE Transactions Biomedical Engineering*, 3, 19–28, 1966.
- [48] Kent, E., "An educable waveform recognition program suitable for on line discrimination of extracellular single units", *Electroencephalography and Clinical Neurophysiology*, 31, 615–620, 1971.

- [49] Kope, J. and I. Housmanona, "Histogram of muscle potentials recorded automatically with the aid of the averaging computer ANOPS", *Electromyography*, 19, 371–381, 1969.
- [50] Kranz, H. and G. Baumgartner, "Human alpha motoneurone discharge rates: a statistical analysis", *Brain Research*, 66, 324–329, 1979.
- [51] Kwany, E. et al, "An application of signal processing techniques to the study of myoelectric signals", *IEEE Transactions Biomedical Engineering*, 17, 303–312, 1970.
- [52] Krendal, D., D. Sanders and J. Massey, "Single fiber electromyography in chronic progressive external ophthalmoplegia", *Muscle and Nerve*, 10, 299–302, 1987.
- [53] Lago, P. and R. Scott, "Turning points spectral analysis of the interference myoelectric activity", *Med. Biol. Engineering Computing*, 21, 333, 1983.
- [54] Nandedkar, S. and E. Stalberg, "Simulation of macro EMG motor unit potentials", *Electroencephalography and Clinical Neurophysiology*, 56, 52–62, 1983.
- [55] Nandedkar, S., E. Stalberg, I. Yong and D. Sanders, "Use of signal representation to identify abnormal motor unit potentials in macro EMG", *IEEE Transactions Biomedical Engineering*, 31, 220–226, 1984.
- [56] Nandedkar, S., "Use of signal representation to identify abnormal motor unit potentials in macro EMG", *IEEE Transactions Biomedical Engineering*, 32, 220–227, 1985.
- [57] Stalberg, E., "Macro EMG", *Muscle and Nerve*, 6, 619–630, 1983.

- [58] Stalberg, E., "Macro EMG: a new recording technique", *Journal of Neurol., Neurosurg., and Psychiat.*, 43, 475–482.
- [59] Calencie, B. and B. Bona, "Limitations of the spike triggered averaging technique", *Muscle and Nerve*, 9, 78–84, 1986.
- [60] Lang, A. et al, "Automatic sampling and averaging of electromyographic unit potential", *Electroencephalography and Clinical Neurophysiology*, 31, 404–406, 1971.
- [61] Buchtal, F., C. Guld and P. Rosenflack, "Volume conduction of the spike of the motor unit potential investigated with a new type of multielectrode", *Acta Physiologica Scandinavia*, 38, 331–354, 1957.
- [62] Edwards, R. and O. Lippold, "The relation between force and integrated electrical activity in fatigued muscle", *Journal Physiology*, 132, 677–681, 1956.
- [63] Lippold, E., "The relation between integrated action potentials in human muscles and it's isometric tension", *Journal Physiology*, 117, 492–499, 1952.
- [64] Milner–Brown, H., R. Stein and R. Yemm, "Changes in firing rate of human motor units during linearly changing voluntary contractions", *Journal Physiology*, 230, 371–390, 1973.
- [65] Person, R. and L. Kudina, "Pattern of human motoneuron activity during voluntary muscular contraction", *Neurophysiology*, 3, 455–462, 1971.
- [66] Stulen, F. and C. DeLuca, "The relation between the myo–electric signal and physiological properties of constant–force isometric contractions", *Electroencephalography and Clinical Neurophysiology*, 45, 681– 698, 1978.

- [67] Abeles, M. and M. Goldstein, "Multispikes Train Analysis", Proceedings IEEE, 65, 762–773, 1977.
- [68] Coatrieux, J. et al, "Automatic classification of electromyographic signals", Electroencephalography and Clinical Neurophysiology, 55, 333–341, 1983.
- [69] Coatrieux, V., "Interference electromyogram processing", Electroencephalography and Clinical Neurophysiology, 23, 229–242, 1983.
- [70] Fuglsang–Frederiksen, A. and A. Mansson, "Analysis of electrical activity of normal muscle in man at different degrees of voluntary effort", Journal of Neurology, Neurosurg. and Psychiat., 38, 683–694, 1975.
- [71] Bergmans, J., "Computer assisted on line measurement of motor unit potential parameters in human", Electromyography, 11, 161–181, 1971.
- [72] Qin, F. and Q. Xiong, "Some aspects of nonstationary myoelectric signal processing", IEEE Transactions Biomedical Engineering", 34, 166–172, 1987.
- [73] Kopec, J. et al, "Automatic analysis in electromyography", New Developments in Electromyography and Clinical Neurophysiology, 2, 477–481, 1973.
- [74] McComas, A. and R. Sica, "Automatic quantitative analysis of the electromyogram in partially denervated distal muscles: comparison with motor unit counting", Canadian Journal Neuro. Science, 5, 275–281, 1978.
- [75] Sira, R. et al, "Evaluation of an automated method for analyzing the electromyogram", Canadian Journal Neurophysiological Science, 5, 275–278, 1978.

- [76] Magora, A. and B. Gonen, "Computer analysis of the relation between duration and degree of superposition of electromyographic signals", *Electroencephalography and Clinical Neurophysiology*, 17, 83–98, 1977.
- [77] Fitch, P. and R. Willison, "Automatic measurement of the human electromyogram", *Journal Physiology*, 178, 28–29, 1965.
- [78] Cenkovich, F., S. Hsu and J. Gerstein, "A quantitative electromyographic index that is independent of the force of contraction", *Electroencephalography and Clinical Neurophysiology*, 54, 79–86, 1982.
- [79] Cossi, V. and G. Mazzella, "Frequency analysis in clinical electromyogram", *Electroencephalography and Clinical Neurophysiology*, 27, 100–111, 1969.
- [80] Agarwal, G. and G. Gottlieb, "An analysis of the electromyogram by fourier simulation and experimental techniques", *IEEE Transactions Biomedical Engineering*, 22, 225–229, 1957.
- [81] Bernshtein, V., "Statistical parameters of the electric signal of a muscle model", *Biophysics*, 12, 693–703, 1967.
- [82] Cenkovich, F. and J. Gerstein, "Fourier analysis of the normal human electromyogram", *American Journal Phys. Med.*, 42, 192–204.
- [83] Kadefors, R. et al, "Dynamic spectrum analysis of myo-potentials with special reference to muscle fatigue", *Electromyography*, 7, 39–74, 1968.
- [84] Anderson, D. and J. Manning, "The detection and analysis of point processes in Biological Signals", *Proceedings IEEE*, 65, 773–780, 1977.
- [85] Nandedkar, S., D. Sanders and E. Stalberg, "Simulation and analysis of the EMG interference pattern in normal muscle part II: development of quantitative features", *Muscle and Nerve*, 9, 486–491, 1986.

- [86] Nandedkar, S., D. Sanders and E. Stalberg, "Simulation and analysis of the EMG interference pattern in normal muscle part I: turns and amplitude measurements", *Muscle and Nerve*, 9, 423–431, 1986.
- [87] Nandedkar, S., D. Sanders and E. Stalberg, "Automatic analysis of the electromyogram interference pattern part II: findings in control subjects and in some neuromuscular diseases", *Muscle and Nerve*, 9, 491–500, 1986.
- [88] Nandedkar, S., D. Sanders and E. Stalberg, "Automatic analysis of the electromyogram interference pattern part I: development of quantitative features", *Muscle and Nerve*, 9, 431–439, 1986.
- [89] Buchthal, F. and E. Madsen, "Synchronous activity in normal and atrophic muscle", *Electroencephalography and Clinical Neurophysiology*, 2, 425–444, 1950.
- [90] Harba, M., "A micro-based polarity correlate for the on-line measurement of muscle fibre conduction velocity", *IEEE Transactions Biomedical Engineering*, 32, 1071–1077.
- [91] Buchthal, F., C. Guld and P. Rosenfalck, "Multielectrode study of the territory of a motor unit", *Acta Physiologica Scandinavia*, 39, 83–104, 1958.
- [92] Theile, B. and E. Stalberg, "The bimodal jitter: a single fiber electromyographic study", *Journal Neurol., Neurosurg. and Psychiat.*, 37, 403–411, 1974.
- [93] Ekstedt, J., G. Nilsson and E. Stalberg, "Calculation of the EMG jitter", *Journal of Neurology, Neurosurg. and Psychiat.*, 37, 526–539, 1974.

- [94] Bessou, P. and E. Perl, "Response of cutaneous sensory units with unmyelinated fibres to noxious stimuli", *Journal of Neurophysiology*, 32, 1025–1043, 1969.
- [95] Buchthal, F. and P. Rosenfalck, "Action potential parameters in different human muscles", *Acta Physiologica Scandinavia*, 30, 125–131, 1955.
- [96] Dietz, V. et al, "Correlation between discharges of two simultaneously recorded motor units and physiological tremor", *Electroencephalography and Clinical Neurophysiology*, 40, 97–105, 1970.
- [97] Hayward, M. and R. Willison, "Automatic analysis of the electromyogram in healthy subjects of different ages", *Journal Neur. Science*, 33, 397–413, 1977.
- [98] Hayward, M. and R. Willison, "Automatic analysis of the electromyogram in patients with chronic partial denervation", *Journal Neur. Science*, 33, 415–423, 1977.
- [99] Hirose, K., U. Masonori and I. Sobue, "Quantitative electromyography comparison between manual values and computer ones on normal subjects", *Electromyography and Clinical Neurophysiology*, 14, 315–320, 1974.
- [100] Khashbin, S., M. Hallet and R. Lonbeck, "Predictors of patients experience of pain in EMG", *Muscle and Nerve*, 10, 629–632, 1987.
- [101] Lee, R. and D. White, "Computer analysis of motor unit action potentials in routine clinical electromyography", *New Developments in Electromyography and Clinical Neurophysiology*, 2, 454–461, 1973.
- [102] Miller, R., "Injury to peripheral motor nerves", *Muscle and Nerve*", 10, 698–710, 1987.

- [103] Rose, A. and R. Willison, "Quantitative electromyography using automatic analysis: studies in healthy subjects and patients with primary muscle disease", *Journal Neur., Neurosurg. and Psychiat.*, 30, 403–410, 1967.
- [104] Bigland, B., and O. Lippold, "The relation between force velocity and integrated electrical activity in human muscles", *Journal of Physiology*, 121, 214–224, 1954.
- [105] Burke, R., P. Radomin and F. Zajac, "The effect of activation history on the tension production of individual muscle units", *Brain Research*, 109, 515–529, 1976.
- [106] Clamann, H., "Activity of single motor neurons during isometric tension", *Neurology*, 23, 229–242, 1983.
- [107] DeLuca, C. and E. van Dyk, "Derivation of some parameters of myoelectric signals recorded during sustained constant force isometric contractions", *Biophysics Journal*, 15, 1167–1180, 1975.
- [108] Edstrom, L. and L. Grimby, "Effect of exercise on the motor unit", *Muscle and Nerve*, 9, 104–127, 1986.
- [109] Gilson, A. and W. Mills, "Activities of single motor units in man during slight voluntary efforts", *American Journal Physiology*, 133, 658–669, 1941.
- [110] Komi, P. and J. Viitasalo, "Signal characteristics of EMG at different levels of muscle tension", *Acta Physiologica Scandinavia*, 96, 267–276, 1976.

- [111] Milner-Brown, H. and R. Stein, "The relation between the surface electromyogram and muscular force", *Journal Physiology*, 246, 549-569, 1975.
- [112] DeLuca, C. and W. Forrest, "Some properties of motor unit action potential trains recorded during constant force isometric contractions in man", *Kybernetic*, 12, 160-168, 1973.
- [113] DeLuca, C., "A model for a motor unit train recorded during constant force isometric contractions", *Biol. Cybernetics*, 19, 159-167, 1975.
- [114] Clamann, H., "Statistical analysis of motor unit firing patterns in a human skeletal muscle", *Biophysics Journal*, 9, 1233-1251, 1969.
- [115] Hannerz, J., "Discharge properties of motor units in relation to recruitment order in voluntary contraction", *Acta Physiologica Scandinavia*, 91, 374-384, 1974.
- [116] Milner-Brown, H., R. Stein and R. Lee, "Synchronization of human motor units: possible roles of exercise and supra-spinal reflexes", *Electroencephalography and Clinical Neurophysiology*, 38, 245-254, 1975.
- [117] Milner-Brown, H., R. Stein and R. Yemm, "The orderly recruitment of human motor units during voluntary isometric contractions", *Journal Physiology*, 230, 371-390, 1973.
- [118] Milner-Brown, H., "The contractile properties of human motor units during voluntary isometric contractions", *Journal of Physiology*, 228, 285-306, 1973.
- [119] Person, R. and L. Kudina, "Discharge frequency and discharge pattern in human motor units during voluntary contractions of muscle", *Electroencephalography and Clinical Neurophysiology*, 5, 471-483, 1971.

- [120] Stalberg, E. and B. Thiele, "Discharge pattern of motoneurons in humans: a single fibre EMG study", *New Developments in Electromyography and Clinical Neurophysiology*, 3, 224–231, 1973.
- [121] Cohen, A., "Biomedical signal processing volume II: compression and automatic recognition", CRC Press, Boca Raton, 1986.
- [122] Cohen, A., "Biomedical Signal Processing, Volume I: Time and Frequency Domains Analysis", CRC Press, Boca Raton, 1986.
- [123] Deutsch, S. and E. Micheli–Tzanakou, "Neuroelectric Systems", New York University Press, New York, 1987.
- [124] Calvin, W., "Some simple spike separation techniques for simultaneously recorded neurons", *Electroencephalography and Clinical Neurophysiology*, 6, 166, 1973.
- [125] Agrawala, A., "Machine Recognition of Data", IEEE Press, John Wiley and Sons, New York, 1976.
- [126] Biro, G. and L. Partridge, "Analysis of multiunit spike records", *Journal Applied Physiology*, 30, 521–526, 1971.
- [127] Boyd, D., P. Bratty and P. Lawrence, "A review of methods of automatic analysis in clinical electromyography", *Computers Biology Medicine*, 6, 179–190, 1976.
- [128] Childers, D. and A. Durling, "Digital Filtering and Signal Processing", West Publishing Company, New York, 1975.
- [129] Childers, D. et al, "Multichannel single trial event related potential classification", *IEEE Transactions Biomedical Engineering*, 33, 1069–1075, 1986.

- [130] Dill, J., P. Lockemann and K. Naka, "An attempt to analyze multi-unit recordings", *Electroencephalography and Clinical Neurophysiology*, 28, 367–372, 1972.
- [131] Dinning, G. and A. Sanderson, "Realtime classification multi-unit neural signals using reduced feature sets", *IEEE Transactions Biomedical Engineering*, 28, 804–811, 1981.
- [132] Dowling, M., P. Fitch and G. Willison, "A special purpose digital computer (Biomac) used in the analysis of the human electromyogram", *Electroencephalography and Clinical Neurophysiology*, 25, 570–573, 1968.
- [133] Erbstein, A., and J. Goodgold, "Computer analysis in clinical electromyography", *American Journal Physiol. Med.*, 57, 77–83, 1978.
- [134] Filligoi, G., "Some theoretic results on a digital EMG signal processor", *IEEE Transactions Biomedical Engineering*, 31, 333–341, 1984.
- [135] Freidman, J. and F. Roberge, "Computer detection, classification and analysis of neural spike sequences", *Information*, 9, 1971.
- [136] McCann, G., "Nervous systems research with computers", *Science*, 148, 1565–1575, 1965.
- [137] McGill, K. and L. Dorfman, "Automatic decomposition electromyography: validation and normative data in brachial biceps", *Electroencephalography and Clinical Neurophysiology*, 111, 453–461, 1985.
- [138] McGill, K. and L. Dorfman, "Automatic decomposition of the clinical electromyogram", *IEEE Transactions Biomedical Engineering*, 32, 470–477, 1985.

- [139] O'Connel, R., W. Kocsis and R. Schoenfeld, "Minicomputer identification and timing of nerve impulses mixed in a single recording", Proceedings IEEE, 61, 1615–1621, 1973.
- [140] Schmidt, E., "An instrument for separation of multispikes unit neuro-electric signals", IEEE Transactions Biomedical Engineering, 18, 155–157, 1971.
- [141] Stalberg, E. et al, "Automatic analysis of the EMG interference pattern", Electroencephalography and Clinical Neurophysiology", 56, 672–681, 1983.
- [142] LeFever, R. and C. DeLuca, "A procedure for decomposing the myoelectric signal into its constituent action potentials part I: theory and implementation", IEEE Transactions Biomedical Engineering, 29, 149–157, 1982.
- [143] Miyazaki, S., "An interactive microcomputer system for the analysis of EMG spikes and twitch waveforms of human motor units", Comput. Biol. Res., 10, 287–296, 1977.
- [144] Moosa, A. and B. Brow, "Quantitative electromyography: a new analogue technique for detecting changes in action potential duration", Journal Neurophysiology, 35, 216–220, 1972.
- [145] Young, T. and K. Fu, "Handbook of pattern recognition and image processing", Academic Press, 1986.
- [146] Duda, R. and P. Hart, "Pattern classification and scene analysis", Wiley, New York, 1973.
- [147] Tou, J. and R. Gonzalez, "Pattern recognition principles", Addison–Wesely, Reading Press, 1974.

- [148] Yokoyama, K., "Software system for neuron classification based on simple parameters", IEEE Transactions Biomedical Engineering, 33, 308–314, 1986.
- [149] Simon, W., "The real time sorting of neuro–electric action potentials in multi–unit studies", Electroencephalography and Clinical Neurophysiology, 18, 192–195, 1965.
- [150] Schmidt, E., "Unit activity from peripheral nerve bundles utilizing correlation techniques", Med. Biol. Computing, 9, 665–674, 1971.
- [151] Mischelevich, D., "On line real time digital computer separation of extracellular neur–electric signals", IEEE Transactions Biomedical Engineering, 17, 147–150, 1970.
- [152] Zalud, P. et al, "A 4–parameter discriminator of neuronal spike activity", Medical and Biological Engineering, 14, 636–643, 1976.
- [153] Andreassen, S. and A. Rosenfalck, "Recording from a single motor unit during strong effort", IEEE Transactions Biomedical Engineering, 25, 501–508, 1978.
- [154] DeFigueiredo, R., and A. Gerfer, "Separation of superimposed signals by a cross correlation method", IEEE Transactions Acoustics Speech Signal Processing, 31, 1084, 1983.
- [155] Oppenheim, A. and D. Johnson, "Discrete representation of signals", Proceedings IEEE, 60, 681–691, 1972.
- [156] Oppenheim, A. and R. Schafer, "Digital Signal Processing", Prentice–Hall, Englewood Cliffs, NJ, 1975.

- [157] Nandedkar, S. and D. Sanders, "Special purpose orthonormal basis functions, application to motor unit action potentials", IEEE Transactions Biomedical Engineering, 31, 374–377, 1984.
- [158] Nunez, P., "Representation of evoked potentials by fourier–bessel expansions", IEEE Transactions Biomedical Engineering, 20, 372–374, 1983.
- [159] Chang, Y., "Dynamic programming as applied to feature subset selection in pattern recognition system", IEEE Transactions Systems Man Cybernetics, 6, 166, 1973.
- [160] Nandedkar, S., "Simulation techniques in electromyography", IEEE Transactions Biomedical Engineering, 32, 775–785, 1985.
- [161] Fitch, P., "An analyzer for the use of human electromyography", Electronic Engineering, 39, 240–243, 1967.
- [162] Fusfeld, R., "Classification of the EMG by a pattern recognition method", Med. Biol. Eng. Computing, 20, 496–500, 1982.
- [163] Fusfeld, R., "Instrument for quantitative analysis of the electromyogram", Med. Biol. Eng. Computing, 20, 90–295, 1978.
- [164] Heetderks, W., "Criteria for evaluating multi–unit spike separation techniques", Biological Cybernetics, 29, 215–220, 1978.
- [165] Prochozka, V. and H. Korhuber, "On line multi–unit sorting with resolution of superimposed signals", Electroencephalography and Clinical Neurophysiology, 34, 91–93, 1973.
- [166] Prochozka, V. et al, "Computerized single unit interval analysis and its clinical application", New Developments in Electromyography and Clinical Neurophysiology, 2, 462–468, 1973.

- [167] Prochozka, V., B. Conrad and F. Sinderman, "A neuro-electric signal recognition system", *Electroencephalography and Clinical Neurophysiology*, 34, 91-93, 1973.
- [168] Studer, R., R. Figueirido and G. Moschytz, "An algorithm for sequential signal estimation and system identification for EMG signals", *IEEE Transactions Biomedical Engineering*, 31, 285-295.
- [169] Usui, S. and I. Amidror, "Digital low pass differentiation of biological signal processing", *IEEE Transactions Biomedical Engineering*, 29, 686-693, 1982.
- [170] Roberts, W., and D. Harline, "Separation of multi-unit nerve trains by a multichannel linear filter algorithm", *Brain Research*, 94, 141-149, 1975.
- [171] Horowitz, P., "The Art of Electronics", Cambridge University Press, New York, 1980.
- [172] Cooper, J., "The minicomputer in the Laboratory: with examples using the PDP-11", John Wiley and Sons, Toronto, 1977.
- [173] Desautels, E., "Assembly Language Programming for PDP-11 and LSI Computers: an introduction to computer organization", Wm C. Brown, Toronto, 1982.
- [174] Grady, E., "Assembly Language: Macro-11 and the PDP-11", McGraw-Hill, Toronto, 1984.
- [175] Frank, T., "Introduction to the PDP-11 and its Assembly Language", Prentice-Hall, Toronto, 1983.
- [176] Jermann, W., "Programming 16-Bit Machines: The PDP-11, 8086 and 68000", second edition, Prentice-Hall, Toronto, 1986.

- [177] Katzan, H., "Fortran 77", VanNostrand Reinhold Company, New York, 1978.
- [178] Hamming, R., "Digital Filters", second edition, Prentice-Hall, Englewood Cliffs, 1983.
- [179] Reucher, H., G. Rau and J. Silny, "Spatial filtering of noninvasive multielectrode EMG", IEEE Transactions Biomedical Engineering, 34, 98-106, 1987.
- [180] Bak, M. and E. Schmidt, "An improved window discriminator", IEEE Transactions Biomedical Engineering, 24, 486-489, 1977.
- [181] Guihanec, P., "Segmentation filtering and noise analysis in MUAP analysis", Seminar on automated quantization of MUAPs, 31st Annual Meeting AAEE, Sept. 20, Kansas City, 1984.
- [182] Bose, N., "Digital Filters: Theory and Applications", North-Holland, New York, 1985.
- [183] Bendat, J. and A. Piersol, "Random Data: Analysis and Measurement Procedures", John Wiley and Sons, New York, 1978.
- [184] Bendat, J. and A. Piersol, "Engineering Applications of Correlation and Spectral Analysis", John Wiley and Sons, Toronto, 1980.
- [185] Hamming, R., "Numerical Methods for Scientists and Engineers", second edition, Dover Publications, New York, 1973.
- [186] McGill, K. and L. Dorfman, "High resolution alignment of sampled waveforms", IEEE Transactions Biomedical Engineering, 31, 462-468, 1984.
- [187] Bracewell, R., "The Fourier Transform and its Applications", second edition, McGraw-Hill, Toronto, 1986.

- [188] Brigham, E., "The Fast Fourier Transform", Prentice-Hall, New York, 1974.
- [189] Nussbaumer, H., "Fast Fourier Transform and Convolution Algorithms", second edition, Springer-Verlag, 1982
- [190] Tretter, S., "Introduction to discrete-time signal processing", John Wiley and Sons, Toronto, 1976.
- [191] Wheeler, B. and S. Smith, "High resolution alignment of action potential waveforms using cubic spline interpolation", Journal of Biomedical Engineering, 9, 47-53, 1987
- [192] Flannery, B., S. Teukolsky, W. Vetterling, "Numerical Recipes: the art of scientific computing", Cambridge University Press, New York, 1986.
- [193] Kahaner, D., C. Moler and S. Nash, "Numerical Methods and Software", Prentice-Hall, New Jersey, 1988.
- [194] Johnson, D., J. Johnson and H. Moore, "A Handbook of Active Filters", Prentice-Hall, New Jersey, 1980.
- [195] Stout, D. and M. Kaufman, "Handbook of Microcircuit Design and Application", McGraw Hill, Toronto, 1980.